Bioactive trace metals and their isotopes as paleoproductivity proxies: An assessment using GEOTRACES-era data

Tristan Horner, Susan Little, Tim Conway, Jesse Farmer, Jennifer Hertzberg, Alastair Lough, Jennifer Mckay, Allyson Tessin, Stephen Galer, Sam Jaccard, et al.

Bioactive trace metals and their isotopes as paleoproductivity proxies: An assessment using GEOTRACES-era data

T.J. Horner[1,2,*], S.H. Little[3,*], T.M. Conway[4,*], J.R. Farmer[5,6,*], J.E. Hertzberg[7], A.J.M. Lough[8,9], J. McKay[10], A. Tessin[11], S.J.G. Galer[6], S.L. Jaccard[12], F. Lacan[13], A. Paytan[14], K. Wuttig[15], and GEOTRACES–PAGES Biological Productivity Working Group Members[16].

[1]NIRVANA Labs, [2]Department of Marine Chemistry & Geochemistry, Woods Hole Oceanographic Institution, Woods Hole, MA, USA; [3]Department of Earth Sciences, University College London, London, GBR; [4]College of Marine Science, University of South Florida, FL, USA; [5]Department of Geosciences, Princeton University, Princeton, NJ, USA ; [6]Max-Planck Institute for Chemistry, Mainz, DEU; [7]Department of Ocean, Earth & Atmospheric Sciences, Old Dominion University, Norfolk, VA, USA; [8]National Oceanography Centre, University of Southampton, Southampton, GBR; [9]Now at: School of Geography, University of Leeds, Leeds, GBR; [10]College of Earth, Ocean, and Atmospheric Sciences, Oregon State University, Corvallis, OR, USA; [11]Department of Geology, Kent State University, Kent, OH, USA; [12]Institute of Geological Sciences and Oeschger Center for Climate Change Research, University of Bern, Bern, CHE; [13]LEGOS, University of Toulouse, CNRS, CNES, IRD, UPS, Toulouse, FRA; [14]Institute of Marine Sciences, University of California Santa Cruz, Santa Cruz, CA, USA; [15]Antarctic Climate and Ecosystems Cooperative Research Centre, University of Tasmania, Hobart, AUS; [16]A full list of working group members and their affiliations appears at the end of the manuscript.

*To whom correspondence should be addressed: T.J.H. (Tristan.Horner@whoi.edu), S.H.L. (susan.little@ucl.ac.uk), T.M.C. (tmconway@usf.edu), or J.R.F. (jesse.farmer@princeton.edu).

Key Points

- This review assesses the potential of a number of bioactive trace elements and their isotopes to inform on past ocean productivity
- Distributions, drivers, and depositional archives are described for iron, zinc, copper, cadmium, molybdenum, barium, nickel, and silver
- Future priorities include quantification of 'missing' flux terms, constraining circulation influences, and identifying sedimentary archives

Keywords: marine chemistry; iron; zinc; copper; cadmium; molybdenum; barium; nickel; silver.

Abstract

The ocean's biological carbon pump redistributes climatically-significant quantities of carbon from the atmosphere to the ocean interior and seafloor. How the biological pump operated in the past is therefore important for understanding past atmospheric carbon dioxide concentrations and Earth's climate history. Due to their intimate association with biological processes, several bioactive trace metals and their isotopes are thought to be promising proxies for productivity, including: iron, zinc, copper, cadmium, molybdenum, barium, nickel, and silver. Here we review the oceanic distributions, driving processes, and depositional archives for these eight elements and their isotopes based on GEOTRACES-era datasets. We offer an assessment of the overall maturity of each isotope system to serve as a proxy for diagnosing aspects of past ocean export productivity, and identify priorities for future research. Despite many of the elements reviewed here sharing a common biological driving processes, we show that key aspects of the biogeochemical cycle of each element are often unique. Rather than being a source of confusion, it is our hope that combining the unique perspectives afforded by each bioactive trace element will enable painting a more complete picture of marine paleoproductivity, biogeochemical cycles, and Earth's climate history.

1. Introduction

The ocean plays host to three carbon 'pumps' that redistribute climatically-significant quantities of carbon dioxide (CO_2) from the atmosphere to the ocean interior and seafloor (Volk & Hoffert, 1985). These ocean carbon pumps—biological, carbonate, and solubility— influence Earth's climate over timescales ranging from decades to millions of years (e.g., Volk & Hoffert, 1985; Sigman et al., 2010; Khatiwala et al., 2019). The biological pump is of particular interest as it connects the cycles of C to those of O_2, (micro)nutrients, and marine biology, and today accounts for as much as 70 % of the 'contribution ' of all three carbon pumps (Sarmiento & Gruber, 2006). The biological pump redistributes atmospheric carbon in two steps. First, phytoplankton, photoautotrophic microbes, use sunlight to transform ambient DIC (dissolved inorganic carbon) into POC (particulate organic carbon), represented here by CO_2 and glucose, respectively, by the simplified reaction:

$$\mathbf{CO_2 + H_2O + } h\nu \rightarrow \mathbf{CH_2O + O_2} \qquad [1]$$

The second step requires that some fraction of the newly-formed POC sinks into the ocean interior through a combination of biological and physical aggregation processes (e.g., Alldredge & Silver 1988). The resulting surface ocean DIC deficit promotes the invasion of atmospheric CO_2 into seawater to maintain air–sea CO_2 equilibrium, driving an overall reduction in atmospheric pCO_2. (This definition of the biological pump neglects dissolved organic carbon export, which is comparatively understudied, though may account for as much as one-third of C export; e.g., Carlson et al., 2010; Giering et al., 2014.) Importantly, Reaction [1] requires sunlight and can only occur in the euphotic layer of the ocean. In contrast, aerobic heterotrophic respiration can occur wherever POC and O_2 are present:

$$\mathbf{CH_2O + O_2 \rightarrow CO_2 + H_2O} \qquad [2]$$

(There are a number of O_2-independent respiration pathways that are reviewed in detail elsewhere; e.g., Froelich et al., 1979.)

While the representation of all POC as glucose (CH_2O) is instructive for illustrating an important biotic transformation in the ocean, it is also simplistic; microbial biomass consists of dozens of bioactive elements that serve many essential functions (e.g., da Silva & Williams, 1991). The elemental stoichiometry of POC can thus be expanded to include a number of major and micronutrient elements, as illustrated by the extended Redfield ratio reported by Ho et al. (2003):

$$\mathbf{C_{124,000}N_{16,000}P_{1,000}S_{1,300}K_{1,700}Mg_{560}Ca_{500}Sr_{5.0}Fe_{7.5}Zn_{0.8}Cu_{0.38}Co_{0.19}Cd_{0.21}Mo_{0.03}} \qquad [3]$$

With this extended stoichiometry in mind, it is clear that Reactions [1] and [2]—the production and regeneration of organic matter, respectively—will not only generate gradients in the dissolved concentration of DIC and O_2, but also for many other bioactive elements associated with POC cycling. These gradients will be steepest for those elements possessing shorter residence times and where biological uptake and regeneration are the most important processes driving their vertical distributions. Likewise, such gradients may be almost absent for elements that possess long residence times or are primarily cycled by processes disconnected from productivity.

For those bioactive metals where biological processes are important, the implication of Reactions [1] and [2] is that many of the metals listed in [3] may, in turn, be used as proxies of POC cycling and hence paleoproductivity. A key motivation for using these elements as tracers of (past) POC cycling is that bioactive metal distributions are often set over significant spatiotemporal scales. For example, temporal changes in POC fluxes from a single sediment core would, at most, reflect local changes in export productivity, though such reconstructions are oftentimes unreliable indicators of productivity owing to significant preservation biases (e.g., Rühlemann et al., 1999). Biases aside, building a regional picture of paleoproductivity in this manner would require sampling many regions of the seafloor (e.g., Cartapanis et al., 2016) and conducting many more analyses. In contrast, the flux and residence time of nutrients in the euphotic ocean can be diagnostic of the productivity of entire ecosystems (e.g., Dugdale & Goering, 1967). Indeed, large-scale features of past ocean productivity are routinely reconstructed using the abundance and stable isotopic compositions of macronutrient elements (C, N, and Si; see Farmer et al., *this issue*). It thus follows that the abundance and isotopic compositions of several bioactive trace elements and their isotopes (TEI's) cycled along with POC could also serve as valuable proxies for past export productivity. However, in order to use systems of trace elements and their isotopes as proxies for productivity, it is necessary to develop a comprehensive understanding of the marine behavior of these elements, including: mapping their distribution in the ocean; elucidating the drivers of the distribution; characterizing sources, sinks, and transformations associated with biological, physical and chemical (notably redox) reactions; and, recognizing if (and how) a given element is incorporated and preserved in marine sediments.

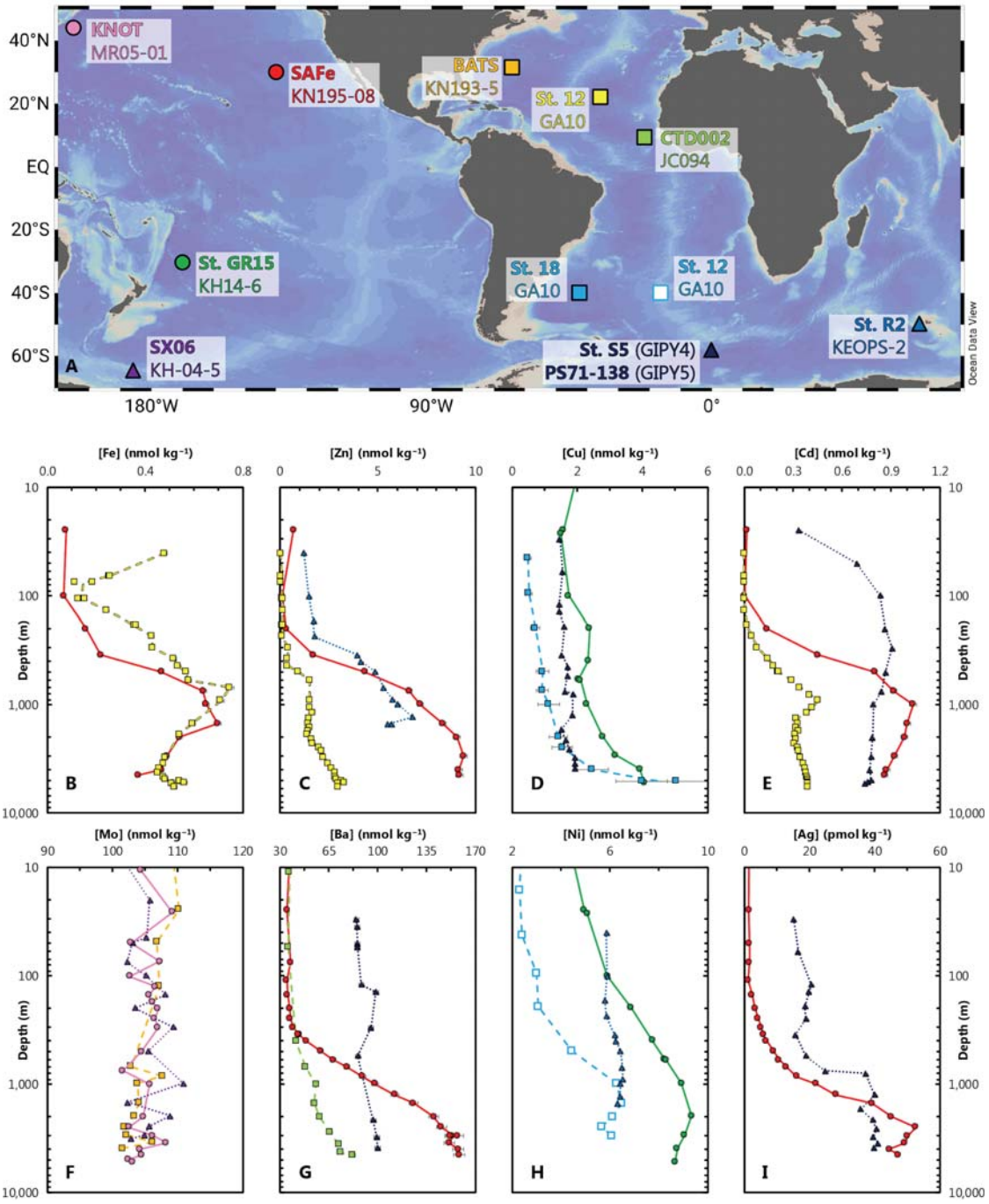

Figure 1 | Overview of bioactive trace metal distributions discussed in this review. A Map showing locations of the representative depth profiles shown in both the lower panels and discussed throughout this review (Sections. 3–10). The specific station (bold) and cruise identifier are given for each location; circles, squares, and triangles denote stations in the Pacific, Atlantic, and Southern Oceans, respectively. The lack of exemplar stations from the Indian Ocean reflects the current paucity of GEOTRACES-compliant campaigns in this basin. Two stations sampled from the Atlantic Sector of the Southern Ocean are designated by a single symbol: St. S5 (GIPY4), situated at 57.55 S, 0.04 W, and PS71-138 (GIPY5) at 61.00 S on the Zero Meridian. **B–I** Depth profiles of bioactive trace metal concentrations for Fe (B), Zn (C), Cu (D), Cd (E), Mo (F), Ba (G), Ni (H), and Ag (I). Profiles are shown in semi-log space to illustrate variations in the epi- and mesopelagic realm. Originators are cited in the Data Sources section. Map created using Ocean Data View (Schlitzer, R., https://odv.awi.de, 2018).

The wealth of new TEI data from the GEOTRACES program (Fig. 1) now permits an assessment of whether certain bioactive metals are promising proxies for past ocean productivity. This contribution represents such an assessment. Our study synthesizes what is known about the processes governing the cycling of several bioactive TEIs in seawater, explores the level of development and readiness of each TEI system to inform on aspects of past ocean productivity, and identifies areas where further research is most needed to improve our understanding of the geochemistry of TEIs in the past and present ocean. We base our assessment on publicly-available results from the international GEOTRACES programme (e.g., Mawji et al. 2015; Schlitzer et al., 2018). Our study is not intended to be a thorough review of all available techniques used to reconstruct paleoproductivity. Instead, we focus on bioactive TEI systems that are either recognized as micronutrients (such as those in Eq. 3) or exhibit nutrient-like dissolved profiles in seawater, regardless of their nutritional status to phytoplankton (e.g., Ba, Ag). This will not be the last word on the topic; our understanding of many of these TEIs has rapidly evolved in recent years, and will continue to evolve as new data are generated.

This contribution is structured such that each bioactive TEI system is reviewed similarly and systematically. The order in which TEI's are assessed follows the extended Redfield ratio—iron (Fe; Sec. 3.), zinc (Zn; Sec. 4), copper (Cu; Sec. 5), cadmium (Cd; Sec. 6), and molybdenum (Mo; Sec. 7)—before describing the nonessential elements barium (Ba; Sec. 8), nickel (Ni; Sec. 9.), and silver (Ag, Sec. 10) in order of decreasing dissolved concentration in seawater. The assessment of each TEI system is organized around four questions:

1. What is the modern marine distribution of this TEI system?
2. Which biological, chemical, and physical processes are most important for maintaining this distribution?
3. In what form is this TEI system incorporated into sediments?
4. Are there clear priorities for improving the utility of this system to track paleoproductivity?

This structure results in some repetition of the main distributions, drivers, and sedimentary archives between individual TEI systems. This redundancy is deliberate: each section can be read independently without reference to other TEIs. We close our review by assessing the 'maturity' of each system based on a comparison to more established productivity proxies, offer suggestions for future studies, and discuss prospects for paleoproductivity reconstructions using bioactive TEI isotope systems.

2. Definitions

2.1. Paleoproductivity

What is (paleo)productivity? This definition is significant since the biological productivity of an ecosystem can be described by a number of nested C cycles, whereby only some sub-cycles contribute to the sequestration of atmospheric CO_2 as POC in the ocean interior and the geological record. Moreover, productivity estimates can diverge depending on the tracer (e.g., Bender et al., 1987) or reference depths (e.g., Buesseler et al., 2020) used as the basis of any calculation. Individual proxies for POC cycling may be sensitive to only certain components of the C cycle and could thus yield conflicting insights into paleoproductivity. For consistency with the macronutrient literature, we use the definitions described by Sigman & Hain (2012): GPP, NPP, and NEP, which correspond to gross primary production, net primary production, and net ecosystem (or 'export') production, respectively. Gross PP refers to total autotrophic production of POC (or O_2; i.e., Eq. [1]). Net PP is defined as GPP minus autotrophic respiration—the metabolic O_2 requirements of primary producers—and is effectively the rate at which phytoplankton produce new biomass. Lastly, NEP refers to GPP minus all autotrophic *and* heterotrophic respiration in an ecosystem (i.e., NPP minus heterotrophic respiration). If considering only the sunlit surface ocean, NEP is equivalent to export production; the flux of POC from the surface ocean must, over sufficiently long timescales, balance the vertical supply of dissolved nutrients. Likewise, integrated over the entire euphotic ocean, NEP represents the upper limit of the CO_2 sequestering capacity of the biological pump: the amount of POC buried in marine sediments must be less than, or equivalent to, annual NEP (minus any contributions from terrestrial OC). Accordingly, NEP is perhaps the most relevant term to understanding how the biological pump draws down and stores atmospheric CO_2. Indeed, variations in NEP are implicated as a key driver of glacial–interglacial variations in pCO_2 and hence climate (e.g., Broecker, 1982; Boyle, 1988a; Berger et al., 1989; Paytan, 2009). Thus, when describing and assessing the utility of each TEI system to inform on past productivity, we are specifically concerned with whether and how that system is related to NEP.

2.2. Key processes

In addition to only being sensitive to certain POC sub-cycles, the TEI systems reviewed here exhibit a number of instances where their cycling may be decoupled from those of POC. Broadly, these processes can be categorized as affecting the sources, internal cycling, or sinks of TEIs, but not always the macronutrients or C. These additional processes may lead to differences between, or even a complete

decoupling of (paleo)productivity estimates using TEI- and macronutrient-based productivity measures. These three areas are introduced here and described in detail in the sections that follow.

First, many elements, including bioactive TEIs, can be decoupled from DIC cycling through 'external' sources that mask any POC-related drawdown. Though rarely significant for DIC, these sources—rivers, dust, desorption from particles, sediments, and hydrothermalism—may be significant terms in local and regional TEI budgets if the magnitude is comparable to the dissolved supply from ocean circulation. Examples include dust-derived Cu to surface planktonic communities (e.g., Paytan et al., 2009) and hydrothermal-derived Fe to the deep ocean (e.g., Resing et al., 2015). Consideration of these external sources is particularly important when close to such point sources and for elements with residence times that are less than or similar to the mixing time of the ocean (~1 kyr).

Second, the internal cycle of TEIs can be complex; TEI distributions can be decoupled from those of the macronutrients through myriad interactions with particles, be they biological (uptake and remineralization), physical (adsorption, desorption), or chemical (e.g., redox transformation leading to precipitation or dissolution; e.g., Boyd et al., 2017).

Biological uptake itself may decouple TEIs from macronutrients since organisms appear to have wider tolerances for the intracellular proportions of certain trace elements compared to those of C, N, and P. The physiological mechanisms enabling this plasticity, and the feedback interactions that drive it, are beyond the scope of this review, and are discussed in detail elsewhere (e.g., Sunda, 2012; Morel et al., 2020). From a proxy perspective, this flexibility may cause uncertainty in paleoproductivity estimates; the more variable the C:TEI stoichiometry of organisms within an ecosystem, the more uncertain the paleoproductivity estimate derived from that trace element. (The corollary being that the more rigid the stoichiometry, the more robust the paleoproductivity estimate.) An extreme example concerns nonessential elements (e.g., Ba), or metals that are only essential for certain groups of organisms within an ecosystem (e.g., Ni for methanotrophs). Productivity estimates derived from the export of these nonessential elements are potentially susceptible to decoupling from productivity cycles as their export is not intrinsically tied to the overall functioning of an ecosystem.

Remineralization—the regeneration of POC to inorganic dissolved nutrients—can similarly decouple the internal cycles of TEIs and macronutrients. In the case of a scarce nutrient, such as Fe, individual organisms (e.g., Saito et al., 2011) and even entire ecosystems (e.g., Rafter et al., 2017) may have evolved mechanisms to retain scarce resources. Likewise, macro- and micronutrient TEIs may be regenerated by heterotrophic

organisms at different rates (e.g., Twining et al., 2014; Ohnemus et al., 2019). Thus, the number of productivity cycles that must occur before a trace element is exported out of the euphotic zone may differ from that of C or other macronutrients.

The processes of adsorption and desorption can also fractionate TEI:macronutrient relationships. Originally developed in the context of dissolved and particulate thorium isotopes (Bacon & Anderson, 1982), reversible scavenging is now suggested to play a role in the vertical cycling of other metals, including Cu (e.g., Little et al., 2013) and Fe (e.g., Abadie et al., 2017). Reversible scavenging is a continuous process that occurs between particle surfaces and dissolved species. While this process can occur at any depth, scavenging intensity is positively correlated with the quantity of particles, and so is most important in the upper water column. Likewise, while dissolved TEIs may be scavenged by any class of particle (e.g., opal, lithogenics), recent modeling efforts indicate that certain particle types may preferentially scavenge certain elements (e.g., Lerner et al., 2018). Scavenging may also affect TEIs primarily cycled by organic matter; secondary phases may scavenge metals during remineralization, which could affect TEI distributions in the upper water column (e.g., Zn, John & Conway, 2014; Co, Hawco et al., 2018; Fe, Tagliabue et al., 2019).

Changes in the ambient redox environment, such as in an oxygen minimum zone (OMZ), may also enhance dissolved–particulate transformations for certain TEIs. Whether OMZs act as a source or a sink depends on the TEI; whereas some elements may be released during reductive dissolution of particulate Fe–Mn oxides, others may exhibit enhanced scavenging onto particles in strongly reducing environments.

Third, many TEIs have significant output fluxes that are not associated with organic matter. The processes mediating these burial fluxes are diverse, ranging from scavenging (e.g., Cu, Mo) to precipitation into (organo)minerals (e.g., Ba; Défarge, 2011). Consequently, changes in the non POC-associated burial flux term(s) may drive the ocean to a new TEI:C stoichiometry that could be difficult to recognize or interpret in the sedimentary record.

While these three categories of processes may appear insurmountable obstacles to the reliable application of TEIs to reconstruct paleoproductivity, there are reasons to be optimistic. Indeed, the fact that so many confounding processes are now recognized highlights just how far our understanding of TEI geochemistry has evolved in recent years. Moreover, many of these processes primarily concern the use of trace element abundances to reconstruct past productivity. As we show in the following sections, the processes controlling the abundance of an element may be distinct from that controlling its isotopic composition. These distinct controls may enable isotopic analyses to reduce, or even eliminate, certain ambiguities in

paleoceanographic data, highlighting a potentially valuable role for TEI systems in the reconstruction of paleoproductivity.

2.3. Isotope notation

The bioactive TEI literature abounds with isotope notations (e.g., ε, δ), reference materials (e.g., JMC, NIST), and isotope ratio pairs (e.g., $^{57}Fe/^{54}Fe$ versus $^{56}Fe/^{54}Fe$; $^{137}Ba/^{134}Ba$ versus $^{138}Ba/^{134}Ba$). There are merits to each choice and it is not our intention to review these here. However, we believe that the sheer number of ways in which TEI data have been reported can be confusing to scientists in other disciplines and this confusion ultimately diminishes the reach and utility of TEI-based research. To avoid furthering this confusion, we have adopted a number of conventions that apply throughout this review, regardless of how literature data were originally reported. First, we use a single isotope notation throughout ('δ'; i.e., the delta notation). Second, we express all data relative to the most widely accepted standard for each isotope system. For many isotope systems, the most widely-accepted standard may have since been exhausted (e.g., JMC Lyon for Zn). In those cases, there are usually cross-calibrated secondary materials that can be used to report new isotope data in terms of 'legacy' materials (e.g. AA-ETH for Zn, Archer et al., 2017). Third, we report TEI data using the same isotope ratio pairs as used in the GEOTRACES data products (e.g., Mawji et al., 2015; Schlitzer et al., 2018). We note that isotope data are a unitless ratio quantity (Coplen, 2011), though are commonly reported with 'units' of ‰ (i.e., parts per one-thousand):

$$\delta^{x}\mathrm{TE} = R_{sample} / R_{standard} - 1 \quad [4]$$

where δ^{x}TE represents $\delta^{56}Fe$, $\delta^{66}Zn$, $\delta^{65}Cu$, $\delta^{114}Cd$, $\delta^{98}Mo$, $\delta^{138}Ba$, $\delta^{60}Ni$, or $\delta^{109}Ag$ and R represents $^{56}Fe/^{54}Fe$, $^{66}Zn/^{64}Zn$, $^{65}Cu/^{63}Cu$, $^{114}Cd/^{110}Cd$, $^{98}Mo/^{95}Mo$, $^{138}Ba/^{134}Ba$, $^{60}Ni/^{58}Ni$, or $^{109}Ag/^{107}Ag$ in either a sample or standard. For clarity, all isotopic data reviewed here have been calculated using notation in Eq. 4, and renormalized to the following standards, regardless of how the data originators reported their results: IRMM-014 for Fe (e.g., Dauphas et al., 2017), JMC-Lyon for Zn (e.g., Moynier et al., 2017), NIST SRM 976 for Cu (*ibid.*), NIST SRM 3108 for Cd (e.g., Abouchami et al., 2013), NIST SRM 3134 +0.25 ‰ for Mo (Nägler et al., 2014), NIST SRM 3104a for Ba (e.g., Horner et al., 2015a), NIST SRM 986 for Ni (e.g., Elliott & Steele, 2017), and NIST SRM 978a for Ag (e.g., Woodland et al., 2005).

We summarize salient features of each TEI in Table 1. The review of each TEI system follows.

240 **Table 1 | Summary of oceanic concentrations, isotopic compositions, and mean ocean residence times for**
241 **bioactive TEIs discussed in this review.** Superscripts denote references listed in the Data Sources section.

Element	Dissolved concentration range (nmol kg^{-1})	Mean Upper Continental Crust composition (‰)	Mean deep ocean isotopic composition (‰)	Range of deep ocean isotope compositions (‰)	Residence time estimates (kyr)
Fe	0.01–100[a]	+0.1[d]	Variable[k]	−2.4 to +1.5[k]	0.004–0.6[r]
Zn	0.01–10[a]	+0.3[e]	≈+0.5[l]	-0.2 to +0.6[l]	1–11[r]
Cu	0.5–4[a]	+0.1[e]	≈+0.7[m]	+0.6 to +0.8[m]	2–5[r]
Cd	0.00003–1.2[a]	0.0[f]	≈+0.3[n]	+0.2 to +0.4[n]	22–105[r]
Mo	100[b]	+0.4[g]	≈+2.3[o]	Homogeneous[o]	440[s]
Ba	35–160[a]	0.0[h]	≈+0.3[p]	+0.2 to +0.4[p]	8[t]
Ni	1.5-11[a]	+0.1[i]	≈+1.3[q]	Homogeneous[q]	10–30[u]
Ag	0.0002–0.1[c]	0.0[j]	Unknown	Unknown	0.4[v]

3. Iron

Iron (Fe) plays a key role within phytoplankton as an electron carrier for photosynthesis and respiration processes, as well as within enzymes necessary for photosynthesis and nitrogen fixation (Morel & Price, 2003). However, in oxygenated seawater, Fe(II) is rapidly oxidized to Fe(III), which is highly insoluble (Liu & Millero, 2002). Intense biological demand coupled to low solubility results in generally sub-nanomolar concentrations for dissolved Fe throughout the oceans, and Fe concentrations approach the low picomolar range in some surface regions far from Fe sources, such as the vast Southern Ocean (Chever et al., 2010; Klunder et al., 2011; Schlitzer et al., 2018). Consequently, biological production in about 30 % of the modern surface ocean is thought to be limited primarily by Fe (Moore et al., 2013), principally in upwelling regions where deep water is depleted in Fe relative to the macronutrients nitrate and phosphate (e.g., Moore, 2016; Boyd et al., 2017). In these regions, termed 'High Nutrient Low Chlorophyll' (HNLC), Fe supply can limit primary productivity (e.g., Martin & Fitzwater, 1988) and potentially the exchange of carbon between the ocean and atmosphere. Furthermore, a changing supply of Fe from sources such as atmospheric dust, hydrothermal venting, or sedimentary release to the surface oceans through geological time can exert a significant control on both the distribution of primary productivity in the oceans and, through this, the global carbon cycle. Changes in supply of dust to the Fe-limited Southern Oceans has been shown to correlate with climate variability on millennial time scales and has also been invoked to explain the dramatic sawtooth glacial–interglacial shifts in atmospheric carbon dioxide (Martin, 1990; Sigman & Boyle, 2000; Martínez-Garcia et al., 2011; 2014). The strong link between Fe supply and primary productivity means that ratios of Fe to other elements and/or Fe isotope ratios ($\delta^{56}Fe$) might be useful proxies for investigating changes in paleoproductivity, provided the processes that fractionate them are dominantly linked to primary production, can be constrained, and suitable archives identified.

3.1. Marine distribution

The distribution of dissolved Fe in seawater is driven by a mixture of competing processes, including biological uptake and (deeper) regeneration; distinct sources of Fe at shallow, intermediate, and deep depths; adsorption/desorption processes onto organic and lithogenic particles; dissolution and precipitation processes; and complexation to organic ligands (Fig. 2; e.g., Boyd & Ellwood, 2010; Labatut et al. 2014; Tagliabue et al., 2017). As a result, dissolved Fe displays what has historically been termed as hybrid-type depth profile in the open ocean, which exhibits a number of similarities between different ocean basins (Fig. 3). Surface Fe is drawn down in surface waters by biological uptake, and can even be as low as 0.01 nmol kg^{-1} in Fe limited regions. However, some areas of the oceans, such as the 'dusty' North Atlantic,

surface Fe concentrations can be driven as high as 2 nmol kg^{-1} as a result of dust events (Sedwick et al., 2005). Below the surface mixed layers, regeneration of biogenic material, reversible particle scavenging, and complexation by organic ligands act to keep the background deep ocean Fe concentrations at around 0.4–0.6 nmol kg^{-1} (e.g., Lauderdale et al., 2020). Against this background, it has been known for decades that Fe concentrations in deeper waters are elevated near point sources such as sedimentary margins (Johnson et al., 1999). Recently, a range of studies including those conducted as part of the GEOTRACES program, have illuminated this picture, showing that deep sources of Fe—such as sedimentary and hydrothermal release—are widespread, may have distinct traceable δ^{56}Fe source signatures, and that this Fe can be transported over large distances through the ocean interior (e.g., Radic et al. 2011; Saito et al., 2013; Conway and John, 2014; Resing et al., 2015; Nishioka et al., 2020). Despite exhibiting well-defined deep maxima close to point sources, Fe distributions at shallow and intermediate depths are much more variable and models have struggled to reproduce these variations (e.g., Tagliabue et al., 2016). The extent to which deeply sourced Fe is supplied to surface seawater is thus equivocal (c.f.., Tagliabue et al., 2010; Roshan et al., 2020).

The origin of Fe variability in the shallow and intermediate ocean is thought to reflect local differences in the competition between uptake, regeneration, sources, and scavenging. The same processes influence δ^{56}Fe; however, unlike variations in Fe concentrations, δ^{56}Fe exhibits dramatic variability between—and even within—ocean basins (Fig. 2; Schlitzer et al., 2017). Such water column variability in δ^{56}Fe, from isotope compositions as light as −3 ‰ (John et al., 2012), to as heavy as ~+1.5 ‰ (Ellwood et al., 2020), is thought to be driven by Fe source signatures and therefore also oceanic circulation, and a combination of biological uptake, Fe complexation to organic ligands in surface waters, and non-reductive release of dissolved Fe from particles (notably lithogenic particles) during desorption and/or ligand-promoted dissolution (e.g. Conway and John, 2014; Abadie et al. 2017; Ellwood et al., 2020; Fig. 3). As such, δ^{56}Fe may provide insight to the contribution of Fe sources at the basin scale (e.g. Conway & John, 2014), as well as for Fe cycling processes such as uptake and regeneration.

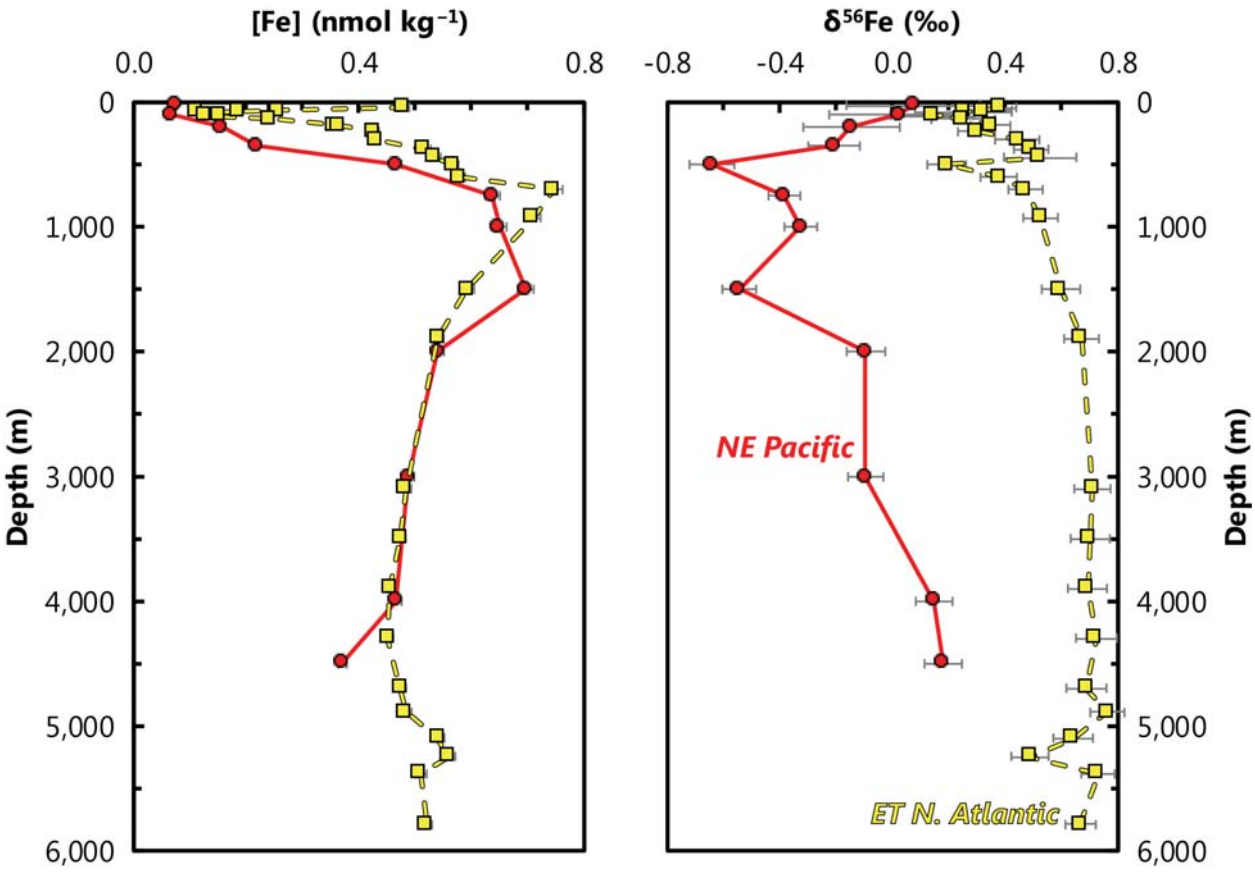

Figure 2 | Representative profiles of dissolved Fe concentrations ([Fe]) and Fe-isotopic compositions (δ^{56}Fe) in the Eastern Tropical North Atlantic (squares, dashed line) and Northeast Pacific (circles, solid line) Oceans. This comparison illustrates that despite possessing similar dissolved concentration profiles, the isotopic behavior of Fe is markedly different between basins.

Despite numerous studies of both small- (e.g., Martin et al., 1990; Coale, 1991; Coale et al., 2003) and large-scale iron fertilization (e.g., de Baar et al., 2005; Boyd et al., 2007; Boyd & Ellwood, 2010), there are still uncertainties in how changing Fe supply to the surface ocean may affect phytoplankton growth in Fe-limited regions, and/or nitrogen fixers under nitrate limitation, leading to gaps in our understanding of linking Fe cycling directly to climate change (Misumi et al., 2014). One major challenge is assessing what portion of the dissolved Fe pool is available for uptake by different microbes, termed 'bioavailable' Fe. Such uncertainties on Fe supply, speciation, and bioavailability in the surface ocean are compounded by limitations in our ability to constrain the supply of dissolved Fe in upwelled deep waters. For example, while the ratio of C to macronutrients such N and P in the deep ocean is well known and the residence time and distribution can be accurately reproduced using apparent oxygen utilization (AOU), this is not the case for Fe. Only around 10–15 % of cellular Fe (Fe:C = 18–33 μmol:mol) appears to be regenerated in the deep ocean (Fe:C 4–6; Twining & Baines, 2013), leading to a weaker correlation between Fe and AOU, even in regions away from Fe sources (Rijkenberg et al., 2014) and upwelling deep waters that are depleted in

dissolved Fe relative to macronutrients. Since incubation experiments show that Fe associated with sinking organic matter from the subsurface is effectively regenerated (Velasquez et al., 2016), much of the released Fe must be rapidly scavenged (Tagliabue et al., 2019). Despite this scavenging, vertical transport is still thought to be the major source of dissolved Fe for phytoplankton in most Fe-limited regions, indicating that additional research into the interplay between Fe supply (sources, stabilization, and transport) and demand (biological uptake, scavenging) are required.

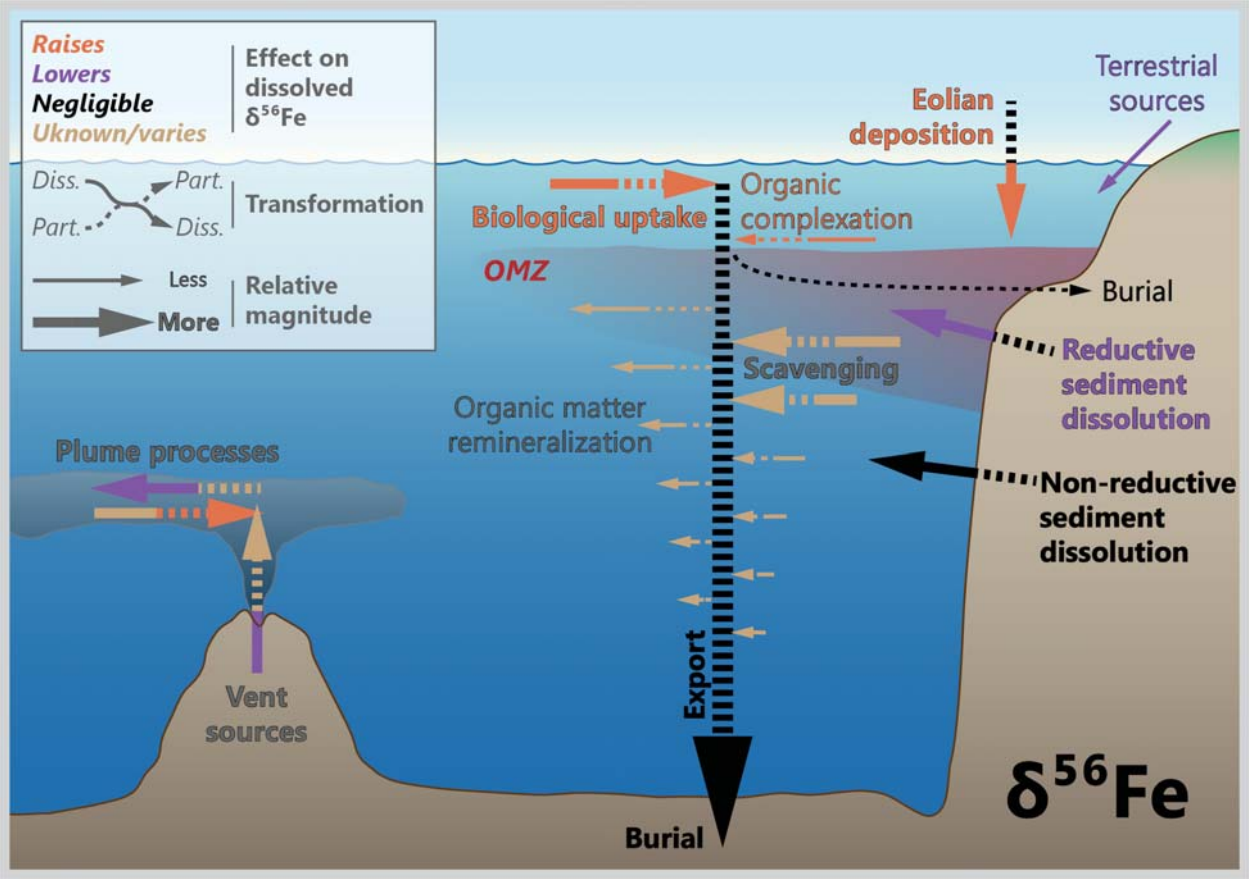

Figure 3 | Processes driving iron isotope variations in modern seawater. The oceans' internal cycle of Fe is perhaps the most complex of the TEIs discussed here, exhibiting several significant sources, sinks, and transformations not directly associated with biological productivity.

3.2. Driving processes

3.2.1. Biological

Initial studies of processes that fractionate Fe isotopes were optimistic that δ^{56}Fe would make for a powerful proxy of physiological 'biosignatures' (Beard et al., 1999), especially once measurement of δ^{56}Fe was

extended to seawater by Lacan et al. (2008). However, much of this early optimism faded once it was found that other factors were also important in setting dissolved δ^{56}Fe, such as external Fe sources (e.g., Radic et al., 2011; John et al., 2012; Sec. 3.2.3.). Moreover, organisms exhibit significant variability in Fe:C ratios (e.g., Twining & Baines, 2013), suggesting that Fe cycling may be partially decoupled from ecosystem productivity. Despite the more nuanced picture, there is a growing body of evidence suggesting that phytoplankton probably preferentially incorporate light Fe isotopes from seawater and, in some circumstances, can render detectable changes in dissolved δ^{56}Fe. For example, studies from isolated eddies, the Mertz Polynya, and the open Southern Ocean showed that surface δ^{56}Fe at picomolar dissolved Fe concentrations are isotopically heavy (>+1‰), which has been attributed to the combination of surface uptake, regeneration, and organic complexation (Lacan et al. 2008; Ellwood et al., 2015; 2020). Estimates for the magnitude of fractionation due to biological uptake range between −0.1 (Radic et al., 2011) and −1.0 ‰ (Ellwood et al., 2020). The magnitude and direction of any Fe isotope fractionation during uptake may depend on the phytoplankton species, uptake mechanism, and Fe species consumed. Additional research is required on all three fronts. Below the surface mixed layer, δ^{56}Fe of dissolved Fe appears to be primarily a reflection of the isotope signature of Fe sources, rather than reflecting a dominant influence from the biological processes of remineralization (e.g. Abadie et al., 2017; Conway & John, 2014a; John et al., 2018a; Labatut et al., 2014). Accordingly, there remains the possibility for δ^{56}Fe of surface seawater to be linked to productivity in some oceanographic settings, though the relative role of other Fe-cycling processes and the degree to which they erase any diagnostic productivity signatures requires further investigation.

3.2.2. Chemical

The chemical behavior of Fe in seawater is complex and has the potential to decouple Fe cycling from macronutrients and thus productivity. Unlike the macronutrients, which are present as aqueous ions in solution, Fe is scarcely soluble in seawater, and much of what constitutes 'dissolved' Fe—operationally defined as that which can pass through a 0.2 or 0.4 μm filter—is in actuality a soup containing organic complexes, nanoparticles, colloids, and a small fraction of truly ionic Fe. The controls governing, and the extent to which exchange occurs between these forms of dissolved Fe, are areas of focused interest (e.g., Fitzsimmons & Boyle, 2014; Fitzsimmons et al., 2015). Additionally, dissolved Fe is subject to strong removal via scavenging, which lowers the Fe:macronutrient ratio of waters returned to the surface via upwelling (Moore, 2016). Chemical processes can also exert a significant influence over the isotopic

composition of Fe in seawater, such as through redox transformations, exchange reactions (e.g., complexation, particle interactions), and by authigenic precipitation, discussed below.

Redox transformations drive large Fe isotope effects (e.g., Johnson et al., 2002; Skulan et al., 2002; Welch et al., 2003; Anbar et al., 2005). Indeed, much of the Fe isotope variation in Earth's ancient, more reducing past likely derives from fractionations associated with redox transformations (e.g., Johnson et al., 2008). While the role of redox relative to other processes is diminished in today's largely-oxygenated ocean, it is nonetheless an important mediator of Fe isotope source compositions, particularly within the ocean interior. This is neatly illustrated using the example of sediment dissolution, which can occur with or without a change in the redox state of Fe. Bulk marine sediments typically possess a composition similar to the crustal composition of +0.1 ‰ (Beard et al., 2003; Poitrasson, 2006). However, dissolved Fe(II) derived from bacterially-mediated reductive dissolution in sediments has been characterized by δ^{56}Fe between −1 and −4 ‰ (Berquist & Boyle, 2006; Severmann et al., 2006; 2010; Homoky et al., 2009; 2013; Klar et al., 2017a; Henkel et al., 2018), whereas Fe derived from non-reductive dissolution processes is thought to be considerably heavier, between +0.1 to +0.3‰ (Homoky et al., 2009; 2013; Radic et al., 2011). Further modification of reductive end-member compositions is possible upon contact with oxidizing seawater, potentially masking true source signatures. Oceanic water column dissolved δ^{56}Fe compositions attributed to either non-reductive (+0.1 to +0.4 ‰) or reductive (−0.3 to −3.3 ‰) release of Fe from sediments have now been observed globally (Radic et al., 2011; John et al., 2012; Staubwasser et al., 2013; Conway & John, 2014a; Labutut et al., 2014; Conway & John 2015a; Chever et al., 2015; Fitszimmons et al., 2016; Klar et al., 2017a; Abadie et al., 2017; Klar et al., 2018; Rolison et al., 2018; John et al., 2018a; Charette et al., 2020).

Exchange reactions can also fractionate primary Fe isotope compositions. For example, natural lithogenic dust is thought to possess a relatively narrow range of Fe isotope compositions (i.e., δ^{56}Fe ≈ +0.1±0.2‰; Waeles et al., 2007; Mead et al., 2013; Conway et al., 2019; Chen et al., 2020), reflecting the overall homogeneity of the upper continental crust. However, dissolved Fe in seawater attributed to dissolving dust particles is isotopically heavy, around +0.7 ‰ (Conway & John, 2014a). This fractionation is thought to reflect dissolution in concert with, and complexation by, strong (organic) ligands (Fishwick et al., 2014), which have been experimentally shown to preferentially bind heavy Fe isotopes (Dideriksen et al., 2008; Morgan et al., 2010). Fractionation effects may also arise during exchange of Fe between dissolved and particulate forms, though the magnitude of the effect depends on whether the exchange is primarily physical

(negligible fractionation; e.g. Fitzsimmons et al., 2017) or chemical (from ≈+0.3 up to +1 ‰; Labutut et al., 2014; Fitzsimmons et al., 2015).

Lastly, authigenic precipitation can control the isotopic composition of Fe released by large point sources, such as hydrothermal vents and margin sediments. Iron in hydrothermal vent fluids possesses end-member compositions ranging from −0.7 to +0.1‰ (Sharma et al., 2001; Beard et al., 2003; Severmann et al., 2004; Rouxel et al., 2008; Bennett et al., 2009; Rouxel et al., 2016; Nasemann et al., 2018; Rouxel et al., 2018). However, precipitation of Fe into authigenic minerals can render significant changes in dissolved δ^{56}Fe (e.g., Severmann et al., 2004; Bennett et al., 2009). The direction of fractionation depends on (e.g., Lough et al., 2017)—and may thus be diagnostic of (e.g., Horner et al., 2015b)—the specific transformations occurring: Fe sulfides and oxides preferentially incorporate isotopically light and heavy Fe, respectively (e.g., Skulan et al. 2002; Rouxel et al., 2008). Mineral precipitation can drive δ^{56}Fe of residual Fe stabilized in seawater to values ranging between −2.4 to +1.5 ‰, depending on the authigenic mineral produced (Conway & John, 2014a; Ellwood et al., 2015; Fitzsimmons et al., 2016; 2017; Klar et al., 2017b; Lough et al., 2017; Rouxel et al., 2018). Analogous processes appear to operate along continental margins, whereby 'light' Fe, mobilized by reductive dissolution, encounters oxidizing seawater and forms precipitates that are heavier than the source Fe (though overall still considerably lighter than background seawater; e.g., Marsay et al., 2018).

Additional nuances relating to δ^{56}Fe signatures of local point sources such as Fe released from anthropogenic aerosol dust, glaciers, icebergs, and rivers are also emerging, with such sources varying dramatically over short spatial and temporal scales and with *in situ* chemical reactions (e.g. Fantle & DePaolo, 2004; Berquist & Boyle, 2006; Ingri et al., 2006; Escoube et al., 2009; Poitrasson et al., 2014; Mead et al., 2013; Ilina et al., 2013; Akerman 2014; Chen et al., 2014; Escoube et al., 2015; Mullholland 2015; Zhang et al., 2015; Kurisu et al., 2016a;b; Stevenson et al., 2017; Conway et al., 2019). The net effect of the dominance of Fe source on dissolved δ^{56}Fe in seawater means that any signal from biological uptake in the Fe-depleted mixed layer, even if could be recorded in an archive, may be easily overprinted by even a small addition of new Fe from either above or below.

3.2.3. Physical

The residence time of Fe in seawater is substantially less than the mixing time of the global ocean (Table 1). Local and regional Fe sources can thus drive large differences in dissolved [Fe] and δ^{56}Fe between ocean basins (Fig. 3). Local source signatures—[Fe], δ^{56}Fe, and perhaps Fe speciation—can be transported and

retained over the scale of individual ocean basins (Fig. 4; Conway & John, 2014a; Abadie et al., 2017). This is arguably one of the marquee findings of the GEOTRACES program, and underpins the utility of sedimentary δ^{56}Fe to reconstruct past marine Fe sources, discussed next.

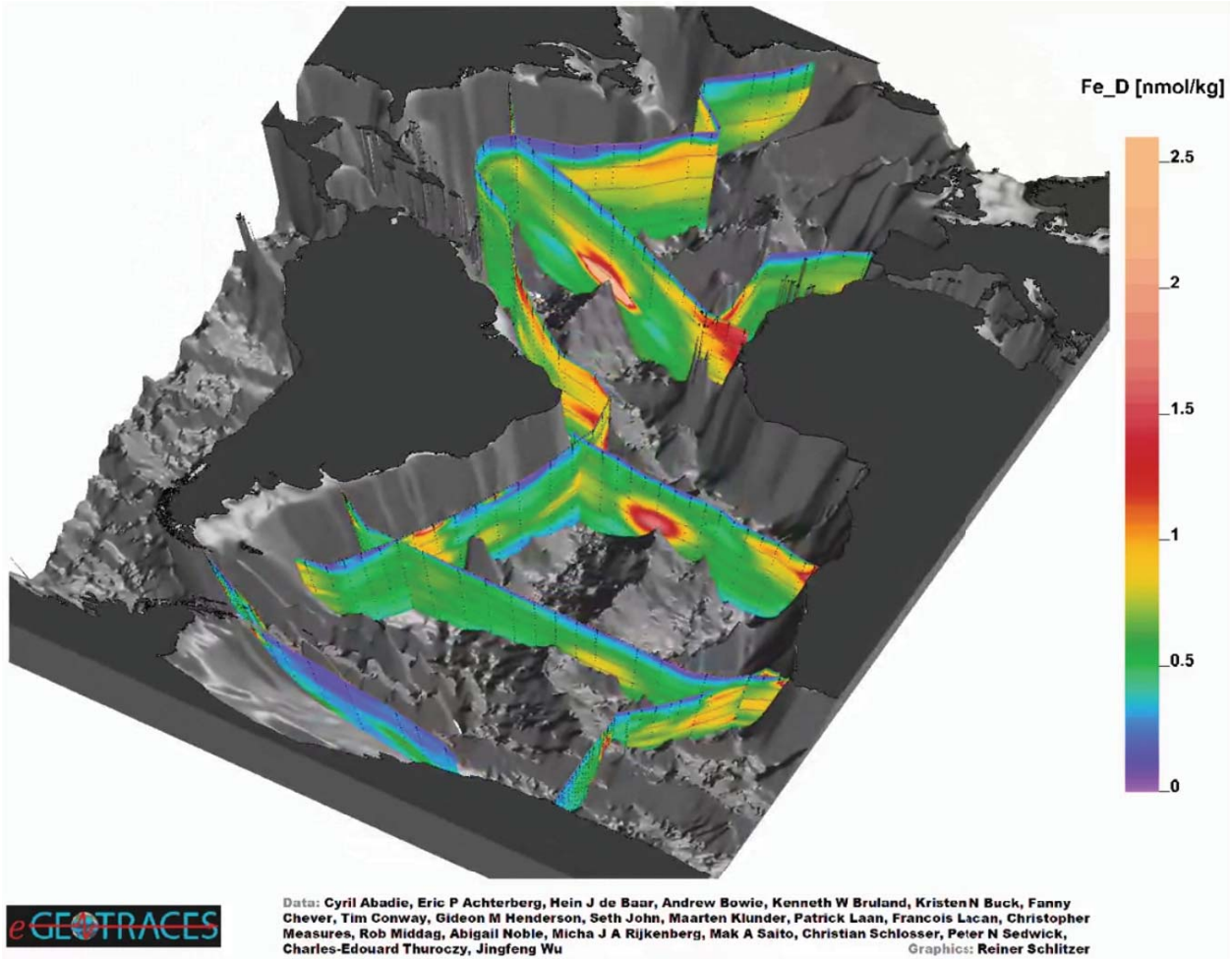

Figure 4 | Three-dimensional scene depicting dissolved iron concentrations in the Atlantic Ocean (Schlitzer, 2017). This perspective illustrates the density of GEOTRACES data in the region as well as the influence of multiple Fe 'hot spots', such as mid-ocean ridges and continental margins. Data are available in the GEOTRACES Intermediate Data Product 2017 (Schlitzer et al., 2018); names of data originators appear in the figure.

3.3. Marine archives

3.3.1. Surface ocean

A requirement of the application of any paleoproxy is the availability of suitable sedimentary archives. These archives must have both a high fidelity for the signal of interest and be robust to post-depositional

alteration. Archives most relevant to reconstructing paleoproductivity should capture surface ocean $\delta^{56}Fe$; however, there are few—if any—reliable archives. The lack of surface-water archives reflects two related challenges. First, most archives for surface seawater are derived from biominerals, such as foraminifera, diatoms, sponges, and corals. These archives possess vanishingly low Fe concentrations, such that Fe isotopic analysis of these substrates has proven difficult. Second, following burial, many biominerals will act as substrates for authigenic mineral formation. These authigenic minerals, such as clays (e.g., Badaut & Risacher, 1983) and Fe–Mn oxides (e.g., Boyle, 1981), possess Fe concentrations far in excess of those in the underlying biomineral, necessitating significant physical and chemical cleaning (e.g., Cheng et al., 2000).

Despite these obstacles, there are three positive signs that reconstructing past surface seawater $\delta^{56}Fe$ is possible. First, biogenic opal may contain Fe at concentrations in the $\mu g\ g^{-1}$ range (Ellwood & Hunter, 2000; Lal et al., 2006; Shemesh et al., 1988; Sun et al., 2016), which is tractable for $\delta^{56}Fe$ analysis. Second, the Fe content of diatoms is correlated with ambient dissolved [Fe] (Twining & Baines, 2013). Lastly, the positive relationship between the Fe content of diatoms and corresponding seawater appears to hold through sinking and sedimentation (Pichevin et al., 2014), indicating that diatoms are a potential window into past surface ocean Fe chemistry. Whether these relationships also extend to $\delta^{56}Fe$ remains to be seen, and will require additional core-top calibrations, incubation experiments, and detailed assessment of the efficacy of chemical cleaning.

3.3.2. Deep ocean

In contrast to surface seawater, there are a number of studies examining Fe sources and fluxes in the meso- and bathypelagic ocean. To constrain Fe sources, researchers have examined the Fe isotope composition of Fe-rich sediments, including red clays (Tegler et al., 2018), polymetallic nodules (Marcus et al., 2015), and Fe–Mn crusts (Zhu et al., 2000; Levasseur et al., 2004; Chu et al., 2006; Horner et al., 2015b; Liu et al., 2020). Ferromanganese crusts are currently the best-studied for Fe isotopes (Fig. 5); Fe–Mn crusts are slowly-accumulating deposits (~mm Myr^{-1}) that record ambient seawater $\delta^{56}Fe$ with a spatially-invariant offset of -0.77 ± 0.06 ‰ (Horner et al., 2015b). The constancy of the offset implies that the Fe isotope composition of individual Fe–Mn crust layers can be interpreted in terms of past dissolved $\delta^{56}Fe$, and thus past Fe sources. Curiously, however, the Fe-isotopic variability of Fe–Mn deposits recovered from the central Pacific—particularly layers formed before ~20 Ma—exceed the range of modern deep-ocean $\delta^{56}Fe$ (though only in the positive direction; Fig. 5). The reasons for elevated $\delta^{56}Fe$ in the past are debated. Horner et al. (2015b) report that heavy $\delta^{56}Fe$ could arise through widespread secondary modification of large Fe

sources through authigenic reactions, such as sulfide precipitation. In contrast, Johnson et al. (2020) contend that the elevated δ^{56}Fe reflects extensive biological modification of dissolved Fe, driven by large-scale Fe fertilization. Regardless, the variation in these records points to a dynamic and enigmatic Fe cycle in Earth's past, and indicates that Fe–Mn crusts have a largely untapped potential to reconstruct spatiotemporal variations in this cycle.

Other approaches are also showing promise to study Fe fluxes to the deep ocean through time. For example, researchers have constrained the rate of sedimentary accumulation of hydrothermally-derived Fe and Cu using constant flux proxies such as extraterrestrial helium-3 (e.g., Middleton et al., 2016) or thorium-230 (Costa et al., 2017). These studies report that hydrothermal activity may be coherent with sea-level changes on Quaternary glacial–interglacial cycles, suggesting a potentially remarkable set of connections between the solid Earth, ocean chemistry, and global climate (e.g., Cullen & Coogan, 2017). Reconstruction of hydrothermal metal fluxes over million-year timescales may also be possible using the geochemistry of pelagic clays (e.g., Dunlea et al., 2015), though such approaches are still in their infancy.

Although existing Fe-isotopic and Fe flux records cannot be directly interpreted in terms of past productivity, the supply and cycling of Fe in seawater is an important control over the biological productivity of the ocean. Thus, records of past oceanic Fe sources may prove most valuable as context for

492 interpreting other proxy records, or for generating novel hypotheses regarding the connections between the
493 Fe cycle and global climate.

494

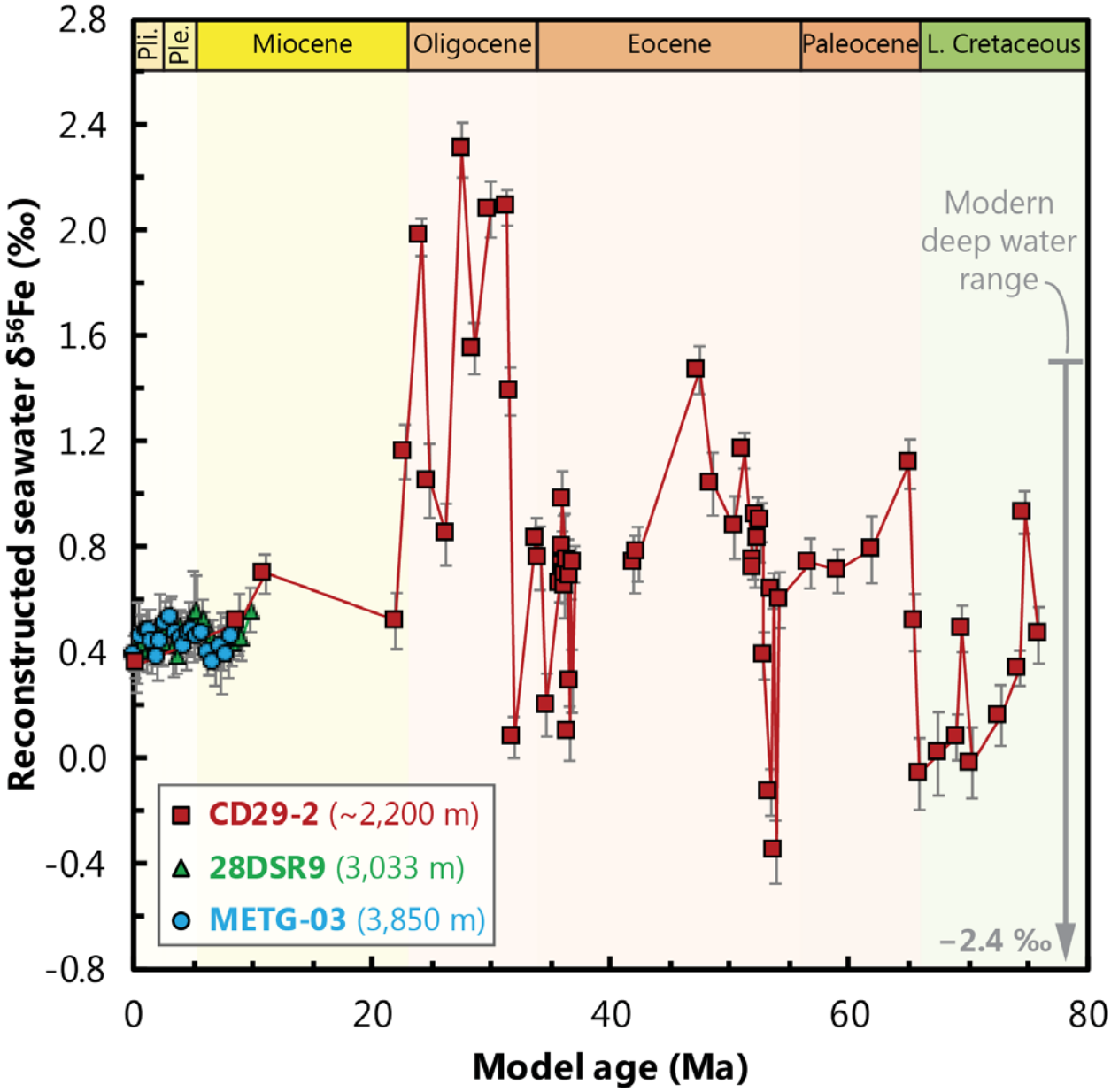

495

496 **Figure 5 | Ferromanganese crust records of central Pacific δ^{56}Fe since the Late Cretaceous.** Records from CD29-
497 2, 28DSR9, and METG-03 from Horner et al. (2015b), Chu et al. (2006) and Liu et al. (2020), respectively. The record
498 from CD29-2 was interpreted by Horner et al. (2015b) as evidencing the importance of deep (non-eolian) Fe sources
499 to central Pacific Fe budgets throughout much of the Cenozoic and Late Cretaceous. In contrast, the δ^{56}Fe recorded
500 by three central Pacific Fe–Mn crusts have been similar since the late Miocene, consistent with a regional Fe source
501 derived largely from non-reductive sediment dissolution and/or eolian deposition.

3.4. Prospects

While the marine Fe cycle is complex, Fe isotopes are proving to be a valuable tool for studying the modern Fe cycle. Detailed study of this cycle reveals that it is driven by a multitude of biological, physical and chemical processes, amongst which productivity is but one small part. In our view, this means that there are considerable obstacles to using δ^{56}Fe as a paleoproductivity tracer. However, this does not preclude δ^{56}Fe from emerging as a powerful tracer for studying the dynamics of the Fe cycle in the (paleo)oceans. Such a tracer would be especially powerful given the proximal connection between Fe supply and the biological productivity of the ocean.

Exploiting δ^{56}Fe will require resolving and refining several ambiguities. First, there is a clear need to better constrain the Fe-isotopic fractionation factor associated with biological uptake (in variable conditions and from different species) and to diagnose locations where dissolved δ^{56}Fe is most affected by productivity. Second, the fractionation factors for remineralization and scavenging are essentially unknown, though field data suggests that the net result of these effects is relatively small (e.g. Radic et al., 2011; Labutut et al., 2104). Constraining these fractionation factors will be particularly important for developing novel archives of the paleo Fe cycle, such as pelagic clays (e.g., Tegler et al., 2018). Third, any sedimentary reconstruction of past Fe-isotopic chemistry will need to consider the high degree of spatial variability in modern δ^{56}Fe. This will necessitate spatially-distributed core sampling, similar to the approach used to constrain basin-scale patterns of dust deposition over glacial–interglacial timescales (e.g., Costa et al., 2016; Winckler et al., 2016). Addressing these priorities will provide valuable constraints on the extent to which the Fe cycle has influenced primary productivity over recent geological history, and provide key insights into the potential sensitivity of Earth's climate to perturbations in marine trace element cycles.

4. Zinc

4.1. Marine distribution

Consistent with its importance as a micronutrient, dissolved Zn has a nutrient-type distribution in the ocean (e.g., Bruland, 1980). Typical surface ocean Zn concentrations are 0.01 to 0.5 nmol kg^{-1}, compared to deep water concentrations of ~2.5 nmol kg^{-1} in the north Atlantic and ~10 nmol kg^{-1} in the north Pacific (Schlitzer et al., 2018; Fig. 6). The dissolved Zn distribution in the ocean closely follows that of the macronutrient Si (Bruland, 1980), at least partially due to the similar behaviour of both elements in the Southern Ocean (Vance et al., 2017; de Souza et al., 2018; Weber et al., 2018; Roshan et al., 2018; Middag et al., 2019). Decoupling of Zn from Si is observed in regions remote from Southern Ocean influence (Janssen & Cullen, 2015; Vance et al., 2019).

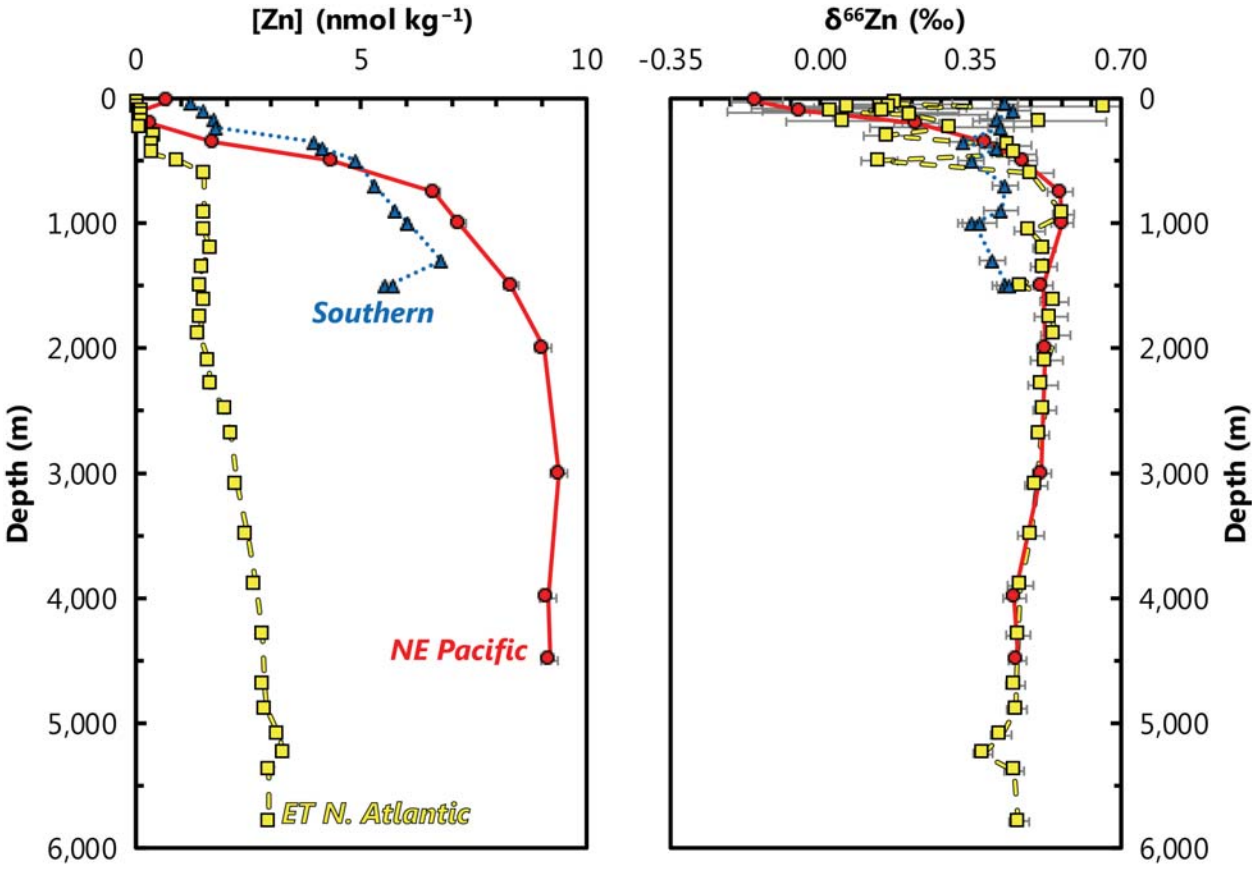

Figure 6 | Representative profiles of dissolved Zn concentrations ([Zn]) and Zn-isotopic compositions ($\delta^{66}Zn$) in the Eastern Tropical North Atlantic (squares, dashed line), Northeast Pacific (circles, solid line) and Southern (triangles, dotted line) Oceans. This comparison illustrates that despite possessing distinct dissolved concentration profiles, the isotopic behavior of Zn is similar between basins.

It was hoped that Zn isotope ratios would provide a means of tracing biological carbon cycling in the past and present ocean (e.g., Maréchal et al., 2000; Pichat et al., 2003; Bermin et al., 2006). Zinc isotope data are reported relative to JMC-Lyon, which has now expired. New δ^{66}Zn data are typically measured relative to AA-ETH or IRMM-3702 Zn standards and corrected by the offset between these and JMC-Lyon (≈0.3‰; Moeller et al., 2006; Archer et al., 2017). The apparent preferential uptake of light Zn isotopes by phytoplankton observed in some culture experiments (John et al., 2007; Köbberich and Vance, 2017; Samanta et al., 2018) predicted an isotopically heavy residual pool in surface seawater, analogous to that observed for δ^{13}C, δ^{15}N, δ^{30}Si and δ^{114}Cd (Cd reviewed in Sec. 6., C, N and Si in Farmer et al., *this issue*). However, the test of this hypothesis, through analyses of δ^{66}Zn in seawater, awaited a GEOTRACES-driven revolution in large volume trace metal clean sampling (Cutter et al., 2017), alongside analytical advances including new chemical separation procedures and MC-ICP-MS (multiple-collector inductively-coupled plasma mass spectrometry; Bermin et al., 2006; Conway et al., 2013; Takano et al., 2017).

A consistent picture of the distribution of δ^{66}Zn in the ocean has since emerged. The deep ocean is isotopically homogeneous, with a δ^{66}Zn signature of about +0.45‰ (Fig. 6.; Conway & John, 2014b; Zhao et al., 2014; Conway & John, 2015a; Samanta et al., 2017; Takano et al., 2017; John et al., 2018b; Wang et al., 2019a; Vance et al., 2019; Sieber et al., 2020; Liao et al., 2020; Lemaitre et al., 2020), and isotopically heavier than the upper continental crust (UCC; δ^{66}Zn +0.3 ‰; Moynier et al., 2017). Deviations to deep ocean δ^{66}Zn compositions as light as -0.2 ‰ have been observed near sediments or hydrothermal Zn sources (Conway and John; 2014b; Lemaitre et al., 2020). In the surface, while heavy δ^{66}Zn isotope compositions have been observed, the upper water column for Zn is often isotopically light or, in the Southern Ocean and North Pacific, only very slightly fractionated towards heavier values (Conway & John, 2014b; 2015a; Zhao et al., 2014; Samanta et al., 2017; Takano et al., 2017; Wang et al., 2019a; Sieber et al., 2020; Vance et al., 2019; Liao et al., 2020; Lemaitre et al., 2020). Possible reasons for the discrepancy between expected and observed upper water column δ^{66}Zn are discussed in detail below. They include preferential scavenging of isotopically heavy Zn on particle surfaces (e.g., John & Conway, 2014; Weber et al., 2018), an isotopically light source of Zn, possibly from shallow remineralization of organic material (Samanta et al., 2017; Vance et al., 2019) or from anthropogenic aerosols (Liao et al., 2020; Lemaitre et al., 2020). We note here that these complexities will likely make it challenging to use Zn isotopes as a paleoproductivity proxy.

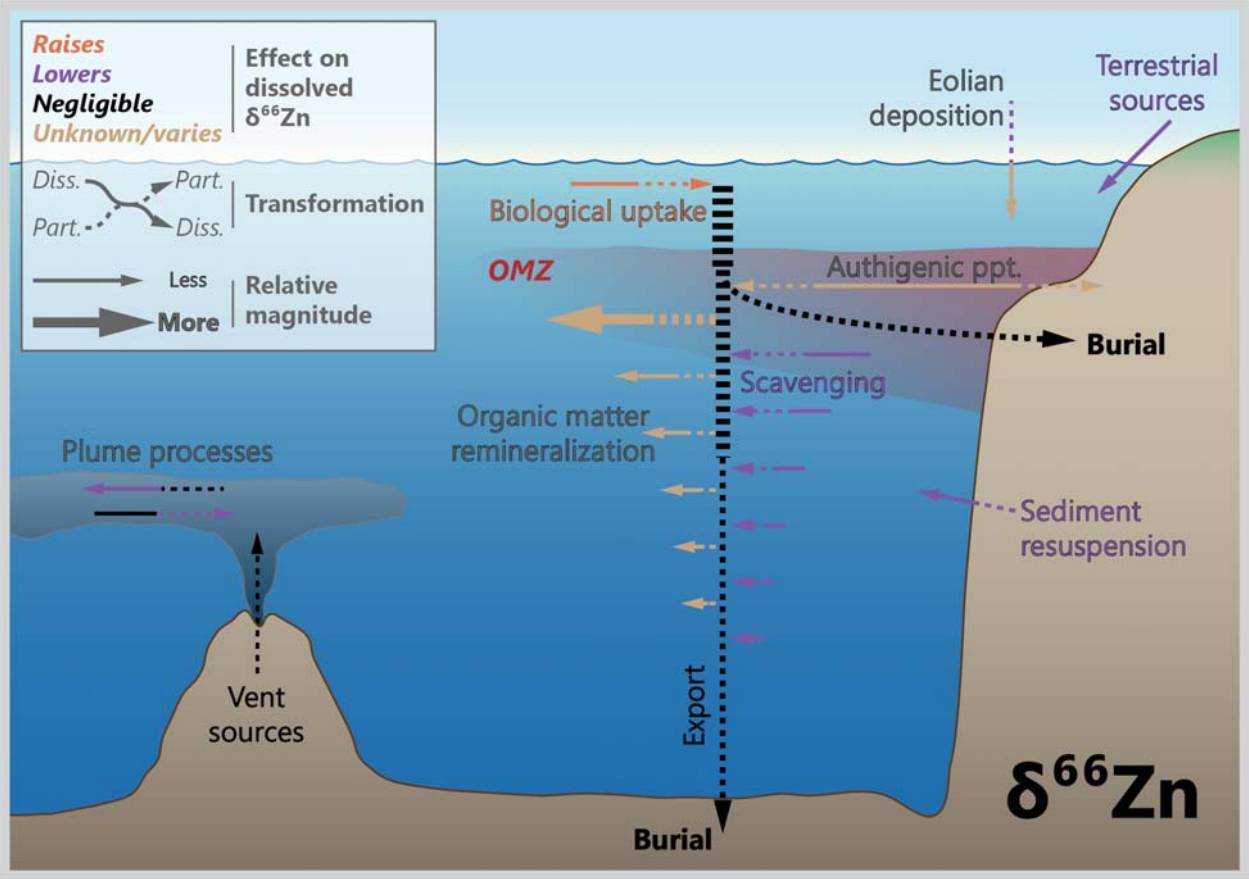

Figure 7 | Processes driving zinc isotope variations in modern seawater. Though biological processes are capable of influencing dissolved $\delta^{66}Zn$, they do not appear to be the dominant driver of Zn isotope variations in the marine realm.

4.2. Driving processes

4.2.1 Biological

Zinc is a metal center in two key enzymes: carbonic anhydrase, necessary for carbon fixation, and alkaline phosphatase, necessary for dissolved organic phosphorus uptake by marine organisms (Morel et al., 1994; Shaked et al., 2006; reviewed by Sinoir et al., 2012). Zinc also has an array of other physiological roles in marine organisms, as exemplified by the observation that Zn contents of phytoplankton cells are of similar magnitude to the micronutrient Fe (Twining & Baines, 2013).

Zinc can be growth-limiting for phytoplankton grown in culture (Anderson et al., 1978; Brand et al., 1983; Morel et al., 1994), but Zn (co)-limitation (with Fe, Co) has only rarely been observed in the open ocean (e.g., Coale, 1991; Coale et al., 2003; Franck et al., 2003; Ellwood, 2004; Lohan et al., 2005). This difference between culture and field may reflect the ability of some phytoplankton to substitute Cd or Co

585 for Zn in some enzyme systems when ambient Zn concentrations are low (e.g., Morel et al., 1994; Lee &
586 Morel, 1995; Yee & Morel, 1996; Kellogg et al., 2020). Nevertheless, Zn availability has been shown to
587 influence species composition and phytoplankton growth, including rates of calcification and alkaline
588 phosphatase activity (Sunda & Huntsman, 1995; Crawford et al., 2003; Schulz et al., 2004; Shaked et al.,
589 2006; Mahaffey et al., 2014). In culture, phytoplankton biomass is typically enriched in the light isotopes
590 of Zn (John et al., 2007; Köbberich and Vance, 2017; 2019; Samanta et al., 2018). Rather than reflecting a
591 kinetic isotope effect on uptake, it has been suggested that Zn speciation in the media controls cellular δ^{66}Zn
592 values; specifically, strong organic ligands (e.g., EDTA) present in the media preferentially complex heavy
593 Zn isotopes, rendering the bioavailable Zn pool isotopically light (John et al., 2007; Köbberich and Vance,
594 2017; 2019; Fig. 7).

595

596 *4.2.2. Chemical*

597 Like most bioessential metals, Zn bioavailability is dictated by its chemical speciation (e.g., Anderson et
598 al., 1978), which is dominated in the ocean by complexation to strong ($K' \sim 10^9 - 10^{11}$) organic ligands
599 (Bruland, 1989; Donat & Bruland, 1990; Ellwood & Van Den Berg, 2000; Jakuba et al., 2012; Kim et al.,
600 2015). Inorganic Zn is considered to make up <5% of the total Zn pool in most ocean regions, with the
601 exception of the Southern Ocean, where strong upwelling of nutrient-rich deep waters leads to Zn
602 concentrations in excess of complexing ligands (Baars & Croot, 2011). Note that while strongly-complexed
603 Zn is unlikely to be bioavailable, the presence of 'weak' ligands (or more labile ligands) can enhance Zn
604 uptake (Aristilde & Xu, 2012). As noted above, the role of the diversity of organic (and inorganic) Zn-
605 binding ligands in determining dissolved and particulate δ^{66}Zn values remains to be fully evaluated.

606 A role for scavenging in the marine cycling of Zn and Zn isotopes has been widely cited (e.g., John &
607 Conway, 2014; Weber et al., 2018; Roshan et al., 2018; Liao et al., 2020; Fig. 7). It is argued that scavenging
608 can a) explain the widespread observation of isotopically light Zn in the upper ocean, via preferential
609 removal of heavy Zn isotopes on particles, and b) explain elevated concentration of Zn in the deep Pacific
610 compared to that supplied in southern-sourced deep waters (Weber et al., 2018; Roshan et al., 2018).
611 Elevated Zn in the deep Pacific has also been attributed to additional Zn input via, e.g., hydrothermalism
612 (Roshan et al., 2018), with a lighter than deep ocean δ^{66}Zn signature (John et al., 2018b). Local and basin
613 scale deviations towards lighter deep ocean δ^{66}Zn compositions in both the Atlantic and Pacific have been
614 attributed to sedimentary input (Conway & John, 2014b; John et al., 2017; Liao et al., 2020; Lemaitre et
615 al., 2020), and could also reflect hydrothermalism (Conway & John, 2014b; John et al., 2018b; Lemaitre et
616 al., 2020). Anthropogenic aerosol deposition is thought to supply significant Zn to regions of the surface

ocean (e.g., Liao & Ho, 2018), with possible direct and indirect (via scavenging) regional impacts on upper ocean δ^{66}Zn values (Liao et al., 2020; Lemaitre et al., 2020).

Lastly, Janssen & Cullen (2015) suggest that decoupling of Zn and Si in the northeast Pacific reflects the formation of Zn sulfides in the oxygen deficient zone (ODZ), directly equivalent to proposed Cd sulfide precipitation; this hypothesis is discussed in more detail in Sec. 6.2.3. To date, however, there remains scant evidence for water column Zn-sulfide precipitation in ODZs (e.g., Conway & John, 2014b; John et al., 2018b; Vance et al., 2019). That said, Zn-sulfide precipitation is undoubtedly important in euxinic basins such as the Black Sea and Cariaco Basin (Vance et al., 2016; Isson et al., 2018), and has been postulated to occur within the porewaters of oxygen deficient, organic-rich sediments (Sec. 4.3.3.; Little et al., 2016).

4.2.3. Physical

In common with many of the TEIs discussed here, the physical ocean circulation exerts a first order control on the distribution of dissolved Zn and δ^{66}Zn compositions (Vance et al., 2017; de Souza et al., 2018; Weber et al., 2018; Sieber et al., 2020). Subantarctic water masses have distinct low Zn:PO_4 and Si:PO_4 ratios, due to the elevated uptake of Zn and Si by diatoms in the surface Southern Ocean (Sarmiento et al., 2004; Vance et al., 2017). Remineralization of these Zn- and Si-rich diatoms at depth imprints a correspondingly high Zn:PO_{-4} and high Si:PO_4 fingerprint on Antarctic bottom waters. This coupling of Zn and Si in the Southern Ocean forms the basis of the global Zn:Si correlation via the advection of southern sourced water masses towards the low latitudes, where they fill much of the ocean interior (de Souza et al., 2012; Holzer et al., 2014). The homogeneity of deep ocean Zn isotope compositions reflects the limited degree of Zn isotope fractionation on uptake by Southern Ocean diatoms (Zhao et al., 2014; Wang et al., 2019a), which results in intermediate and deep southern-sourced water masses with limited or no isotopic contrast (Sieber et al., 2020). The oceanic Zn:Si correlation persists despite shallower remineralization of Zn relative to Si (Twining et al., 2014), and is especially clear in the Atlantic, underlining that the mixing of water masses is the dominant control on dissolved Zn in this basin (Vance et al., 2017; Weber et al., 2018; Middag et al., 2019). Decoupling of Zn and Si is observed in the upper water column of the northeast Pacific, far from the Southern Ocean influence (Janssen & Cullen, 2015; Vance et al., 2019), likely resulting from the shallower remineralisation of Zn (from organic 'soft parts') relative to Si (from opal; Vance et al., 2019).

4.3. Sedimentary archives

4.3.1. Ferromanganese sediments

Manganese oxides are strong sorbents of positively charged, divalent trace metals, due to their negative layer charge at the pH of natural waters (e.g., Koschinsky & Halbach, 1995). The phyllomanganate birnessite is the main Mn- and TE-bearing phase in oxic marine sediments (e.g., Koschinsky and Hein, 2003), as well as for several elements described here, including Zn, Cu, Ni, Cd, and Mo (though Mo exists in seawater as the molybdate anion). Ferromanganese crusts and nodules incorporate TEs during growth, leading to 10^6-fold enrichments compared to seawater concentrations (e.g., Arrhenius, 1963; Aplin and Cronan, 1985). As a result, Fe–Mn sediments are often one of the first marine sediment types to be targeted in the development of a new isotopic tracer.

In the case of Zn, Fe–Mn crusts and nodules are isotopically heavy compared to seawater (≈ +0.45‰), exhibiting compositions between +0.9 to +1 ‰ (Maréchal et al., 2000; Little et al., 2014a; Fig. 8). The heavy signature is broadly consistent with inorganic sorption experiments of Zn on birnessite, with experiments at high ionic strength yielding $\Delta^{66}Zn_{sorbed\text{-}aqueous}$ (where $\Delta^{66}Zn_{sorbed\text{-}aqueous} = \delta^{66}Zn_{sorbed} - \delta^{66}Zn_{aqueous}$) of +0.16 to +2.7‰ (Bryan et al., 2015). The magnitude of fractionation observed in experiments is typically considerably larger than in natural Fe–Mn crusts and nodules, which Bryan et al. (2015) suggest may reflect sorption of Zn on birnessite via two different molecular mechanisms, each associated with different isotopic fractionation factors, as is the case for thallium (e.g., Nielsen et al., 2013). In addition, the influence of organic and inorganic speciation of Zn in seawater may play a role, though this remains to be fully evaluated (e.g., Little et al., 2014b).

Little et al. (2014a) observed no marked temporal changes in $\delta^{66}Zn$ values for three Fe–Mn crusts from each of the major ocean basins over the last ~20 Ma. Assuming no significant diffusion or resetting of crust Zn isotope compositions on this timescale, this observation suggests that, on a global basis, the marine Zn cycle has been in isotopic steady state for at least 20 Myr (Fig. 8)

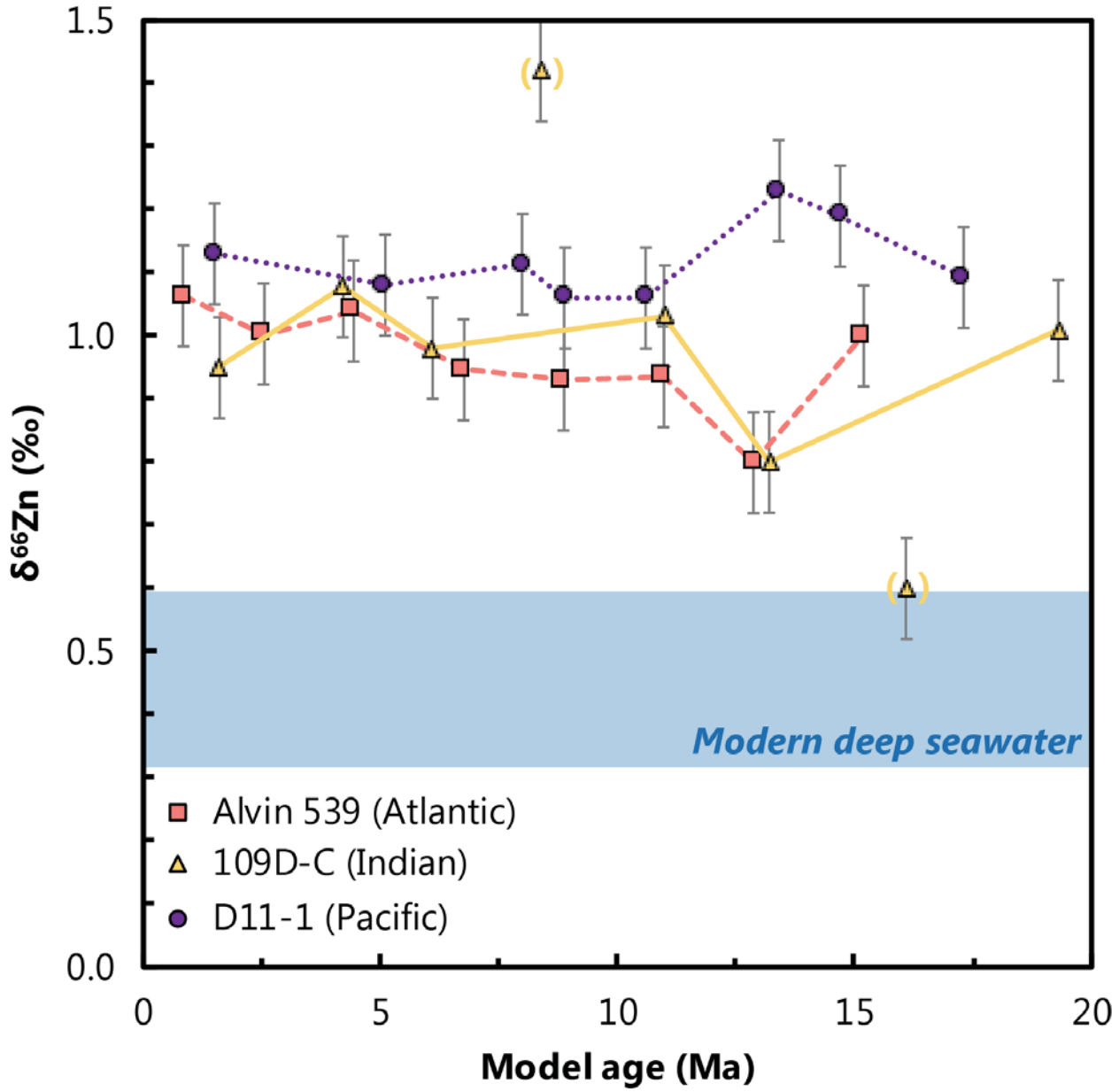

669

670 **Figure 8 | Deep ocean Zn isotope constancy over the past 20 Myr.** These records are derived from Fe–Mn crusts
671 recovered from the Atlantic (square, dashed line), Indian (triangle, solid line), and Pacific (circle, dotted line) Oceans.
672 Assuming the isotopic offset between dissolved Zn in seawater and Fe–Mn crusts has remained unchanged at ≈0.55
673 ‰ over this time, these records imply only minimal Zn-isotopic variations in the deep ocean over the past ~20 Myr. Two
674 anomalous measurements from 109D-C (in parentheses) possess low levels of authigenic Zn enrichment, indicative of
675 detrital contamination (Little et al., 2014a).

676

4.3.2. Biogenic silica

The correlation of Zn with Si in the modern ocean led to the suggestion that Zn/Si measured in diatom opal may be a proxy for Zn/Si (and thus [Zn]) of past seawater. However, culturing and µ-XRF analyses revealed that only a small fraction (1–3%) of the diatom Zn quota is incorporated into the opal frustules, with the remainder present in the organic 'soft parts' of the diatom cells (Ellwood & Hunter, 2000; Twining et al., 2004). The Zn concentration in opal (Zn_{opal}) also more closely reflects the bioavailable Zn in seawater than ambient Zn:Si (Ellwood & Hunter, 2000). Nevertheless, if the mechanisms of Zn incorporation into biogenic opal can be understood, and calibrated, a Zn:Si proxy of Zn bioavailability could help shed light on micronutrient limitation of the biological pump.

Andersen et al. (2011) analyzed Zn isotopes ($\delta^{66}Zn_{opal}$) and Zn/Si_{opal} in diatom opal isolated from core top sediments from the Southern Ocean. They observed isotopically heavy Zn in opal (at +0.7 to +1.5‰), and an inverse relationship of $\delta^{66}Zn_{opal}$ with Zn/Si_{opal}. Consistent with culturing studies, core top Zn/Si_{opal} appears to be linked to bioavailable Zn concentrations in ambient surface seawater. The authors suggested that $\delta^{66}Zn_{opal}$ should also reflect the isotope composition of bioavailable Zn in surface seawater, which, they predicted, should be isotopically heavy due to the predicted preferential incorporation of light isotopes into phytoplankton organic material. In this view, the extent of uptake—nutrient utilization—would be recorded by the systematics of Zn/Si_{opal} and $\delta^{66}Zn_{opal}$. However, this study predated the recent surge in seawater $\delta^{66}Zn$ measurements. As discussed above, surface water $\delta^{66}Zn$ analyses in the Southern Ocean have not borne out the prediction of isotopically-heavy residual surface waters, with little to no fractionation observed (Zhao et al., 2014; Wang et al., 2019a; Sieber et al., 2020).

More recently, Hendry and Andersen (2013) have shown that some sponge spicules faithfully record seawater $\delta^{66}Zn$. Sponges are primarily deep-sea organisms. Hence, if we can deconvolve the controls on diatom Zn/Si and $\delta^{66}Zn_{opal}$, a combination of Zn/Si and $\delta^{66}Zn$ measurements in diatoms and sponges (as used for Si isotopes, Farmer et al., *this issue*) could provide a strong basis for unravelling the past ocean global Zn cycle, including the role of Southern Ocean processes in the biological carbon pump.

4.3.3. Carbonates

Carbonates may provide an alternative archive for Zn (as Zn/Ca) and $\delta^{66}Zn$. For example, Marchitto et al. (2000) showed that Zn/Ca ratios in benthic foraminifera reflect bottom water dissolved Zn concentrations. However, Zn concentrations in individual microfossil shells are extremely low (of the order ~0.1 ng); at

this level, with current analytical capabilities and blank contributions, more than one hundred benthic foraminifera would be required for a single Zn isotope measurement.

To circumvent the issue of low Zn contents of individual shells, Pichat et al. (2003) utilized a selective carbonate dissolution procedure on bulk sediment from the equatorial Pacific, mostly consisting of coccoliths. These authors argued that isotopically heavy $\delta^{66}Zn_{carb}$ reflected ambient surface seawater, with values modulated by changes in biological productivity due to varying seasonal insolation. Similarly isotopically heavy Zn in ancient carbonates has also been argued to reflect strong biological utilization in surface waters (Kunzmann et al., 2013; cf. John et al., 2017; Liu et al., 2017). However, as discussed, the interpretation of these data should be revisited in the light of recent seawater $\delta^{66}Zn$ data, where isotopically heavy surface ocean Zn isotope compositions are rarely observed.

Selective carbonate dissolution procedures present two problems. First, Zn is present at high concentrations in potential contaminating material, e.g., lithogenic or authigenic (e.g. Fe-Mn oxide) phases, and second, non-quantitative leaching introduces the potential for stable isotope fractionation (Revels et al., 2015). Nevertheless, several lab groups are now investing considerable effort to systematically assess these procedures, with promising results (e.g., Clarkson et al., 2018).

Finally, deep-sea coral skeletons also provide promise as a potential intermediate-deep water archive of $\delta^{66}Zn$ (e.g., Little et al., 2017a). Their size and global distribution, combined with the ability to assign precise ages to individual specimens, gives corals some distinct advantages over traditional sedimentary paleoclimate archives (Robinson et al., 2014).

4.3.4. Organic-rich sediments

Quantitative removal of Zn into Zn sulfides in the euxinic Black Sea water column leads to sedimentary $\delta^{66}Zn$ values that preserve the global seawater signature (Vance et al., 2016). This behaviour is analogous to the Mo isotope system (Sec. 7; e.g., Neubert et al., 2008; Nägler et al., 2011), and suggests that euxinic black shales represent an archive for seawater $\delta^{66}Zn$ values. By extension, Isson et al. (2018) propose that a chemically isolated sulfide-bound Zn fraction also preserves seawater $\delta^{66}Zn$ values, demonstrating the effectiveness of their approach for core top sediments from the euxinic Cariaco Basin. However, it is not yet clear if the sulfide fraction of organic shales from non-euxinic sites will necessarily record seawater $\delta^{66}Zn$, as (non-quantitative) precipitation of Zn sulfides is associated with light isotope fractionation (Fujii et al., 2011a; Vance et al., 2016).

Authigenic Zn in organic rich sediments deposited in productive continental margin settings is isotopically light (on average, about +0.1‰) compared to seawater (at about +0.45 ‰; Little et al., 2016). One possible explanation for this signature is the preferential biological uptake of light isotopes into organic matter (Little et al., 2016; John et al., 2017). The second possible explanation, touched upon above, is light Zn isotope fractionation during Zn sulfide precipitation, either in sediments or, possibly, in reducing microenvironments in the water column (Janssen & Cullen, 2015; Little et al., 2016; Vance et al., 2016; Bianchi et al., 2018). While a biologically-driven signature would suggest utility for δ^{66}Zn in organic-rich sediments as a paleoproductivity proxy, a role for sulfidation highlights the importance of redox conditions during diagenesis, particularly sulphate reduction, in driving the δ^{66}Zn values preserved in organic-rich sediments. We note that sedimentary redox is linked to overlying productivity (e.g., Hartnett et al., 1998), but in a complex manner that would make a purely productivity based interpretation of preserved δ^{66}Zn values in black shales challenging.

4.4. Prospects

To summarize, recent seawater, experimental, and sedimentary Zn isotope research implies that the relationship between Zn isotopes and (paleo)productivity is not straightforward. This adds uncertainty to the application of using Zn isotopes as a tracer of paleoproductivity. Fundamental to the application of Zn isotopes as a paleoproductivity proxy (or other type of paleoenvironmental tracer) is a better understanding of the mechanisms driving the modern upper water column distribution of δ^{66}Zn. Future work should target coupled dissolved and particulate phase δ^{66}Zn data, in concert with detailed biological and chemical speciation data. To date, particulate phase δ^{66}Zn data has proved particularly challenging due to Zn being extremely contamination prone.

We recommend revisiting existing archive data in the context of modern seawater δ^{66}Zn data. In general, we encourage that the future interpretation of Zn/Si, Zn/Ca, Zn-TOC and δ^{66}Zn data be made within a mechanistic framework, via careful sequential extraction procedures, application of appropriate micro-analytical techniques (e.g., LA-ICP-MS, nano-SIMS, μ-XAFS), and further experimental and theoretical work.

We note that there are systematic variations in sedimentary Zn isotope compositions on Gyr timescales. For example, Isson et al. (2018) reported δ^{66}Zn of black-shale associated Zn spanning ~3.5 Gyr, as well as bitumen and kerogen spanning the last 1.5 Gyr. The black shale record shows a shift from UCC-like values (centered on ≈+0.4 ‰) to more marine-like δ^{66}Zn (centered on ≈+0.6 ‰) around 800 Ma, which the authors

768 interpret as evidencing a transition to a more eukaryote-dominated marine ecosystem. While this feature is
769 consistent with the higher affinity of eukaryotes for Zn compared to prokaryotes (Dupont et al., 2006; 2010),
770 there remains considerable uncertainty regarding the influence of Earth's overall redox state on marine Zn
771 isotope systematics.

772 In carbonates, Yan et al. (2019) compile three δ^{66}Zn datasets from contemporaneous Ediacaran (635 Ma,
773 Marinoan) post-glacial cap carbonates (Kunzmann et al., 2013; John et al., 2017; Lv et al., 2018), which
774 show systematic changes in Zn isotope compositions over this period of marked global change. Similarly,
775 Sweere et al. (2018) present data showing marked shifts in carbonate-bound Zn isotope compositions in
776 several geological sections spanning a Cretaceous ocean anoxic event (OAE 2). As yet, there is no
777 consensus on the drivers of these intriguing isotopic shifts, but these and similar records serve to motivate
778 the future of Zn isotope research.
779

5. Copper

5.1. Marine distribution

The distribution of Cu in the ocean has been described as 'hybrid-type', because it is intermediate between nutrient- and scavenged-type elements (Bruland & Lohan, 2003). Depth profiles of dissolved Cu typically show approximately linear increases in concentration with depth (e.g., Boyle et al., 1977). Surface dissolved Cu concentrations are typically about 0.5 to 1 nmol kg^{-1}, compared to deep Atlantic concentrations of ~2.5 nmol kg^{-1} and deep Pacific concentrations of ~4 nmol kg^{-1} (Fig. 9). The distribution of dissolved Cu has been attributed to a combination of biological uptake and remineralization, benthic flux from sediments (e.g., Boyle et al., 1977; Roshan & Wu, 2015a; Little et al., 2018), and/or reversible scavenging (Little et al., 2013; Richon et al., 2019). These processes are superimposed on the first-order distribution established via the physical ocean circulation (Roshan & Wu, 2015a).

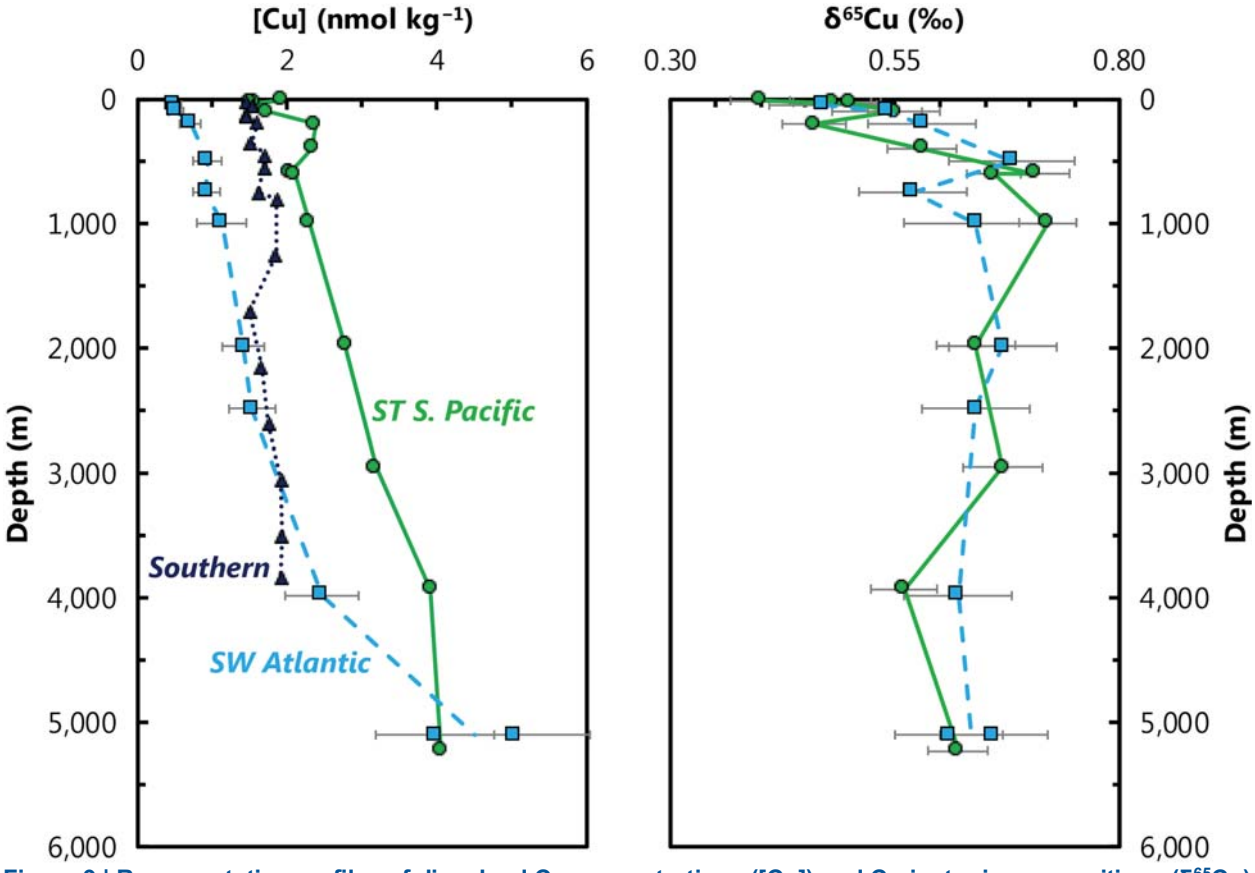

Figure 9 | Representative profiles of dissolved Cu concentrations ([Cu]) and Cu-isotopic compositions ($\delta^{65}Cu$) in the Southwest Atlantic (squares, dashed line), Subtropical South Pacific (circles , solid line) and Southern (triangles, dotted line) Oceans. This comparison illustrates that the isotopic behavior of Cu is similar between basins, reflecting the importance of complexation by strong organic ligands.

Copper isotopes are reported as relative to the NIST SRM 976 standard, though due to a shortage of this material, two other certified reference standards are now available: ERM-AE633 ($\delta^{65}Cu_{SRM976} = -0.01 \pm 0.05$ ‰) and ERM-AE647 ($\delta^{65}Cu_{SRM976} = +0.21 \pm 0.05$ ‰; Moeller et al., 2012; Moynier et al., 2017). For consistency and ease of comparison, Moynier et al. (2017) recommend that future data be reported relative to NIST SRM 976. We adopt this convention. The analysis of Cu isotopes in seawater is challenging, due to both Cu's strong organic complexation, and only two isotopes precluding the use of a double spike technique (reviewed in Little et al., 2018). The data presented to date indicate that deep seawater $\delta^{65}Cu$ values are isotopically heavy (at about +0.7 ‰) compared to the upper continental crust (UCC; at about +0.1 ‰; Table 1; Moynier et al., 2017). Lighter Cu isotope compositions in the upper water column and along margins are thought to reflect local sources of isotopically light Cu (e.g., aerosols, riverine particulates, sediments; Takano et al., 2014; Little et al., 2018).

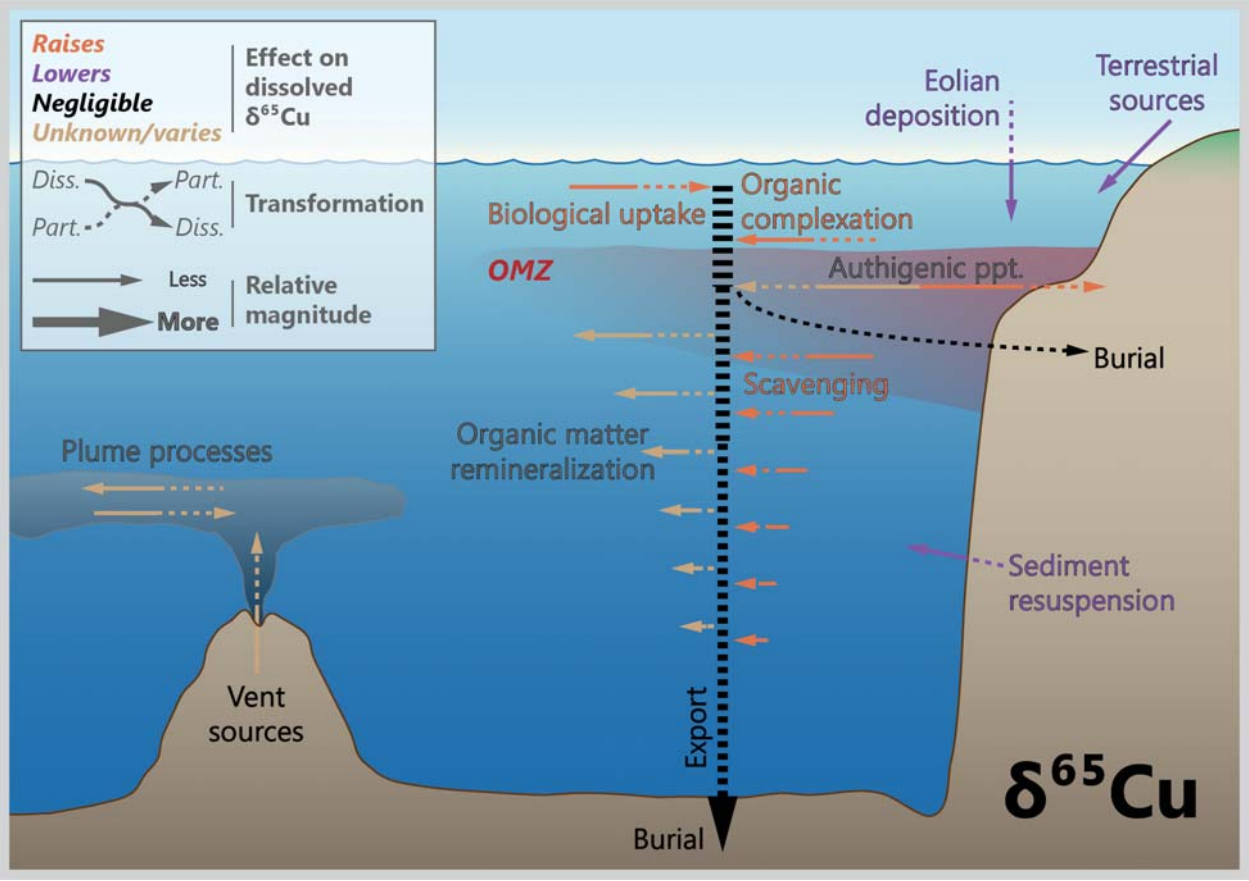

Figure 10 | Processes driving copper isotope variations in modern seawater. Biological productivity exerts only a modest impact on the marine Cu isotope cycle and thus there is no obvious route to developing Cu isotopes (or Cu concentrations) as a paleoproductivity proxy.

5.2. Driving processes

5.2.1. Biological

Copper is bioessential, but cellular Cu contents are approximately 2–10 fold lower than the micronutrients Fe and Zn (Twining & Baines, 2013). The redox-active behaviour of Cu (existing as Cu^{2+} or Cu^{+} in biological systems) enables its role in electron transport, for example in the Cu-containing proteins plastocyanin and cytochrome c oxidase (Ridge et al., 2008). Copper uptake of some Fe-limited phytoplankton may increase, either due to the replacement of Fe-containing with Cu-containing enzymes (e.g., Peers and Price, 2006), or the involvement of Cu in the high-affinity Fe uptake systems (Annett et al., 2008; Maldonado et al., 2006; Guo et al., 2012). Despite its biological function, Cu is also extremely toxic due to the formation of reactive oxygen species, which pose a threat to DNA, lipids, and proteins (Ridge et al., 2008). Copper toxicity thresholds vary by phytoplankton group, with smaller organisms generally more sensitive than larger ones (e.g., cyanobacteria cf. diatoms; Brand et al., 1986), and coastal strains more resistant than open ocean strains (e.g., Peers et al., 2005).

A small number of studies have investigated Cu isotope fractionation during cellular uptake or cell surface adsorption by microorganisms (Pokrovsky et al., 2008; Navarrete et al., 2011; Cadiou et al., 2017; Coutaud et al., 2018; 2019). The results of these experiments are somewhat variable, with enrichment of either light or heavy Cu isotopes observed during assimilation and adsorption. However, assimilation in culture generally favours light Cu isotopes (Navarrete et al., 2011; Cadiou et al., 2017; Fig. 10). The complexity in Cu isotopic behaviour has been attributed to small changes in Cu speciation or redox during uptake and/or release of Cu (Coutaud et al., 2018; 2019).

5.2.2. Chemical

In seawater, the vast majority of Cu is complexed to strong organic ligands (more than 99.8% complexed in surface northeast Pacific), which lower free Cu^{2+} concentrations to below toxic levels (e.g., Coale & Bruland, 1988; 1990; Moffett & Dupont, 2007). It is thought that ligands are primarily produced by biota for the purpose of detoxification (e.g., Moffett et al., 1990; Moffett & Brand, 1996), albeit recent work suggesting that strongly complexed Cu is bioavailable to some eukaryotes, which appear to have a higher cellular Cu requirement (and higher thresholds of Cu toxicity) than prokaryotes (Semeniuk et al., 2009; 2015).

Both theory and experiments predict preferential complexation of heavy isotopes by strong organic ligands (Sherman, 2013; Fujii et al., 2013; Ryan et al., 2014; Sherman et al., 2015), and organic complexation is thought to play a key role in the modern oceanic budget and distribution of Cu isotopes (Vance et al., 2008; Little et al., 2014a; Thompson & Ellwood, 2014; Takano et al., 2014; Little et al., 2018). The small pool of non-complexed Cu^{2+} in seawater is thus expected to be isotopically light (e.g., Little et al., 2014b, 2018).

Based on a surface complexation model with the phyllomanganate birnessite, the principal scavenging phase of divalent trace metals in oxic sediments, Sherman & Peacock (2010) calculated that the concentration of dissolved Cu in deep waters should be orders of magnitude lower than is actually observed. They attribute this difference to the chelation of "*essentially all dissolved Cu*" by organic ligands (Sherman & Peacock, 2010), consistent with observations (e.g., Moffett & Dupont, 2007; Heller & Croot, 2015; Jacquot & Moffett, 2015). Nevertheless, some form or forms of scavenging are also thought to play a role in the oceanic Cu distribution.

Reversible scavenging, a term used to describe the equilibrium between a scavenged and dissolved metal pool, has been proposed as the driving process behind the generally monotonic, linear increases in dissolved [Cu] depth (Little et al., 2013; Richon et al., 2019; Fig. 9). In some regions with high particulate loads (e.g., some hydrothermal plumes, benthic nepheloid layers), scavenging removal of Cu has been observed (Jacquot and Moffett, 2015; Roshan & Wu, 2015a). Preferential scavenging of light Cu isotopes by particulate (e.g., oxyhydroxide) phases has also been proposed as an explanation for isotopically heavy seawater Cu isotope compositions (e.g., Takano et al., 2014), though the driving mechanisms leading to isotopically light particulate Cu remain to be fully established (see section 5.3; Fig. 10).

The shorter residence time of Cu (2-3.3 kyr; Little et al., 2017b), compared to metals with longer residence times (e.g., Cd, Zn, Ni), mean that, as for Fe, regional and local sources of Cu to the ocean play a relatively larger role in determining dissolved Cu distributions than for some other TEIs. Sources of Cu include aerosols (both natural and anthropogenic; e.g., Takano et al., 2014; Yang et al., 2019), benthic fluxes from sediments (e.g., Boyle et al., 1977; Heller & Croot, 2015; Roshan & Wu, 2015a; Little et al., 2018), and dissolved or particulate riverine sources (e.g., Vance et al., 2008; Little et al., 2018; Richon et al., 2019). A possible small hydrothermal source has been identified in the South Pacific from the East Pacific Rise (Roshan & Wu, 2018), which is in contrast to the scavenging removal of Cu observed around hydrothermal vents elsewhere (e.g., Jacquot and Moffett, 2015).

871

872 *5.2.3. Physical*

873 Copper's shorter residence time relative to Cd, Zn and Ni also means that the Southern Ocean and wider
874 physical ocean circulation play a somewhat smaller role in oceanic Cu and δ^{65}Cu distributions compared to
875 many of the other TEIs discussed herein. Nonetheless, the imprint of circulation is evident in certain
876 circumstances, such as in the Atlantic and the upper 2 km of the South Pacific where dissolved Cu is
877 correlated with dissolved silicate (Roshan & Wu, 2015a; 2018; Little et al., 2018).

878

879 **5.3. Marine archives**

880 *5.3.1. Ferromanganese sediments*

881 Ferromanganese sediments (crusts and nodules) exhibit Cu isotope compositions of +0.3 to +0.5 ‰
882 (Albarède, 2004; Little et al., 2014). This means that, on average, Fe–Mn sediments are approximately 0.35
883 ‰ lighter than deep seawater, which averages +0.7 ‰ (Fig. 11). The explanation for this offset is uncertain,
884 but may reflect either strong organic complexation of Cu in seawater (Little et al., 2014b), or the enrichment
885 of light Cu isotopes on the birnessite mineral surface, as recently observed in inorganic experiments
886 whereby sorbed Cu exhibited δ^{65}Cu that was 0.45±0.18 ‰ lighter than cu in solution (Ijichi et al., 2018).
887 At equilibrium in seawater, however, the strong complexation and mineral sorption effects should be
888 additive, leading to a much larger isotopic offset than the ~0.35 ‰ observed, suggesting that one of the two
889 effects is not expressed in nature for reasons as yet unclear.

890 Little et al. (2014a) observed no marked changes in deep-ocean δ^{65}Cu recovered from three Fe–Mn crusts
891 from each of the major ocean basins over the last ~20 Ma. Assuming Cu diffusion is slower than crust
892 growth rate, the lack of Cu isotope variation indicates that, on a global basis, the marine Cu cycle has been
893 in isotopic steady state for at least 20 Myr (Fig. 10).

894

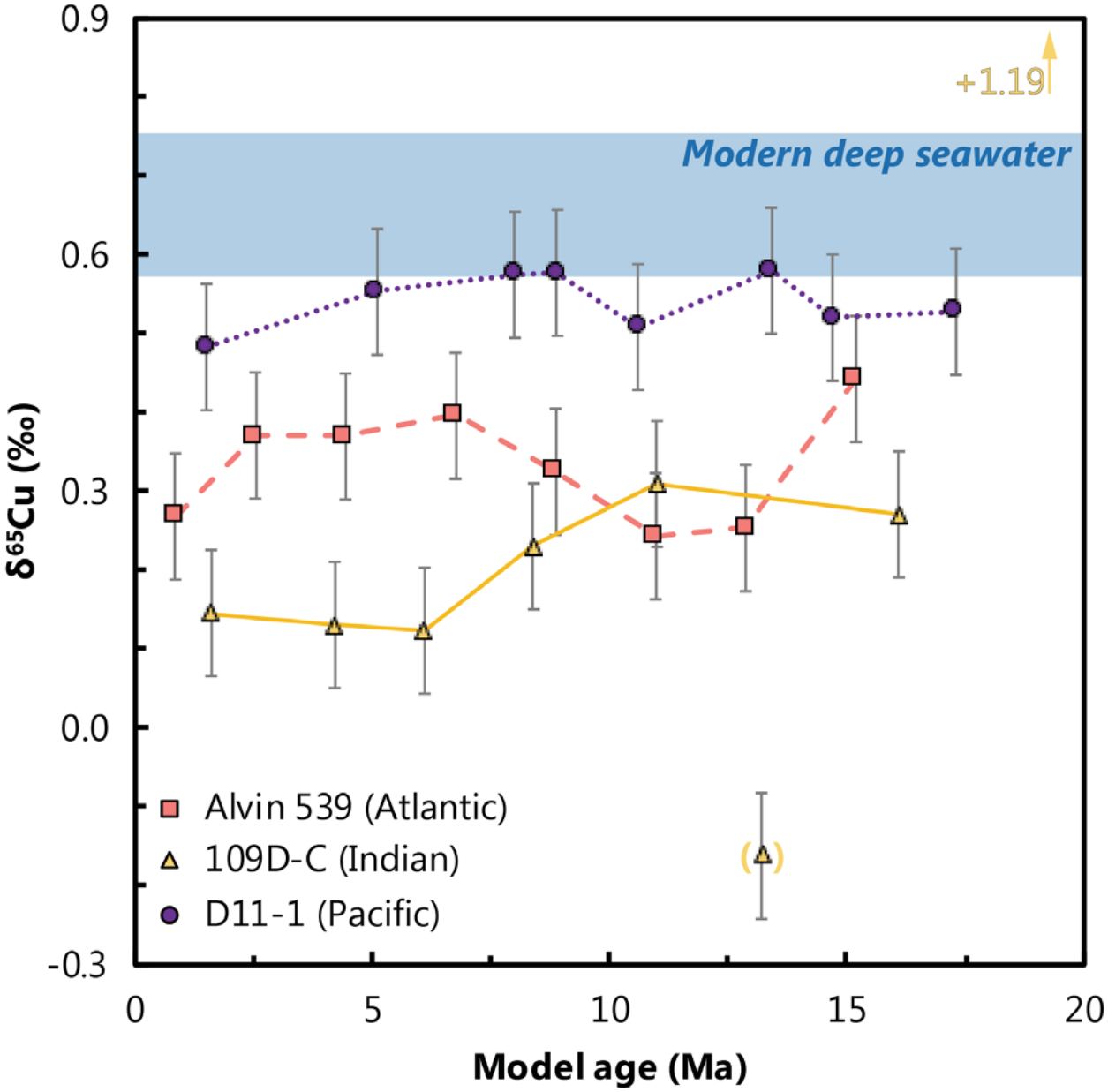

Figure 11 | Deep ocean Cu isotope constancy over the past 20 Myr. These records are derived from Fe–Mn crusts recovered from the Atlantic (square, dashed line), Indian (triangle, solid line), and Pacific (circle, dotted line) Oceans. Assuming the isotopic offset between dissolved Cu in seawater and Fe–Mn crusts has remained unchanged at ≈0.35 ‰ over this time, these records imply that the inter-basin Cu-isotopic variations observed in modern crusts and the Cu isotope cycle itself have remained relatively stable for at least 20 Myr. Two samples from 109D-C possess low levels of authigenic Cu enrichment indicating detrital contamination (parentheses, arrow; Little et al., 2014a).

5.3.2. Organic-rich sediments

Qualitative arguments for high organic matter fluxes (i.e., higher paleoproductivity) have been made based on elevated Cu and Ni concentrations in ancient organic-rich sediments (e.g., Tribovillard et al., 2006). This approach is supported by positive correlations between Cu and Ni with TOC in modern continental margin sediments (Sec. 9.3). Applying this [metal]–TOC approach to study past productivity has three prerequisites:

1. Organic matter is the primary vector supplying the TE to sediments;
2. Sediments are reducing, and must remain reducing during diagenesis and burial (note that this differs for Ba, since $BaSO_4$ preservation requires more oxidizing conditions; Sec. 8);
3. The system is open marine

A significant challenge to this approach for Cu (as well as Zn, Cd, Mo, and other chalcophile elements) is its reactivity towards sulfide, as illustrated by the quantitative removal of Cu from the euxinic Black Sea water column and resultant enrichment in underlying sediments (Tankéré et al., 2001; Little et al., 2015). Thus, for Cu, prerequisite number (1), that the metal is primarily supplied to sediment associated with organic matter, is not fulfilled. We return to this approach for Ni in Sec. 9.3.2.

Authigenic Cu in modern organic-rich sediments is generally similar in isotopic composition to Fe–Mn sediments and suspended particulate material collected from the South Atlantic, all at about +0.3‰ (Little et al., 2017b; 2018; Ciscato et al., 2019). This homogeneity in authigenic Cu isotope compositions has been suggested to reflect an equilibrium isotope fractionation in the aqueous phase between organically complexed Cu and inorganic Cu^{2+}, with the latter approximately 0.4‰ lighter than ligand-bound Cu, followed by near quantitative scavenging of inorganic Cu^{2+} by (any type of) particulate material (Little et al., 2017b; 2018). If correct, this hypothesis suggests that authigenic Cu isotope compositions in marine sediments may reflect the evolution of organic complexation on geological timescales.

Ciscato et al. (2018; 2019) developed a new approach to isolate TEIs associated with two different fractions in organic-rich sediments, the 'organic-pyrite fraction' (OPF) and 'HF-digestible fraction' (HFD). They find that the OPF of modern Peru margin sediments typically contains >50 % of total Cu and is variably isotopically light compared to bulk authigenic Cu. They suggest this signature reflects incomplete sulfidation under variable water column and sedimentary redox conditions (e.g., Bianchi et al., 2018). Unlike in modern sediments, in ancient shales (ranging in age from 0.4 to 3.4 Ga) bulk Cu concentrations do not correlate with TOC and >80% of Cu is hosted in the HFD fraction. In addition, the OPF fraction in ancient shales is markedly isotopically heavier than it is in modern sediments (Ciscato et al., 2019). This

difference between modern and ancient Cu partitioning may reflect diagenetic or metamorphic processing, or it may be a primary feature relating to differences in the Cu isotope composition of seawater, or differences in the mechanism(s) of Cu sequestration into sediments.

5.4. Prospects

Despite the biological importance of Cu, the modern biogeochemical cycle of Cu suggests there is no clear route to developing Cu isotopes (or Cu concentrations) as a paleoproductivity proxy. However, organic ligands play a key role in the cycling of Cu and Cu isotopes, suggesting potential for the use of Cu isotopes in tracing the evolution of organic complexation on geological timescales. Additionally, careful sequential extraction procedures, such as those described by Ciscato et al. (2019), may allow for the direct probing of past seawater properties, such as redox state.

At present, there are few applications of Cu isotopes to study ancient biogeochemical cycles. Interestingly however, there are two black shale records that indicate a shift from UCC-like to heavy Cu isotope values across the Great Oxidation Event (GOE, ~2.4 Ga; Chi Fru et al., 2016; Ciscato et al., 2019). Chi Fru et al. (2016) interpreted this shift as reflecting the onset of oxidative weathering and waning of iron formation deposition, with the latter process driving pre-GOE seawater isotopically light due to the preferential scavenging of heavy Cu isotopes to Fe oxides. However, a recent analysis of two classic pre-GOE sequences containing iron formations do not support this earlier hypothesis, with δ^{65}Cu remaining close to 0 ‰ (Thibon et al., 2019). Thus, while the limited available data preclude confident interpretations, there are tantalizing tastes of future research directions in Cu isotope geochemistry.

6. Cadmium

Dissolved cadmium (Cd) concentrations closely correlate with the macronutrient phosphate in the oceans (PO_4^{3-}; e.g., Boyle et al., 1976; Bruland, 1980). The nutrient-like properties of Cd—and attendant correlations with PO_4^{3-}—have been documented in multiple ocean basins and in multiple dimensions (i.e., vertically, spatially, and temporally). This overall behavior implies that Cd somehow participates in marine biological processes and that the resulting distribution captured by sediments can be connected to underlying patterns of primary productivity. Recently, results from the GEOTRACES program have highlighted new nuances to this cycle that act to decouple phosphate and Cd in certain situations, which affect the interpretation of Cd distributions in the modern ocean as well as in the sedimentary record. Accordingly, this section will review the first-order features of marine Cd (and Cd isotope) distributions, discuss known driving mechanisms, highlight recent progress on identifying suitable sedimentary archives, and offer recommendations for future studies.

6.1. Marine distribution

Away from major upwelling regions, surface water dissolved Cd concentrations are typically between 1–100 pmol kg^{-1}, but can reach as low as 30 fmol kg^{-1} (Schlitzer et al., 2017; Fig. 12). The majority of this small surface inventory is thought to be complexed by strong organic ligands (e.g., Bruland, 1992; Ellwood, 2004). In intermediate and deep waters, dissolved Cd concentrations are significantly elevated relative to surface waters, ranging from 0.5 nmol kg^{-1} in intermediate and deep waters in the north Atlantic to ≈1.2 nmol kg^{-1} in the oldest deep waters of the north Pacific (Schlitzer et al., 2018). As with Zn (Sec. 4.), the overall distribution of dissolved Cd throughout the oceans is driven principally by biological and physical processes in the Southern Ocean, and the lateral circulation of Southern Ocean water masses (e.g., Baars et al., 2014; Middag et al., 2018; Sieber et al., 2019a). Thus, the shape of vertical Cd concentration profiles at lower latitudes arises largely from horizontal transport and mixing of high-Cd Southern Ocean-sourced water masses, with a modest contribution from regeneration of sinking particles (i.e., 5–40 %; Middag et al., 2018). These processes result in Cd having ‘nutrient-type’ one dimensional water column profiles, with

a progressive increase in intermediate- and deep-water [Cd] along the pathways of meridional overturning circulation (e.g., de Baar et al., 1994; Middag et al., 2018).

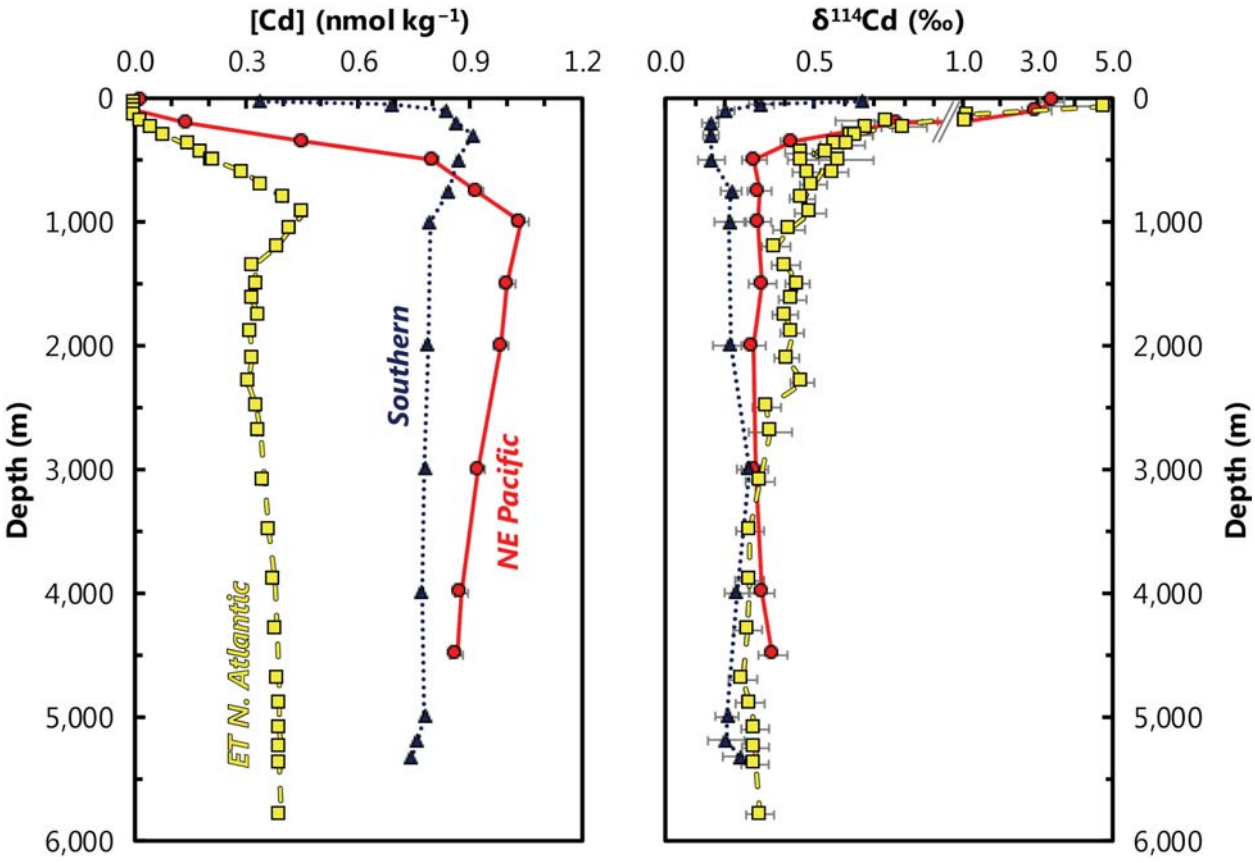

Figure 12 | Representative profiles of dissolved Cd concentrations ([Cd]) and Cd-isotopic compositions (δ^{114}Cd) in the Eastern Tropical North Atlantic (squares, dashed line), Northeast Pacific (circles, solid line), and Southern (triangles, dotted) Oceans. Note the break in scale in δ^{114}Cd above 1 ‰, illustrating the extreme isotopic compositions observed in the most Cd-depleted surface samples. Notably, such extreme compositions are not observed in the similarly Cd-depleted surface waters of the southern hemisphere gyres (e.g., Gault-Ringold et al., 2011; Xie et al., 2017; George et al., 2019), nor in the surface of the high-latitude Southern Ocean, where dissolved [Cd] is elevated (e.g., Abouchami et al., 2011; 2014). This comparison illustrates that the processes leading to distinct dissolved concentration profiles effect only modest changes in dissolved δ^{114}Cd between basins.

The past decade has seen an explosion in the number of studies employing Cd stable isotopes to investigate marine Cd cycling. The majority of extant Cd isotope data are reported relative to the NIST SRM 3108 standard, though several earlier studies, reviewed by Rehkämper et al. (2012), were reported relative to other in-house materials. Cross-calibration of these materials is described in detail by Abouchami et al. (2013). While the earliest study of Cd isotope variations in seawater was unable to unambiguously identify systematic patterns in the water column, the authors noted that cultures of phytoplankton preferentially

incorporated isotopically-light Cd relative to the media (Lacan et al., 2006). Assuming biological processes were responsible for Cd uptake, this observation led to two key predictions for marine Cd isotope systematics: that Cd-depleted surface waters should exhibit isotopically 'heavier' compositions than Cd-replete deep waters; and, that the degree of isotopic fractionation should be proportional to the extent of Cd removal into particles. Indeed, this is precisely the pattern that was first reported by Ripperger et al. (2007).

Subsequent studies have corroborated this general one-dimensional pattern in the Southern (e.g., Abouchami et al., 2011; 2014; Xue et al., 2013; Sieber et al. 2019a), Atlantic (e.g., Xue et al., 2012; Conway & John, 2015a; Xie et al., 2017; Xie et al., 2019a), Arctic (Zhang et al., 2019), and Pacific Oceans (Yang et al., 2012; Yang et al., 2014; Conway & John, 2015b; Janssen et al., 2017; John et al., 2018; Yang et al., 2018; Xie et al., 2019b; Sieber et al., 2019b). These studies have shown that the deep ocean (>500–1,000 m) is largely homogenous in Cd isotope composition (δ^{114}Cd of +0.2 to +0.3 ‰). This deep water δ^{114}Cd value is heavier than the upper continental crust δ^{114}Cd signature of ~0‰ (Schmitt et al., 2009a), similar to that observed for other metals such as Zn, Ba, and Ni (Sections 4, 8, and 9.). Intermediate-depth waters relating to water masses such as Antarctic Intermediate Water (AAIW) exhibit slightly heavier δ^{114}Cd values (+0.4 to +0.5 ‰), while surface waters generally exhibit heavier isotopic compositions (up to ~+1‰). As for Cd concentrations, these one dimensional δ^{114}Cd profile shapes arise largely from the combination of Southern Ocean biological processes and lateral circulation of water masses, as well as some contribution from local surface uptake and regeneration (Abouchami et al., 2014; Sieber et al., 2019b). Some studies have reported δ^{114}Cd values of up to +5 ‰ in surface waters of the northern hemisphere gyres (Ripperger et al., 2007; Xue et al., 2012; Conway & John, 2015a; 2015b), while others have reported more muted fractionation or even a switch to lighter than deep-ocean compositions in surface waters (Gault-Ringold et al., 2012; Xie et al., 2017; Janssen et al., 2017; Xie et al., 2019a; George et al., 2019; Sieber et al., 2019b; Xie et al., 2019). The origin of these extreme δ^{114}Cd values remains ambiguous.

Overall, although the first-order distributions of dissolved Cd concentration and isotope composition in surface waters are consistent with intense cycling by biological processes, this range of observations suggests that the processes influencing surface Cd isotope compositions may be more complex. For example, interactions with ligands, effects arising from recycling of organic matter, differences in fractionation factor between different organisms, and supply of Cd from external Cd sources may all influence surface water dissolved δ^{114}Cd. This raises three related questions to be addressed in the remainder of this section: What are the candidate biological processes that drive these patterns? How do other physical

or chemical processes play a role in setting marine Cd distributions? Can Cd-based reconstructions of these processes be used to inform on past productivity?

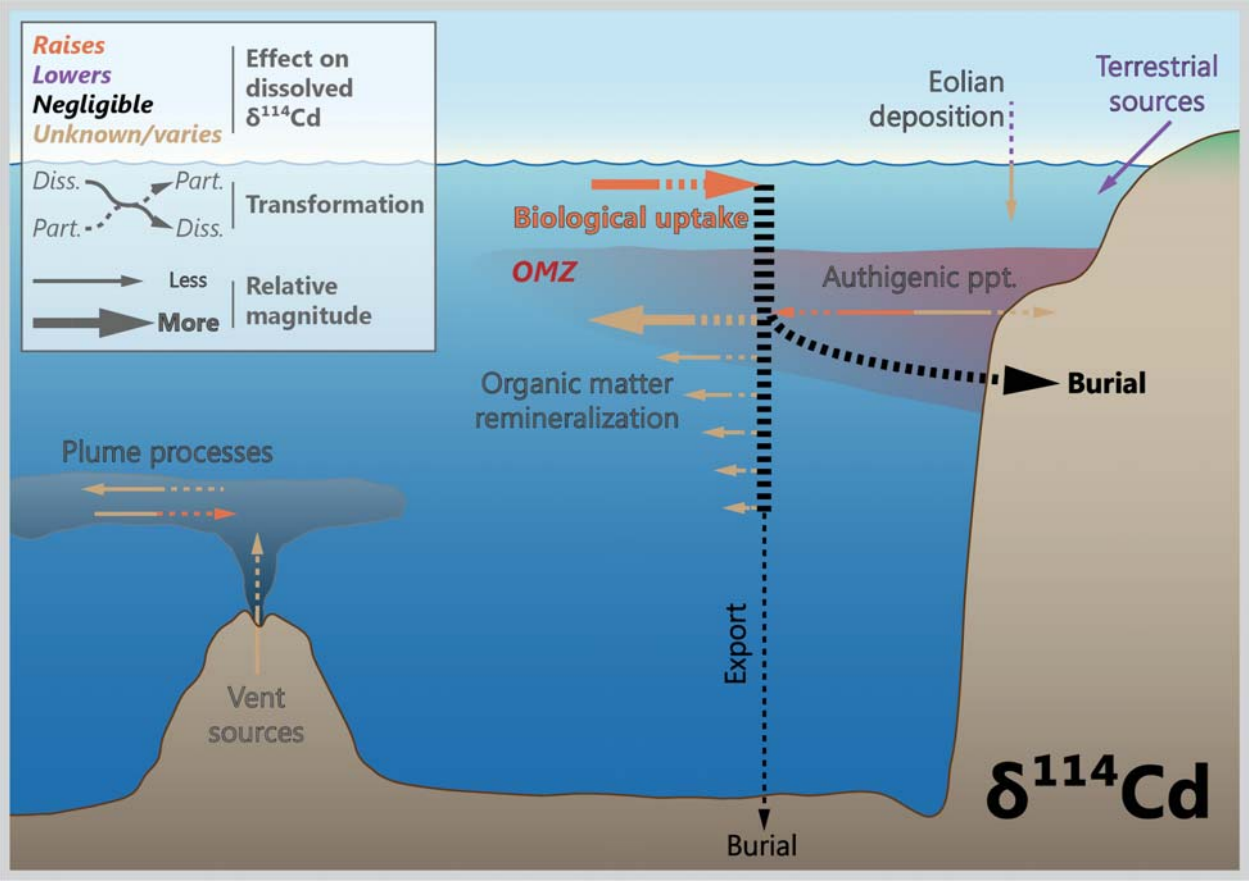

Figure 13 | Processes driving cadmium isotope variations in modern seawater. Biological processes exert a significant control on surface water Cd cycling, implying that $\delta^{114}Cd$ is broadly responsive to productivity. However, important redox-dependent processes remain to be fully elucidated, particularly those occurring around OMZs.

6.2. Driving processes

6.2.1. Biological

As noted above, the nutrient-like distribution of Cd implies intense biological cycling in seawater, even though Cd is considered toxic (e.g., Waldron & Robinson, 2009). This dichotomy has inspired a significant body of research investigating the role that Cd plays in microbial physiology. These studies showed that Cd uptake by marine microbes exhibits three noteworthy dependencies. First, cellular Cd quotas are strongly positively correlated with the Cd content of their environment, both in culture (see compilation by Twining & Baines, 2013) and from oceanographic data (Middag et al., 2018). Second, microbial Cd uptake

is diminished when the concentration of other divalent cations increases, particularly so for Fe, Mn, and Zn. Likewise, lower concentrations of these divalent cations cause increases in Cd uptake (e.g., Sunda & Huntsman, 2000; Cullen et al., 2003). Some diatoms have even shown capacity to substitute much of their metabolic Zn requirements with Cd (Price & Morel, 1990). Third, Cd uptake is also influenced by speciation of inorganic carbon, with low pCO_2 promoting higher cellular Cd quotas (e.g., Cullen et al., 1999; Cullen & Sherrell, 2005; de Baar et al., 2017). The connection between Cd and carbon speciation is particularly intriguing given the discovery of the ζ-class of carbonic anhydrase that can utilize Cd (or Zn) as the catalytic metal (e.g., Lane et al., 2005; Xu et al., 2008).

Despite these dependencies, the extent to which active physiological utilization of Cd controls global patterns of Cd uptake is unclear. For example, genes encoding the ζ carbonic anhydrase metalloenzyme were not found in green algae nor coccolithophores, and were similarly absent from many species of diatom (Park et al., 2007). Thus, it is similarly plausible that some part of the biological Cd cycle is driven by organisms inadvertently removing Cd from seawater while attempting to source other metals (e.g., Boyle, 1988b; Horner et al., 2013), or that microbes require Cd to populate other Cd-centered metalloenzymes that await discovery.

The role of microbial physiology in mediating Cd isotope fractionation is comparatively understudied. Despite this, it appears that biological fractionation of Cd isotopes is ubiquitous; fresh- (Lacan et al., 2006) and saltwater (John & Conway, 2014) green algae, incubations of unfiltered seawater (Xue et al., 2012), heterotrophic bacteria (Horner et al., 2013), and shallow marine particles (e.g., Yang et al., 2015; Janssen et al., 2019) all indicate that biological particles accumulate isotopically-light Cd from their environment with a fractionation between −0.3 to −0.8 ‰ (Fig. 13). How—and perhaps even whether—this range of offsets is related to environmental context, experimental setup, species, or specific microbial functions is unknown.

6.2.2. Chemical

The role of chemical processes in mediating global Cd distributions is the most under-constrained. Recent studies suggested that pelagic partitioning of Cd into sulfides in oxygen-minimum zones may be a significant loss term (Janssen et al., 2014; Bianchi et al., 2018; Plass et al., 2020). Moreover, the Cd isotope effect associated with sulfide precipitation identified by Guinoiseau et al. (2018) is consistent with field data, and particulate Cd is known to accumulate more rapidly in sediments that are bathed by bottom waters containing low dissolved oxygen (e.g., van Geen et al., 1995; Sec. 6.3; Fig. 13). Collectively, these

observations suggest a potential redox sensitivity in sedimentary Cd isotope distributions that deserves additional scrutiny. Indeed, the influence of sediments as the most important marine Cd sink can be seen in some water column profiles of δ^{114}Cd (Xie et al., 2019b). Similarly, data from the hydrothermal TAG site in the North Atlantic suggests that hydrothermal plumes may scavenge Cd from seawater, constituting a small sink of isotopically-light Cd, though this does not have an observable effect on deep ocean δ^{114}Cd values outside of the plume itself (Conway & John, 2015b; Fig. 13).

Other potential sources and sinks include rivers, atmospheric deposition, and sediments; however, none of these interfaces exhibit significant anomalies in Cd concentration or δ^{114}Cd in GEOTRACES-era datasets. This finding is in accord with earlier research by Martin & Thomas (1994), though there exist two possible exceptions. The first concerns the role of atmospheric aerosols, which have been invoked to explain the Cd isotope composition of surface waters in the Southwest Pacific (e.g., George et al., 2019) and South China Sea (e.g., Yang et al., 2012). Modern aerosol inputs may be largely anthropogenic in origin. Anthropogenic forms of Cd exhibit a relatively narrow range of isotopic compositions that are typically—though not always (e.g., Shiel et al., 2010)—lighter than dust-derived Cd (e.g., Bridgestock et al., 2017). Second, interactions with organic ligands have also been invoked to explain the relatively muted pattern of Cd isotope fractionation in the surface of the south Atlantic Ocean (e.g. Xie et al., 2017; Guinoiseau et al., 2018), but there are as yet no corroborating field or experimental data examining the role of organic ligands in mediating Cd isotope fractionation in seawater.

6.2.3. Physical

Physical processes are similarly influential in mediating the global distribution and isotopic composition of Cd throughout the global ocean, particularly those processes occurring in the Southern Ocean. Antarctic Intermediate- and Bottom Waters masses possess higher dissolved [Cd]:[PO_4^{3-}] than North Atlantic Deep Water (e.g., de Baar et al., 1994; Middag et al., 2018). Mixing between these southern- and northern-sourced water masses likely contributes to the well-known 'kink' in the Cd–PO_4^{3-} relationship (e.g., Frew & Hunter, 1992; Elderfield & Rickaby, 2000; Quay & Wu, 2015). Why northern- and southern-sourced intermediate and deep waters possess different dissolved [Cd]:[PO_4^{3-}] is debated, and likely reflects regionally-distinct fractionation of Cd and P during biological uptake (e.g., Sunda & Huntsman, 2000; Cullen et al., 2003) and during remineralization (e.g., Baars et al., 2014; Roshan & Wu, 2015). In the Atlantic, however, the importance of remineralization to deep water Cd budgets is of secondary significance: the ratio of regenerated-to-preformed [Cd] is ~30 % in the mesopelagic, and generally <10 % in the deep ocean (Roshan & Wu, 2015b; Middag et al., 2018). Given the low proportion of regenerated Cd in the deep Atlantic, the

ratio of dissolved [Cd]:[PO_4^{3-}] and the overall distribution of [Cd] are essentially governed by the [Cd]:[PO_4^{3-}] of the source waters (Middag et al., 2018) and the prevailing geometry of ocean circulation, respectively (Boyle, 1988b).

Recent Cd isotope data from the South Atlantic (Xie et al., 2017), South Pacific (George et al., 2019; Sieber et al., 2019a), and Arctic (Zhang et al., 2019) also support the importance of mixing in mediating deep-ocean Cd distributions, though it should be noted that the isotopic contrast between mixing end-members is small, relative to measurement precision (e.g., Janssen et al., 2017; Fig. 12). For example, biological uptake of light Cd in the source regions of intermediate waters in the surface Southern Ocean results in isotopically-heavy pre-formed δ^{114}Cd signatures being imparted to Cd-depleted intermediate water masses (e.g., +0.45 ‰ in AAIW; +0.65 ‰ in Subantarctic Mode Water, SAMW; Xue et al., 2013; Abouchami et al., 2014; Sieber et al., 2019b). Lateral circulation of these southern-sourced water masses then transfer this signature northward to intermediate depths in the Atlantic and Pacific Oceans (e.g. Xue et al., 2012; Abouchami et al., 2014; Conway & John, 2015a; Sieber et al., 2019b). This effect is more pronounced in the North Atlantic than in the Pacific, where southward flowing NADW also carries isotopically-heavy Cd southward at depths of 1,000–3,000m (Xue et al., 2012; Conway & John, 2015a).

6.3. Marine archives

6.3.1. Carbonates

There is a long history of Cd concentration measurements in marine carbonates, particularly corals and foraminifera, most commonly reported as Cd:Ca molar ratios. In principle, carbonates are an appealing archive of ambient Cd chemistry since inorganic partition coefficients are ≫1 (e.g., Tesoriero & Pankow, 1996) and the Cd:Ca of many types of carbonate exhibit a strong proportionality with ambient dissolved [Cd]. In practice, however, most biogenic carbonates exhibit partition coefficients closer to unity (Boyle, 1988b), and resultant Cd:Ca is also sensitive to the species (Boyle, 1992) and temperature of calcification (e.g., Rickaby & Elderfield, 1999). As such, Cd:Ca in carbonates has found the most utility where ambient dissolved [Cd]—and attendant carbonate Cd:Ca—exceeds several 100 pmol kg^{-1}, such as in tracing industrial fallout (e.g., Shen et al., 1987) or in studies of Quaternary deep ocean circulation (e.g., Boyle & Keigwin, 1985; van Geen et al., 1992; Adkins et al., 1998; Farmer et al., 2019).

There are far fewer studies examining the Cd isotope composition of marine carbonates as tracers of historical Cd isotope chemistry. Inorganic partitioning experiments indicate that Cd isotopes are fractionated during incorporation into calcite by ≈−0.5 ‰ (Horner et al., 2011). The isotopic effect is

temperature- and Mg-independent, but vanishes at low salinity. This inorganic calibration has been used to interpret patterns of Cd isotope fractionation preserved in bulk carbonates from the Neoproterozoic Eon (1,000–541 Ma). The variations in these sediments are interpreted as evidencing changes in biological productivity (e.g., Hohl et al., 2017) and Cd sinks (e.g., John et al., 2017) through time. Applications of Cd isotopes to foraminifera to study problems in Quaternary paleoceanography are precluded by the large sample requirements; obtaining 1 ng of Cd—the minimum quantity needed for a reasonable isotope measurement (Ripperger & Rehkämper, 2007; Schmitt et al., 2009b)—requires picking (and cleaning) of 10's of mg of foraminiferal tests. Alleviation of such limitations awaits development of automated picking and screening systems, or vast improvements in ion transmission efficiency for isotope ratio mass spectrometry.

6.3.2. Ferromanganese sediments

Ferromanganese sediments have shown the most promise for recording deep-ocean Cd isotope chemistry. Both ferromanganese nodules (Schmitt et al., 2009a) and crusts (Horner et al., 2010) reflect ambient seawater Cd isotope compositions with negligible fractionation (Fig. 14A), consistent with Cd–Mn-oxyhydroxide partitioning experiments conducted at high ionic strength that show only minor Cd isotope fractionation (Wasylenki et al., 2014). Cadmium is predicted to have a similar diffusivity in Fe-Mn crusts to Hf (Horner et al., 2010), implying that long-term records are likely to exhibit some diffusive smoothing while preserving larger variations (e.g., Henderson & Burton, 1999). As with Zn and Cu isotopes however, time-resolved records of δ^{114}Cd recovered from Fe–Mn crusts indicate minimal variation over the last 20 Myr, and perhaps even the Cenozoic (Fig. 14B); modeling conducted by Murphy (2016) suggests that Cd diffusion may occur much faster than predicted by the diffusion model of Henderson & Burton (1999). If

so, the lack of variation in $\delta^{114}Cd$ over the Cenozoic may simply reflect a 'resetting' of all crust layers toward modern deep-ocean Cd isotope compositions.

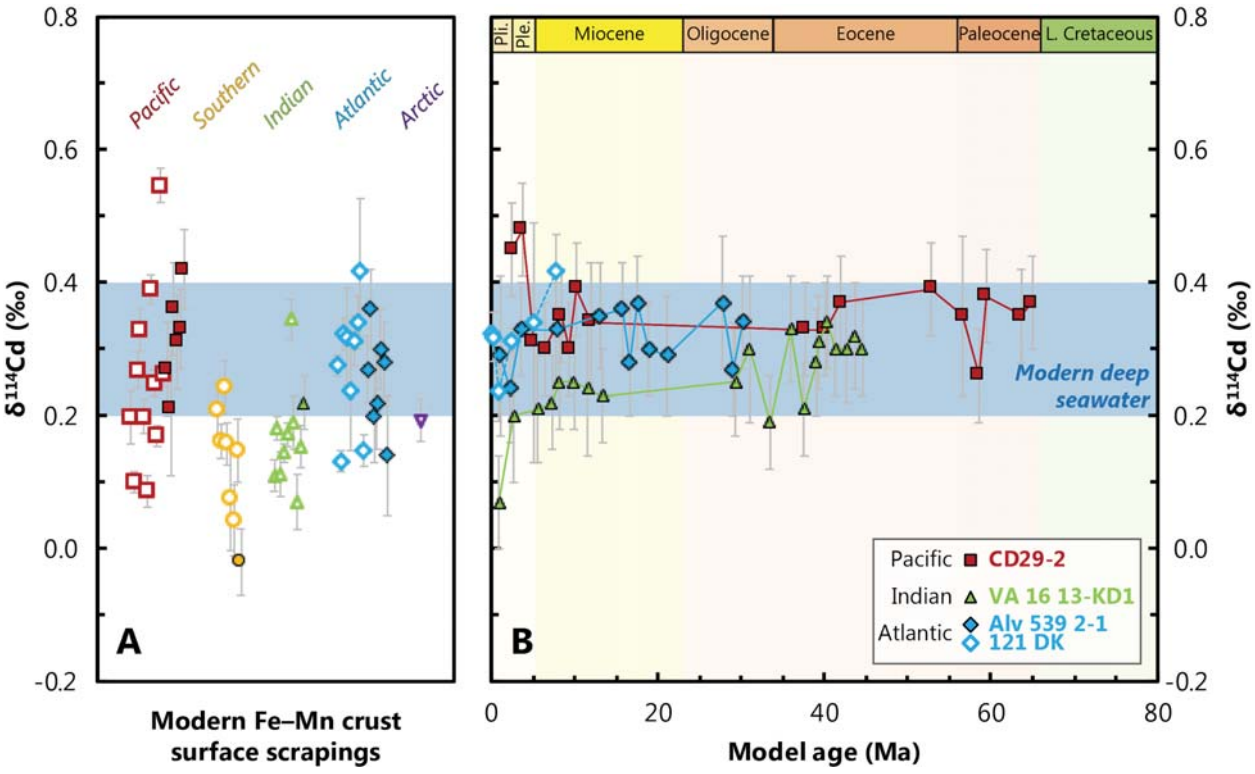

Figure 14 | Ferromanganese crusts records of deep-water Cd isotope compositions. (A) Compilation of 'core-top' Fe–Mn crust $\delta^{114}Cd$; data from Schmitt et al. (2009a; open symbols) and Horner et al. (2010; closed symbols). In general, Southern Ocean samples exhibit lighter $\delta^{114}Cd$ than other basins, consistent with profiles of $\delta^{114}Cd$ (e.g., Fig. 12). **(B)** Cenozoic records of deep-water $\delta^{114}Cd$ recovered from four Fe–Mn crusts; data from Murphy, 2016 (closed symbols) and Schmitt et al. (2009a; open symbols). These records have been plotted using the authors' preferred age models, meaning that there are some differences between the chronology of CD29-2 shown here compared to Fig. 5. Such differences may be immaterial however, given that Cd isotopes in Fe–Mn crusts are potentially subject to diffusive 'resetting' over time (Murphy, 2016).

6.3.3. Organic-rich sediments

Organic-rich sediments are the principal sink of dissolved Cd from the modern oceans (e.g., Rosenthal et al., 1995; van Geen et al., 1995; Little et al., 2015). A significant fraction of the total Cd in organic-rich sediments is derived from sinking organic matter. Accordingly, the Cd content of organic-rich sediments has been applied as a proxy for past productivity (e.g., Brumsack, 2006). However, there is also a redox sensitivity: Cd contents are generally elevated in organic-rich sediments that are bathed by low-oxygen waters (Fig. 15). This enrichment likely derives from three processes. First, low-oxygen environments may limit oxidation—and thus favor preservation—of settling Cd sulfide particles formed in the water column. Second, the chalcophile nature of Cd means that even trace levels of hydrogen sulfide may cause Cd to (co-

)precipitate. Thus, as organic matter is remineralized within the sediment column, any Cd liberated to porewaters is proportionally more likely to re-precipitate into sulfide minerals, relative to harder metals (and carbon), effectively 'trapping' remineralized Cd in sediments (e.g., Rosenthal et al., 1995). Third, recent evidence suggests that Cd may also directly (co-)precipitate from seawater and into sediments when plumes of hydrogen sulfide interact with bottom waters (e.g., Xie et al., 2019b; Plass et al., 2020). The relative importance of these three processes to the O_2-dependent pattern of Cd accumulation remains to be fully elucidated.

While the contribution of organic-rich sediments to the isotopic mass balance of Cd is presently unknown, their significance to the marine Cd budget suggests that, globally, the Cd isotope composition of these sediments should balance the riverine flux $\delta^{114}Cd \approx +0.1 \pm 0.1$‰ (Lambelet et al., 2013). Alternatively, the other minor sinks of Cd—carbonates, ferromanganese oxides, clays—must possess large isotopic offsets relative to seawater, which seems unlikely given existing field and experimental data. Obtaining modern calibrations of Cd isotope partitioning into organic-rich sediments should be considered a priority.

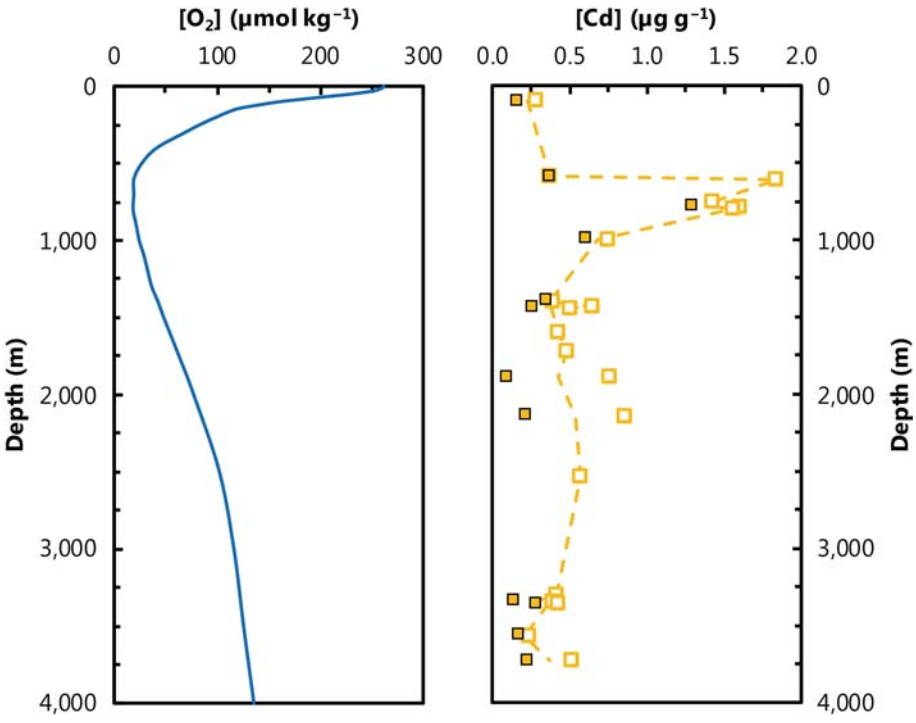

Figure 15 | Cadmium concentrations in California Margin sediments. Left: Regionally-representative dissolved $[O_2]$ profile from the northeast Pacific showing broad minimum between 600–800 m. Profile from 35.5°N, 122.5°W (from World Ocean Atlas; Garcia et al., 2013). **Right:** Solid-phase Cd concentrations for northeast Pacific core-top (closed symbols) and "*slightly deeper*" (8–10 cm; open symbols) sediment samples; dashed line indicates arithmetic mean. These samples evidence a maximum in authigenic Cd deposition at the top of the OMZ, which may originate from processes occurring in the water or sediment column.

6.4 Prospects

The overview provided above indicates that Cd participates in marine biological processes and that its distribution is sensitive to the biological productivity of the oceans. How this sensitivity is transcribed into marine sediments remains uncertain, however. Additionally, there are several other processes that have the potential to render isotope effects that require further exploration before Cd isotopes can be solely interpreted as a productivity proxy, such as: biological fractionation effects, authigenic transformations, and redox sensitivities. Relatedly, the fidelity of many types of marine sediment to record ambient Cd isotope chemistry remain inadequately constrained. With these two themes in mind, we suggest several areas for additional research that may help to address the overarching question as to whether Cd isotope-based reconstructions can be used to inform on past ocean productivity.

6.4.1. Modern

Several questions persist regarding the modern Cd isotope cycle. We list five of the most pressing below and offer possible remedies to each.

- Are the 'extreme' (i.e., δ^{114}Cd of + 5 ‰; Fig. 12) values seen in surface waters of the northern-hemisphere gyres real? That is, are these heavy compositions true oceanographic features that are absent from the southern hemisphere, or do they represent analytical artifacts unique to MC-ICP-MS? This issue will require intercalibration between the two main approaches—the other being thermal ionization mass spectrometry (TIMS)—that various groups use to measure Cd isotopes in seawater.
- To what extent do local Cd isotope compositions in surface waters reflect larger-scale processes? Addressing this issue will require elucidating the role of organismal uptake, ligands, and mixing, which would benefit from conducting additional experimentation with plankton, coupling of isotope methods with electrochemistry, and numerical modeling, respectively.
- Is there a 'Redfield' stoichiometry for Cd in organic matter? If so, what controls it? Existing culture (Ho et al., 2003) and field (Ohnemus et al., 2017) data suggest a wide range of cellular Cd:P, which

have been suggested as reflecting species and local supply ratios, respectively (in addition to the aforementioned feedback interactions). Further experimentation with model organisms is needed.

- Do all organisms contribute to Cd isotope fractionation in seawater? Uptake of Cd into cells is widespread, whereas the genes encoding the ζ-class of carbonic anhydrases are not. Again, further experimentation with marine-relevant organisms is necessary.
- How are the 'light' Cd isotope compositions seen in suspended particles above oxygen-minimum zones related to those putatively accumulating in sediments? Do these values relate to sulfide precipitation and what is their influence on the global mass balance? What controls the Cd isotope composition of these particles? Addressing these questions will require examining the Cd isotope composition of particles from oxygen-rich oceanographic regions, identifying whether processes associated with particle regeneration affect Cd isotope compositions, and surveying core-top sediments.

6.4.2. Paleo

As with the modern cycle, several ambiguities persist, though the most pressing relates to archives. Indeed, it appears that a major obstacle preventing the widespread application of Cd isotope-based proxies in paleoceanography has been the lack of suitable archives.

- Concerning carbonates, the main question is still whether it is possible to isolate sufficient quantities of foraminiferal-bound Cd to reconstruct past seawater δ^{114}Cd. Does species matter, or can mixed assemblages be used?
- For organic-rich sediments, the role of biology itself must be considered. That is, how important might it be that different organisms exhibit different magnitudes of Cd isotope fractionation (and Cd:C stoichiometry)? If important, how best to interpret Cd isotope records—species, evolutionary innovations, productivity?

7. Molybdenum

7.1. Marine distribution

Today, Mo is one of the most abundant trace metals in seawater (Morris, 1975; Bruland 1983; Collier 1985). Molybdenum possesses a long residence time (~440,000 yr; Miller et al., 2011), is conservative with respect to salinity, and exhibits a uniform isotopic composition in oxygenated seawater (e.g., Barling et al., 2001; Siebert et al., 2003). Based on 168 seawater samples from the Atlantic, Pacific, and Southern Oceans analyzed by Nakagawa et al. (2012), the average salinity-normalized dissolved [Mo] and δ^{98}Mo of the ocean are 107±6 nmol kg^{-1} and +2.36±0.10 ‰, respectively (both values ±2 SD; Fig. 16).

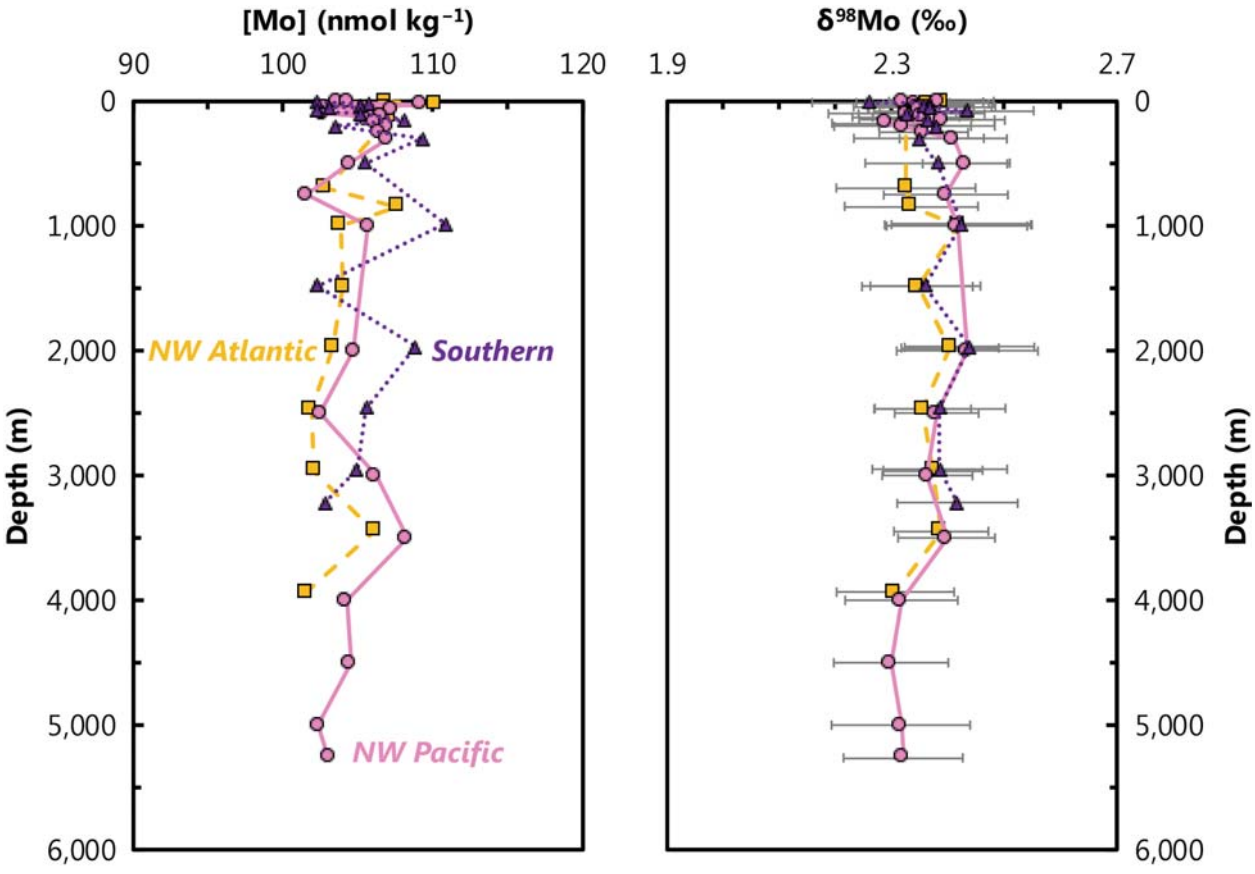

Figure 16 | Representative profiles of dissolved Mo concentrations ([Mo]) and Mo-isotopic compositions (δ^{98}Mo) in the Northwest Atlantic (squares, dashed line), Southern (triangles, dotted line), and Northwest Pacific (circles, solid line) Oceans. This comparison illustrates that the dissolved behavior of Mo is essentially invariant throughout the global oceans.

Given that no significant gradients in dissolved [Mo] are expected, there are few new open-ocean δ^{98}Mo data measured as part of GEOTRACES. However, dissolved [Mo] has been measured on two GEOTRACES transects (GP16 and GA02), demonstrating four intriguing instances where [Mo] deviated

from an otherwise conservative distribution. These instances are briefly described below and covered in detail by Ho et al. (2018). First, the most significant dissolved [Mo] anomalies (~5 % drawdown) are associated with intense scavenging by particulate Fe (oxy)hydroxides close to the Peruvian OMZ. Second, dissolved [Mo] is slightly drawn down (<5 %) in some samples directly above the East Pacific Rise hydrothermal ridge crest, again mostly likely driven by scavenging onto hydrothermally-derived Fe–Mn oxides. Some Mo drawdown is also observed in some far-field hydrothermal samples, though the mechanism is unclear. Third, following normalization to a salinity of 35, surface seawater shows a minor dissolved [Mo] drawdown, implying either biological uptake or adsorption to biotic particles. Though not a true oceanographic feature, a fourth type of dissolved Mo anomaly is also noteworthy: bottle storage artefacts. Ho et al. (2018) found that many samples with initially low values showed an increase in dissolved [Mo] with increasing storage time, implying a change in Mo speciation to a form that is detectable by ICP-MS. In contrast to the relative constancy of dissolved [Mo] in open ocean settings, there are a number of studies of showing striking dissolved Mo variations in coastal and estuarine systems (e.g., Dalai et al., 2005; Dellwig et al., 2007; Joung and Shiller, 2016; Wang et al., 2016) as well as in modern restricted settings, such as the Black and Baltic Seas (Nägler et al., 2011).

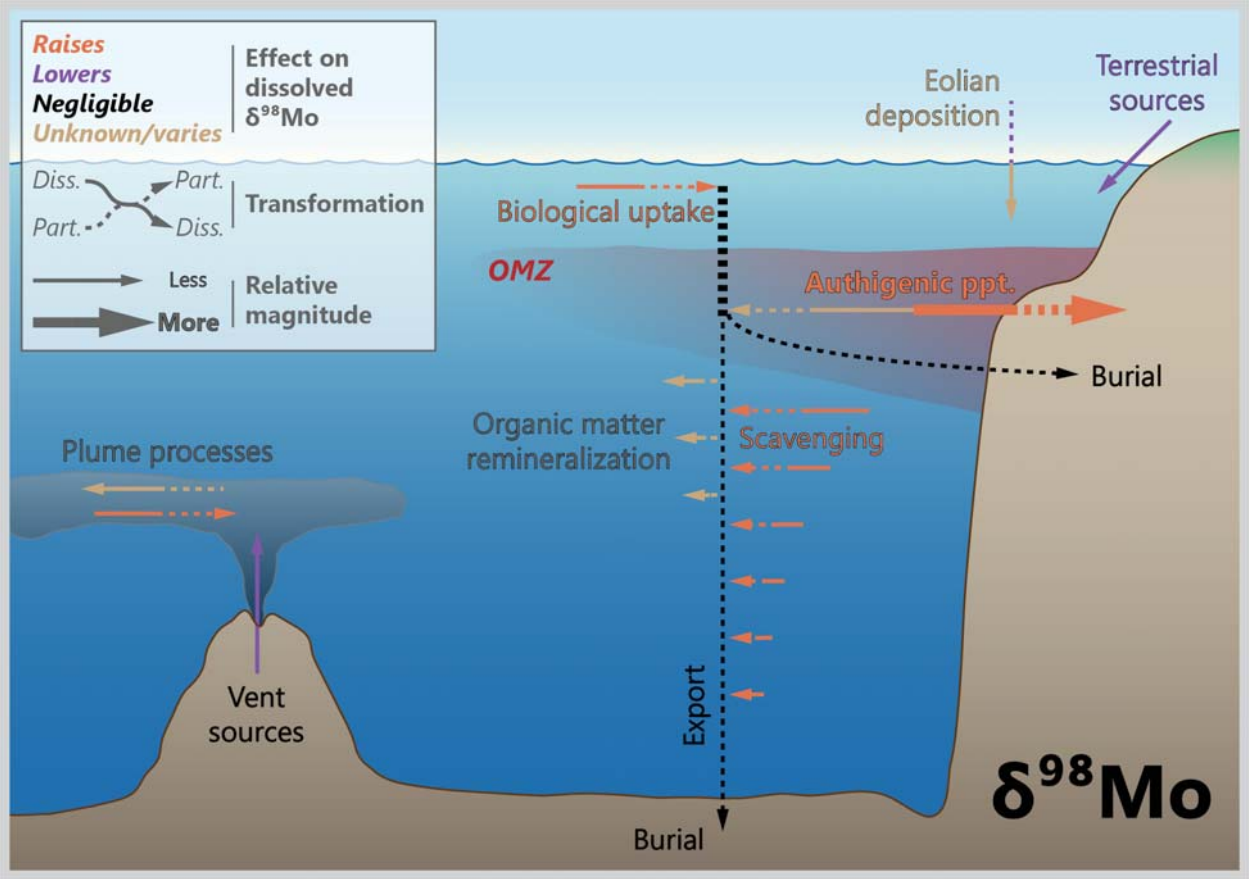

Figure 17 | Processes driving molybdenum isotope variations in modern seawater. While biological processes may exert a slight influence on surface water Mo distributions, the main drivers of marine Mo cycling are related to the balance between scavenging pathways, which are redox dependent.

7.2. Driving processes

7.2.1. Biological

Molybdenum is a bio-essential micronutrient required by enzymes that catalyze key reactions in the global C, N, and S cycles (Mendel & Bittner, 2006). Importantly, Mo is a co-factor of the primary nitrogenase enzyme complex, meaning that Mo is required for energy-efficient nitrogen fixation. Additionally, Mo is required for over 30 other enzymes that control biologically essential redox processes (Kendall et al., 2017). Despite its biological importance, biological activity does not appear to be a dominant process in setting the distribution of Mo in seawater (Fig. 17), likely due to the high abundance of Mo in the modern ocean. Results from the East Pacific Zonal Transect do, however, suggest some Mo removal by biological uptake and/or adsorption onto biogenic particles within regions of elevated chlorophyll (Ho et al., 2018). Experimental data indicate that biological uptake of Mo imparts a small negative isotope fractionation on the order of 0.3 ‰ (Wasylenki et al., 2007).

Enhanced removal of Mo from seawater in regions with high export of organic carbon likely explains some of the non-conservative behavior observed in modern coastal regions. A significant relationship between Mo and total organic carbon has also been observed in marine euxinic sediments (e.g. Helz et al., 1996; Algeo & Lyons, 2006; McManus et al., 2006; Lyons et al., 2009). Furthermore, it has been shown that Mo interactions with organic matter can control Mo cycling in both soils (Wichard et al., 2009; King et al., 2014, 2016; Marks et al., 2015; Siebert et al., 2015) and marine sediments (Wagner et al., 2017; Tessin et al., 2019). The formation of Mo complexes containing organic ligands has been proposed as an explanation for the correlation between sedimentary Mo and organic carbon, suggesting that organic matter may play an important role in both the delivery and burial of Mo in sediments (Wagner et al., 2017). Accordingly, it is possible that Mo accumulation in marine sediments is linked to export production and, more specifically, delivery and burial of organic carbon in sediments.

7.2.2. Chemical

Due to the long residence time and abundance of Mo, non-conservative Mo behavior is typically localized to areas with high particle concentrations, such as close to the continental margin, in the euphotic ocean, or around hydrothermal vents (e.g., Goto et al., 2020). In the present oxic water column, Mo is present primarily as the oxyanion molybdate (MoO_4^{2-}) and Mo sorption onto Mn oxyhydroxides represents the most significant modern Mo sink (Fig. 17; Bertine & Turekian, 1973; Scott & Lyons, 2012). Since the Fe–Mn oxide sink preferentially incorporates isotopically light Mo from seawater with an isotopic effect of ≈3.0 ‰, the fraction of Mo that is buried in Fe–Mn oxides exerts a major control over the Mo isotope composition of seawater.

In the presence of sulfide, the oxygen atoms in molybdate are progressively substituted for sulfur, producing particle reactive thiomolybdate species ($MoO_{4-x}S_x^{2-}$; Erickson & Helz, 2000; Vorlicek et al., 2015). Dissolved Mo can thus be strongly drawn down in sulfidic environments, such as the Black Sea. Importantly, this drawdown occurs with a small, but non-zero isotope effect of ≈0.5±0.3 ‰, whereby isotopically light Mo is preferentially scavenged (e.g., Nägler et al., 2011). Thiomolybdate is also scavenged in from sulfidic sediment porewaters leading to significant Mo accumulations within sediments deposited in anoxic and euxinic environments (e.g., Emerson & Huested, 1991; Crusius et al., 1996; Scott & Lyons, 2012). Long-term Mo burial is associated with Fe–S minerals (Chappaz et al., 2014; Vorlicek et al., 2018) and/or organic matter (Dahl et al., 2017; Tessin et al., 2019), depending on the biogeochemical conditions prevailing at a given basin.

7.2.3. Physical

The residence time of dissolved Mo is significantly longer than the mixing time of the ocean (Table 1). Thus, variations in dissolved [Mo] and δ^{98}Mo are not influenced by the geometry of modern overturning circulation. Whole-ocean changes in dissolved [Mo] and δ^{98}Mo are, however, possible, and much of what we know about such changes is gleaned from studies of the geological past, particularly during periods of ocean anoxia. Based on this research, it has been suggested that during intervals of lower ocean oxygenation, the ocean Mo inventory may have been low enough to limit marine primary productivity (Anbar & Knoll, 2002; Algeo, 2004; Glass et al., 2009; Reinhard et al., 2013). This limitation has been demonstrated in certain lake ecosystems (Goldman, 1960; Glass et al., 2012). Under strongly euxinic conditions ($[H_2S]_{aq}$>11 μM), thermodynamic calculations predict that tetrathiomolybdate (MoS_4^{2-}) becomes the most predominant species (Erickson and Helz, 2000), which can result in quantitative Mo drawdown from seawater into seawater with negligible isotope fractionation. Evidence from Lake Cadagno, the Black and Baltic Seas, and seasonally anoxic fjords supports the occurrence of near-quantitative drawdown of Mo from seawater in these environments (Neubert et al., 2008; Dahl et al., 2010; Nägler et al., 2011; Noordmann et al., 2015). Indeed, this hypothesis is the foundation of several paleoceanographic studies that assume that the sedimentary Mo isotopic signatures, deposited in euxinic settings, faithfully capture the δ^{98}Mo of oxygenated (surface) seawater and can be further interpreted in terms of the fraction of the seafloor that is oxygenated (e.g., Kendall et al., 2015; Dickson, 2017).

7.3. Sedimentary archives

The majority of Mo paleoceanographic studies focus on the measurement of Mo concentrations and isotopes within bulk sediments. While many applications of Mo within the sedimentary record focus on early Earth, Mo proxies have been used to constrain environmental conditions in the Holocene (e.g. Hardisty et al., 2016; van Helmond et al., 2018) and Pleistocene (e.g. Dean et al., 2006; Scholz et al., 2017). However, Mo and its isotopes are predominantly used as tracers of redox conditions and not productivity.

Research on biological archives of Mo concentrations and isotopes has met with mixed results. Research examining δ^{98}Mo in corals indicates that corals may accurately record seawater Mo isotope concentrations (Voegelin et al., 2009). However, follow-up studies suggested a temperature-dependent fractionation between seawater and corals that is related to the activity of symbiotic zooxanthellae (Wang et al., 2019b). Moreover, bivalve shell Mo:Ca ratios have been determined to have no relationship to oceanographic

conditions (Vihtakari et al., 2017), whereas Tabouret et al. (2012) suggest a mechanism related to trophic uptake, but not to ambient dissolved [Mo]. A third study proposed that Mo:Ca peaks in bivalve carbonate are controlled by ingestion of phytoplankton grown on nitrate due to high concentrations of Mo associated with nitrate reductase, indicating that bivalves may provide an archive for surface water nitrate uptake and a potential proxy for the balance between new and regenerated productivity (Thebault et al., 2009).

7.4. Prospects

At present, it does not appear that bulk sediment δ^{98}Mo will be useful for reconstructing biological productivity, even though Mo is cycled by organic matter both actively (e.g., Liermann et al., 2005; Wasylenki et al., 2007) and passively (e.g., Kowalski et al., 2013; King et al., 2018). That we see no pathway to using Mo as a productivity tracer reflects, in part, the difficulty in disentangling biological processes that exert relatively modest Mo isotope fractionations from those associated with thiomolybdate transformations (Tossell, 2005), or scavenging processes that possess large fractionation effects (e.g., Mn- or Fe-oxide scavenging; Siebert et al., 2003; Barling & Anbar, 2004; Wasylenki et al., 2008; Brucker et al., 2009; Goldberg et al, 2009; 2012). Additionally, within the modern ocean and likely within the recent geologic past, the global ocean reservoir of Mo is too large and well mixed for biological associated fractionations to significantly impact the global Mo isotopic composition.

The use of bulk sedimentary Mo concentrations as a proxy for export of organic carbon to the seafloor is more promising, but numerous caveats exist. Specifically, other mechanisms for enhanced delivery, sequestration, and burial complicate any efforts to quantitatively relate Mo enrichments to increased export productivity (e.g., Scholz et al., 2017). Redox conditions and, in particular, the presence of sulfide in the water column and sediment pore waters will be a primary control on Mo accumulation (e.g., Hardisty et al., 2018). Sedimentary Mo enrichments can also be produced through shuttling of Mo adsorbed to the surface of Fe and Mn oxides to the seafloor (Algeo & Lyons, 2006; Algeo & Tribovillard, 2009; Dellwig et al., 2010; Scholz et al., 2013). At a minimum, independent constraints on water column and pore water redox conditions using Fe speciation, other trace metals and/or fossil redox proxies are required before an argument can be made relating Mo concentrations to export productivity. Additionally, the quantitative relationship between Mo and organic carbon may be impacted by aqueous Mo concentrations, which may have varied over Earth's history, or if depositional environments become restricted (i.e., Mo drawdown leads to a lower Mo:TOC ratio; Algeo & Lyons, 2006). Conversely, the utility of bulk sediment Mo

concentrations and isotopes may lie in constraining redox conditions to improve the interpretation of other trace metal proxies that are more strongly controlled by primary and/or export productivity.

The most promising future avenue for Mo-based productivity proxies may emerge from fossil-specific measurements of Mo concentrations (and perhaps δ^{98}Mo). Currently, research has focused on large fossils (corals and bivalves) and has led to mixed results on the utility of Mo in reconstructing productivity-related parameters. However, analytical progress may allow for measurement of smaller sample sizes, which may provide opportunities to explore new archives of past marine Mo geochemistry.

8. Barium

Barium is a widely-used tracer of marine export production, past and present. This section provides an overview of marine Ba geochemistry, focusing on driving mechanisms, palaeoceanographic applications, and emerging insights from Ba stable isotopes. We close by suggesting several areas for additional research.

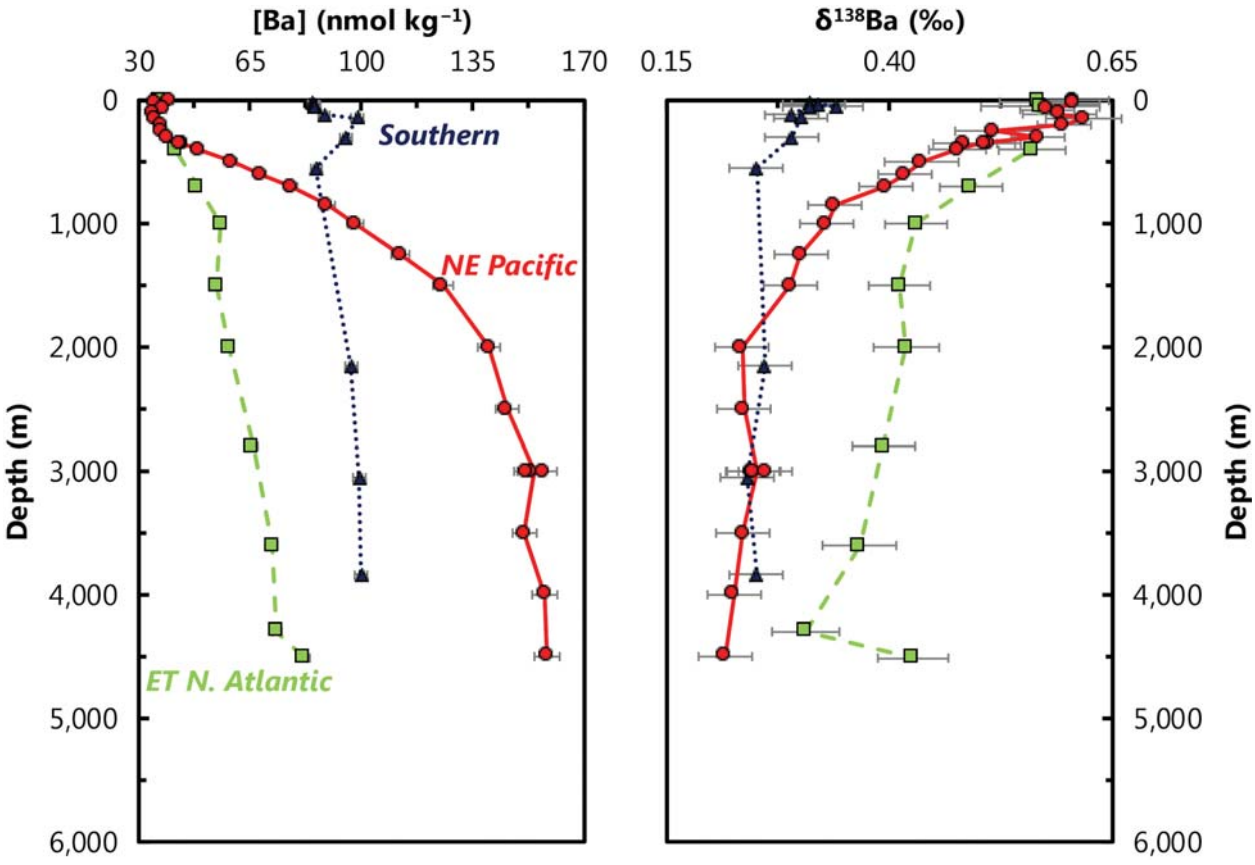

Figure 18 | Representative profiles of dissolved Ba concentrations ([Ba]) and Ba-isotopic compositions (δ^{138}Ba) from the Eastern Tropical North Atlantic (squares, dashed line), northeast Pacific (circles, solid line line), and Southern (triangles, dotted lines) Oceans. This comparison illustrates that the oceanographic processes leading to distinct dissolved concentration profiles render significant changes in dissolved δ^{138}Ba between basins.

8.1. Marine distribution

The nutrient-like distribution of dissolved Ba has been documented in the literature since the 1970's (e.g., Wolgemuth & Broecker, 1970). However, it was not until later in the decade that the GEOSECS Program fully revealed the three-dimensional marine distribution of Ba (e.g., Chan et al., 1976; 1977). These geochemical ocean sections highlighted vertical, zonal, and meridional variations in dissolved [Ba] related to the major biogeochemical and hydrographic features of the ocean. In nutrient-depleted surface waters, dissolved [Ba] exhibits low concentrations between 35–45 nM. Similarly, nutrient-replete deep waters are

enriched in [Ba], though typically by no more than a factor of four above surface values. The spatial resolution of GEOSECS illustrated the importance of hydrography; [Ba] increases along the meridional overturning circulation from ≈50 nM in deep waters of the North Atlantic, to ≈90 nM in the Southern Ocean, up to ≈180 nM in the deep northeast Pacific (Fig. 18; Chan et al., 1976; 1977).

Though it was long suspected that the major dissolved–particulate transformation of Ba was related to the mineral barite ($BaSO_4$; e.g., Chow & Goldberg, 1960; Turekian, 1968), this was not confirmed until the 1980's (e.g., Dehairs et al., 1980; Bishop, 1988). Barite crystals are now recognized as an ubiquitous component of marine particulate matter, with up to 10^4 discrete, micron-sized crystals present per L of seawater (Dehairs et al., 1980). However, the distribution of particulate $BaSO_4$ is distinct from primary biogenic phases that exhibit Martin-like distributions with maxima in the euphotic zone. The minimum particulate Ba concentration is typically situated in the euphotic zone and the maximum slightly below, usually in the upper mesopelagic (e.g., Ohnemus & Lam, 2015; Ohnemus et al., 2019). This distribution likely reflects the fact that neither Ba nor $BaSO_4$ are utilized for physiological processes by any of the major marine primary producers. Particulate Ba fluxes are nevertheless strongly correlated with export productivity in well-oxygenated environments (e.g., Bishop, 1988; Dymond et al., 1992; Francois et al., 1995; Dymond & Collier, 1996; McManus et al., 2002) and therefore sedimentary Ba abundances have been widely used as a proxy to reconstruct past changes in ocean export production (e.g., Francois et al., 1995; Paytan et al., 1996; Paytan & Griffith, 2007 and references therein; Costa et al., 2016, Winckler et al., 2016).

Recent studies of Ba stable isotope geochemistry have added a new dimension with which to study marine Ba cycling. Von Allmen et al. (2010) first reported that isotopically light Ba is preferentially incorporated into $BaSO_4$, with a particulate–dissolved Ba-isotopic offset of ≈−0.3 ‰. The direction of this offset implies that residual solutions, such as seawater, should exhibit Ba-isotopic compositions heavier than those of sedimented $BaSO_4$. This was corroborated for Atlantic seawater by Horner et al. (2015a), showing that dissolved $\delta^{138}Ba$ displays a mirror image of dissolved [Ba]: Ba-depleted surface water masses exhibited 'heavy' Ba-isotopic compositions (≈+0.6 ‰), whereas Ba-replete deep waters possessed 'lighter' values ≈+0.3 ‰. (Notably, all values are considerably heavier than the upper continental crust, which possesses $\delta^{138}Ba \approx 0.0 \pm 0.1$‰; Nan et al., 2018.) Similar patterns have since been corroborated in other ocean basins (Bates et al., 2017; Hsieh & Henderson, 2017; Bridgestock et al., 2018; Geyman et al., 2019; Cao et al., 2020; Fig. 18).

These isotopic studies have yielded a number of novel insights into the marine Ba cycle. First, these data underscore the importance of physical mixing (i.e., ocean circulation) in mediating patterns of dissolved

1462 δ^{138}Ba and, by extension, [Ba]. Second, both the regression of dissolved Ba-isotopic data (Bates et al., 2017;
1463 Hsieh & Henderson, 2017) and comparison of co-located seawater and particulates (Horner et al., 2017)
1464 imply an average particulate–dissolved Ba-isotopic offset ≈−0.5 ‰, somewhat larger than the experimental
1465 results reported by Von Allmen et al. (2010). Third, marine sediments—both bulk (Bridgestock et al., 2018)
1466 and $BaSO_4$ isolates therefrom (Crockford et al., 2019)—faithfully reflect the ≈−0.5 ‰ Ba-isotopic offset
1467 from surface seawater. Consequently, the mean δ^{138}Ba of globally-sedimented $BaSO_4$ is ≈+0.1±0.1 ‰
1468 (Crockford et al., 2019). Since $BaSO_4$ is the dominant oceanic output (e.g., Paytan & Kastner, 1996), these
1469 data imply that mean isotopic composition of Ba delivered to the ocean should possess an average
1470 composition ≈+0.1±0.1 ‰. At present however, the main Ba inputs are unable to close the marine Ba-
1471 isotopic budget: rivers, the principal Ba source to seawater, rivers, are too heavy, exhibiting compositions
1472 generally ≥+0.2 ‰ (e.g., Cao et al., 2020; Gou et al., 2020); and, groundwater discharge, while possessing
1473 the necessary 'light' composition of ≈+0.1 ± 0.1 ‰, is too small a Ba flux to balance the budget (Mayfield

et al., in press). Thus, either the marine Ba-isotopic budget is currently out of steady state, or an additional Ba source possessing a light isotopic composition remains to be identified.

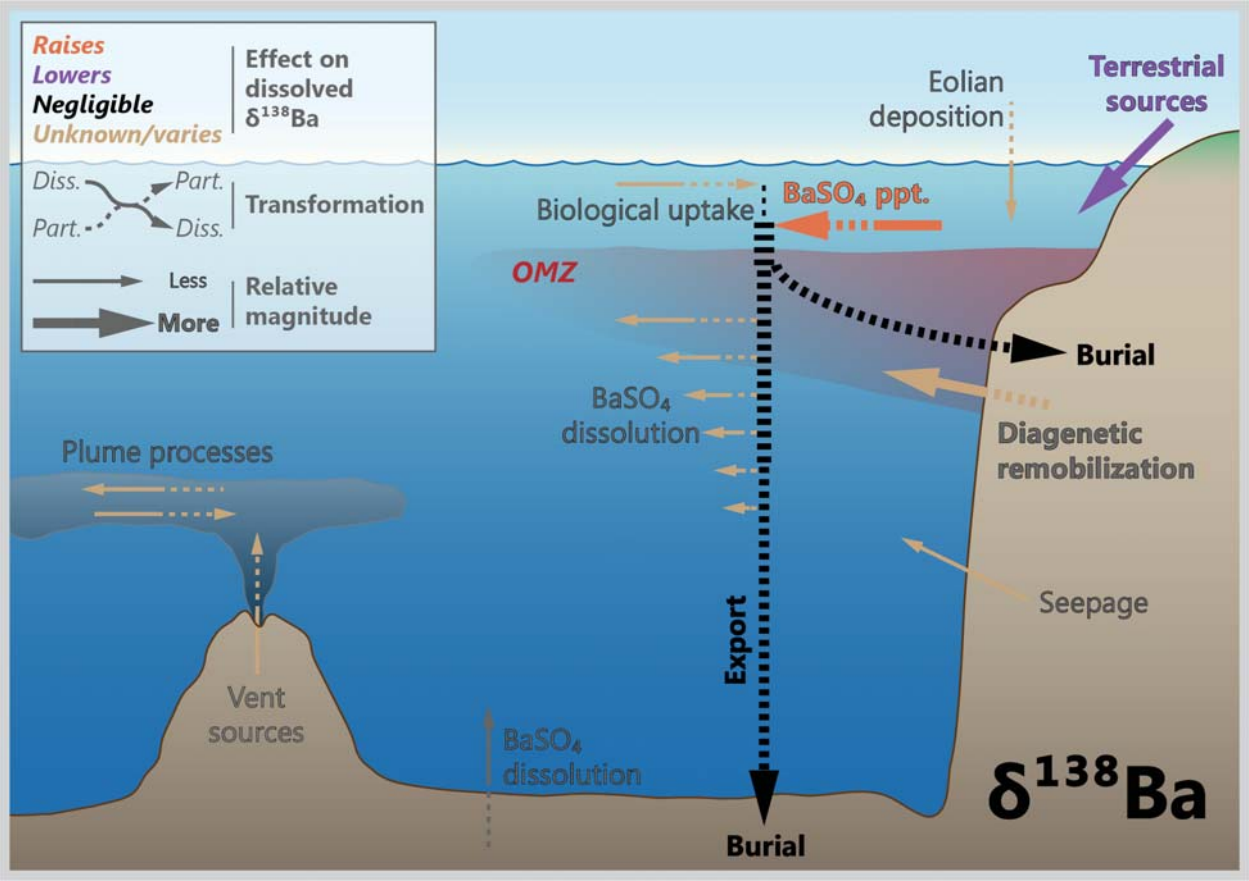

Figure 19 | Processes driving barium isotope variations in modern seawater. Though biological processes exert only a minor direct influence on δ^{138}Ba, the biologically-mediated cycling of $BaSO_4$ drives large variations in marine Ba isotope cycling, thereby connecting δ^{138}Ba to (paleo)productivity.

8.2. Driving processes

Seawater is undersaturated with respect to $BaSO_4$ almost everywhere (Monnin et al., 1999; Rushdi et al., 2000; Monnin & Cividini, 2006). However, micro-crystalline $BaSO_4$ is ubiquitous in the ocean. This 'barite

paradox' remains an area of active research. Proposed driving mechanisms broadly fall into two categories: 'active' biological and 'passive' chemical precipitation.

8.2.1. Biological

Several organisms are known to precipitate $BaSO_4$ intracellularly, possibly for the purposes of gravitropism (e.g., Gooday & Nott, 1982; Finlay et al., 1983). However, the organisms known to actively precipitate $BaSO_4$ are not abundant in seawater, nor do they constitute a significant fraction of marine primary productivity. Likewise, acantharea—organisms that precipitate $SrSO_4$ (celestite) tests that can contain considerable quantities of Ba (e.g., Bernstein & Byrne, 2004)—are not necessary for driving significant dissolved [Ba] drawdown in the ocean (Esser & Volpe, 2002) or for barite precipitation (Ganeshram et al., 2003). Thus, existing evidence does not support a significant role for active biological processes in driving marine Ba cycling (Fig. 19).

8.2.2. Chemical

Passive chemical precipitation is likely the major contributor to particulate $BaSO_4$ stocks and sedimentation. Given that seawater is largely undersaturated with respect to $BaSO_4$, passive precipitation is thought to occur within particle-associated microenvironments that are supersaturated with respect to $BaSO_4$ (e.g., Chow & Goldberg, 1960; Dehairs et al., 1987). The development of $BaSO_4$-supersaturated microenvironments is hypothesized to relate to the heterotrophic oxidation of organic matter (Chow & Goldberg, 1960), whereby Ba and sulfate ions are concentrated in chemically-isolated micro-zones during bacterially-mediated mineralization of organic matter. Once sufficient quantities of Ba and sulfate ions have accumulated and the microenvironment becomes supersaturated, $BaSO_4$ precipitation occurs. Thus, passive precipitation of $BaSO_4$ is possible even in strongly undersaturated environments with low ambient sulfate (e.g., Horner et al., 2017). Continued mineralization destroys the microenvironment, ceasing precipitation and exposing $BaSO_4$ precipitates to undersaturated seawater where they begin to dissolve.

The widespread association between pelagic $BaSO_4$ and aggregates of decaying organic matter provides indirect support for this process (Dehairs et al., 1980; Bishop, 1988). Indeed, the peak in particulate Ba—and presumably $BaSO_4$—abundance is found in the upper mesopelagic zone where most organic matter mineralization occurs (e.g., Sternberg et al., 2008). Microscale mechanisms remain unresolved, however; recent studies indicate that biofilms may play an important role accumulating Ba (e.g., Martinez-Ruiz et

al., 2018; 2019), which can promote precipitation of $BaSO_4$ nanoparticles from undersaturated solutions (Deng et al., 2019).

Regardless of the precise microscale mechanism, precipitation of particulate $BaSO_4$ is ubiquitous in the marine realm. Given that $BaSO_4$ precipitation renders a substantial negative isotope fractionation of ≈0.5 ‰, it is highly likely that $BaSO_4$ cycling drives much of the Ba isotope variability in the ocean (Fig. 19). From a paleoproxy perspective, this is ideal; $BaSO_4$ formation is related to the decay of organic matter and not by the presence of any specific organism (e.g., Jacquet et al., 2007; Dehairs et al., 2008). Downward transport of particulate $BaSO_4$ is driven by aggregation with larger particles (Lam & Marchal, 2014). The efficiency of this downward transport depends on the same biophysical processes that export organic matter, thus connecting the export flux of $BaSO_4$ to that of organic carbon (Fig. 19).

Barites formed in the ocean through this passive chemical pathway are commonly termed marine, pelagic, authigenic, or biogenic. Though none of these terms are perfect descriptors of the chemical processes involved, 'marine' and 'biogenic' are the most ambiguous and their use is discouraged; the former encompasses all $BaSO_4$ formed in the marine realm—including diagenetic, cold seep, and hydrothermal—whereas the latter could be taken to imply only those precipitates brought about by active biological processes. While 'authigenic' is an informative descriptor, it has also been used to describe sedimentary $BaSO_4$ that formed via diagenetic redistribution on or below the seafloor (e.g., Torres et al., 1996). Thus, we recommend use of the term 'pelagic' when describing chemically-precipitated microcrystalline $BaSO_4$, and encourage authors to include this definition in their works.

8.2.3. Physical

Barium exhibits a nutrient-like profile in the oceans, similar to that of Si (silicic acid) and alkalinity (Fig. 18). However, the extent to which this pattern arises from non-conservative biogeochemical processes versus physical mixing remains unresolved. Results from the GEOTRACES program are facilitating renewed interest into this topic, which is being investigated using two complementary approaches. In the first, biogeochemical contributions to basin-scale Ba distributions are isolated using statistical methods, such as OMPA (Optimum Multiparameter water mass Analysis). These statistical methods showed that mixing is dominant in the Mediterranean (Jullion et al., 2017) and North Atlantic (Le Roy et al., 2018), but that sea ice-related processes may be important in the Arctic (Hendry et al., 2018). Second, the influence of mixing is evidenced from emerging Ba stable isotope data. Indeed, the importance of mixing has been documented vertically (Horner et al., 2015a), zonally (Bates et al., 2017; Bridgestock et al., 2018), and

meridionally (Bates et al., 2017; Hsieh & Henderson, 2017). Together, these new approaches imply that *in situ* biogeochemical processes exert a relatively minor influence on basin-scale Ba distributions.

8.3. Marine archives

Given the connections between export production and $BaSO_4$ fluxes, the major archive of historical changes in Ba cycling is $BaSO_4$ itself. Indeed, the sedimentary accumulation of $BaSO_4$—most commonly determined as the fraction of Ba in excess of the detrital Ba background or the deposition rate of $BaSO_4$ itself—has been extensively used to reconstruct past changes in export production (e.g., Schmitz, 1987; Francois et al., 1995; Paytan et al., 1996; Frank et al., 2000; Jaccard et al., 2005; Jaccard et al., 2013; Ma et al., 2014; 2015, Costa et al. 2016, Winckler et al., 2016). An estimated 30 % of the $BaSO_4$ microcrystals formed in seawater are buried in oxygenated sediments (e.g. Dymond et al., 1992), a considerably higher fraction than for organic carbon (Paytan & Kastner, 1996). However, in oligotrophic regimes where both $BaSO_4$ fluxes and sedimentation rates are low, prolonged exposure to undersaturated seawater results in poor preservation (Eagle et al., 2003; Serno et al., 2014). Similarly, in high-productivity coastal upwelling settings, sedimentary mineralization of organic matter consumes oxygen present in pore waters, driving conditions down the redox tower and toward sulfate reduction, hampering $BaSO_4$ preservation (McManus et al., 1998; Paytan & Griffith, 2007; Carter et al., 2020).

Recently, the isotopic composition of Ba in bulk sediments has been investigated as a proxy for the Ba isotope composition of the Ba source (i.e., dissolved Ba in epipelagic and upper-mesopelagic seawater). Applications to date have explored the recovery of the biological carbon pump following the PETM (~56 Ma; Bridgestock et al., 2019) and the origin of enigmatic sedimentary $BaSO_4$ deposited in the aftermath of the Marinoan glaciation (~635 Ma; Crockford et al., 2019) and Great Oxidation Event (~2,000 Ma; Hodgskiss et al., 2019). Proceedings from recent geochemistry conferences indicate that many more investigations are underway.

Lastly, the amount—and, more recently the isotopic composition (e.g., Hemsing et al., 2018; Geyman et al., 2019; Liu et al., 2019)—of Ba in marine carbonates has been extensively used to reconstruct the Ba content of past environments. These studies are not discussed here as they only indirectly relate to productivity, and instead pertain primarily to reconstructing ocean circulation and/or terrestrial runoff.

8.4. Prospects

Barium exhibits several nutrient-like properties. Dissolved Ba distributions resemble those of other nutrients and particulate abundances are intimately associated with the processes of organic carbon remineralization and export. Despite these connections, several aspects of Ba cycling—both in the modern and past oceans—remain unresolved. We suggest several areas for additional research that will help widen the applicability of Ba-based proxies in paleoceanography.

8.4.1. Modern

Several questions persist regarding the modern Ba cycle. Below we list three and offer possible remedies to each.

- To what extent do the similar distributions in [Ba], [Si], alkalinity, and [^{226}Ra] reflect true biogeochemical coupling versus passive physical mixing? As noted above, statistical analysis of Ba (and Si, Ra) distributions in regions will offer valuable insights, particularly if conducted in regions with weaker overturning circulation. Likewise, additional profiles of dissolved Ba isotope distributions will enable quantification of mixing relationships.
- Closing the Ba-isotopic mass balance of the ocean. This will require detailed evaluation of other putative Ba sources, such as hydrothermal vents, cold seeps and other benthic sources (e.g., Hoppema et al., 2010), atmospheric deposition, and the importance of estuarine enhancement of riverine Ba fluxes (e.g., Hanor & Chan, 1977; Edmond et al., 1978) as well as Ba fractionation associated with other phases like the adsorption on Fe-Mn oxyhydroxides.
- What is the mechanism of $BaSO_4$ precipitation? While the microenvironment-mediated model appears most likely, the (bio)chemical mechanisms of precipitation remain ambiguous: How and from what are Ba and sulfate ions liberated during bacterial mineralization? How are they accumulated? Do different substrate organisms and/or heterotrophic communities influence the amount of $BaSO_4$ precipitated? Addressing these questions will require additional field and laboratory studies, which can then be compared against distributions of particulate $BaSO_4$ in the ocean interior. Depending on their importance, these nuances may require ecological parameterizations in numerical models of Ba cycling.
- Narrowing estimates of the fractionation factor between $BaSO_4$ and seawater. Existing laboratory studies place this estimate ≈ -0.3 ‰, whereas a wide-range of field data suggest that it is considerably larger at ≈ -0.5 ‰. Accounting for this ≈ 0.2 ‰ difference is both important and

justifies additional experimentation, as it indicates incomplete understanding of the processes that fractionate Ba isotopes in the marine realm.

8.4.2. Paleo

As with the modern cycle, several ambiguities persist. Assuming that $BaSO_4$ remains the preferred archive of past Ba cycle variations, the most pressing relates to diagenesis.

- What is the effect of early diagenesis on the Ba isotope composition of sedimentary $BaSO_4$? Likewise, do diagenetic $BaSO_4$ retain any primary Ba isotope information? Assessing these questions will require studies of co-located $BaSO_4$ and porewaters from environments at various stages of early diagenesis. Answering these questions is critical in establishing the validity of Ba isotopes in barite as a paleoceanographic proxy.
- Are $BaSO_4$ accumulation rates impacted by ambient [Ba]? Related to the question concerning $BaSO_4$ precipitation mechanisms above, it is presently unknown if the quantity of $BaSO_4$ yielded by remineralization is impacted by ambient [Ba]—does more $BaSO_4$ precipitation occur at higher ambient [Ba]? Likewise, to what extent does $BaSO_4$ preservation depend on ambient [Ba]? These considerations are significant when considering longer-term records, particularly when marine sulfate levels were lower-than-modern (and [Ba] presumably higher; e.g., Hanor, 2000; Wei & Algeo, in press). Finally, does the seawater temperature at the depth of POC mineralization impact the relationship between POC and barite formation? These questions are best addressed through a combination of experimentation (e.g., cultures, precipitation), field studies in basins with large gradients in [Ba], and numerical experiments incorporating saturation state modeling.

9. Nickel

9.1. Marine distribution

Nickel has a classic nutrient-type distribution in the oceans with one unusual feature; surface dissolved Ni concentrations never drop below around 1.8–2 nmol kg^{-1} (e.g., Sclater et al., 1976; Bruland, 1980; Fig. 20). There is evidence, however, that this residual pool in surface waters is not bioavailable, as summarized recently by Archer et al. (2020). Deep water dissolved Ni concentrations are 4–5 nmol kg^{-1} in the Atlantic, and ~9 nmol kg^{-1} in the north Pacific (Fig. 20).

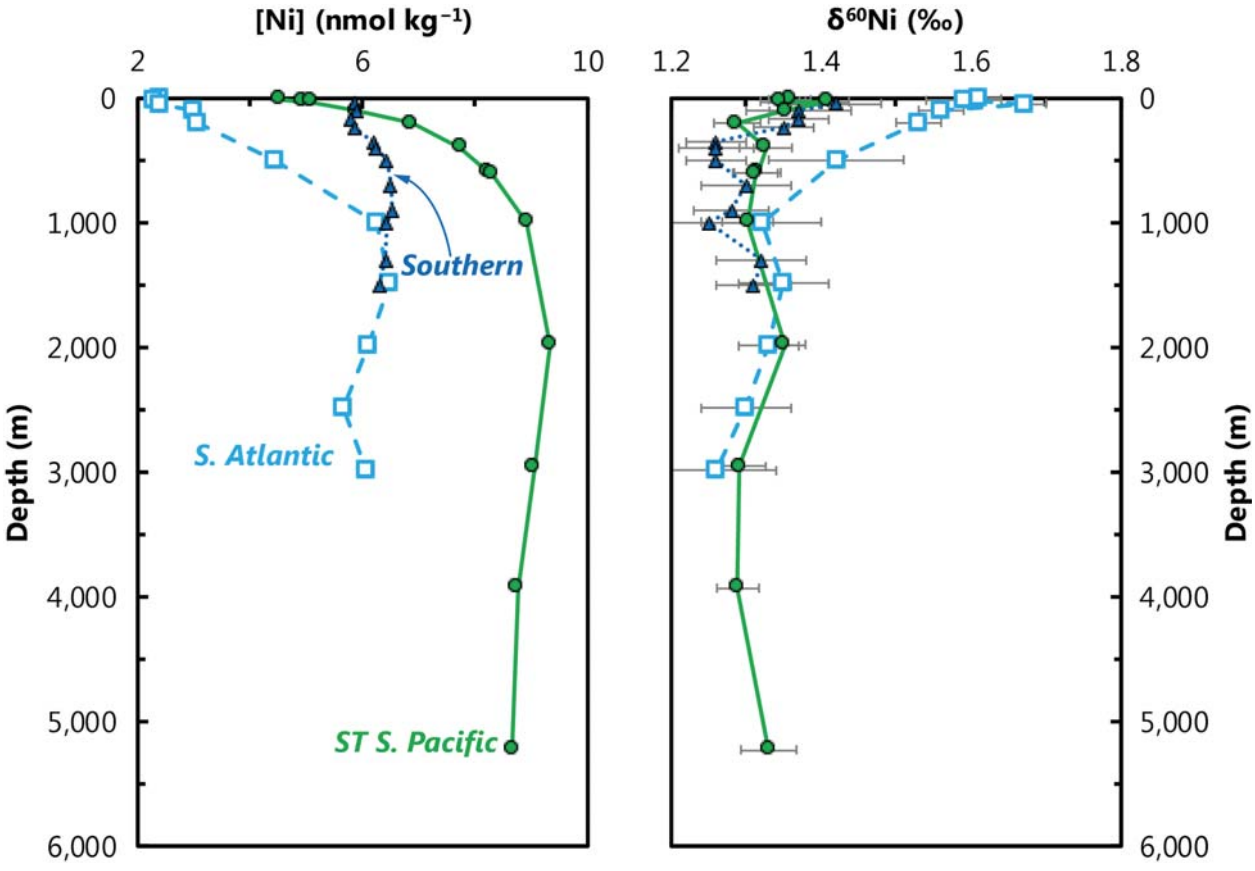

Figure 20 | Representative profiles of dissolved Ni concentrations ([Ni]) and Ni-isotopic compositions (δ^{60}Ni) from the South Atlantic (squares, dashed line), Southern (triangles, dotted line), and Subtropical South Pacific (circles, solid line) Oceans. This comparison illustrates that the oceanographic processes leading to distinct dissolved concentration profiles render only small changes in dissolved δ^{60}Ni between basins.

Developing robust analytical protocols for analyzing Ni isotopes for a range of sample matrices has proven somewhat more challenging than for some of the other TEIs discussed here due to the difficulty in separating Ni from interfering elements (e.g., Fe, a major isobaric interference on ^{58}Ni). Chemical purification protocols now use a sequence of resins including anion exchange (e.g., AG MP-1M or AG1-

X8, Bio-Rad) and either a Ni-specific resin (containing dimethylglyoxime) or Nobias PA-1 (Hitachi High Technologies; e.g., Cameron et al., 2009; Gueguen et al., 2013; Wang et al., 2019a; Yang et al., 2020). The limited data subsequently reported for the oceanic dissolved pool of Ni is isotopically homogeneous at depth (δ^{60}Ni ≈+1.3 ‰), with a small shift towards heavier values (up to +1.7 ‰) in the upper water column (Takano et al., 2017; Wang et al., 2019a; Yang et al., 2020; Archer et al., 2020). The latter is proposed to reflect a small kinetic isotope fractionation during biological uptake. Similar to Zn, Cu, Cd, Mo, and Ba, the isotopic composition of Ni in seawater is isotopically heavy compared to the UCC (Table 1).

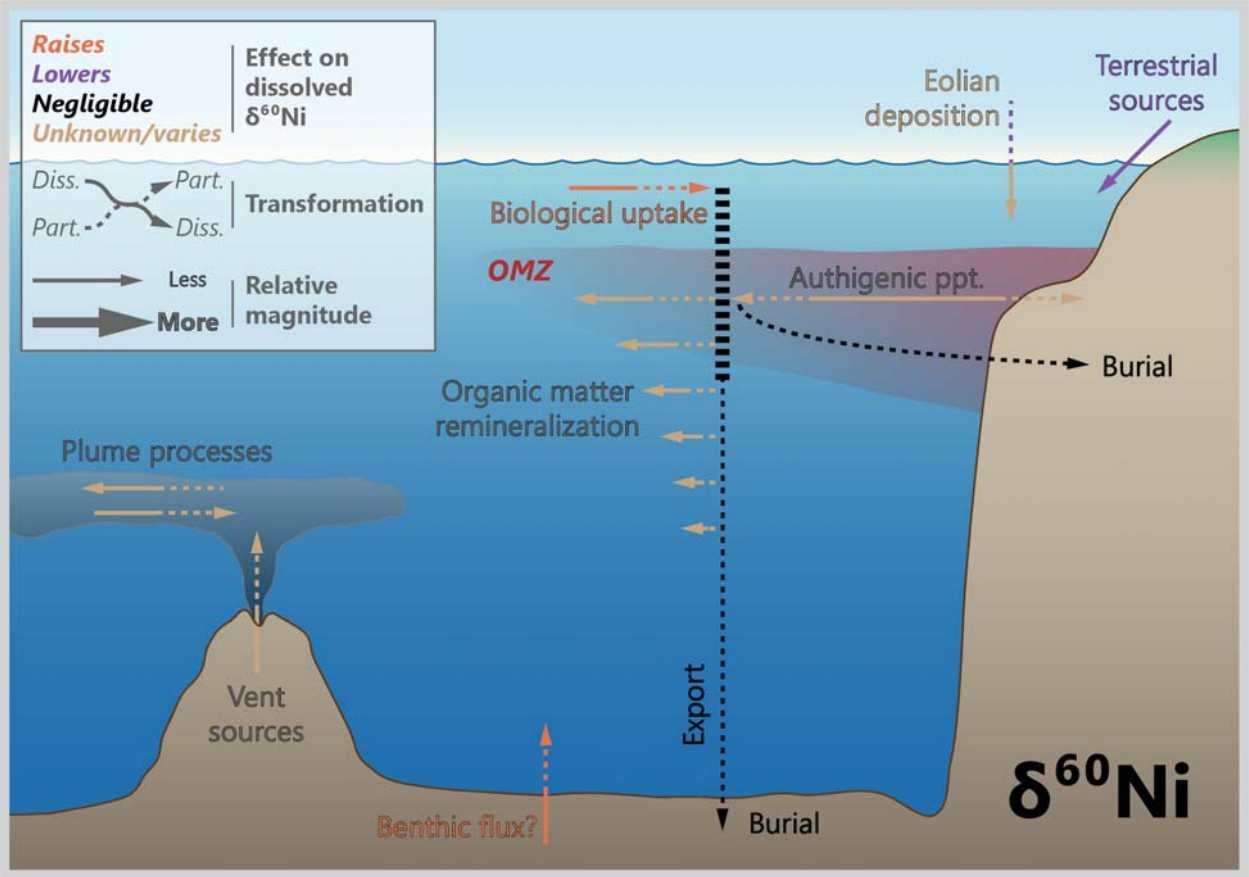

Figure 21 | Processes driving nickel isotope variations in modern seawater. Biological processes are recognized to drive a small, but systematic increase in dissolved δ^{60}Ni and marine Ni isotope values are preserved in certain sediments. Other abiotic Ni cycling processes may be important however, such as sorption to Mn-oxide minerals, and the significance of these fractionations to global Ni cycling remains to be fully elucidated.

9.2. Driving processes

9.2.1 Biological

To date, eight Ni-based enzyme systems have been identified (Ragsdale, 2009), including urease, which is key to the global nitrogen cycle, and methyl-CoM reductase, which catalyses the production of all biologically generated methane on Earth. The obligate requirement of methanogens for Ni has led to interest in developing Ni and Ni isotopes as a tracer of methane production on the early Earth (e.g. Cameron et al., 2009; Konhauser et al., 2009; Wang et al., 2019c). In the modern ocean the highest Ni quotas are found in diazotrophs (N-fixers), thought to reflect the presence of Ni-Fe hydrogenases (which catalyse H_2 produced during N fixation), Ni-superoxide dismutase (Ni-SOD) and urease (Tamagnini et al., 2002; Dupont et al., 2008a; 2008b; Nuester et al., 2012). Nickel limitation of phytoplankton grown on urea has been shown in culture and in natural assemblages, suggesting the Ni-N co-limitation of phytoplankton growth may be relevant in the ocean (Price & Morel, 1991; Dupont et al. 2008a; 2010). Significant Ni is also found in diatom frustules (about 50 % of diatom cellular quotas; Twining et al., 2012). The latter observation is thought to play a role in the similarity of Ni and Si oceanic distributions (Twining et al., 2012).

No culture data are available to determine the degree of Ni isotope fractionation during biological uptake. Upper ocean data suggest no fractionation or a small preference for the light isotope (up to $\alpha \approx 0.9997$; Takano et al., 2017; Archer et al., 2020; Yang et al., 2020; Fig. 21), consistent with the Ni isotope systematics observed in organic-rich sediments (Ciscato et al., 2018) and water column particulates (Takano et al., 2020). Interestingly, new water column data from the South Atlantic suggest distinct ecological differences in Ni drawdown and Ni isotope fractionation compared to other TEIs (e.g., Zn, Cd). Limited drawdown and Ni isotope fractionation is observed in the diatom-dominated regime south of the Polar Front in the Southern Ocean. In contrast, more marked drawdown and significant Ni isotope fractionation is observed north of the Polar Front, which has been attributed to the predominance of nitrate-limited, Ni-requiring cyanobacteria (Archer et al., 2020).

9.2.2 Chemical

Nickel is partially complexed by strong organic ligands in coastal and open ocean environments (5–70 %; e.g., Donat et al., 1994; Saito et al., 2004; Boiteau et al., 2016), though slow water exchange kinetics of Ni make these complexation measurements particularly challenging (Hudson & Morel, 1993). Slow exchange kinetics may also explain the residual pool of non-bioavailable Ni in the surface ocean (e.g., Mackay et al.,

2002; Dupont et al., 2010). Speciation models suggest that the remainder of the Ni is present as free Ni^{2+} and $NiCl^{+}$, with a small fraction present as $NiCO_3^{0}$ (Zirino and Yamamoto, 1972; Turner et al., 1981).

Nickel cycling is tightly coupled to that of Mn, in sediments, pore waters, and across the redoxcline of the Black Sea (e.g., Klinkhammer, 1980; Koschinsky and Hein, 2003; Vance et al., 2016). In the Black Sea, for example, Mn redox cycling is associated with preferential sorption of light Ni isotopes, with a large negative fractionation of ≈–4‰ (Vance et al., 2016). This large fractionation is consistent with experimental sorption of Ni on birnessite (Wasylenki et al., 2014; Sorensen et al., 2020).

Unlike more strongly chalcophile elements like Cd, Cu, and Zn, dissolved Ni is not strongly drawn down in the euxinic portion of the Black Sea water column (Tankéré et al., 2001; Vance et al., 2016). However, Ni is enriched in Black Sea sediments (Little et al., 2015), with δ^{60}Ni compositions notably lighter (at +0.3 to +0.6‰) than Ni sources to the basin (at about +1.3‰; Vance et al., 2016; Fig. 21). Vance et al. (2016) attributed these light isotope compositions to the scavenging of sulfidized Ni species, which are predicted to be isotopically light (Fujii et al., 2011b).

9.2.3 Physical

The most recent estimate for residence time of Ni in the ocean is approximately ~20 kyr (Little et al., 2020), considerably longer than the mixing time of the ocean. As a result, in parallel with the other TEIs discussed herein, Ni and Ni isotope distributions are modulated at first order by the geometry of physical ocean circulation. The importance of diatom uptake in the Southern Ocean in partially coupling oceanic Ni and Si (Twining et al., 2012) was introduced above, and the homogeneity of deep ocean Ni isotope compositions supports an important role for southern-sourced water masses in the Ni distribution (Takano et al., 2017; Wang et al., 2019a; Archer et al., 2020).

9.3. Marine archives

9.3.1. Ferromanganese sediments

Ferromanganese crusts exhibit variable Ni isotope compositions (Fig. 22; Gall et al., 2013; Gueguen et al., 2016), which are, on average, slightly isotopically heavier (at δ^{60}Ni of +1.6‰) than seawater (δ^{60}Ni at about +1.3‰). However, experiments suggest that sorption of Ni to birnessite (the primary Ni-hosting phase in Fe–Mn sediments) should be associated with a large negative isotope effect (of about 3 to 4 ‰; Wasylenki

et al., 2014; Sorensen et al., 2020). It remains unclear why the full isotope effect is not expressed in Fe–Mn crusts. Intense Mn cycling occurs across the redoxcline of the Black Sea; this cycling is associated with large variations in Ni and Ni isotopes, consistent with the experimentally observed light isotope effect on sorption to birnessite (Vance et al., 2016). Recent data from Mn-rich sediments that have undergone diagenesis also point to the preservation of a large negative Ni isotope effect (Little et al., 2020).

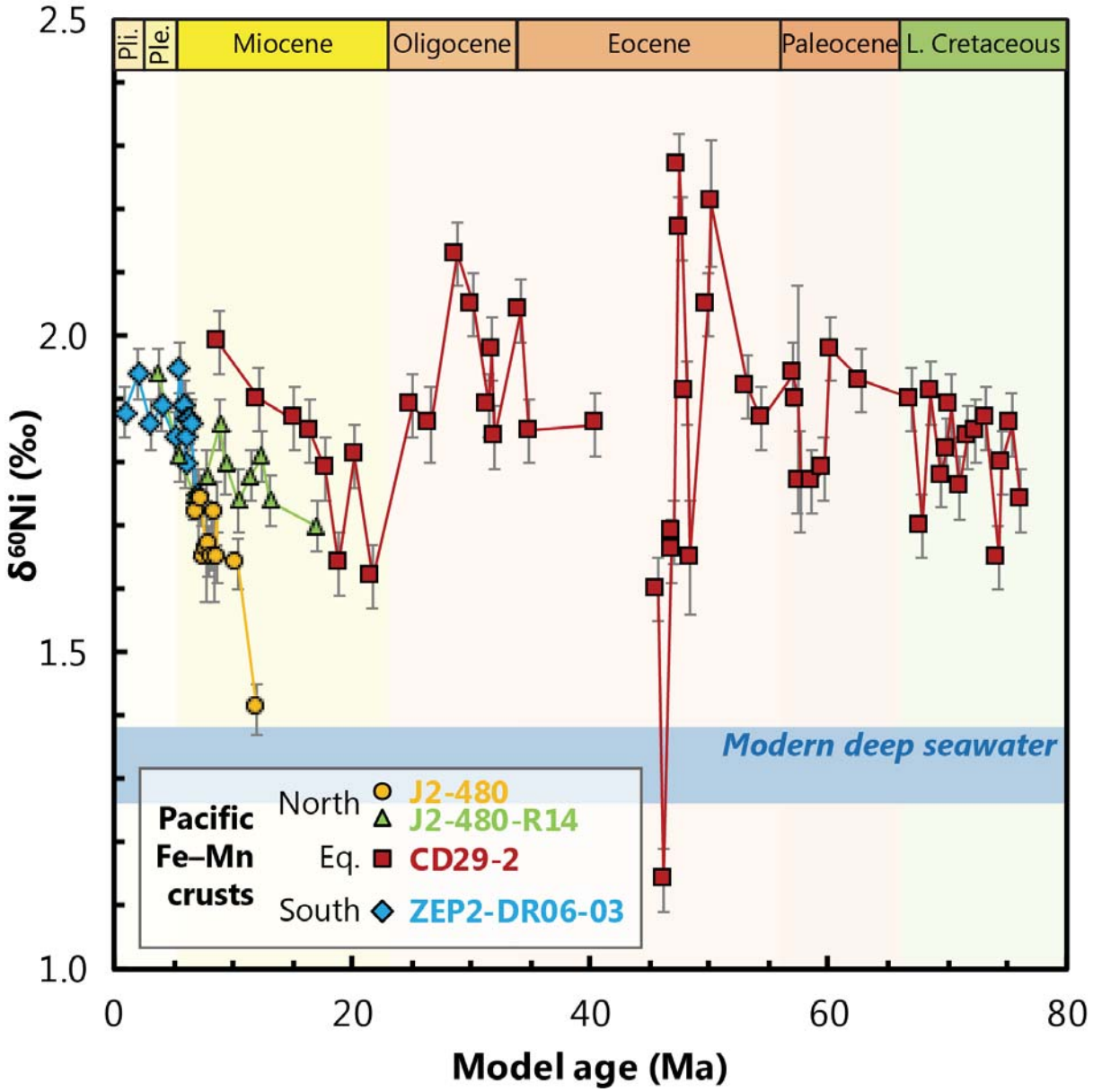

Figure 22 | Four Fe–Mn records of Ni isotope compositions from the Pacific Ocean. Assuming that Fe–Mn crusts have always formed with an offset ≈+0.5 ‰ with respect to ambient dissolved Ni in seawater, these records illustrate that the Ni isotope composition of seawater has varied by only ±0.2 ‰ over the Cenozoic. Data for J2-480, J2-480-R14, and ZEP2-DR06-03 are from Gueguen et al. (2016). Data from CD29-2 are from Gall et al. (2013). All four records have been plotted using the authors' preferred age model, meaning that there are some differences between the chronology of CD29-2 shown here compared to Figs. 5, 14.

Though promising, the development of Fe–Mn crusts as a tracer of past oceanic Ni cycling awaits a mechanistic understanding of the processes driving their variably isotopically heavy signature, as well as an awareness of the likely complicating role of diagenetic remobilisation of Ni (e.g., Atkins et al., 2016; Little et al., 2020).

9.3.2. Organic-rich sediments

As introduced in section 5.3.2 (Cu), qualitative arguments for high organic matter fluxes (i.e., increased paleoproductivity) have been made based on elevated Cu and Ni concentrations in ancient organic-rich sediments (e.g., Tribovillard et al., 2006). For Ni, this approach is supported by positive correlations with TOC in modern continental margin sediments (Fig. 23).

Nickel does not precipitate in the presence of water column dissolved sulfide and is therefore a better candidate for the Metal–TOC approach than the more strongly chalcophile elements, like Cu. Nevertheless, Ni cycling is strongly linked to the redox cycling of Mn, so prerequisite (2)—that depositional environments remain reducing—is critical. In addition, sedimentary and water column data from the Black Sea indicate that the Fe–Mn redox shuttle provides an alternative supply route for Ni to sediments in these settings (Little et al., 2015; Vance et al., 2016). Finally, an open marine setting (prerequisite 3) would be required to make estimates of the relative productivity of two different sites based on their absolute measured Ni:TOC ratios. Otherwise the degree of basin restriction will exert the primary control on nutrient supply, and therefore the degree of trace metal enrichment (Algeo & Maynard, 2008; Little et al., 2015).

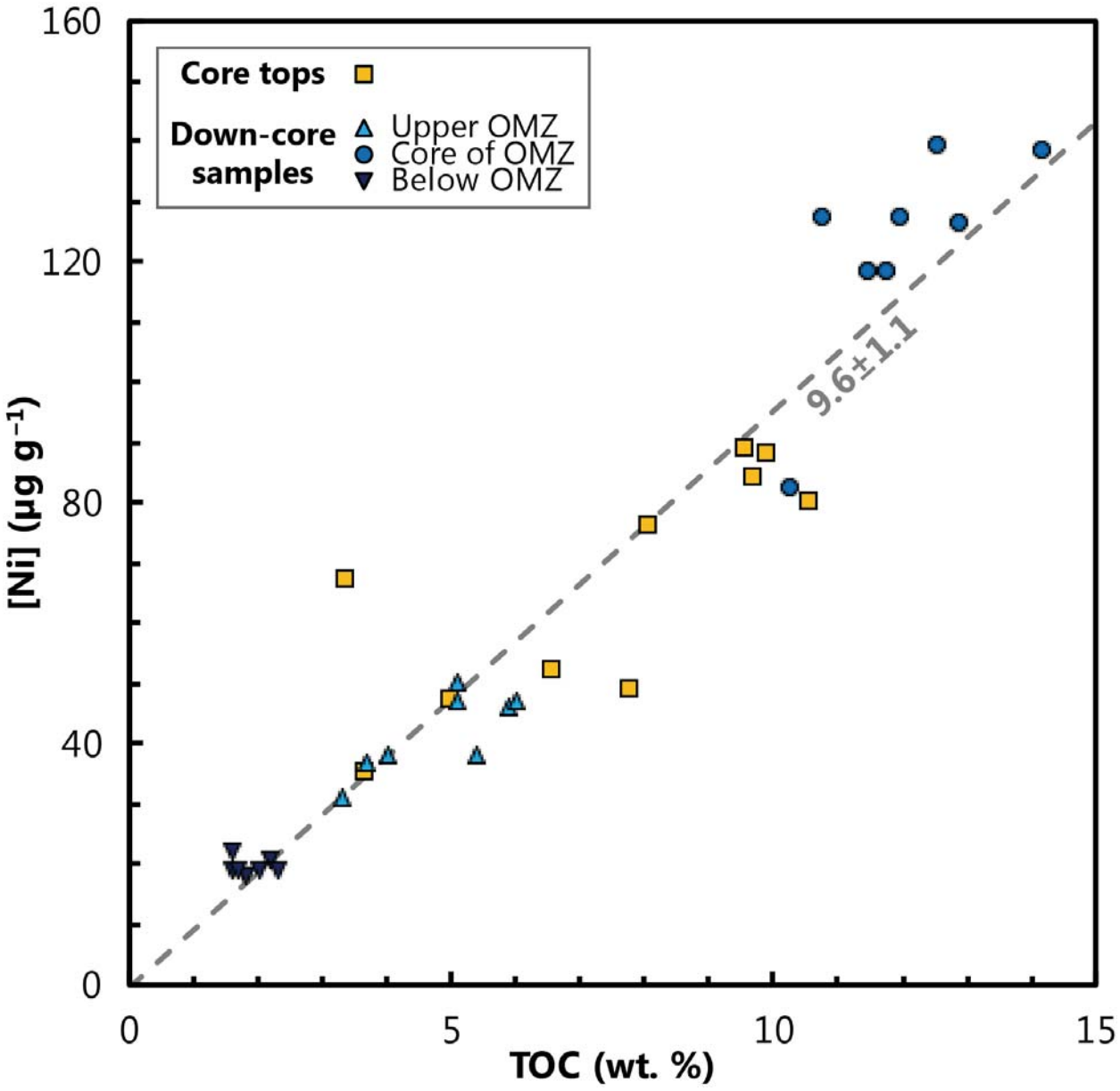

Figure 23 | Correlation of Ni and TOC content in organic-rich sediments from the Peru Margin. Data from Ciscato et al. (2018). The best-fit regression of these data yields a Ni–TOC slope of 9.6±1.1 (mean ± 2 SD), similar to the "≈9" reported by Böning et al. (2015).

Ciscato et al. (2018) investigated the distribution of Ni and its isotopes in two fractions isolated from Peru margin organic-rich sediments. The HF-HCl digestible fraction (usually containing >80% of total Ni) exhibited δ^{60}Ni values similar to modern deep seawater (at about +1.2‰). Meanwhile, these authors found variable Ni isotope compositions in the organic-pyrite fraction (OPF), which they suggested record the fractionation imparted by biological uptake in the photic zone. Systematic relationships between Ni–TOC,

1761 $\delta^{60}Ni_{OPF}$, and $\delta^{13}C$ indicate that there is merit in continuing to investigate Ni and Ni isotopes as a
1762 paleoproductivity tracer (Ciscato et al., 2018).

1763

1764 **9.4. Prospects**

1765 To date, Ni and its isotopes have been under-developed as a potential paleoproductivity proxy. Recent data,
1766 both from the dissolved phase in seawater and in two different fractions isolated from anoxic organic-rich
1767 sediments, suggest promise in the coupling of Ni and C and their isotopes. However, in oxic-to-suboxic
1768 settings, Ni and its isotopes in sediments are strongly influenced by the diagenetic redox cycling of Mn. In
1769 these settings, we recommend exploratory Ni and $\delta^{60}Ni$ work focusing on carbonate and siliceous
1770 biominerals, work that is increasingly tractable with new and improved chemical separation and analytical
1771 techniques.

1772 Finally, in a completely different approach, Wang et al. (2019c) present $\delta^{60}Ni$ values of Precambrian glacial
1773 diamictites, which are suggested to represent the chemical weathering residues of the UCC. They find a
1774 small shift towards heavier Ni isotope compositions across the Great Oxidation Event, which they relate to
1775 the onset of oxidative weathering of crustal sulfides (Wang et al., 2019c). Combined with the proposed
1776 importance of Ni to the maintenance of methanogenesis during this time period (e.g. Konhauser et al.,
1777 2009), it is hoped that future Ni stable isotope analyses will shed further light on the paleoenvironmental
1778 conditions on the early Earth.

1779

10. Silver

10.1. Marine distribution

Silver is the scarcest of the TEIs described here, both within Earth's crust and in the modern ocean. Moreover, Ag is an usual candidate for a paleoproductivity proxy given that it possesses no known biological function and is most widely known for its antimicrobial properties. Despite this, Ag exhibits a characteristic nutrient-like profile in seawater, most similar to that of Si (and Zn, Ba; Fig. 24).

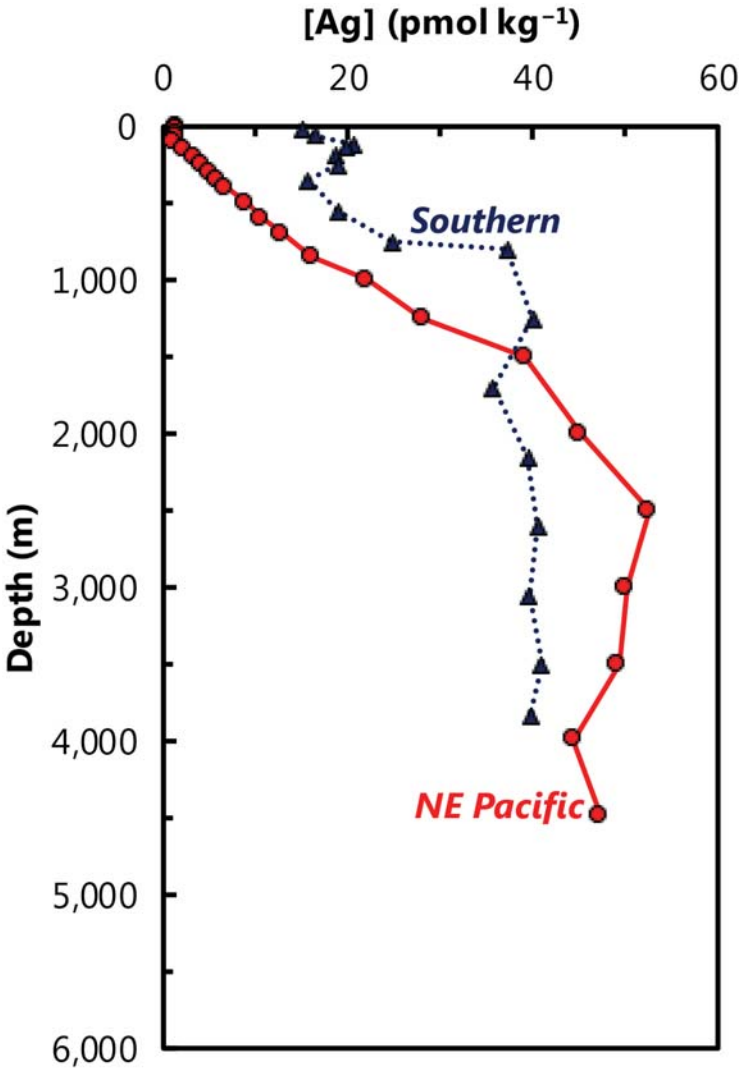

Figure 24 | Representative profiles of dissolved Ag concentrations ([Ag]) from the Northeast Pacific (circles, solid line) and Southern (triangles, dotted line) Ocean. No Ag-isotopic data for seawater are available at this time.

Dissolved Ag occurs primarily as chloride complexes in seawater (Cowan et al., 1985, Miller & Bruland, 1995) and exhibits a nutrient-type depth profile. Dissolved [Ag] in surface waters is typically <5 pmol kg^{-1}, and ranges from 5–30 pmol kg^{-1} in deep waters of the Atlantic Ocean to 50–114 pmol kg^{-1} in the Pacific

Ocean (Fig. 24; Flegal et al., 1995; Rivera-Duarte et al., 1999; Ndung'u et al., 2001; Zhang et al., 2001; 2004; Ranville and Flegal, 2005; Boye et al., 2012). The total observed range in seawater is 0.2–115 pmol kg^{-1} (Gallon and Flegal. 2014). Despite its potential as a biogeochemical proxy, no Ag isotope data yet exist for dissolved or particulate phases in the water column, nor in marine sedimentary archives. Accordingly, we cannot directly assess the utility of Ag isotopes to infer paleoproductivity, though we can deduce a number of processes that are likely to influence dissolved δ^{109}Ag based on the processes known to cycle Ag (Fig. 25).

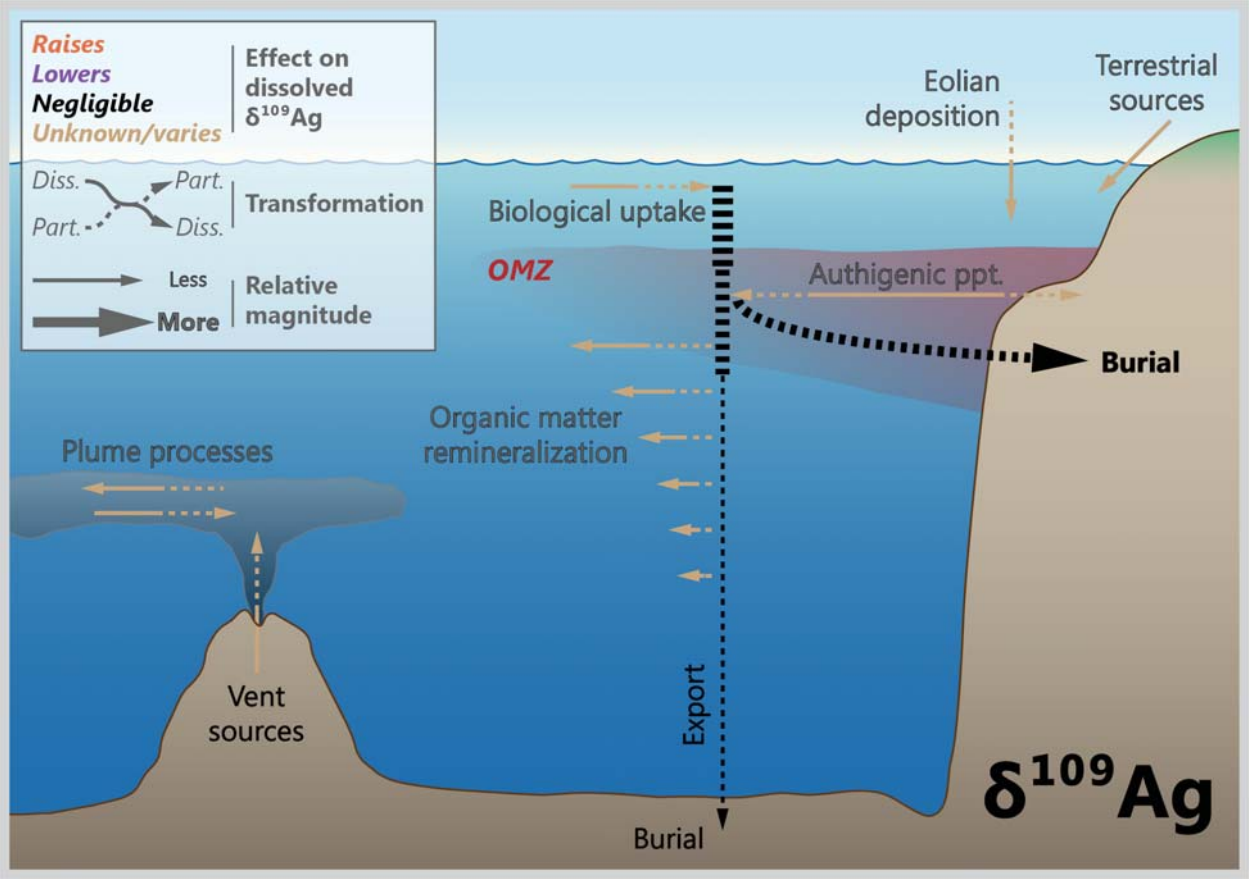

Figure 25 | Processes likely to drive silver isotope variations in modern seawater. Despite there being no Ag isotope data for seawater at this time, we can infer a number of processes that are most likely to influence dissolved δ^{109}Ag from measurements of [Ag] in seawater and sediments.

10.2. Driving processes

The 1D depth profile for dissolved Ag is similar to that of Si (and Zn, Ba), resulting in a strong positive correlation between these elements (Fig. 1). This has led researchers to suggest that Ag is taken up by diatoms, incorporated into their frustules, and then released as the frustules dissolve (e.g., Flegal et al.,

1995). Silver might then be delivered to the seafloor with opal, potentially making it useful as a paleoproductivity proxy (Friedl & Pedersen, 2002). However, the correlation between dissolved Ag and Si is non-linear, indicating that other factors are at play (Zhang et al., 2001; 2004). Furthermore, while Ag is taken up by various types of phytoplankton, including diatoms (Fisher & Wente, 1993), experiments conducted using the marine diatom *Thalassiosira pseudonana* show that most of the Ag is associated with the organic fraction rather than the opal (Wagner, 2013; Fig. 25). Martin et al. (1983) also hypothesized that high particulate Ag concentration within the euphotic zone (40–70 m) off the west coast of Mexico were due to the formation of Ag-organic complexes. Interestingly, particulate Ag concentrations are even higher well below the euphotic zone, at a depth corresponding to the upper portion of the oxygen minimum zone (Martin et al., 1983). It could also be that a global Ag:Si correlation arises at least in part from biological processes occurring int he surface of the Southern Ocean, whereby intermediate and mode water masses with low preformed [Ag] are advected to lower latitudes, analogous to the mechanism proposed for Zn–Si (Vance et al., 2017) and Ba–Si coupling (Horner et al., 2015a). If correct, Ag is unlikely to be coupled directly to opal with a simple relationship that can be used to reconstruct past diatom productivity.

Dissolved Ag cycling may become decoupled from productivity by possessing different source and sink terms relative to carbon and the macronutrients (Gallon and Flegal, 2014 and references therein). For example, Ranville & Flegal (2005) and Ranville et al. (2010) invoked an anthropogenic aerosol source of Ag to surface and intermediate waters to explain north Pacific water column data. Other complications may arise in low-oxygen environments—waters from the northeast Pacific (Kramer et al., 2011) and southeastern Atlantic (Boye et al., 2012) exhibit a deficit in dissolved Ag relative to Si within their respective OMZs. These deficits imply preferential removal of Ag over Si, which may occur locally or 'upstream'. If occurring locally, a putative mechanism is (co-)precipitation with other chalcophile elements, analogous to the sulfide-mediated mechanism proposed for Cd in OMZs (Janssen et al., 2014; Sec. 6). Alternatively, the deficit may reflect low preformed Ag:Si in intermediate waters, which is inherited from preferential drawdown of Ag over Si in regions upstream where these intermediate waters were last ventilated. Both interpretations have implications for the use of Ag (isotopes) as a paleoproxy: the former implies a redox sensitivity that depends on the changing location, spatial extent, and intensity of low-oxygen regions in the oceans over time. The latter implies a sensitivity to ecology and the geometry of ocean circulation. Both warrant additional scrutiny.

10.3. Marine archives

Bulk sediments are the main archive that has been investigated for their potential to record information about the marine Ag cycle. Silver concentrations in bulk sediments from open-marine environments range from ≤100 ng g^{-1} (i.e., typical lithogenic values) up to 100s of ng g^{-1} (Koide et al., 1986). In general, low concentrations are typical of well-oxygenated sediments, while higher concentrations are found in oxygen-poor and sulfidic environments. The general consensus has been that Ag enrichment in anoxic sediments is the result of post-depositional precipitation of Ag_2S (Koide et al., 1986) or possibly Ag selenide (Crusius & Thomson, 2003; Böning et al., 2005). However, high Ag concentrations are also documented in marine sediments that are only weakly reducing (Böning et al., 2004, 2005; McKay & Pedersen, 2008; Morford et al., 2008). Furthermore, even in anoxic sediments, the degree of Ag enrichment exceeds what would be expected from post-depositional Ag precipitation alone (Borchers et al., 2005; McKay and Pedersen, 2008; Böning et al., 2009). Thus, redox-controlled, post-depositional precipitation is not the primary control on Ag accumulation in marine sediments; there must also be a flux of non-lithogenic, particulate Ag to the seafloor (McKay & Pedersen, 2008).

McKay & Pedersen (2008) hypothesized that Ag, like Ba, accumulates in organic-rich settling particles. However, in contrast to Ba, Ag precipitation requires a reduced microenvironment within the particle, which is only favored in oxygen-poor waters. The analysis of sediment trap samples from the northeast Pacific show that the fluxes of particulate Ag and particulate organic carbon flux positively correlate (Martin et al., 1983). This correlation is also seen in surface sediments (McKay & Pedersen, 2008) and sediment cores from the northeastern Pacific (Fig. 26). These data broadly support the use of Ag concentrations as a paleoproductivity proxy, with an important caveat: the post-depositional preservation of particulate Ag requires that sediments remain reducing (prerequisite 2.), as settling particulate Ag formed below the euphotic zone is not preserved if sediments are oxidizing (McKay and Pedersen, 2008; Morford et al., 2008). Thus, while the delivery of Ag to sediments appears related to productivity (Wagner et al., 2013), Ag preservation will likely depend on the depositional environment. Regardless, these observations are promising from the point of view of tracing past productivity.

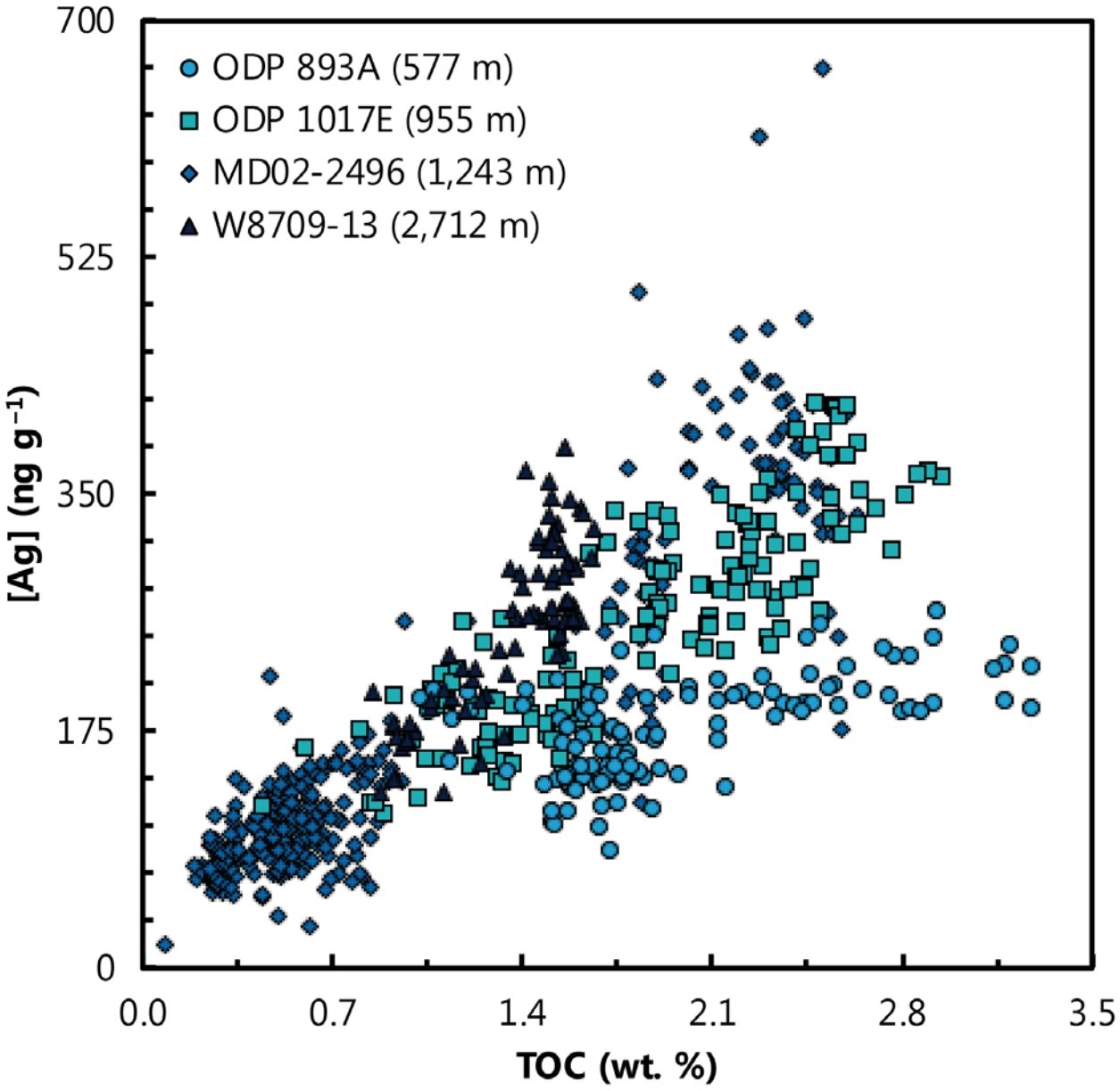

Figure 26 | Concentrations of silver and total organic carbon in sediment cores from the northeast Pacific Ocean. These data illustrate that Ag is broadly correlated with organic matter in bulk sediments, which is highly promising from the perspective of developing Ag as a paleoproductivity proxy.

10.4. Prospects

The apparent linkages between dissolved and particulate [Ag], macronutrients, and organic matter provides tantalizing evidence that Ag may be coupled to surface productivity (Fig. 24). Moreover, core-top studies indicate that the geochemical signature of this coupling is preserved under certain environmental conditions

(Fig. 26). Despite this progress, the study of Ag in marine biogeochemical cycles remains in its infancy, particularly compared to many of the other elements described here. Additional constraints are needed in several areas, including: the role of biogeochemical processes in mediating Ag distributions in the water column, the dominant controls on the downward transport of Ag through the oceans, and on the controls on Ag preservation in sediments. Given what has been learned from the application of the other TEI systems described here, new analytical developments in Ag isotope geochemistry could help place valuable constraints in several of these areas.

11. Synthesis

We now assess the overall readiness of each TEI system to reconstruct productivity, summarized in Table 2. This exercise is analogous to the assessment of analytical techniques used in chemical oceanography described by Fassbender et al. (2017). Our assessment is similarly conducted in two dimensions. First, we identify five objectives toward the development of a reliable productivity proxy, ranging from development of the analytical capabilities necessary to measure that species, to constraining diagenetic effects, and ending with the goal of using that species to reliably reconstruct paleoproductivity itself. Second, we assess the level of development within each objective. Our reasoning behind the assignments is described above in Sections 3–10.

Reliable application of a proxy requires that five objectives be serially met (e.g., Hillaire-Marcel & Vernal, 2007; Table 2). In practical terms, however, the final stage (proxy application) is often realized before many of the supporting objectives; variations in TEI ratios in the sedimentary record commonly provide the motivation for developing a more holistic understanding of that TEI system in the modern environment. (A common critique of this approach being that subsequent studies often invalidate earlier interpretations.) The five objectives that follow are common to the development of almost any proxy. First, it is essential to develop the analytical capability to measure the species of interest commensurate with the quantities typically encountered in the environment. In the case of TEI abundance proxies, the development and widespread adoption of ICP-MS instrumentation coupled to automated sample preparation systems has enabled low-blank–high-throughput–high-sensitivity analyses of multiple TE's in both seawater (e.g., Wuttig et al., 2019) and sediments alike (e.g., Wefing et al., 2017). In contrast, the techniques required to measure many TEI systems have only been developed within the past decade—or are still in development—and generally remain labor intensive and time consuming. Second, it is important to map the broad vertical and spatial patterns of a TEI system in the modern ocean. The GEOTRACES program has provided a coordinated opportunity to study the basin-scale distributions of multiple TEIs. Third, the utility of a proxy is significantly increased if the driving processes are understood. These processes may be isolated through a number of approaches, including: lab-based analogue experimentation, numerical modeling, and high-resolution spatiotemporal environmental studies. Fourth, paleoceanographic proxies require sedimentary archives—a substrate from which to reconstruct the variable of interest. The latter necessitates knowledge of how a TEI system partitions between seawater and sediment, such as through a core-top study, ideally conducted across large environmental gradients. Since many marine sedimentary archives are biogenic in origin, additional experimentation isolating 'vital effects' may be necessary. Fifth, proxies are only as

reliable as their archives are hardy. Diagenetic processes may alter primary environmental signatures, and recognizing these effects is imperative for reliably reconstructing past environmental conditions.

We assess the level of development within each objective on a four-point scale: unknown, developing, applied, and unlikely. The levels define a continuum from least to most understood, and are a useful shorthand for illustrating where additional work is most needed. Assignment of 'unknown,' implies that too little is presently known to reliably assess progress towards that objective. These TEI systems may or may not ultimately be useful in reconstructing ocean productivity. 'Developing' objectives are those where there are pilot studies on that topic, but overall there are an insufficient number to define general rules for that TEI system. If a TEI system is widely recognized to be useful towards some objective, it is given a score of 'applied'. Though these scores are subjective, they are roughly equivalent to the number of spatiotemporal and lab studies of that TEI system, and the number of inter-calibrated laboratories. If the evidence indicates that a TEI system is not suitable for reconstruction of past productivity, a score of 'unlikely' is given. This does not rule out future developments, such as identification of environmental control variables or new sedimentary archives, only that current data (and archives) do not support use of the TEI system towards this goal. Lastly, we recognize that there are continual refinements to analytical protocols, environmental distributions, etc. and thus, at some level, all five objectives could reasonably be described as 'developing'. Rather, our assignments are intended to give a relative sense of understanding between different TEI systems toward the overarching goal of reconstructing past ocean productivity.

Table 2 | Proxy development assessment. The progress toward five objectives is assessed for each TE proxy system and assigned a development level ranging unknown to unlikely, corresponding to the least and most certain assignments, respectively. Some TEI systems possess split designations. Definitions of each development level are described in Sec. 11. and discussed in detail for each TEI system in the corresponding TEI section.

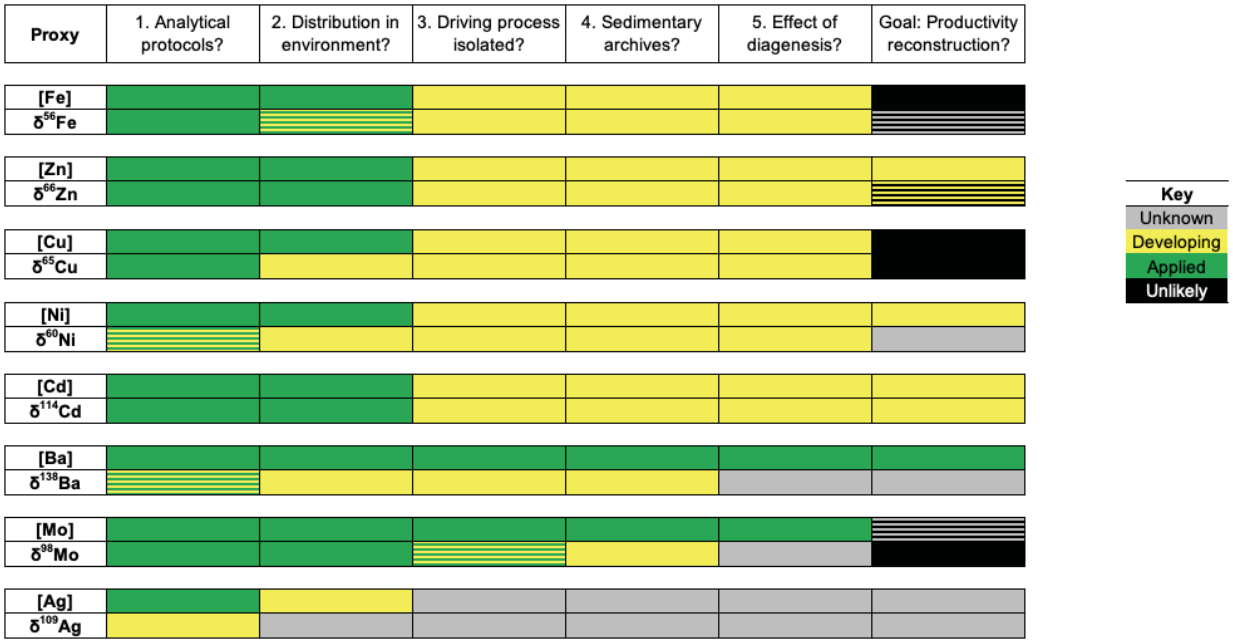

12. Conclusions and outlook

This review and synthesis allows us to draw a number of inferences regarding the overall suitability, similarities, and research priorities for using Fe, Zn, Cu, Cd, Mo, Ba, Ni, and Ag and their isotopes as paleoproductivity proxies. Regarding suitability, our proxy development assessment highlights that our knowledge of bioactive trace metal isotope systematics lags far behind those of trace-element abundances. This field is nascent; excepting Mo, the very first isotope data for seawater for all of the elements reviewed here were published within the last 15 year, or are yet to be reported, as is the case for Ag. The field is thus decades behind the trace element concentration community. Despite the lack of detail however, we can classify the elements reviewed here into three broad categories: those where the preponderance of evidence indicates that a particular bioactive metal isotope system is unlikely to inform on paleoproductivity, such as δ^{56}Fe, δ^{65}Cu, and δ^{98}Mo; those where there are promising signs, but significant calibration and validation remains to be completed, such as for δ^{66}Zn and δ^{114}Cd; and, those elements where simply too little is presently known to confidently assign utility in diagnosing paleoproductivity such as for δ^{138}Ba, δ^{60}Ni, and δ^{109}Ag.

Our review highlights a number of instances where the bioactive metals and their isotopes share similarities or—perhaps more importantly—exhibit divergent behaviors, despite sharing a common biological driver. The most significant similarity is ocean circulation; trace element isotope distributions reflect a mixture of local (i.e., *in situ)* processes, and regional (or *ex situ*) conditions that are set 'upstream' of any given locality. Indeed, researchers are recognizing that, much like the macronutrients (see Farmer et al., *this issue*), the first-order features of marine δ^{66}Zn, δ^{65}Cu, δ^{114}Cd, δ^{138}Ba, and δ^{60}Ni distributions are not controlled locally by dissolved–particulate transformations, but reflect a regionally-integrated history of vertical cycling and mixing that is imparted over the scale of an ocean basin. Today, the Southern Ocean represents the common starting point in controlling nutrient and bioactive metal inventories for much of the low latitude thermocline; whether, when, and how this pattern might have changed in Earth's past will be an important consideration for interpreting paleoproductivity records derived from these proxies. Where the bioactive metals diverge in their response is equally instructive from the point of view of proxy development. For example, if experiencing a common forcing, such as a temporary shift in the loci of most intense primary productivity, subtle differences in the response of the various bioactive metals reviewed here may hold the key to understanding whether the underlying change was truly productivity related. For example, sedimentary accumulation and preservation of Cd and Ba exhibit opposing redox sensitivities; Cd burial is enhanced at low [O_2], whereas Ba is oftentimes diminished. Recognizing these opposing controls may

enable reconciling inconsistent proxy records, thus building a more holistic picture of marine biogeochemistry at key points in Earth's history.

Lastly, we outline three priorities for further study. First, a number of modern ambiguities require addressing. Most notable is the apparent 'missing' source and/or sink terms for the whole-ocean isotopic budgets of several elements, including Cu, Cd, Ba, and Ni. Though it is possible that these missing source and sink terms represent actual short-term imbalances in the flux of these elements to and from the ocean, we view it more likely that there are major fluxes that remain uncharacterized. The origin of these imbalances is most pressing for elements where the output flux associated with organic matter constitutes a secondary sink (e.g., Zn, Ni), as the isotopic budget of these elements is most susceptible to decoupling from productivity. Second, the significance of ocean circulation in mediating basin-scale bioactive metal isotope distributions implies that paleoceanographic interpretations made from a single site cannot be uniquely interpreted in terms of either changes in productivity or ocean circulation without additional constraints. Such constraints could take the form of independent circulation estimates—from numerical models or canonical circulation proxies measured in the same samples—or by measuring bioactive metal isotope distributions in spatially-distributed sediment samples. Third, the lack of suitable archives with which to reconstruct surface water bioactive metal isotope compositions afflicts almost every element reviewed here. Overcoming this limitation will require the most creativity; we suggest more studies testing the fidelity of non-traditional substrates (e.g., mixed foraminiferal assemblages, coccolith calcite, diatom opal), periodic re-assessment of the feasibility of traditional substrates following analytical advancements (e.g., improvements in ion transmission efficiency, large-scale [automated and/or crowd-sourced] picking of monospecific foraminiferal assemblages), and development and validation of selective extraction protocols that can be used to isolate phases of interest from complex matrices. Though attempting to overcome these limitations may be considered high risk, we believe that this risk is more than justified by the reward of developing a more complete understanding of Earth's biogeochemical history.

Postscripts

Acknowledgments

This contribution grew (and grew) out of the joint GEOTRACES–PAGES workshop held in Aix-en-Provence in December 2018. The authors extend tremendous thanks to the workshop organizers, and in particular Bob Anderson, Catherine Jeandel, Laurence Vidal, and Kazuyo Tachikawa. T.J.H. acknowledges support from the U.S. National Science Foundation; S.H.L. from the U.K. Natural Environment Research Council (NE/P018181/1); T.M.C. from the University of South Florida; and, J.R.F. from the Max Planck Society, the Tuttle Fund of the Department of Geosciences of Princeton University, the Grand Challenges Program of the Princeton Environmental Institute, and the Andlinger Center for Energy and the Environment of Princeton University. Most importantly, we acknowledge the hundreds of scientists who have generated GEOTRACES-compliant TEI data that made this synthesis possible.

Data sources

Dissolved TEI data are sourced from the GEOTRACES Intermediate Data Products in 2014 (Mawji et al., 2015) and 2017 (Schlitzer et al., 2018). Citations to the primary data sources used in the figures and Table 1 are given below.

Figures

Iron: Conway & John, 2014a (Atlantic); Conway & John, 2015a (Pacific); Horner et al., 2015b (CD29-2 record); Chu et al., 2006 (28DSR9 record); Liu et al., 2020 (METG-03 record). Zinc: Conway & John, 2014b (Atlantic); Conway & John, 2015a (Pacific); Wang et al., 2019a (Southern); Little et al., 2014 (Fe–Mn crust records). Copper: Little et al., 2018 (Atlantic); Takano et al., 2017 (Pacific); Boye et al., 2012 (Southern); Little et al., 2014 (Fe–Mn crust records). Cadmium: Conway and John, 2015b (Atlantic); Conway & John, 2015a (Pacific); Abouchami et al., 2014 (Southern); Schmitt et al., 2009a (Fe–Mn crust data); Horner et al., 2010 (Fe–Mn crust 'core-top' data); Murphy, 2016 ('down core' Fe–Mn crust records); Schmitt et al., 2009a ('down core' Fe–Mn crust record); van Geen et al., 1995 (California Margin core-top data). Molybdenum: Nakagawa et al., 2012 (all basins). Barium: Bates et al., 2017 (Atlantic); Geyman et al., 2019 (Pacific); Hsieh & Henderson, 2017 (Southern). Nickel: Archer et al., 2020 (Atlantic); Takano et al., 2017 (Pacific); Wang et al., 2019a (Southern); Gall et al., 2013 (CD29-2 record); Gueguen et al., 2016 (Fe–Mn crust records). Silver: Fischer et al., 2018 (Pacific); Boye et al., 2012 (Southern). Core MD02-2496 (Vancouver Island Margin; 48.97°N, 127.04°W, 1,243 m water depth) from Chang et al., 2014; Core

W8709-13PC (Oregon Margin; 42.116°N, 125.75°W; 2,712 m water depth) from Kienast, 2003; ODP 1017E (Southern California; 34.53°N, 121.1°W; 955 m water depth) from Hendy & Pedersen, 2005; ODP 893A (Santa Barbara Basin; 34.287°N, 120.036°W; 576.5 m water depth) from Ivanochko, 2001.

Table 1

[a]Schlitzer (2017); [b]Morris et al. (1975); [c]Gallon and Flegal, 2014; [d]Beard et al. (2003); [e]Moynier et al. (2017) and references therein; [f]Schmitt et al. (2009a); [g]Willbold & Elliott (2017); [h]Nan et al., 2018; [i]Cameron et al. (2009); [j]USGS reference material SCO-1 (Cody Shale) is used given paucity of representative data; Schönbächler et al. (2007); [k]Section 3 and references therein; [l]Section 4 and references therein; [m]Section 5 and references therein; [n]Section 6 and references therein; [o]Data from Nakagawa et al. (2012) renormalized to NIST SRM 3134 + 0.25 ‰ based on Goldberg et al. (2013); [p]Section 8 and references therein; [q]Section 9 and references therein; [r]Hayes et al. (2018) and references therein; [s]Miller et al. (2011); [t]Dickens et al. (2003); [u]Cameron & Vance (2014) and references therein; Little et al. (2015; 2020); [v]Broecker & Peng (1982).

Competing interests

The authors declare that they are not aware of any financial conflicts of interest, real or perceived.

GEOTRACES–PAGES Biological Productivity Working Group Members

C. Bolton (CEREGE, Univ. Aix-Marseille, CNRS, IRD, Collège de France, INRAE, Aix-en-Provence, France); E. Calvo (Institut de Ciències del Mar, CSIC, Barcelona, Spain); D. Cardinal (LOCEAN (UMR7159), Sorbonne Université, IRD, CNRS, MNHN, Paris, France); T. de Garidel-Thoron (CEREGE, Univ. Aix-Marseille, CNRS, IRD, Collège de France, INRAE Aix-en-Provence, France); S. Fietz (Department of Earth Sciences, Stellenbosch University, Stellenbosch South Africa); K. R. Hendry (School of Earth Sciences, University of Bristol, Bristol, UK); F. Marcantonio (Department of Geology and Geophysics, Texas A&M University), P. A. Rafter (Department of Earth System Science, University of California, Irvine, CA, USA); H. Ren (Department of Geosciences, National Taiwan University, Taipei, Taiwan); C. J. Somes (GEOMAR Helmholtz Centre for Ocean Research Kiel, 24105 Kiel, Germany); J. N. Sutton (Univ Brest, CNRS, IRD, Ifremer, Institut Universitaire Européen de la Mer, LEMAR, Plouzané, France); A. Torfstein (Institute of Earth Sciences, Hebrew University, Jerusalem, & InterUniversity Institute for Marine Sciences, Eilat, Israel); G. Winckler (Lamont-Doherty Earth Observatory of Columbia University, Palisades, NY, USA).

References

Abadie, C., Lacan, F., Radic, A., Pradoux, C., & Poitrasson, F. (2017). Iron isotopes reveal distinct dissolved iron sources and pathways in the intermediate versus deep Southern Ocean. *Proc. Natl. Acad. Sci.,* **114**, 858-863.

Abouchami, W., Galer, S. J. G., de Baar, H. J. W., Alderkamp, A. C., Middag, R., Laan, P., Feldmann, H., & Andreae, M. O. (2011). Modulation of the Southern Ocean cadmium isotope signature by ocean circulation and primary productivity. *Earth Planet. Sci. Lett.*, **305**(1-2), 83-91.

Abouchami, W., Galer, S. J. G., Horner, T. J., Rehkämper, M., Wombacher, F., Xue, Z., Lambelet, M., Gault-Ringold, M., Stirling, C. H., Schönbächler, M., Shiel, A. E., Weis, D., & Holdship, P. F. (2013). A common reference material for cadmium isotope studies–NIST SRM 3108. *Geostandards and Geoanalytical Research*, **37**(1), 5-17.

Abouchami, W., Galer, S. J. G., de Baar, H. J. W., Middag, R., Vance, D., Zhao, Y., Klunder, M., Mezger, K., Feldmann, H., & Andreae, M. O. (2014). Biogeochemical cycling of cadmium isotopes in the Southern Ocean along the Zero Meridian. *Geochim. Cosmochim. Acta*, **127**, 348-367.

Adkins, J. F., Cheng, H., Boyle, E. A., Druffel, E. R., & Edwards, R. L. (1998). Deep-sea coral evidence for rapid change in ventilation of the deep North Atlantic 15,400 years ago. *Science*, **280**(5364), 725-728.

Akerman, A., Poitrasson, F., Oliva, P., Audry, S., Prunier, J., & Braun, J. J. (2014). The isotopic fingerprint of Fe cycling in an equatorial soil-plant-water system: The Nsimi watershed, South Cameroon. *Chem. Geol.*, **385**, 104–116.

Albarède, F. (2004). The stable isotope geochemistry of copper and zinc. *Reviews in Mineralogy and Geochemistry*, *55*(1), 409-427.

Algeo, T. J. (2004). Can marine anoxic events draw down the trace element inventory of seawater? *Geology*, **32** (12), 1057-1060, doi:10.1130/G20896.1.

Algeo, T. J., & Lyons, T. W. (2006). Mo-total organic carbon covariation in modern anoxic marine environments: Implications for analysis of paleoredox and paleohydrographic conditions: *Paleoceanography*, **21**, doi:10.1029/2004PA001112.

Algeo T. J., & Maynard J. B. (2008). Trace-metal covariation as a guide to water-mass conditions in ancient anoxic marine environments. *Geosphere* **4**, 872.

Algeo, T. J., & Tribovillard, N. (2009). Environmental analysis of paleoceanographic systems based on molybdenum-uranium covariation: *Chem. Geol.*, **268**, 211–225, doi:10.1016/j.chemgeo.2009.09.001.

Alldredge, A. L., & Silver, M. W. (1988). Characteristics, dynamics and significance of marine snow. *Prog. Oceanogr.*, **20**(1), 41-82.

Anbar, A. D., & Knoll, A. H. (2002). Proterozoic Ocean Chemistry and Evolution: A Bioinorganic Bridge? *Science*, **297**, 1137–1142, doi:10.1126/science.1069651.

Anbar, A. D., Jarzecki, A. A., & Spiro, T. G. (2005) Theoretical investigation of iron isotope fractionation between $Fe(H_2O)_6^{3+}$ and $Fe(H_2O)_6^{2+}$: Implications for iron stable isotope geochemistry. *Geochim. Cosmochim. Acta.* **69**, 825–837. https://doi.org/10.1016/j.gca.2004.06.012.

Andersen, M. B., Vance, D., Archer, C., Anderson, R. F., Ellwood, M. J., & Allen, C. S. (2011). The Zn abundance and isotopic composition of diatom frustules, a proxy for Zn availability in ocean surface seawater. *Earth Planet. Sci. Lett.,* **301**, 137–145. http://dx.doi.org/10.1016/j.epsl.2010.10.032.

2117 Anderson, M. A., Morel, F. M. M., & Guillard, R. R. L. (1978). Growth limitation of a coastal diatom by
2118 low zinc ion activity. *Nature*, **276**, 70-71.

2119 Annett, A. L., Lapi, S., Ruth, T. J., & Maldonado, M. T. (2008). The effects of Cu and Fe availability on
2120 the growth and Cu:C ratios of marine diatoms. *Limnol. Oceanogr.* **53**, 2451–2461.

2121 Aplin, A. C., & Cronan, D. S. (1985). Ferromanganese oxide deposits from the central Pacific Ocean, I.
2122 Encrustations from the Line Islands Archipelago. *Geochim. Cosmochim. Acta*, **49**(2), 427-436.

2123 Archer, C., Andersen, M. B., Cloquet, C., Conway, T. M., Dong, S., Ellwood, M., Moore, R, Nelson, J.,
2124 Rehkämper, M., Rouxel, O., Samanta, M., Shin, K.-C., Sohrin, Y., Takano, S., & Wasylenki, L.
2125 (2017). Inter-calibration of a proposed new primary reference standard AA-ETH Zn for zinc
2126 isotopic analysis. *Journal of Analytical Atomic Spectrometry*, **32**(2), 415-419.

2127 Archer, C., Vance, D., Milne, A., & Lohan, M. C. (2020). The oceanic biogeochemistry of nickel and its
2128 isotopes: New data from the South Atlantic and the Southern Ocean biogeochemical divide. *Earth*
2129 *Planet. Sci. Lett.*, **535**, 116118.

2130 Aristilde, L., & Xu, Y. (2012). Weak organic ligands enhance Zinc uptake in Marine phytoplankton.
2131 *Environ. Sci. Technol.,* **46**, 5438-5445.

2132 Arrhenius, G. (1963). *Pelagic sediments*. Scripps Institution of Oceanography, University of California.

2133 Atkins, A. L., Shaw, S., & Peacock, C. L. (2016). Release of Ni from birnessite during transformation of
2134 birnessite to todorokite: Implications for Ni cycling in marine sediments. *Geochim. Cosmochim.*
2135 *Acta*, **189**, 158-183.

2136 Baars, O., & Croot, P. L. (2011). The speciation of dissolved zinc in the Atlantic sector of the Southern
2137 Ocean. *Deep. Res. Part II Top. Stud. Oceanogr.,* **58**, 2707–2719.
2138 http://dx.doi.org/10.1016/j.dsr2.2010.10.041.

2139 Baars, O., Abouchami, W., Galer, S. J., Boye, M., & Croot, P. L. (2014). Dissolved cadmium in the
2140 Southern Ocean: distribution, speciation, and relation to phosphate. *Limnol. Oceanogr.*, **59**(2), 385-
2141 399.

2142 Bacon, M.P. and Anderson, R.F. (1982). Distribution of thorium isotopes between dissolved and particulate
2143 forms in the deep sea. *J. Geophys. Res. Oceans*, **87**(C3), 2045-2056.

2144 Badaut, D., & Risacher, F. (1983). Authigenic smectite on diatom frustules in Bolivian saline lakes.
2145 *Geochim. Cosmochim. Acta*, **47**(3), 363-375.

2146 Barling, J., Arnold, G., & Anbar, A. D., (2001). Natural mass-dependent variations in the isotopic
2147 composition of molybdenum. *Earth Planet. Sci. Lett.*, **193**, 447–457, doi:10.1016/S0012-
2148 821X(01)00514-3.

2149 Barling, J., & Anbar, A. D. (2004). Molybdenum isotope fractionation during adsorption by manganese
2150 oxides. *Earth Planet. Sci. Lett.*, **217**, 315-329, doi:10.1016/S0012-821X(03)00608-3.

2151 Bates, S. L., Hendry, K. R., Pryer, H. V., Kinsley, C. W., Pyle, K. M., Woodward, E. M. S., & Horner, T.
2152 J. (2017). Barium isotopes reveal role of ocean circulation on barium cycling in the Atlantic.
2153 *Geochim. Cosmochim. Acta*, **204**, 286-299.

2154 Beard, B.L., Johnson, C.M., Cox, L., Sun, H., Nealson, K.H., & Aguilar, C. (1999). Iron Isotope
2155 Biosignatures. *Science* **285**, 1889-1892.

2156 Beard, B. L., Johnson, C. M., Skulan, J. L., Nealson, K. H., Cox, L., & Sun, H. (2003). Application of Fe
2157 isotopes to tracing the geochemical and biological cycling of Fe. *Chem. Geol.*, **195**(1-4), 87-117.

Bender, M., Grande, K., Johnson, K., Marra, J., Williams, P. J. L., Sieburth, J., Pilson, M., Langdon, C., Hitchcock, G., Orchado, J., Hunt, C., Donaghy, P., & Heinemann, K.(1987). A comparison of four methods for determining planktonic community production. *Limnol. Oceanogr.*, **32**(5), 1085-1098.

Bennett, S. A., Rouxel, O., Schmidt, K., Garbe-Schönberg, D., Statham, P. J., & German, C. R. (2009). Iron isotope fractionation in a buoyant hydrothermal plume, 5 S Mid-Atlantic Ridge. *Geochim. Cosmochim. Acta*, **73**(19), 5619-5634.

Bergquist, B. A., & Boyle, E. A. (2006). Iron isotopes in the Amazon River system: Weathering and transport signatures. *Earth Planet, Sci. Lett.*, **248**(1–2), 54–68. https://doi.org/10.1016/j.epsl.2006.05.004.

Berger, W. H., Smetacek, V., & Wefer, G. (1989). Ocean productivity and paleoproductivity - an overview. In W. H. Berger, V. S. Smetacek, G. Wefer (Eds) *Productivity of the Oceans present and past: Report of the Dahlem Workshop on Productivity of the Ocean, Berlin, 1988*, Life Sciences Research Reports 44, Wiley & Sons, Chichester, pp. 1-34.

Bermin, J., Vance, D., Archer, C., & Statham, P. J. (2006). The determination of the isotopic composition of Cu and Zn in seawater. *Chem. Geol.,* **226**, 280–297.

Bernstein, R. E., & Byrne, R. H. (2004). Acantharians and marine barite. *Mar. Chem.*, **86** (1-2), 45-50.

Bertine, K. K., & Turekian, K. K. (1973). Molybdenum in marine deposits. *Geochim. Cosmochim. Acta*, **37** (6), 1415-1434.

Bianchi, D., Weber, T. S., Kiko, R., & Deutsch, C. (2018). Global niche of marine anaerobic metabolisms expanded by particle microenvironments. *Nat. Geosci.,* **11**, 1–6.

Bishop, J. K. (1988). The barite-opal-organic carbon association in oceanic particulate matter. *Nature*, **332** (6162), 341.

Böning, P., Brumsack, H.-J., Böttcher, M.E., Schnetger, B., Kriete, C., Kallmeyer, J., & Borchers, S.L. (2004). Geochemistry of Peruvian near-surface sediments. *Geochim. Cosmochim. Acta*, **68**, 4429-4451.

Böning, P., Cuypers, S., Grunwald, M., Schnetger, B., & Brumsack, H.-J. (2005). Geochemical characteristics of Chilean upwelling sediments at ~36°S. *Mar. Geol.*, **220**, 1-21.

Böning, P., Brumsack, H.-J., Schnetger, B., & Grunwald, M. (2009). Trace element signatures of Chilean upwelling sediments at ~36°S. *Mar. Geol.*, **259**, 112-121.

Böning, P., Shaw, T., Pahnke, K., & Brumsack, H.-J. (2015). Nickel as an indicator of fresh organic matter in upwelling sediments. *Geochim. Cosmochim. Acta*, **162**, 99-108, doi:10.1016/j.gca.2015.04.027.

Borchers, S.L., Schnetger, B., Boning, P., & Brumsack, H.-J. (2005). Geochemical signatures of the Namibian diatom belt: Perennial upwelling and intermittent anoxia. *Geochemistry, Geophysics, Geosystems*, **6**(4), Q06006, doi:10.1029/2004GC000886.

Boyd, P. W., Jickells, T., Law, C. S., Blain, S., Boyle, E. A., Buesseler, K. O., Coale, K. H., Cullen, J. J., de Baar, H. J. W., Follows, M., Harvey, M., Lancelot, C., Levasseur, M., Owens, N. P. J., Pollard, R., Rivkin, R. B., Sarimento, J., Schoemann, V., Smetacek, V., Takeda, S., Tsuda, A., Turner, S., & Watson, A. J.. (2007). Mesoscale iron enrichment experiments 1993-2005: synthesis and future directions. *Science*, **315**(5812), 612-617.

Boyd, P. W., & Ellwood, M. J. (2010). The biogeochemical cycle of iron in the ocean. *Nat. Geosci.* **3**(10), 675-682.

Boyd, P. W., Ellwood, M. J., Tagliabue, A., & Twining, B. S. (2017). Biotic and abiotic retention, recycling and remineralization of metals in the ocean. *Nat. Geosci.*, **10**(3), 167-173.

Boye, M., Wake, D. B., Lopez Gracia, P., Bown, J., Baker, A. R., & Achterberg, E. P. (2012). Distributions of dissolved trace metals (Cd, Cu, Mn, Pb, Ag) in the southeastern Atlantic and the Southern Ocean. *Biogeosciences*, **9**, 3231-3246, doi:10.5194/bg-9-3231-2012.

Boyle, E. A. (1981). Cadmium, zinc, copper, and barium in foraminifera tests. *Earth Planet. Sci. Lett.*, **53**(1), 11-35.

Boyle, E. A. (1988a). Vertical oceanic nutrient fractionation and glacial/interglacial CO_2 cycles. *Nature*, **331**(6151), 55-56.

Boyle, E. A. (1988b). Cadmium: Chemical tracer of deepwater paleoceanography. *Paleoceanography*, **3**(4), 471-489.

Boyle, E. A. (1992). Cadmium and $\delta^{13}C$ paleochemical ocean distributions during the stage 2 glacial maximum. *Annual Review of Earth and Planetary Sciences*, **20**(1), 245-287.

Boyle, E. A., & Keigwin, L. D. (1985). Comparison of Atlantic and Pacific paleochemical records for the last 215,000 years: Changes in deep ocean circulation and chemical inventories. *Earth Planet. Sci. Lett.*, **76**(1-2), 135-150.

Boyle, E. A., Sclater, F., & Edmond, J. M. (1976). On the marine geochemistry of cadmium. *Nature*, **263**(5572), 42.

Boyle, E. A., Sclater, F. R., & Edmond, J. M. (1977). The distribution of dissolved copper in the Pacific. *Earth Planet. Sci. Lett.*, **37**, 38-54.

Brand, L. E., Sunda, W. G., & Guillard, R. R. L. (1983). Limitation of marine phytoplankton by zinc, manganese, and iron. *Limnol. Oceanogr.*, **28**, 1182–1198.

Brand L. E., Sunda, W. G., & Guillard, R. R. L. (1986). Reduction of marine phytoplankton reproduction rates by copper and cadmium. *J. Exp. Mar. Bio. Ecol.* **96**, 225–250.

Bridgestock, L., Rehkämper, M., van de Flierdt, T., Murphy, K., Khondoker, R., Baker, A. R., Chance, R., Strekopytov, S., Humphreys-Williams, E., Achterberg, E. P. (2017). The Cd isotope composition of atmospheric aerosols from the Tropical Atlantic Ocean. *Geophys. Res. Lett.* **44**(6), 2932-2940. https://doi.org/10.1002/2017GL072748.

Bridgestock, L., Hsieh, Y. T., Porcelli, D., Homoky, W. B., Bryan, A., & Henderson, G. M. (2018). Controls on the barium isotope compositions of marine sediments. *Earth Planet. Sci. Lett.*, **481**, 101-110.

Bridgestock, L., Hsieh, Y. T., Porcelli, D., & Henderson, G. M. (2019). Increased export production during recovery from the Paleocene–Eocene thermal maximum constrained by sedimentary Ba isotopes. *Earth Planet. Sci. Lett.*, **510**, 53-63.

Broecker, W.S. (1982). Glacial to interglacial changes in ocean chemistry. *Prog. Oceanogr*. **11**, 151-197.

Broecker, W.S., & Peng, T. H. (1982). Tracers in the Sea. Eldigo Press, Palisades, NY.

Brucker, R. L. P., McManus, J., Severmann, S., & Berelson, W. M. (2009). Molybdenum behavior during early diagenesis: Insights from Mo isotopes. *Geochemistry, Geophysics, Geosystems*, **10**, doi:10.1029/2008GC002180.

Bruland, K. W. (1980). Oceanographic distributions of cadmium, zinc, nickel, and copper in the North Pacific. *Earth Planet. Sci. Lett.*, **47**(2), 176-198.

Bruland, K. W. (1989). Complexation of zinc by natural organic ligands in the central North Pacific. *Limnol. Oceanogr.*, **34**, 269–285.

Bruland, K. W. (1992). Complexation of cadmium by natural organic ligands in the central North Pacific. *Limnol. Oceanogr.*, **37**(5), 1008-1017.

Bruland, K. W., & Lohan, M. C. (2003). Controls of Trace Metals in Seawater. In *Treatise on Geochemistry*, Elsevier, 23-47.

Brumsack, H. J. (2006). The trace metal content of recent organic carbon-rich sediments: implications for Cretaceous black shale formation. *Palaeogeography, Palaeoclimatology, Palaeoecology*, **232**(2-4), 344-361.

Bryan, A. L., Dong, S., Wilkes, E. B., & Wasylenki, L. E. (2015). Zinc isotope fractionation during adsorption onto Mn oxyhydroxide at low and high ionic strength. *Geochim. Cosmochim. Acta*, **157**, 182-197.

Buesseler, K. O., Boyd, P. W., Black, E. E., & Siegel, D. A. (2020). Metrics that matter for assessing the ocean biological carbon pump. *Proc. Natl. Acad. Sci.*, **117**(18), 9679-9687.

Cadiou, J. L., Pichat, S., Bondanese, V. P., Soulard, A., Fujii, T., Albarède, F., & Oger, P. (2017). Copper transporters are responsible for copper isotopic fractionation in eukaryotic cells. *Sci. Rep.*, **7**(1), 1-10.

Cameron, V., Vance, D., Archer, C., & House, C. H. (2009). A biomarker based on the stable isotopes of nickel. *Proceedings of the National Academy of Sciences*, *106*(27), 10944-10948.

Carlson, C. A., Hansell, D. A., Nelson, N. B., Siegel, D. A., Smethie, W. M., Khatiwala, S., Meyers, M. M., & Halewood, E. (2010). Dissolved organic carbon export and subsequent remineralization in the mesopelagic and bathypelagic realms of the North Atlantic basin. *Deep Sea Res. Pt. II*, **57**(16), 1433-1445.

Cao, Z., Siebert, C., Hathorne, E. C., Dai, M., & Frank, M. (2020). Corrigendum to "Constraining the oceanic barium cycle with stable barium isotopes" [*Earth Planet. Sci. Lett.*, **434** (2016) 1-9], doi: 10.1016/j.epsl.2019.116003/

Cartapanis, O., Bianchi, D., Jaccard, S. L., & Galbraith, E. D. (2016). Global pulses of organic carbon burial in deep-sea sediments during glacial maxima. *Nat. Commun.*, **7**, 10796, doi:10.1038/ncomms10796.

Carter, S. C., Paytan, A., & Griffith, E. M. (2020). Toward an Improved Understanding of the Marine Barium Cycle and the Application of Marine Barite as a Paleoproductivity Proxy. *Minerals*, **10**(5), 421.

Chan, L. H., Edmond, J. M., Stallard, R. F., Broecker, W. S., Chung, Y. C., Weiss, R. F., & Ku, T. L. (1976). Radium and barium at GEOSECS stations in the Atlantic and Pacific. *Earth Planet. Sci. Lett.*, **32**(2), 258-267.

Chan, L. H., Drummond, D., Edmond, J. M., & Grant, B. (1977). On the barium data from the Atlantic GEOSECS expedition. *Deep Sea Res.*, **24**(7), 613-649.

Chang, A. S., Pedersen, T. F., & Hendy, I. L. (2014). Effects of productivity, glaciation, and ventilation on late Quaternary sedimentary redox and trace element accumulation on the Vancouver Island margin, western Canada. *Paleoceanogr.*, **29**(7), 730-746.

Chappaz, A., Lyons, T. W., Gregory, D. D., Reinhard, C. T., Gill, B. C., Li, C., & Large, R. R. (2014). Does pyrite act as an important host for molybdenum in modern and ancient euxinic sediments? *Geochim. Cosmochim. Acta*, **126**, 112–122, doi:10.1016/j.gca.2013.10.028.

Charette, M. A., et al. (2020). The Transpolar Drift as a Source of Riverine and Shelf-Derived Trace Elements to the Central Arctic Ocean. *J. Geophys. Res. Oceans*, **125**(5), e2019JC015920. https://doi.org/10.1029/2019JC015920.

Chen, J.-B., Busigny, V., Gaillardet, J., Louvat, P., & Wang, Y.-N. (2014). Iron isotopes in the Seine River (France): Natural vs anthropogenic sources. *Geochim. Cosmochim. Acta,* **128**, 128-143.

2287 Chen., T., Wenqiang, L., Gao, B., Liu, R., Li, G., Zhao, L., and Ji, J. (2020). Reactive iron isotope signatures
2288 of the East Asian dust particles: Implications for iron cycling the deep North Pacific. *Chem. Geol.*
2289 **531**, 119342. https://doi.org/10.1016/j.chemgeo.2019.119342.

2290 Cheng, H., Adkins, J., Edwards, R. L., & Boyle, E. A. (2000). U-Th dating of deep-sea corals. *Geochim.*
2291 *Cosmochim. Acta*, **64**(14), 2401-2416.

2292 Chever, F., Bucciarelli, E., Sarthou, G., Speich, S., Arhan, M., Penven, P., & Tagliabue, A. (2010). Physical
2293 speciation of iron in the Atlantic sector of the Southern Ocean along a transect from the subtropical
2294 domain to the Weddell Sea Gyre. *J. Geophys. Res. Oceans*, **115**, C10059,
2295 doi:10.1029/2009JC005880.

2296 Chever. F., Rouxel, O. J., Croot, P. L., Ponzevera, E., Wuttig, K., & Auro, M. (2015). Total dissolvable and
2297 dissolved iron isotopes in the water column of the Peru upwelling regime. *Geochim. Cosmochim.*
2298 *Acta*, **162**, 66-82. https://doi.org/10.1016/j.gca.2015.04.031.

2299 Chow, T. J., & Goldberg, E. D. (1960). On the marine geochemistry of barium. *Geochim. Cosmochim.*
2300 *Acta,* **20**(3-4), 192-198.

2301 Chu, N., Johnson, C., Beard, B., German, C., Nesbitt, R., Frank, M., Bohn, M., Kubik, P., Usui, A., &
2302 Graham, I. (2006). Evidence for hydrothermal venting in Fe isotope compositions of the deep
2303 Pacific Ocean through time. *Earth Planet. Sci. Lett.*, **245**, 202-217.

2304 Ciscato E. R., Bontognali T. R. R., & Vance, D. (2018). Nickel and its isotopes in organic-rich sediments:
2305 implications for oceanic budgets and a potential record of ancient seawater. *Earth Planet. Sci. Lett.*
2306 **494**, 239–250. https://doi.org/10.1016/j.epsl.2018.04.061.

2307 Ciscato, E. R., Bontognali, T. R., Poulton, S. W., & Vance, D. (2019). Copper and its Isotopes in Organic-
2308 Rich Sediments: From the Modern Peru Margin to Archean Shales. *Geosciences*, **9**(8), 325.

2309 Clarkson, M., Müsing, K., Andersen, M. B., & Vance, D. (2018). Reducing the role of contaminant phases
2310 for metal isotopes in carbonates. In *Goldschmidt Abstracts* p. 441.

2311 Coale, K. H. (1991). Effects of iron, manganese, copper and zinc enrichments on productivity and biomass
2312 in the subarctic Pacific. *Limnol. Oceanogr.,* **36**, 1851–1864.

2313 Coale K. H., & Bruland K. W. (1988). Copper complexation in the Northeast Pacific. *Limnol. Oceanogr.*
2314 **33**, 1084–1101.

2315 Coale K. H., & Bruland K. W. (1990). Spatial and temporal variability in copper complexation in the North
2316 Pacific. *Deep Sea Res. Part A, Oceanogr. Res. Pap.* **37**, 317–336.

2317 Coale, K. H., Wang, X., Tanner, S. J., & Johnson, K. S. (2003). Phytoplankton growth and biological
2318 response to iron and zinc addition in the Ross Sea and Antarctic Circumpolar Current along 170°W.
2319 *Deep. Res. Part II Top. Stud. Oceanogr.,* **50**, 635–653.

2320 Collier, R. W. (1985). Molybdenum in the Northeast Pacific Ocean. *Limnol. Oceanogr.*, **30**, 1351–1354,
2321 doi:10.4319/lo.1985.30.6.1351

2322 Conway, T. M., & John, S. G. (2014a). Quantification of dissolved iron sources to the North Atlantic Ocean.
2323 *Nature*, 511, 212-215.

2324 Conway, T. M., & John, S. G. (2014b). The biogeochemical cycling of zinc and zinc isotopes in the North
2325 Atlantic Ocean. *Global Biogeochem. Cycles*, 1111–1128.

2326 Conway, T. M., & John, S. G. (2015a). The cycling of iron, zinc and cadmium in the North East Pacific
2327 Ocean–Insights from stable isotopes. *Geochim. Cosmochim. Acta*, **164**, 262-283.

2328 Conway, T. M., & John, S. G. (2015b). Biogeochemical cycling of cadmium isotopes along a high-
2329 resolution section through the North Atlantic Ocean. *Geochim. Cosmochim. Acta*, **148**, 269-283.

2330 Conway, T. M., Rosenberg, A. D., Adkins, J. F., & John, S. G. (2013). A new method for precise
2331 determination of iron, zinc and cadmium stable isotope ratios in seawater by double-spike mass
2332 spectrometry. *Anal. Chim. Acta,* **793**, 44–52.

2333 Conway, T. M., Hamilton, D. S., Shelley, R. U., Aguilar-Islas, A. M., Landing, W. M., Mahowald, N. M.,
2334 & John, S. G. (2019). Tracing and constraining anthropogenic aerosol iron fluxes to the North
2335 Atlantic Ocean using iron isotopes. *Nat. Commun.*, **10**, 2628, doi:10.1038/s41467-019-10457-w.

2336 Coplen, T. B. (2011). Guidelines and recommended terms for expression of stable-isotope-ratio and gas-
2337 ratio measurement results. *Rapid communications in mass spectrometry*, **25**(17), 2538-2560.

2338 Costa, K. M., McManus, J. F., Anderson, R. F., Ren, H., Sigman, D. M., Winckler, G., Fleisher, M. Q.,
2339 Marcantonio, F., & Ravelo, A. C. (2016). No iron fertilization in the equatorial Pacific Ocean
2340 during the last ice age. *Nature*, **529**(7587), 519-522.

2341 Costa, K. M., McManus, J. F., Middleton, J. L., Langmuir, C. H., Huybers, P. J., Winckler, G., &
2342 Mukhopadhyay, S. (2017). Hydrothermal deposition on the Juan de Fuca Ridge over multiple
2343 glacial–interglacial cycles. *Earth Planet. Sci. Lett.*, **479**, 120-132.

2344 Coutaud, M., Méheut, M., Glatzel, P., Pokrovski, G. S., Viers, J., Rols, J. L., & Pokrovsky, O. S. (2018).
2345 Small changes in Cu redox state and speciation generate large isotope fractionation during
2346 adsorption and incorporation of Cu by a phototrophic biofilm. *Geochim. Cosmochim. Acta*, **220**, 1-
2347 18.

2348 Coutaud, M., Méheut, M., Viers, J., Rols, J. L., & Pokrovsky, O. S. (2019). Copper isotope fractionation
2349 during excretion from a phototrophic biofilm. *Chem. Geol.*, **513**, 88-100.

2350 Cowan, C .E., Jenne, E. A., & Crecelius, E. A. (1985). Silver speciation in seawater: The importance of
2351 sulfide and organic complexes. In: A.C. Sigleo and A. Hattori (Eds.), *Marine and Estuarine*
2352 *Geochemisty*, Lewis Publishers Inc., Chelsea, MI, USA.

2353 Crawford, D. W. W., Lipsen, M. S. S., Purdie, D. A. A., Lohan, M. C. C., Statham, P. J. J., Whitney, F. A.
2354 A., Putland, J. N. N., Johnson, W. K. K., Sutherland N., Peterson, T. D. D., Harrison, P. J. J., &
2355 Wong C. S. S. (2003). Influence of zinc and iron enrichments on phytoplankton growth in the
2356 northeasten subarctic Pacific. *Limnol. Oceanogr.,* **48**, 1583–1600.

2357 Crockford, P. W., Wing, B. A., Paytan, A., Hodgskiss, M. S., Mayfield, K. K., Hayles, J. A., Middleton, J.
2358 E., Ahm, A.-S. C., Johnston, D. T., Caxito, F., Uhlein, G., Halverson, G. P., Eickmann, B., Torres,
2359 M., & Horner, T. J. (2019). Barium-isotopic constraints on the origin of post-Marinoan barites.
2360 *Earth Planet. Sci. Lett.*, **519**, 234-244.

2361 Crusius, J., & Thomson, J. (2003). Mobility of authigenic rhenium, silver, and selenium during
2362 postdepositional oxidation in marine sediments. *Geochim. Cosmochim. Acta*, **67**(2), 265-273.

2363 Crusius, J., Calvert, S., Pedersen, T., & Sage, D. (1996). Rhenium and molybdenum enrichments in
2364 sediments as indicators of oxic, suboxic and sulfidic conditions of deposition. *Earth Planet. Sci.*
2365 *Lett.*, **145**, 65–78, doi:10.1016/S0012-821X(96)00204-X.

2366 Cullen, J. T. (2006). On the nonlinear relationship between dissolved cadmium and phosphate in the modern
2367 global ocean: could chronic iron limitation of phytoplankton growth cause the kink? *Limnol.*
2368 *Oceanogr.*, **51**(3), 1369-1380.

2369 Cullen, J. T., & Sherrell, R. M. (2005). Effects of dissolved carbon dioxide, zinc, and manganese on the
2370 cadmium to phosphorus ratio in natural phytoplankton assemblages. *Limnol. Oceanogr.*, **50**(4),
2371 1193-1204.

Cullen, J. T., Chase, Z., Coale, K. H., Fitzwater, S. E., & Sherrell, R. M. (2003). Effect of iron limitation on the cadmium to phosphorus ratio of natural phytoplankton assemblages from the Southern Ocean. *Limnology and Oceanography*, **48**(3), 1079-1087.

Cullen, J. T., Lane, T. W., Morel, F. M., & Sherrell, R. M. (1999). Modulation of cadmium uptake in phytoplankton by seawater CO_2 concentration. *Nature*, **402**(6758), 165.

Cullen, J. T., Chase, Z., Coale, K. H., Fitzwater, S. E., & Sherrell, R. M. (2003). Effect of iron limitation on the cadmium to phosphorus ratio of natural phytoplankton assemblages from the Southern Ocean. *Limnol. Oceanogr.*, **48**(3), 1079-1087.

Cullen, J. T., & Coogan, L. A. (2017). Changes in Fe Oxidation Rate in Hydrothermal Plumes as a Potential Driver of Enhanced Hydrothermal Input to Near-Ridge Sediments During Glacial Terminations. *Geophys. Res. Lett.*, **44**(23), 11-951.

Cutter, G., Casciotti, K., Croot, P., Geibert, W., Heimbürger, L.-E., Lohan, M., & van de Flierdt, T. (2017). *Sampling and Sample-handling Protocols for GEOTRACES Cruises*, Version 3. http://www.geotraces.org/images/stories/documents/intercalibration/Cookbook.pdf [accessed 2020-06-23].

da Silva, J. F., & Williams, R. J. P. (1991). *The biological chemistry of the elements: the inorganic chemistry of life*. Oxford University Press.

Dahl, T. W., Anbar, A. D., Gordon, G. W., Rosing, M. T., Frei, R., & Canfield, D. E. (2010). The behavior of molybdenum and its isotopes across the chemocline and in the sediments of sulfidic Lake Cadagno, Switzerland. *Geochim. Cosmochim. Acta*, **74**, 144–163, doi:10.1016/j.gca.2009.09.018.

Dahl, T. W., Chappaz, A., Hoek, J., McKenzie, C. J., Svane, S., and Canfield, D. E. (2017). Evidence of molybdenum association with particulate organic matter under sulfidic conditions. *Geobiology*, **15**, 311–323, doi:10.1111/gbi.12220.

Dalai, T.K., Nishimura, K., & Nozaki, Y. (2005). Geochemistry of molybdenum in the Chao Phraya River estuary, Thailand: Role of suboxic diagenesis and porewater transport. *Chem. Geol.*, **218**, 189–202, doi:10.1016/j.chemgeo.2005.01.002.

de Baar, H. J. W., Saager, P. M., Nolting, R. F., & van der Meer, J. (1994). Cadmium versus phosphate in the world ocean. *Mar. Chem.,* **46**(3), 261-281.

de Baar, H. J., Boyd, P. W., Coale, K. H., Landry, M. R., Tsuda, A., Assmy, P., ... & Buesseler, K. O. (2005). Synthesis of iron fertilization experiments: from the iron age in the age of enlightenment. *Journal of Geophysical Research: Oceans*, **110**(C9).

de Baar, H. J. W., van Heuven, S. M., Abouchami, W., Xue, Z., Galer, S. J. G., Rehkämper, M., Middag, R. & van Ooijen, J. (2017). Interactions of dissolved CO_2 with cadmium isotopes in the Southern Ocean. *Mar. Chem.* **195**, 105-121.

de Souza, G. F., Reynolds, B. C., Rickli, J., Frank, M., Saito, M. A., Gerringa, L. J., & Bourdon, B. (2012). Southern Ocean control of silicon stable isotope distribution in the deep Atlantic Ocean. *Global Biogeochem. Cycles*, **26**(2).

de Souza, G. F., Khatiwala, S. P., Hain, M. P., Little, S. H., & Vance, D. (2018). On the origin of the marine zinc–silicon correlation. *Earth Planet. Sci. Lett.,* **492**, 22-34.

Dean, W. E., Zheng, Y., Ortiz, J. D., & van Geen, A. (2006). Sediment Cd and Mo accumulation in the oxygen-minimum zone off western Baja California linked to global climate over the past 52 kyr. *Paleoceanography*, **21**, PA4209, doi:10.1029/2005PA001239.

Défarge, C. (2011). Organomineralization. Reitner, J., & Thiel, V. (eds.). *Encyclopedia of Geobiology*, Springer Verlag, pp.697-701, 2011, doi:10.1007/978-1-4020-9212-1_159.

Dehairs, F., Chesselet, R., & Jedwab, J. (1980). Discrete suspended particles of barite and the barium cycle in the open ocean. *Earth Planet. Sci. Lett.*, **49**(2), 528-550.

Dehairs, F., Lambert, C. E., Chesselet, R., & Risler, N. (1987). The biological production of marine suspended barite and the barium cycle in the Western Mediterranean Sea. *Biogeochemistry*, **4**(2), 119-140.

Dehairs, F., Jacquet, S., Savoye, N., Van Mooy, B. A., Buesseler, K. O., Bishop, J. K., Lamborg, C. H., Elskens, M., Baeyens, W., Boyd, P. W., Casciotti, K. L., & Monnin, C. (2008). Barium in twilight zone suspended matter as a potential proxy for particulate organic carbon remineralization: Results for the North Pacific. *Deep Sea Res. Pt. II*, **55**(14-15), 1673-1683.

Dellwig, O., Beck, M., Lemke, A., Lunau, M., Kolditz, K., Schnetger, B., & Brumsack, H.-J. (2007). Non-conservative behaviour of molybdenum in coastal waters: Coupling geochemical, biological, and sedimentological processes. *Geochim. Cosmochim. Acta*, **71**, 2745–2761, doi:10.1016/j.gca.2007.03.014.

Dellwig, O., Leipe, T., März, C., Glockzin, M., Pollehne, F., Schnetger, B., Yakushev, E. V., Böttcher, M. E., & Brumsack, H. J. (2010). A new particulate Mn-Fe-P-shuttle at the redoxcline of anoxic basins. *Geochim. Cosmochim. Acta*, **74**, 7100–7115, doi:10.1016/j.gca.2010.09.017.

Deng, N., Stack, A. G., Weber, J., Cao, B., De Yoreo, J. J., & Hu, Y. (2019). Organic–mineral interfacial chemistry drives heterogeneous nucleation of Sr-rich $(Ba_x, Sr_{1-x})SO_4$ from undersaturated solution. *Proc. Natl. Acad. Sci.*, 201821065.

Dickens, G.R., Fewless, T., Thomas, E. & Bralower, T.J. (2003). Excess barite accumulation during the Paleocene–Eocene Thermal Maximum: Massive input of dissolved barium from seafloor gas hydrate reservoirs. In Wing, S. L, Gingerich, P. D., Schmitz, B., & Thomas, E. (Eds.) *Causes and consequences of globally warm climates in the early Paleogene*, **369**, 11-23, Geological Society of America Special Papers; doi:10.1130/0-8137-2369-8.11.

Dickson, A. J. (2017). A molybdenum-isotope perspective on Phanerozoic deoxygenation events. *Nat. Geosci.*, **10**, 721–726, doi:10.1038/NGEO3028.

Dideriksen, K., Baker, J. A., & Stipp, S. L. S. (2008). Equilibrium Fe isotope fractionation between inorganic aqueous Fe (III) and the siderophore complex, Fe (III)-desferrioxamine B. *Earth Planet. Sci. Lett.*, **269**(1-2), 280-290.

Donat, J. R., & Bruland, K. W. (1990). A comparison of two voltammetric techniques for determining zinc speciation in Northeast Pacific Ocean waters. *Mar. Chem.*, **28**, 301–323.

Donat J. R., Lao, K. A., & Bruland, K. W. (1994) Speciation of dissolved copper and nickel in South San Francisco Bay: a multi-method approach. *Anal. Chim. Acta* **284**, 547–571.

Dunlea, A. G., Murray, R. W., Sauvage, J., Spivack, A. J., Harris, R. N., & D'Hondt, S. (2015). Dust, volcanic ash, and the evolution of the South Pacific Gyre through the Cenozoic. *Paleoceanogr.*, **30**(8), 1078-1099.

Dugdale, R. C., & Goering, J. J. (1967). Uptake of new and regenerated forms of nitrogen in primary production. *Limnol. Oceanogr.*, **12**(2), 196–206.

Dupont, C. L., Moffett, J. W., Bidigare, R. R., & Ahner, B. A. (2006). Distributions of dissolved and particulate biogenic thiols in the subarctic Pacific Ocean. *Deep. Res. Part I Oceanogr. Res. Pap.*, **53**, 1961–1974.

Dupont, C. L., Butcher, A., Valas, R. E., Bourne, P. E., & Caetano-Anolles, G. (2010). History of biological metal utilization inferred through phylogenomic analysis of protein structures. *Proc. Natl. Acad. Sci.*, **107**, 10567–10572.

2460 Dymond, J., Suess, E., & Lyle, M. (1992). Barium in deep-sea sediment: A geochemical proxy for
2461 paleoproductivity. *Paleoceanography*, **7**(2), 163-181.

2462 Dymond, J., & Collier, R. (1996). Particulate barium fluxes and their relationships to biological
2463 productivity. *Deep Sea Research Part II: Topical Studies in Oceanography*, **43**(4-6), 1283-1308.

2464 Eagle, M., Paytan, A., Arrigo, K. R., van Dijken, G., & Murray, R. W. (2003). A comparison between
2465 excess barium and barite as indicators of carbon export. *Paleoceanography*, **18**(1), 1021,
2466 https://doi.org/10.1029/2002PA000793.

2467 Edmond, J. M., Boyle, E. D., Drummond, D., Grant, B., & Mislick, T. (1978). Desorption of barium in the
2468 plume of the Zaire (Congo) River. *Netherlands Journal of Sea Research*, **12**(3-4), 324-328.

2469 Elderfield, H., & Rickaby, R. E. M. (2000). Oceanic Cd/P ratio and nutrient utilization in the glacial
2470 Southern Ocean. *Nature*, **405**(6784), 305-310.

2471 Elliott, T., & Steele, R. C. (2017). The isotope geochemistry of Ni. *Reviews in Mineralogy and*
2472 *Geochemistry*, **82**(1), 511-542.

2473 Ellwood, M. J. (2004). Zinc and cadmium speciation in subantarctic waters east of New Zealand. *Mar.*
2474 *Chem.*, **87**(1-2), 37-58.

2475 Ellwood, M. J., & Hunter, K. A. (2000). The Incorporation of Zinc and Iron into the Frustule of the Marine
2476 Diatom *Thalassiosira pseudonana*. *Limnol. Oceanogr.,* **45**, 1517–1524.

2477 Ellwood, M. J., & Van Den Berg, C. M. G. (2000). Zinc speciation in the Northeastern Atlantic Ocean.
2478 *Mar. Chem,*. **68**, 295–306.

2479 Ellwood, M.J., Hutchins, D.A., Lohan, M.C., Milne, A., Nasemann, P., Nodder, S.D., Sander, S.G.,
2480 Strzepek, R., Wilhelm, S.W., & Boyd, P.W. (2015). Iron stable isotopes track pelagic iron cycling
2481 during a subtropical phytoplankton bloom. *Proc. Natl. Acad. Sci. U. S. A.* **112**, E15-E20.

2482 Ellwood, M. J., Strzepek, R. F., Strutton, P. G., Trull, T. W., Fourquez, M., & Boyd, P. W. (2020). Distinct
2483 iron cycling in a Southern Ocean eddy. *Nature Communications*, **11**(1), 1-8.

2484 Emerson, S. R., & Huested, S. S. (1991). Ocean anoxia and the concentrations of molybdenum and
2485 vanadium in seawater. *Mar. Chem.* **34**, 177–196, doi:10.1016/0304-4203(91)90002-E.

2486 Erickson, B. E., & Helz, G. R. (2000). Molybdenum(VI) speciation in sulfidic waters: Stability and lability
2487 of thiomolybdates. *Geochim. Cosmochim. Acta*, **64**, 1149–1158, doi:10.1016/S0016-
2488 7037(99)00423-8.

2489 Escoube, R., Rouxel, O. J., Pokrovsky, O. S., Schroth, A., Max Holmes, R., & Donard, O. F. X. (2015).
2490 Iron isotope systematics in Arctic rivers. *Comptes Rendus Geosci*,, **347**(7–8), 377–385.

2491 Escoube, R., Rouxel, O. J., Sholkovitz, E., & Donard, O. F. X. (2009). Iron isotope systematics in estuaries:
2492 The case of North River, Massachusetts (USA). *Geochim. Cosmochim. Acta*, **73**(14), 4045–4059.

2493 Esser, B. K., & Volpe, A. M. (2002). At-sea high-resolution chemical mapping: extreme barium depletion
2494 in North Pacific surface water. *Mar. Chem.*, **79**(2), 67-79.

2495 Fantle, M. S., & DePaolo, D. J., (2004). Iron isotopic fractionation during continental weathering. *Earth*
2496 *Planet. Sci. Lett.*, **228**(3-4), 547-562.

2497 Farmer, J. R., Hönisch, B., Haynes, L. L., Kroon, D., Jung, S., Ford, H. L., Raymo, M. E., Jaume-Seguí,
2498 M., Bell, D. B., Goldstein, S. L., Pena, L. D., Yehudai, M., & Kim, J. (2019). Deep Atlantic Ocean
2499 carbon storage and the rise of 100,000-year glacial cycles. *Nat. Geosci.* **12**, 355-360,
2500 https://doi.org/10.1038/s41561-019-0334-6.

Fassbender, A. J., Palevsky, H. I., Martz, T. R., Ingalls, A. E., Gledhill, M., Fawcett, S. E., Brandes, J. A., Aluwihare, L. I., & the participants of COME ABOARD and DISCO XXV (2017). Perspectives on Chemical Oceanography in the 21st century: Participants of the COME ABOARD Meeting examine aspects of the field in the context of 40 years of DISCO. *Mar. Chem.*, **196**, 181-190.

Finlay, B. J., Hetherington, N. B., & Da Vison, W. (1983). Active biological participation in lacustrine barium chemistry. *Geochim. Cosmochim. Acta*, **47**(7), 1325-1329.

Fischer, L., Smith, G., Hann, S., & Bruland, K. W. (2018). Ultra-trace analysis of silver and platinum in seawater by ICP-SFMS after off-line matrix separation and pre-concentration. *Mar. Chem.*, **199**, 44-52.

Fisher, N.S., & Wente, M. (1993). The release of trace elements by dying marine phytoplankton. *Deep-Sea Research I*, 40(4), 671-694.

Fishwick, M. P., Sedwick, P. N., Lohan, M. C., Worsfeld, P. J., Buck, K. N., Church, T. M., Ussher, S. J. (2014). The impact of changing surface ocean conditions on the dissolution of aerosol iron. *Global Biogeochem. Cycles,* **28**(11), 1235-1250. https://doi.org/10.1002/2014GB004921.

Fitzsimmons, J. N., & Boyle, E. A. (2014). Both soluble and colloidal iron phases control dissolved iron variability in the tropical North Atlantic Ocean. *Geochim. Cosmochim. Acta*, **125**, 539-550.

Fitzsimmons, J. N., Carrasco, G. G., Wu, J., Roshan, S., Hatta, M., Measures, C. I., Conway, T. M., John, S.G., & Boyle, E. A. (2015). Partitioning of dissolved iron and iron isotopes into soluble and colloidal phases along the GA03 GEOTRACES North Atlantic Transect. *Deep Sea Res. Pt. II*, **116**, 130-151.

Fitzsimmons, J. N., Conway, T. M., Lee, J.-M., Kayser, R., Thyng, K. M., John, S. G. and Boyle, E. A. (2016). Dissolved iron and iron isotopes in the Southeastern Pacific Ocean. *Global Biogeochem. Cycles,* **30**(10), 1372-1395. https://doi.org/10.1002/2015GB005357.

Fitzsimmons, J. N., John, S. G., Marsay, C. M., Hoffman, C. L., Nicholas, S. L., Toner, B. M., German, C. R., & Sherrell, R. M. (2017). Iron persistence in a distal hydrothermal plume supported by dissolved–particulate exchange. *Nature Geoscience*, **10**(3), 195-201.

Flegal, A.R., Sanudo-Wilhelmy, S.A., & Scelfo, G.M. (1995). Silver in the eastern Atlantic Ocean. *Mar. Chem.*, **49**, 315-320.

Franck, V. M., Bruland, K. W., Hutchins, D. A., & Brzezinski, M. A. (2003). Iron and zinc effects on silicic acid and nitrate uptake kinetics in three high-nutrient, low-chlorophyll (HNLC) regions. *Mar. Ecol. Prog. Ser.,* **252**, 15–33.

Francois, R., Honjo, S., Manganini, S. J., & Ravizza, G. E. (1995). Biogenic barium fluxes to the deep sea: Implications for paleoproductivity reconstruction. *Global Biogeochem. Cycles*, **9**(2), 289-303.

Frew, R. D., & Hunter, K. A. (1992). Influence of Southern Ocean waters on the cadmium–phosphate properties of the global ocean. *Nature*, **360**(6400), 144.

Friedl, G., & Pedersen, T. (2002). Silver as a new tracer for diatom production. *Eawag News*, 52, 14-15.

Froelich, P., Klinkhammer, G. P., Bender, M. L., Luedtke, N. A., Heath, G. R., Cullen, D., Dauphin, P., Hammond D., Hartman, B., & Maynard, V. (1979). Early oxidation of organic matter in pelagic sediments of the eastern equatorial Atlantic: suboxic diagenesis. *Geochimica et Cosmochimica Acta*, **43**(7), 1075-1090.

Fru, E. C., Rodríguez, N. P., Partin, C. A., Lalonde, S. V., Andersson, P., Weiss, D. J., El Albani, A., Rodushkin, I., & Konhauser, K. O. (2016). Cu isotopes in marine black shales record the Great Oxidation Event. *Proceedings of the National Academy of Sciences*, **113**(18), 4941-4946.

Fujii, T., Moynier, F., Pons, M. L., & Albarède, F. (2011a). The origin of Zn isotope fractionation in sulfides. *Geochim. Cosmochim. Acta*, **75**(23), 7632-7643.

Fujii, T., Moynier, F., Dauphas, N., & Abe, M. (2011b). Theoretical and experimental investigation of nickel isotopic fractionation in species relevant to modern and ancient oceans. *Geochim. Cosmochim. Acta*, **75**(2), 469-482.

Fujii, T., Moynier, F., Abe, M., Nemoto, K., & Albarède, F. (2013). Copper isotope fractionation between aqueous compounds relevant to low temperature geochemistry and biology. *Geochim. Cosmochim. Acta*, **110**, 29-44.

Gall, L., Williams, H. M., Siebert, C., Halliday, A. N., Herrington, R. J., & Hein, J. R. (2013). Nickel isotopic compositions of ferromanganese crusts and the constancy of deep ocean inputs and continental weathering effects over the Cenozoic. *Earth Planet. Sci. Lett.*, **375**, 148-155.

Gallon, C., & Flegal, A. R. (2015). Sources, Fluxes, and Biogeochemical Cycling of Silver in the Oceans. In: Whitacre, D. (eds) *Rev. Environ. Contamin. Toxicol.* **235**. Springer, Cham. https://doi.org/10.1007/978-3-319-10861-2_2.

Ganeshram, R. S., François, R., Commeau, J., & Brown-Leger, S. L. (2003). An experimental investigation of barite formation in seawater. *Geochim. Cosmochim. Acta*, **67**(14), 2599-2605.

Garcia, H. E., R. A. Locarnini, T. P. Boyer, J. I. Antonov, O.K. Baranova, M.M. Zweng, J.R. Reagan, D.R. Johnson, 2014. World Ocean Atlas 2013, Volume 3: Dissolved Oxygen, Apparent Oxygen Utilization, and Oxygen Saturation. S. Levitus, Ed., A. Mishonov Technical Ed.; *NOAA Atlas NESDIS 75*, 27 pp.

Gault-Ringold, M., Adu, T., Stirling, C. H., Frew, R. D., & Hunter, K. A. (2012). Anomalous biogeochemical behavior of cadmium in Subantarctic surface waters: mechanistic constraints from cadmium isotopes. *Earth Planet. Sci. Lett.*, **341**, 94-103.

George, E., Stirling, C. H., Gault-Ringold, M., Ellwood, M. J., & Middag, R. (2019). Marine biogeochemical cycling of cadmium and cadmium isotopes in the extreme nutrient-depleted subtropical gyre of the South West Pacific Ocean. *Earth Planet. Sci. Lett.*, **514**, 84-95.

Georgiev, S. V., Horner, T. J., Stein, H. J., Hannah, J. L., Bingen, B., & Rehkämper, M. (2015). Cadmium-isotopic evidence for increasing primary productivity during the Late Permian anoxic event. *Earth Planet. Sci. Lett.*, **410**, 84-96.

Geyman, B. M., Ptacek, J. L., LaVigne, M., & Horner, T. J. (2019). Barium in deep-sea bamboo corals: Phase associations, barium stable isotopes, & prospects for paleoceanography. *Earth Planet. Sci. Lett.*, **525**, 115751.

Giering, S. L., Sanders, R., Lampitt, R. S., Anderson, T. R., Tamburini, C., Boutrif, M., Zubkov, M. V., Marsay, C. M., Henson, S. A., Saw, K., Cook, K., & Mayor, D. J.(2014). Reconciliation of the carbon budget in the ocean's twilight zone. *Nature*, **507**(7493), 480-483.

Glass, J. B., Axler, R. P., Chandra, S., & Goldman, C. R. (2012). Molybdenum limitation of microbial nitrogen assimilation in aquatic ecosystems and pure cultures. *Frontiers in Microbiology*, **3**, 1–11, doi:10.3389/fmicb.2012.00331.

Glass, J. B., Wolfe-Simon, F., & Anbar, A. D. (2009). Coevolution of metal availability and nitrogen assimilation in cyanobacteria and algae. *Geobiology*, **7**, 100–123, doi:10.1111/j.1472-4669.2009.00190.x.

Goldberg, T., Archer, C., Vance, D., & Poulton, S. W. (2009). Mo isotope fractionation during adsorption to Fe (oxyhydr)oxides. *Geochim. Cosmochim. Acta*, **73**, 6502–6516, doi:10.1016/j.gca.2009.08.004.

Goldberg, T., Archer, C., Vance, D., Thamdrup, B., McAnena, A., & Poulton, S. W. (2012). Controls on Mo isotope fractionations in a Mn-rich anoxic marine sediment, Gullmar Fjord, Sweden. *Chem. Geol.*, **296-297**, 73-82, doi:10.1016/j.chemgeo.2011.12.020.

Goldberg, T., Gordon, G., Izon, G., Archer, C., Pearce, C. R., McManus, J., Anbar, A. D., & Rehkämper, M. (2013). Resolution of inter-laboratory discrepancies in Mo isotope data: an intercalibration. *Journal of Analytical Atomic Spectrometry*, **28**(5), 724-735.

Goldman, C. R. (1960). Molybdenum as a Factor Limiting Primary Productivity in Castle Lake, California. *Science*, **132**, 1016–1017, doi:10.1126/science.132.3433.1016.

Gooday, A. J., & Nott, J. A. (1982). Intracellular barite crystals in two xenophyophores, Aschemonella ramuliformis and *Galatheammina sp.* (Protozoa: Rhizopoda) with comments on the taxonomy of *A. ramuliformis. Journal of the Marine Biological Association of the United Kingdom*, **62**(3), 595-605.

Goto, K. T., Sekine, Y., Shimoda, G., Hein, J. R., Aoki, S., Ishikawa, A., Suzuki, K., Gordon, G. W., & Anbar, A. D. (2020). A framework for understanding Mo isotope records of Archean and Paleoproterozoic Fe-and Mn-rich sedimentary rocks: Insights from modern marine hydrothermal Fe-Mn oxides. *Geochim. Cosmochim. Acta*, **280**, 221-236.

Gou, L. F., Jin, Z., Galy, A., Gong, Y. Z., Nan, X. Y., Jin, C., Wang, X.-D., Bouchez, J., Cai, H.-M., Chen, J.-B., Yu, H.-M., & Huang, F. (2020). Seasonal riverine barium isotopic variation in the middle Yellow River: Sources and fractionation. *Earth and Planetary Science Letters*, **531**, 115990.

Gueguen, B., Rouxel, O., Ponzevera, E., Bekker, A., & Fouquet, Y. (2013). Nickel isotope variations in terrestrial silicate rocks and geological reference materials measured by MC-ICP-MS. *Geostandards and Geoanalytical Research*, **37**(3), 297-317.

Gueguen, B., Rouxel, O., Rouget, M. L., Bollinger, C., Ponzevera, E., Germain, Y., & Fouquet, Y. (2016). Comparative geochemistry of four ferromanganese crusts from the Pacific Ocean and significance for the use of Ni isotopes as paleoceanographic tracers. *Geochim. Cosmochim. Acta*, **189**, 214-235.

Guinoiseau, D., Galer, S. J., & Abouchami, W. (2018). Effect of cadmium sulphide precipitation on the partitioning of Cd isotopes: Implications for the oceanic Cd cycle. *Earth Planet. Sci. Lett.*, **498**, 300-308.

Guo, J., Lapi, S., Ruth, T. J., & Maldonado, M. T. (2012). The effects of iron and copper availability on the copper stoichiometry of marine phytoplankton. *J. Phycol.* **48**, 312–325.

Hanor, J. S., & Chan, L. H. (1977). Non-conservative behavior of barium during mixing of Mississippi River and Gulf of Mexico waters. *Earth and Planetary Science Letters*, **37**(2), 242-250.

Hanor, J. S. (2000). Barite–celestine geochemistry and environments of formation. *Reviews in Mineralogy and Geochemistry*, **40**(1), 193-275.

Hardisty, D. S., Riedinger, N., Planavsky, N. J., Asael, D., Andrén, T., et al. (2016). A Holocene history of dynamic water column redox conditions in the Landsort Deep, Baltic Sea. *Am. J. Sci.*, **316**, 713-745, doi:10.2475/08.2016.01.

Hardisty, D. S., Lyons, T. W., Riedinger, N., Isson, T. T., Owens, J. D., Aller, R. C., Rye, D. M., Planavsky, N. J., Reinhard, C. T., Gill, B. C., Masterson, A. L., Asael, D., & Johnston, D. T. (2018). An evaluation of sedimentary molybdenum and iron as proxies for pore fluid paleoredox conditions. *Am. J. Sci.*, **318**(5), 527-556.

Hartnett, H. E., Keil, R. G., Hedges, J. I., & Devol, A. H. (1998). Influence of oxygen exposure time on organic carbon preservation in continental margin sediments. *Nature*, **391**(6667), 572-575.

Hawco, N. J., Lam, P. J., Lee, J. M., Ohnemus, D. C., Noble, A. E., Wyatt, N. J., Lohan, M. C., & Saito, M. A. (2018). Cobalt scavenging in the mesopelagic ocean and its influence on global mass balance: Synthesizing water column and sedimentary fluxes. *Marine Chemistry*, **201**, 151-166.

Hayes, C. T., Anderson, R. F., Cheng, H., Conway, T. M., Edwards, R. L., Fleisher, M. Q., Ho, P., Huang, K.-F., John, S. G., Landing, W. M., Little, S. H., Lu, Y., Morton, P. L., Moran, S. B., Robinson, L. F., Shelley, R. U., Shiller, A. M., & Zheng, X.-Y. (2018). Replacement times of a spectrum of elements in the North Atlantic based on thorium supply. *Global Biogeochem. Cycles*, **32**(9), 1294-1311.

Heller, M. I., & Croot, P. L. (2015). Copper speciation and distribution in the Atlantic sector of the Southern Ocean. *Mar. Chem.,* **173**, 253-268.

Helz, G. R., Miller, C. V., Charnock, J. M., Mosselmans, J. F. W., Pattrick, R. A. D., Garner, C. D., & Vaughan, D. J. (1996). Mechanism of molybdenum removal from the sea and its concentration in black shales: EXAFS evidence. *Geochim. Cosmochim. Acta*, **60**, 3631–3642, doi:10.1016/0016-7037(96)00195-0.

Hemsing, F., Hsieh, Y. T., Bridgestock, L., Spooner, P. T., Robinson, L. F., Frank, N., & Henderson, G. M. (2018). Barium isotopes in cold-water corals. *Earth and Planetary Science Letters*, **491**, 183-192.

Henderson, G. M., & Burton, K. W. (1999). Using (234U/238U) to assess diffusion rates of isotope tracers in ferromanganese crusts. *Earth Planet. Sci. Lett.*, **170**(3), 169-179.

Hendry, K. R., & Andersen, M. B. (2013). The zinc isotopic composition of siliceous marine sponges: Investigating nature's sediment traps. *Chem. Geol.,* **354**, 33–41. Available at: http://dx.doi.org/10.1016/j.chemgeo.2013.06.025.

Hendry, K. R., Pyle, K. M., Barney Butler, G., Cooper, A., Fransson, A., Chierici, M., Leng, M. J., Meyer, A., & Dodd, P.A. (2018). Spatiotemporal Variability of Barium in Arctic Sea-Ice and Seawater. *J. Geophys. Res. Oceans*, **123**(5), 3507-3522.

Hendy, I. L., & Pedersen, T. F. (2005). Is pore water oxygen content decoupled from productivity on the California Margin? Trace element results from Ocean Drilling Program Hole 1017E, San Lucia slope, California. *Paleoceanography*, **20**(4).

Henkel, S., Kasten, S., Hartmann, J. F., Silva-Busso, A., & Staubwasser, M. (2018). Iron cycling and stable Fe isotope fractionation in Antarctic shelf sediments, King George Island. *Geochim. Cosmochim. Acta,* **237**, 320-338. https://doi.org/10.1016/j.gca.2018.06.042.

Hillaire-Marcel, C., & De Vernal, A. (Eds.). (2007). *Proxies in Late Cenozoic Paleoceanography*. Elsevier.

Ho, P., Lee, J. M., Heller, M. I., Lam, P. J., and Shiller, A. M. (2018). The distribution of dissolved and particulate Mo and V along the U.S. GEOTRACES East Pacific Zonal Transect (GP16): The roles of oxides and biogenic particles in their distributions in the oxygen deficient zone and the hydrothermal plume. *Mar. Chem.*, **201**, 242–255, doi:10.1016/j.marchem.2017.12.003.

Ho, T. Y., Quigg, A., Finkel, Z. V., Milligan, A. J., Wyman, K., Falkowski, P. G., & Morel, F. M. (2003). The elemental composition of some marine phytoplankton 1. *Journal of Phycology*, **39**(6), 1145-1159.

Hodgskiss, M. S., Crockford, P. W., Peng, Y., Wing, B. A., & Horner, T. J. (2019). A productivity collapse to end Earth's Great Oxidation. *Proc. Natl. Acad. Sci.,* **116**(35), 17207-17212.

Hohl, S. V., Galer, S. J. G., Gamper, A., & Becker, H. (2017). Cadmium isotope variations in Neoproterozoic carbonates–A tracer of biologic production?. *Geochemical Perspective Letters*, **3**, 32-44.

Hohl, S. V., Jiang, S. Y., Wei, H. Z., Pi, D. H., Liu, Q., Viehmann, S., & Galer, S. J. (2019). Cd Isotopes trace periodic (bio)geochemical metal cycling at the verge of the Cambrian animal evolution. *Geochim. Cosmochim. Acta*, **263**, 195-214, doi:10.1016/j.gca.2019.07.036.

Holzer, M., Primeau, F. W., DeVries, T., & Matear, R. (2014). The Southern Ocean silicon trap: Data-constrained estimates of regenerated silicic acid, trapping efficiencies, and global transport paths. *J. Geophys. Res. Oceans*, **119**(1), 313-331.

Homoky, W. B.., Severmann, S., Mills, R. A., & Fones, G. R. (2009). Pore-fluid Fe isotopes reflect the extent of benthic Fe redox recycling: evidence from continental shelf and deep-sea sediments. *Geology,* **37**, 751–754. https://doi.org/10.1130/G25731A.1.

Homoky, W. B., John, S. G., Conway T. M., & Mills, R. A. (2013). Distinct iron isotopic signatures and supply from marine sediment dissolution. *Nat. Comms*, **4**, 2143. https://doi.org/10.1038/ncomms3143.

Hoppema, M., Dehairs, F., Navez, J., Monnin, C., Jeandel, C., Fahrbach, E., & De Baar, H. J. W. (2010). Distribution of barium in the Weddell Gyre: Impact of circulation and biogeochemical processes. *Marine Chemistry*, **122**(1-4), 118-129.

Horner, T. J., Schönbächler, M., Rehkämper, M., Nielsen, S. G., Williams, H., Halliday, A. N., Xue, Z., & Hein, J. R. (2010). Ferromanganese crusts as archives of deep water Cd isotope compositions. *Geochemistry, Geophysics, Geosystems*, **11**(4), Q04001, https://doi.org/10.1029/2009GC002987.

Horner, T. J., Rickaby, R. E., & Henderson, G. M. (2011). Isotopic fractionation of cadmium into calcite. *Earth Planet. Sci. Lett.*, **312**(1-2), 243-253.

Horner, T. J., Lee, R. B., Henderson, G. M., & Rickaby, R. E. (2013). Nonspecific uptake and homeostasis drive the oceanic cadmium cycle. *Proc. Natl. Acad. Sci.,* **110**(7), 2500-2505.

Horner, T. J., Kinsley, C. W., & Nielsen, S. G. (2015a). Barium-isotopic fractionation in seawater mediated by barite cycling and oceanic circulation. *Earth Planet. Sci. Lett.*, **430**, 511-522.

Horner, T. J., Williams, H. M., Hein, J. R., Saito, M. A., Burton, K. W., Halliday, A. N., & Nielsen, S. G. (2015b). Persistence of deeply sourced iron in the Pacific Ocean. *Proc. Natl. Acad. Sci.*, **112**, 1292-1297.

Horner, T. J., Pryer, H. V., Nielsen, S. G., Crockford, P. W., Gauglitz, J. M., Wing, B. A., & Ricketts, R. D. (2017). Pelagic barite precipitation at micromolar ambient sulfate. *Nat. Commun.*, **8**(1), 1342.

Hsieh, Y. T., & Henderson, G. M. (2017). Barium stable isotopes in the global ocean: tracer of Ba inputs and utilization. *Earth Planet. Sci. Lett.*, **473**, 269-278.

Hudson, R. J. M., & Morel, F. M. M. (1993). Trace metal transport by marine microorganisms: Implications of metal coordination kinetics. *Deep Sea Res.* **40**, 129–150.

Ijichi, Y., Ohno, T., & Sakata, S. (2018). Copper isotopic fractionation during adsorption on manganese oxide: Effects of pH and desorption. *Geochemical Journal*, *52*(2), e1-e6.

Ilina, S. M., Poitrasson, F., Lapitskiy, S. A., Alekhin, Y. V., Viers, J., & Pokrovsky, O. S. (2013). Extreme iron isotope fractionation between colloids and particles of boreal and temperate organic-rich waters. *Geochim. et Cosmochim. Acta*, **101**, 96–111.

Ingri, J., Malinovsky, D., Rodushkin, I., Baxter, D.C., Widerlund, A., Andersson, P., Gustafsson, Ö., Forsling, W. & Öhlander, B. (2006). Iron isotope fractionation in river colloidal matter. *Earth Planet. Sci. Lett.*, **245**(3–4), 792–798.

Isson, T. T., Love, G. D., Dupont, C. L., Reinhard, C. T., Zumberge, A. J., Asael, D., Gueguen, B., McCrow, J., Gill, B. C., Owens, J., Rainbird, R. H., Rooney, A. D., Zhao, M. Y., Stueeken, E. E., Konhauser,

K. O., John, S. G., Lyons, T. W,. & Planavsky, N. J. (2018). Tracking the rise of eukaryotes to ecological dominance with zinc isotopes. *Geobiology,* **16**, 341–352.

Ivanochko, T. S. (2001). Productivity influences on oxygenation of the Santa Barbara Basin, California, during the Late Quaternary (Doctoral dissertation, University of British Columbia).

Jaccard, S. L., Haug, G. H., Sigman, D. M., Pedersen, T. F., Thierstein, H. R., & Röhl, U. (2005). Glacial/interglacial changes in subarctic North Pacific stratification. Science, **308**(5724), 1003-1006.

Jaccard, S. L., Hayes, C. T., Martínez-García, A., Hodell, D. A., Anderson, R. F., Sigman, D. M., & Haug, G. H. (2013). Two modes of change in Southern Ocean productivity over the past million years. *Science*, **339**(6126), 1419-1423.

Jacquet, S. H., Dehairs, F., Elskens, M., Savoye, N., & Cardinal, D. (2007). Barium cycling along WOCE SR3 line in the Southern Ocean. *Mar. Chem.*, **106**(1-2), 33-45.

Jacquot, J. E., & Moffett, J. W. (2015). Copper distribution and speciation across the International GEOTRACES Section GA03. *Deep Sea Res. Pt. II*, **116**, 187-207, doi:10.1016/j.dsr2.2014.11.013.

Jakuba, R. W., Saito, M. A., Moffett, J. W., & Xu, Y. (2012). Dissolved zinc in the subarctic North Pacific and Bering Sea: Its distribution, speciation, and importance to primary producers. *Global Biogeochem. Cycles,* **26**, 1–15.

Janssen, D. J., & Cullen, J. T. (2015). Decoupling of zinc and silicic acid in the subarctic northeast Pacific interior. *Mar. Chem.,* **177**, 124–133. http://dx.doi.org/10.1016/j.marchem.2015.03.014.

Janssen, D. J., Conway, T. M., John, S. G., Christian, J. R., Kramer, D. I., Pedersen, T. F., & Cullen, J. T. (2014). Undocumented water column sink for cadmium in open ocean oxygen-deficient zones. *Proc. Natl. Acad. Sci.,* **111**(19), 6888-6893.

Janssen, D. J., Abouchami, W., Galer, S. J. G., & Cullen, J. T. (2017). Fine-scale spatial and interannual cadmium isotope variability in the subarctic northeast Pacific. *Earth Planet. Sci. Lett.*, **472**, 241-252.

Janssen, D. J., Abouchami, W., Galer, S. J., Purdon, K. B., & Cullen, J. T. (2019). Particulate cadmium stable isotopes in the subarctic northeast Pacific reveal dynamic Cd cycling and a new isotopically light Cd sink. *Earth Planet. Sci. Lett.*, **515**, 67-78.

John, S. G., & Conway, T. M. (2014). A role for scavenging in the marine biogeochemical cycling of zinc and zinc isotopes. *Earth Planet. Sci. Lett.*, **394**, 159-167.

John, S. G., Geis R. W., Saito M. A., & Boyle E. A. (2007). Zinc isotope fractionation during high affinity and low-affinity zinc transport by the marine diatom *Thalassiosire oceanica*. *Limnol. Oceanogr.,* **52**, 2710–2714.

John, S. G., Mendez, J., Moffett, J., & Adkins, J. (2012). The flux of iron and iron isotopes from San Pedro Basin sediments. *Geochim. Cosmochim. Acta*, **93**, 14-29.

John, S. G., Kunzmann, M., Townsend, E. J., & Rosenberg, A. D. (2017). Zinc and cadmium stable isotopes in the geological record: A case study from the post-snowball Earth Nuccaleena cap dolostone. *Palaeogeography, Palaeoclimatology, Palaeoecology*, **466**, 202-208.

John, S. G., Helgoe, J., Townsend, E., Weber, T., DeVries, T., Tagliabue, A., Moore, K., Lam, P., Marsay, C.M., & Till, C. (2018a). Biogeochemical cycling of Fe and Fe stable isotopes in the Eastern Tropical South Pacific. *Mar. Chem.* **201**, 66-76.

John, S. G., Helgoe, J., & Townsend, E. (2018b). Biogeochemical cycling of Zn and Cd and their stable isotopes in the Eastern Tropical South Pacific. *Mar. Chem.*, **201**, 256-262.

2761 Johnson, C.M., Skulan, J.L., Beard, B. L., Sun, H., Nealson, K. H., & Braterman, P. S. (2002). Isotopic
2762 fractionation between Fe(III) and Fe(II) in aqueous solutions. *Earth. Planet. Sci. Lett.,* **195**, 141–
2763 153. https://doi.org/10.1016/S0012-821X(01)00581-7.

2764 Johnson, C. M., Beard, B. L., & Roden, E. E. (2008). The iron isotope fingerprints of redox and
2765 biogeochemical cycling in modern and ancient Earth. *Annu. Rev. Earth Planet. Sci.*, **36**, 457-493.

2766 Johnson, C. M., Beard, B. L., & Weyer, S. (2020). *Iron Geochemistry: An Isotopic Perspective*. Springer.
2767 doi:10.1007/978-3-030-33828-2.

2768 Joung, D. J., and Shiller, A. M. (2016). Temporal and spatial variations of dissolved and colloidal trace
2769 elements in Louisiana Shelf waters. *Mar. Chem.* **181**, 25–43, doi:10.1016/j.marchem.2016.03.003.

2770 Jullion, L., Jacquet, S. H. M., & Tanhua, T. (2017). Untangling biogeochemical processes from the impact
2771 of ocean circulation: First insight on the Mediterranean dissolved barium dynamics. *Global*
2772 *Biogeochem. Cycles*, **31**(8), 1256-1270.

2773 Kellogg, M. M., McIlvin, M. R., Vedamati, J., Twining, B. S., Moffett, J. W., Marchetti, A., Moran, D. M.,
2774 & Saito, M. A. (2020). Efficient zinc/cobalt inter-replacement in northeast Pacific diatoms and
2775 relationship to high surface dissolved Co: Zn ratios. *Limnol. Oceanogr*. doi:10.1002/lno.11471.

2776 Kendall, B., Komiya, T., Lyons, T. W., Bates, S. M., Gordon, G. W., Romaniello, S. J., Jiang, G., Creaser,
2777 R. A., Xiao, S., McFadden, K., Sawaki, Y., Tahata, M., Shu, D., Han, J., Li, Y., Chu, X., & Anbar,
2778 A. D. (2015). Uranium and molybdenum isotope evidence for an episode of widespread ocean
2779 oxygenation during the late ediacaran period. *Geochim. Cosmochim. Acta*, **156**, 173–193,
2780 doi:10.1016/j.gca.2015.02.025.

2781 Kendall, B., Dahl, T. W., & Anbar, A. D. (2017). The Stable Isotope Geochemistry of Molybdenum. *Rev.*
2782 *Min. Geochem.*, **82**, 683–732, doi:10.2138/rmg.2017.82.16.

2783 Khatiwala, S., Schmittner, A., & Muglia, J. (2019). Air-sea disequilibrium enhances ocean carbon storage
2784 during glacial periods. *Science Advances*, **5**(6), eaaw4981.

2785 Kienast, S. (2003). Palaeoceanography of the mid-latitude North East Pacific: during the late Pleistocene
2786 (Doctoral dissertation, University of British Columbia).

2787 Kim, T., Obata, H., Kondo, Y., Ogawa, H., & Gamo, T. (2015). Distribution and speciation of dissolved
2788 zinc in the western North Pacific and its adjacent seas. *Mar. Chem.,* **173**, 330–341.
2789 http://dx.doi.org/10.1016/j.marchem.2014.10.016.

2790 King, E. K., Thompson, A., Hodges, C., & Pett-Ridge, J. C. (2014). Towards Understanding Temporal and
2791 Spatial Patterns of Molybdenum in the Critical Zone. *Procedia Earth and Planetary Science*, **10**,
2792 56–62, doi:10.1016/j.proeps.2014.08.011.

2793 King, E. K., Thompson, A., Chadwick, O. A., & Pett-Ridge, J. C. (2016). Molybdenum sources and isotopic
2794 composition during early stages of pedogenesis along a basaltic climate transect. *Chem. Geol.*, **445**,
2795 54–67, doi:10.1016/j.chemgeo.2016.01.024.

2796 King, E. K., Perakis, S. S., & Pett-Ridge, J. C. (2018). Molybdenum isotope fractionation during adsorption
2797 to organic matter. *Geochim. Cosmochim. Acta*, **222**, 584–598, doi:10.1016/j.gca.2017.11.014.

2798 Klar, J. K., James, R. H., Gibbs, D., Lough, A., Parkinson, I., Milton, J. A., Hawkes, J. A., & Connelly, D.
2799 P. (2017a). Isotopic signature of dissolved iron delivered to the Southern Ocean from hydrothermal
2800 vents in the East Scotia Sea. *Geology*, 4**5**(4), 351-354. https://doi.org/10.1130/G38432.1.

2801 Klar, J. K., Homoky, W. B., Statham, P. J., Birchill, A. J., Harris, E. L., Woodward, E. M. S., Silburn, B.,
2802 Cooper, M. J., James, R. H., Connelly, D. P., Chever, F., Lichtschlag, A., & Graves, C. (2017b).
2803 Stability of dissolved and soluble Fe(II) in shelf sediment pore waters and release to an oxic water
2804 column. *Biogeochem.*, **135,** 1-19. https://doi.org/10.1007/s10533-017-0309-x.

2805 Klar, J. K., Schlosser, C., Milton, J. A., Woodward, E. M. S., Lacan, F., Parkinson, I. J., Achterberg, E., &
2806 James, R. H. (2018). Sources of dissolved iron to oxygen minimum zone waters on the Senegalese
2807 continental margin in the tropical North Atlantic Ocean: Insights from iron isotopes. *Geochim. Cosmochim. Acta*, **236**, 60-78. https://doi.org/10.1016/j.gca.2018.02.031.

2809 Klinkhammer, G. P. (1980). Early diagenesis in sediments from the eastern equatorial Pacific, II. Pore water
2810 metal results. *Earth Planet. Sci. Lett.*, **49**(1), 81-101.

2811 Klunder, M. B., Laan, P., Middag, R., De Baar, H. J. W., & van Ooijen, J. C. (2011). Dissolved iron in the
2812 Southern Ocean (Atlantic sector). *Deep Sea Res. Pt. II*, **58**, 2678-2694,
2813 doi:10.1016/j.dsr2.2010.10.042.

2814 Köbberich, M., & Vance, D. (2017). Kinetic control on Zn isotope signatures recorded in marine diatoms.
2815 *Geochim. Cosmochim. Acta,* **210**, 97–113. http://dx.doi.org/10.1016/j.gca.2017.04.014.

2816 Köbberich, M., & Vance, D. (2019). Zn isotope fractionation during uptake into marine phytoplankton:
2817 Implications for oceanic zinc isotopes. *Chem. Geol.*, **523**, 154-161,
2818 doi:10.1016/j.chemgeo.2019.04.004.

2819 Koide, M., Hodge, V.F., Yang, J.S., Stallard, M., & Goldberg, E.G. (1986). Some comparative marine
2820 chemistries of rhenium, gold, silver and molybdenum. *Appl. Geochem.*, **1**, 705-714.

2821 Konhauser, K. O., Pecoits, E., Lalonde, S. V., Papineau, D., Nisbet, E. G., Barley, M. E., Arndt, N. T.,
2822 Zahnle, K., & Kamber, B. S. (2009). Oceanic nickel depletion and a methanogen famine before the
2823 Great Oxidation Event. *Nature*, **458**(7239), 750-753.

2824 Koschinsky, A., & Halbach, P. (1995). Sequential leaching of marine ferromanganese precipitates: Genetic
2825 implications. *Geochim. Cosmochim. Acta*, **59**(24), 5113-5132.

2826 Koschinsky, A., & Hein, J. R. (2003). Uptake of elements from seawater by ferromanganese crusts: solid-
2827 phase associations and seawater speciation. *Mar. Geol.*, **198**(3-4), 331-351.

2828 Kowalski, N., Dellwig, O., Beck, M., Gräwe, U., Neubert, N., Nägler, T. F., Badewien, T. H., Brumsack,
2829 H. J., van Beusekom, J. E. E., & Böttcher, M. E. (2013). Pelagic molybdenum concentration
2830 anomalies and the impact of sediment resuspension on the molybdenum budget in two tidal systems
2831 of the North Sea. *Geochim. Cosmochim. Acta*, **119**, 198–211, doi:10.1016/j.gca.2013.05.046.

2832 Kramer, D., Cullen, J. T., Christian, J. R., Johnson, W. K., & Pedersen, T. F. (2011). Silver in the subarctic
2833 northeast Pacific Ocean: Explaining the basin scale distribution of silver. *Mar. Chem.*, **123**, 133-
2834 142.

2835 Kurisu, M., Takahashi, Y., Iizuka, T. & Uematsu, M. (2016a). Very low isotope ratio of iron in fine aerosols
2836 related to its contribution to the surface ocean. *J. Geophys. Res. Atmos*. **121**, 11,119–11,136.
2837 https://doi.org/10.1002/2016JD024957.

2838 Kurisu, M., Sakata, K., Miyamoto, C., Takaku, Y., Iizuka, T., & Takahashi, Y. (2016b).Variation of iron
2839 isotope ratios in anthropogenic materials emitted through combustion processes. *Chem. Lett.* 45,
2840 970–972 (2016). https://doi.org/10.1246/cl.160451.

2841 Kunzmann, M., Halverson, G. P., Sossi, P. A., Raub, T. D., Payne, J. L., & Kirby, J. (2013). Zn isotope
2842 evidence for immediate resumption of primary productivity after snowball Earth. *Geology,* **41**, 27–
2843 30.

2844 Labatut, M., Lacan, F., Pradoux, C., Chmeleff, J., Radic, A., Murray, J. W., Poitrasson, F., Johansen, A.
2845 M., & Thil, F. (2014). Iron sources and dissolved-particulate interactions in the seawater of the
2846 Western Equatorial Pacific, iron isotope perspectives. *Global Biogeochem. Cycles* **28**, 1044-1065.

2847 Lacan, F., Francois, R., Ji, Y., & Sherrell, R. M. (2006). Cadmium isotopic composition in the ocean.
2848 *Geochim. Cosmochim. Acta*, **70**(20), 5104-5118.

2849 Lacan, F., Radic, A., Jeandel, C., Poitrasson, F., Sarthou, G., Pradoux, C., & Freydier, R. (2008).
2850 Measurement of the isotopic composition of dissolved iron in the open ocean. *Geophys. Res. Lett.*,
2851 **35**, L24610, doi:10.1029/2008GL035841.

2852 Lal, D., Charles, C., Vacher, L., Goswami, J. N., Jull, A. J. T., McHargue, L., & Finkel, R. C. (2006). Paleo-
2853 ocean chemistry records in marine opal: Implications for fluxes of trace elements, cosmogenic
2854 nuclides (Be-10 and Al-26), and biological productivity. *Geochim. Cosmochim. Acta* **70**, 3275-
2855 3289.

2856 Lam, P. J., & Marchal, O. (2015). Insights into particle cycling from thorium and particle data. *Annual*
2857 *Review of Marine Science*, **7**, 159-184.

2858 Lambelet, M., Rehkämper, M., van de Flierdt, T., Xue, Z., Kreissig, K., Coles, B., Porcelli, D., &
2859 Andersson, P. (2013). Isotopic analysis of Cd in the mixing zone of Siberian rivers with the Arctic
2860 Ocean—New constraints on marine Cd cycling and the isotope composition of riverine Cd. *Earth*
2861 *Planet. Sci. Lett.*, **361**, 64-73.

2862 Lane, T. W., Saito, M. A., George, G. N., Pickering, I. J., Prince, R. C., & Morel, F. M. (2005).
2863 Biochemistry: a cadmium enzyme from a marine diatom. *Nature*, **435**(7038), 42.

2864 Lauderdale, J. M., Braakman, R., Forget, G., Dutkiewicz, S., & Follows, M. J. (2020). Microbial feedbacks
2865 optimize ocean iron availability. *Proc. Natl. Acad. Sci.,* **117**(9), 4842-4849.

2866 Lee, J. G., & Morel, F. M. M. (1995). Replacement of zinc by cadmium in marine phytoplankton. *Mar.*
2867 *Ecol. Prog. Ser.,* **127**, 305–309.

2868 Lemaitre, N., de Souza, G. F., Archer, C., Wang, R. M., Planquette, H., Sarthou, G., & Vance, D. (2020).
2869 Pervasive sources of isotopically light zinc in the North Atlantic Ocean. *Earth Planet. Sci. Lett.*,
2870 **539**, doi:10.1016/j.epsl.2020.116216.

2871 Lerner, P., Marchal, O., Lam, P. J., & Solow, A. (2018). Effects of particle composition on thorium
2872 scavenging in the North Atlantic. *Geochimica et Cosmochimica Acta*, **233**, 115-134.

2873 Liao, W. H., & Ho, T. Y. (2018). Particulate trace metal composition and sources in the Kuroshio adjacent
2874 to the East China Sea: The importance of aerosol deposition. *Journal of Geophysical Research:*
2875 *Oceans*, **123**(9), 6207-6223.

2876 Liao, W. H., Takano, S., Yang, S. C., Huang, K. F., Sohrin, Y., & Ho, T. Y. (2020). Zn isotope composition
2877 in the water column of the Northwestern Pacific Ocean: the importance of external sources. *Global*
2878 *Biogeochem. Cycles*, **34**(1), e2019GB006379.

2879 Liermann, L. J., Guynn, R. L., Anbar, A., & Brantley, S. L. (2005). Production of a molybdophore during
2880 metal-targeted dissolution of silicates by soil bacteria. *Chem. Geol.*, **220**, 285–302,
2881 doi:10.1016/j.chemgeo.2005.04.013.

2882 Little, S.H., Vance, D., Siddall, M. and Gasson, E. (2013). A modeling assessment of the role of reversible
2883 scavenging in controlling oceanic dissolved Cu and Zn distributions. *Global Biogeochem. Cycles*
2884 **27**(3), 780-791.

2885 Little, S.H., Sherman, D.M., Vance, D. and Hein, J.R. (2014a). Molecular controls on Cu and Zn isotopic
2886 fractionation in Fe–Mn crusts. *Earth Planet. Sci. Lett.* **396**, 213-222.

2887 Little, S. H., Vance, D., Walker-Brown, C., & Landing, W. M. (2014b). The oceanic mass balance of copper
2888 and zinc isotopes, investigated by analysis of their inputs, and outputs to ferromanganese oxide
2889 sediments. *Geochim. Cosmochim. Acta* **125**, 673–693.

2890 Little, S. H., Vance, D., Lyons, T. W., & McManus, J. (2015). Controls on trace metal authigenic
2891 enrichment in reducing sediments: insights from modern oxygen-deficient settings. *Am. J. Sci.*,
2892 **315**(2), 77-119.

Little, S. H., Vance, D., McManus, J., & Severmann, S. (2016). Key role of continental margin sediments in the oceanic mass balance of Zn and Zn isotopes. *Geology,* **44**, 207–210.

Little, S. H., van de Flierdt, T., Rehkämper, M., Wilson, D. J., Adkins, J. F., & Robinson, L. F. (2017a). Deep sea corals as archives of seawater Zn isotopes. In *Goldschmidt Abstracts,* p. 2387.

Little, S.H., Vance, D., McManus, J., Severmann, S. and Lyons, T.W. (2017b). Copper isotope signatures in modern marine sediments. *Geochim. Cosmochim. Acta*, *212*, pp.253-273.

Little, S. H., Archer, C., Milne, A., Schlosser, C., Achterberg, E. P., Lohan, M. C., & Vance, D. (2018). Paired dissolved and particulate phase Cu isotope distributions in the South Atlantic. *Chem. Geol.*. **502**, 29-43.

Little, S.H., Archer, C., McManus, J., Najorka, J., Wegorzewski, A.V. and Vance, D. (2020). Towards balancing the oceanic Ni budget. *Earth Planet. Sci. Lett.* **547**, p.116461.

Liu, R., Guo, B., Wang, M., Li, W., Yang, T., Ling, H., & Chen, T. (2020). Isotopic fingerprinting of dissolved iron sources in the deep western Pacific since the late Miocene. *Science China Earth Sciences*, **63**, doi:10.1007/s11430-020-9648-6.

Liu, S. A., Wu, H., Shen, S. Z., Jiang, G., Zhang, S., Lv, Y., Zhang, H., & Li, S. (2017). Zinc isotope evidence for intensive magmatism immediately before the end-Permian mass extinction. *Geology,* **45**, 343–346.

Liu, X., & Millero, F. J. (2002). The solubility of iron in seawater. *Mar. Chem.*, **77**(1), 43-54.

Le Roy, E. L., Sanial, V., Charette, M. A., van Beek, P., Lacan, F., Jacquet, S. H., Henderson, P. B., Souhaut, M., García-Ibáñez, M. I., Jeandel, C., Pérez, F. F., & Sarthou, G. (2018). The ^{226}Ra–Ba relationship in the North Atlantic during GEOTRACES-GA01. *Biogeosciences*, **15**(9), 3027-3048.

Levasseur, S., Frank, M., Hein, J. R., & Halliday, A. N. (2004). The global variation in the iron isotope composition of marine hydrogenetic ferromanganese deposits: implications for seawater chemistry? *Earth Planet. Sci. Lett.*, **224**(1-2), 91-105.

Liu, Y., Li, X., Zeng, Z., Yu, H. M., Huang, F., Felis, T., & Shen, C. C. (2019). Annually-resolved coral skeletal $\delta^{138/134}$Ba records: A new proxy for oceanic Ba cycling. *Geochim. Cosmochim. Acta*, **247**, 27-39.

Lohan, M. C., Crawford, D. W., Purdie, D. A., & Statham, P. J. (2005). Iron and Zinc Enrichments in the Northeastern Subarctic Pacific : Ligand Production and Zinc Availability in Response to Phytoplankton Growth. *Limnol. Oceanogr.,* **50**, 1427–1437.

Lough, A. J. M., Klar, J. K., Homoky, W. B., Comer-Warner, S. A., Milton, J. A., Connelly, D. P., James, R. H., & Mills, R. A. (2017). Opposing authigenic controls on the isotopic signature of dissolved iron in hydrothermal plumes. *Geochim. Cosmochim. Acta*, **202**, 1-20.

Lv, Y., Liu, S. A., Wu, H., Hohl, S. V., Chen, S., & Li, S. (2018). Zn-Sr isotope records of the Ediacaran Doushantuo Formation in South China: diagenesis assessment and implications. *Geochim. Cosmochim. Acta*, *239*, 330-345.

Lyons, T. W., Anbar, A. D., Severmann, S., Scott, C., & Gill, B. C. (2009). Tracking Euxinia in the Ancient Ocean: A Multiproxy Perspective and Proterozoic Case Study. *Annu. Rev. Earth Planet. Sci.*, **37**, 507–534, doi:10.1146/annurev.earth.36.031207.124233.

Ma, Z., Gray, E., Thomas, E., Murphy, B., Zachos, J., & Paytan, A. (2014). Carbon sequestration during the Palaeocene–Eocene Thermal Maximum by an efficient biological pump. *Nat. Geosci.*, **7**(5), 382.

Ma, Z., Ravelo, A. C., Liu, Z., Zhou, L., & Paytan, A. (2015). Export production fluctuations in the eastern equatorial Pacific during the Pliocene-Pleistocene: Reconstruction using barite accumulation rates. *Paleoceanography*, **30**(11), 1455-1469.

Mahaffey, C., Reynolds, S., Davis, C. E., & Lohan, M. C. (2014). Alkaline phosphatase activity in the subtropical ocean: insights from nutrient, dust and trace metal addition experiments. *Front. Mar. Sci.*, **1**, 1–13.

Maldonado, M. T., Allen, A. E., Chong, J. S., Lin, K., Leus, D., Karpenko, N., & Harris, S. L. (2006). Copper-dependent iron transport in coastal and oceanic diatoms. *Limnol. Oceanogr.* **51**, 1729–1743.

Marchitto, T. M., Curry, W. B., & Oppo, D. W. (2000) Zinc concentrations in benthic foraminifera reflect seawater chemistry. *Paleoceanography,* **15**, 299–306.

Marcus, M. A., Edwards, K. J., Gueguen, B., Fakra, S. C., Horn, G., Jelinski, N. A., Rouxel, O., Sorensen, J., & Toner, B. M. (2015). Iron mineral structure, reactivity, and isotopic composition in a South Pacific Gyre ferromanganese nodule over 4 Ma. *Geochim. Cosmochim. Acta*, **171**, 61-79.

Maréchal, C. N., Nicolas, E., Douchet, C., & Albarède, F. (2000). Abundance of zinc isotopes as a marine biogeochemical tracer. *Geochem. Geophys. Geosyst.*, **1**, 1015, http://doi.wiley.com/10.1029/1999GC000029.

Marks, J. A., Perakis, S. S., King, E. K., & Pett-Ridge, J. (2015). Soil organic matter regulates molybdenum storage and mobility in forests. *Biogeochemistry*, **125**, 167–183, doi:10.1007/s10533-015-0121-4.

Marsay, C. M., Lam, P. J., Heller, M. I., Lee, J. M., & John, S. G. (2018). Distribution and isotopic signature of ligand-leachable particulate iron along the GEOTRACES GP16 East Pacific Zonal Transect. *Mar. Chem.*, **201**, 198-211.

Martin, J. H. (1990). Glacial-interglacial CO_2 change: the iron hypothesis. *Paleoceanography* **5**, 1-13.

Martin, J. H., & Fitzwater, S. E. (1988). Iron deficiency limits phytoplankton growth in the north-east Pacific subarctic. *Nature*, **331**(6154), 341-343.

Martin, J. H., Fitzwater, S. E., & Gordon, R. M. (1990). Iron deficiency limits phytoplankton growth in Antarctic waters. *Global Biogeochem. Cycles*, **4**(1), 5-12.

Martin, J. H., Knauer, G. A. and Gordon, R. M. (1983) Silver distributions and fluxes in north-east Pacific waters. *Nature*, **305**, 306-309.

Martin, J. M., & Thomas, A. J. (1994). The global insignificance of telluric input of dissolved trace metals (Cd, Cu, Ni and Zn) to ocean margins. *Mar. Chem.*, **46**(1-2), 165-178.

Martínez-Garcia, A., Rosell-Melé, A., Jaccard, S. L., Geibert, W., Sigman, D. M., & Haug, G. H. (2011). Southern Ocean dust–climate coupling over the past four million years. *Nature*, **476**(7360), 312-315.

Martínez-Garcia, A., Sigman, D. M., Ren, H., Anderson, R. F., Straub, M., Hodell, D. A., et al. (2014). Iron fertilization of the Subantarctic Ocean during the last ice age. *Science*, **343**, 1347-1350, doi:10.1126/science.1246848.

Martinez-Ruiz, F., Jroundi, F., Paytan, A., Guerra-Tschuschke, I., del Mar Abad, M., & González-Muñoz, M. T. (2018). Barium bioaccumulation by bacterial biofilms and implications for Ba cycling and use of Ba proxies. *Nat. Commun.*, **9**.

Martinez-Ruiz, F., Paytan, A., Gonzalez-Muñoz, M. T., Jroundi, F., Abad, M. M., Lam, P. J., Bishop, J. K. B., Horner, T. J., Morton, P. L., & Kastner, M. (2019). Barite formation in the ocean: Origin of amorphous and crystalline precipitates. *Chem. Geol.*, **511**, 441-451.

2978 Mathur, R., Arribas, A., Megaw, P., Wilson, M., Stroup, S., Meyer-Arrivillaga, D., & Arribas, I. (2018).
2979 Fractionation of silver isotopes in native silver explained by redox reactions. *Geochim. Cosmochim.*
2980 *Acta*, **224**, 313-326.

2981 Mawji, E. et al. (2015). The GEOTRACES Intermediate Data Product 2014. *Mar. Chem.,* **177**, 1-8,
2982 doi:10.1016/j.marchem.2015.04.005.

2983 Mayfield, K .K., A. Eisenhauer, D. Santiago Ramos, J. A. Higgins, T. J. Horner, M. E. Auro, T. Magna, N.
2984 Moosdorf, M. A. Charette, M. E. Gonneea, C. E. Brady, N. Komar, B. Peucker-Ehrenbrink, and A.
2985 Paytan (in press) The Importance of Groundwater Discharge in Marine Isotope Budgets, *Nature*
2986 *Communications*.

2987 McKay, J. L., & Pedersen, T. F. (2008). The accumulation of silver in marine sediments: A link to biogenic
2988 Ba and marine productivity. *Global Biogeochem. Cycles*, **22**, GB4010,
2989 doi:10.1029/2007GB003136

2990 McManus, J., Berelson, W. M., Klinkhammer, G. P., Johnson, K. S., Coale, K. H., Anderson, R. F., Kumar,
2991 N., Burdige, D. J., Hammond, D. E., Brumsack, H. J., McCorkle, D. C., & Rushdi, A. (1998).
2992 Geochemistry of barium in marine sediments: Implications for its use as a paleoproxy. *Geochim.*
2993 *Cosmochim. Acta*, **62**(21-22), 3453-3473.

2994 McManus, J., Dymond, J., Dunbar, R. B., & Collier, R. W. (2002). Particulate barium fluxes in the Ross
2995 Sea. *Mar. Geol.*, **184**(1-2), 1-15.

2996 McManus, J., Berelson, W. M., Severmann, S., Poulson, R. L., Hammond, D. E., Klinkhammer, G. P., &
2997 Holm, C. (2006). Molybdenum and uranium geochemistry in continental margin sediments:
2998 Paleoproxy potential. *Geochim. Cosmochim. Acta*, **70**, 4643–4662,
2999 doi:10.1016/j.gca.2006.06.1564.

3000 Mead, C., Herckes, P., Majestic, B. J., & Anbar, A. D. (2013). Source apportionment of aerosol iron in the
3001 marine environment using iron isotope analysis. *Geophys. Res. Lett.*, **40**(21), 5722-5727.

3002 Mendel, R. R., & Bittner, F. (2006) Cell biology of molybdenum. *Biochim. Biophys. Acta*, **1763**(7), 621-
3003 635, doi:10.1016/j.bbamcr.2006.03.013.

3004 Middag, R., van Heuven, S. M., Bruland, K. W., & de Baar, H. J. (2018). The relationship between cadmium
3005 and phosphate in the Atlantic Ocean unraveled. *Earth Planet. Sci. Lett.*, **492**, 79-88.

3006 Middag, R., de Baar, H. J. W., & Bruland, K. W. (2019). The relationships between dissolved zinc and
3007 major nutrients phosphate and silicate along the GEOTRACES GA02 transect in the west Atlantic
3008 Ocean. *Global Biogeochem. Cycles*, **33**, 63-84, doi:10.1029/2018GB006034.

3009 Middleton, J. L., Langmuir, C. H., Mukhopadhyay, S., McManus, J. F., & Mitrovica, J. X. (2016).
3010 Hydrothermal iron flux variability following rapid sea level changes. *Geophys. Res. Lett.,* **43**, 3848-
3011 3856.

3012 Miller, C. A., Peucker-Ehrenbrink, B., Walker, B. D., & Marcantonio, F. (2011). Re-assessing the surface
3013 cycling of molybdenum and rhenium. *Geochim. Cosmochim. Acta*, **75**, 7146–7179,
3014 doi:10.1016/j.gca.2011.09.005.

3015 Miller, L. A., & Bruland, K. W. (1995). Organic speciation of silver in marine waters. *Environ. Sci.*
3016 *Technol.*, **29**, 2616-2621.

3017 Misumi, K., Lindsay, K., Moore, J. K., Doney, S. C., Bryan, F. O., Tsumune, D., & Yoshida, Y. (2014).
3018 The iron budget in ocean surface waters in the 20th and 21st centuries: projections by the
3019 Community Earth System Model version. *Biogeosciences*, **11**, 33-55.

Moeller, K., Schoenberg, R., Pedersen, R. B., Weiss, D., & Dong, S. (2012). Calibration of the new certified reference materials ERM-AE633 and ERM-AE647 for copper and IRMM-3702 for zinc isotope amount ratio determinations. *Geostan. Geoanal. Res.* **36**(2), 177-199.

Moffett, J. W., & Brand ,L. E. (1996). Production of strong, extracellular Cu chelators by marine cyanobacteria in response to Cu stress. *Limnol. Oceanogr.* **41**, 388–395.

Moffett, J. W., & Dupont, C. (2007). Cu complexation by organic ligands in the sub-arctic NW Pacific and Bering Sea. *Deep. Res. Part I Oceanogr. Res. Pap.* **54**, 586–595.

Moffett, J. W., Zika, R. G., & Brand, L. E. (1990). Distribution and potential sources and sinks of copper chelators in the Sargasso Sea. *Deep Sea Res. Part A, Oceanogr. Res. Pap.* **37**, 27–36.

Monnin, C., Jeandel, C., Cattaldo, T., & Dehairs, F. (1999). The marine barite saturation state of the world's oceans. M*ar. Chem.*, **65**(3-4), 253-261.

Monnin, C., & Cividini, D. (2006). The saturation state of the world's ocean with respect to (Ba, Sr)SO_4 solid solutions. *Geochim. Cosmochim. Acta*, **70**(13), 3290-3298.

Moore, C. M., Mills, M. M., Arrigo, K. R., Berman-Frank, I., Bopp, L., Boyd, P. W., Galbraith, E. D., Geider, R. J., Guieu, C., Jaccard, S. L., Jickells, T. D., La Roche, J., Lenton, T. M., Mahowald, N. M., Maranon, E., Marinov, I., Moore, J.K., Nakatsuka, T., Oschlies, A., Saito, M. A., Thingstad, T. F., Tsuda, A., & Ulloa, O. (2013). Processes and patterns of oceanic nutrient limitation. *Nat. Geosci.* **6**, 701-710.

Moore, C. M. (2016). Diagnosing oceanic nutrient deficiency. *Philosophical Transactions of the Royal Society A: Mathematical, Physical and Engineering Sciences*, **374**(2081), 20150290.

Morel, F. M. M., & Price, N. M. (2003). The biogeochemical cycles of trace metals in the oceans. *Science*, **300**, 944-947, doi:10.1126/science.1083545.

Morel, F. M. M., Reinfelder, J. R., Roberts, S. B., Chamberlain, C. P., Lee, J. G., & Yee, D. (1994) Zinc and carbon co-limitation of marine phytoplankton. *Nature*, **369**, 740-742.

Morel, F. M., Lam, P. J., & Saito, M. A. (2020). Trace Metal Substitution in Marine Phytoplankton. *Annual Review of Earth and Planetary Sciences*, **48**.

Morford, J. L., Kalnejais, L. H., Helman, P., Yen, G., & Reinard, M. (2008). Geochemical cycling of silver in marine sediments along an offshore transect. *Mar. Chem.*, **110**, 77-88.

Morgan, J. L., Wasylenki, L. E., Nuester, J., & Anbar, A. D. (2010). Fe isotope fractionation during equilibration of Fe–organic complexes. *Environ. Sci. Technol.*, **44**(16), 6095-6101.

Morris, A. W. (1975). Dissolved molybdenum and vanadium in the northeast Atlantic Ocean. *Deep Sea Research and Oceanographic Abstracts*, **22**, 49–54, doi:10.1016/0011-7471(75)90018-2.

Moynier, F., Vance, D., Fujii, T., & Savage, P. (2017). The Isotope Geochemistry of Zinc and Copper. *Rev. Mineral. Geochemistry* **82**, 543–600.

Murphy, K. L. (2016). *Isotopic studies in marine geochemistry* (Doctoral dissertation, Imperial College London), doi:10.25560/68270.

Mulholland, D.S., Poitrasson, F., Boaventura, G.R., Allard, T., Vieira, L.C., Santos, R.V., Mancini, L. & Seyler, P. (2015). Insights into iron sources and pathways in the Amazon River provided by isotopic and spectroscopic studies. *Geochim. Cosmochim. Acta*, **150**, 142–159.

Nägler, T. F., Neubert, N., Böttcher, M. E., Dellwig, O., & Schnetger, B. (2011). Molybdenum isotope fractionation in pelagic euxinia: Evidence from the modern Black and Baltic Seas. *Chem. Geol.*, **289**, 1–11, doi:10.1016/j.chemgeo.2011.07.001.

Nägler, T. F., Anbar, A. D., Archer, C., Goldberg, T., Gordon, G. W., Greber, N. D., Seibert, C., Sohrin, Y., & Vance, D. (2014). Proposal for an international molybdenum isotope measurement standard and data representation. *Geostand. Geoanal. Res.*, **38**(2), 149-151.

Nakagawa, Y., Takano, S., Firdaus, M. L., Norisuye, K., Hirata, T., Vance, D., & Sohrin, Y. (2012). The molybdenum isotopic composition of the modern ocean. *Geochemical Journal*, **46**, 131–141, doi:10.2343/geochemj.1.0158.

Nan, X. Y., Yu, H. M., Rudnick, R. L., Gaschnig, R. M., Xu, J., Li, W.-Y., Zhang, Q., Jin, Z.-D., Li, X.-H., & Huang, F. (2018). Barium isotopic composition of the upper continental crust. *Geochim. Cosmochim. Acta*, **233**, 33-49.

Nasemann, P., Gault-Ringold, M., Stirling, C. H., Koschinsky, A., & Sander, S. G. (2018). Processes affecting the isotopic composition of dissolved iron in hydrothermal plumes: A case study from the Vanuatu back-arc. *Chem. Geol.* **476**, 70-84. https://doi.org/10.1016/j.chemgeo.2017.11.005.

Navarrete, J. U., Borrok, D. M., Viveros, M., & Ellzey, J. T. (2011). Copper isotope fractionation during surface adsorption and intracellular incorporation by bacteria. *Geochim. Cosmochim. Acta*, **75**(3), 784-799.

Nishioka, J., Obata, H., Ogawa, H., Ono, K., Yamashita, Y., Lee, K., Takeda, S., & Yasuda, I. (2020). Subpolar marginal seas fuel the North Pacific through the intermediate water at the termination of the global ocean circulation. *Proc. Natl Acad. Sci. U. S. A.* **117**(23), 12665-12673 https://doi.org/10.1073/pnas.2000658117.

Ndung'u, K., Thomas, M.A., & Flegal, A.R. (2001). Silver in the western equatorial and South Atlantic Ocean. *Deep-Sea Research II,* **48**, 2933-2945.

Neubert, N., Nägler, T. F., and Böttcher, M. E. (2008). Sulfidity controls molybdenum isotope fractionation into euxinic sediments: Evidence from the modern Black Sea. *Geology*, **36**, 775–778, doi:10.1130/G24959A.1.

Nielsen, S. G., Wasylenki, L. E., Rehkämper, M., Peacock, C. L., Xue, Z., & Moon, E. M. (2013). Towards an understanding of thallium isotope fractionation during adsorption to manganese oxides. *Geochim. Cosmochim. Acta*, **117**, 252-265.

Noordmann, J., Weyer, S., Montoya-Pino, C., Dellwig, O., Neubert, N., Eckert, S., Paetzel, M., & Böttcher, M. E. (2015). Uranium and molybdenum isotope systematics in modern euxinic basins: Case studies from the central Baltic Sea and the Kyllaren fjord (Norway). *Chem. Geol.*, **396**, 182–195, doi:10.1016/j.chemgeo.2014.12.012.

Ohnemus, D. C., & Lam, P. J. (2015). Cycling of lithogenic marine particles in the US GEOTRACES North Atlantic transect. *Deep Sea Res. Pt. II*, **116**, 283-302.

Ohnemus, D. C., Rauschenberg, S., Cutter, G. A., Fitzsimmons, J. N., Sherrell, R. M., & Twining, B. S. (2017). Elevated trace metal content of prokaryotic communities associated with marine oxygen deficient zones. *Limnol. Oceanog.*, **62**(1), 3-25.

Ohnemus, D. C., Torrie, R., & Twining, B. S. (2019). Exposing the Distributions and Elemental Associations of Scavenged Particulate Phases in the Ocean Using Basin-Scale Multi-Element Data Sets. *Global Biogeochem. Cycles*, **33**(6), 725-748.

Park, H., Song, B., & Morel, F. M. (2007). Diversity of the cadmium-containing carbonic anhydrase in marine diatoms and natural waters. *Environmental Microbiology*, **9**(2), 403-413.

Paytan, A. (2009). Ocean Paleoproductivity. In: Gornitz V. (eds) *Encyclopedia of Paleoclimatology and Ancient Environments.* Encyclopedia of Earth Sciences Series, Springer, Dordrecht.

Paytan, A., & Kastner, M. (1996). Benthic Ba fluxes in the central Equatorial Pacific, implications for the oceanic Ba cycle. *Earth Planet. Sci. Lett.*, **142**(3-4), 439-450.

Paytan, A., Kastner, M., & Chavez, F. P. (1996). Glacial to interglacial fluctuations in productivity in the equatorial Pacific as indicated by marine barite. *Science*, **274**(5291), 1355-1357.

Paytan, A., & Griffith, E. M. (2007). Marine barite: Recorder of variations in ocean export productivity. *Deep Sea Res. Pt. II*, **54**(5-7), 687-705.

Paytan, A., Mackey, K. R., Chen, Y., Lima, I. D., Doney, S. C., Mahowald, N., Labiosa, R., & Post, A. F. (2009). Toxicity of atmospheric aerosols on marine phytoplankton. *Proc. Natl. Acad. Sci.*, **106**(12), 4601-4605.

Peers, G., & Price, N. M. (2006). Copper-containing plastocyanin used for electron transport by an oceanic diatom. *Nature* **441**, 341–344.

Peers, G., Quesnel, S., & Price, N. M. (2005). Copper requirements for iron acquisition and growth of coastal and oceanic diatoms. *Limnol. Oceanogr.* **50**, 1149–1158.

Pichat, S., Douchet, C., & Albarède, F. (2003). Zinc isotope variations in deep-sea carbonates from the eastern equatorial Pacific over the last 175 ka. *Earth Planet. Sci. Lett.*, **210**, 167–178.

Pichevin, L. E., Ganeshram, R. S., Geibert, W., Thunell, R., & Hinton, R. (2014). Silica burial enhanced by iron limitation in oceanic upwelling margins. *Nat. Geosci.*, **7**(7), 541-546.

Plass, A., Schlosser, C., Sommer, S., Dale, A. W., Achterberg, E. P., & Scholz, F. (2020). The control of hydrogen sulfide on benthic iron and cadmium fluxes in the oxygen minimum zone off Peru. *Biogeosciences*, **17**(13), 3685-3704.

Poitrasson, F. (2006). On the iron isotope homogeneity level of the continental crust. *Chem. Geol.*, **235**(1-2), 195-200.

Poitrasson, F., Vieira, L. C., Seyler, P., dos Santos Pinheiro, G. M., Mulholland, D. S., Bonnet, M. P., Martinez, J.-M., Lima, B. A., Boaventura, G. R., Chmeleff, J., Dantas, E. L., Guyot, J.-L., Mancini, L., Pimentel, M. M., Santos, R. V., Sondag, F., & Vauchel, P. (2014). Iron isotope composition of the bulk waters and sediments from the Amazon River Basin. *Chem. Geol.*, **377**, 1-11.

Pokrovsky, O. S., Viers, J., Emnova, E. E., Kompantseva, E. I., & Freydier, R. (2008). Copper isotope fractionation during its interaction with soil and aquatic microorganisms and metal oxy (hydr) oxides: Possible structural control. *Geochim. Cosmochim. Acta*, **72**(7), 1742-1757.

Price, N. M., & Morel, F. M. M. (1990). Cadmium and cobalt substitution for zinc in a marine diatom. *Nature*, **344**(6267), 658.

Price, N. M., & Morel, F. M. M. (1991). Colimitation of phytoplankton growth by nickel and nitrogen. *Limnol. Oceanogr.* **50**, 1071-1077.

Quay, P., & Wu, J. (2015). Impact of end-member mixing on depth distributions of $\delta^{13}C$, cadmium and nutrients in the N. Atlantic Ocean. *Deep Sea Res. Pt. II*, **116**, 107-116.

Radic, A., Lacan, F., & Murray, J. W. (2011). Iron isotopes in the seawater of the equatorial Pacific Ocean: New constraints for the oceanic iron cycle. *Earth Planet. Sci. Lett.*, **306**, 1-10.

Rafter, P. A., Sigman, D. M., & Mackey, K. R. (2017). Recycled iron fuels new production in the eastern equatorial Pacific Ocean. *Nat. Commun.*, **8**(1), 1100.

Ragsdale, S. W. (2009). Nickel-based enzyme systems. *J. Biol. Chem.* **284**, 18571–18575.

Ranville, M. A., & Flegal, A.R. (2005). Silver in the North Pacific Ocean. *Geochemistry, Geophysics, Geosystems*, **6**(3), doi:10.1029/2004GC000770

Ranville, M. A., Cutter, G. A., Buck, C. S., Landing, W. M., Cutter, L. S., Resing. J. A, & Flegal, A. R. (2010). Aeolian contamination of Se and Ag in the North Pacific from Asian fossil fuel combustion. *Environ. Sci. Tech.*, **44**, 1587–1593.

Rehkämper, M., Wombacher, F., Horner, T. J., & Xue, Z. (2012). Natural and anthropogenic Cd isotope variations. In Baskaran, M. (Ed.) *Handbook of Environmental Isotope Geochemistry* (pp. 125-154). Springer, Berlin, Heidelberg, doi:10.1007/978-3-642-10637-8_8.

Reinhard, C. T., Planavsky, N. J., Robbins, L. J., Partin, C. A., Gill, B. C., Lalonde, S. V., Bekker, A., Konhauser, K. O., & Lyons, T. W. (2013). Proterozoic ocean redox and biogeochemical stasis. *Proc. Natl. Acad. Sci.*, **110**, 5357–5362, doi:10.1073/pnas.1208622110.

Resing, J. A., Sedwick, P. N., German, C. R., Jenkins, W. J., Moffett, J. W., Sohst, B. M., & Tagliabue, A. (2015). Basin-scale transport of hydrothermal dissolved metals across the South Pacific Ocean. *Nature*, **523**(7559), 200-203.

Revels, B. N., Zhang, R., Adkins, J. F., & John, S. G. (2015). Fractionation of iron isotopes during leaching of natural particles by acidic and circumneutral leaches and development of an optimal leach for marine particulate iron isotopes. *Geochim. Cosmochim. Acta,* **166**, 92–104.

Richon, C., & Tagliabue, A. (2019). Insights into the major processes driving the global distribution of copper in the ocean from a global model. *Global Biogeochem. Cycles*, *33*(12), 1594-1610.

Rickaby, R. E. M., & Elderfield, H. (1999). Planktonic foraminiferal Cd/Ca: paleonutrients or paleotemperature?. *Paleoceanography*, **14**(3), 293-303.

Ridge, P. G., Zhang, Y., & Gladyshev, V. N. (2008). Comparative genomic analyses of copper transporters and cuproproteomes reveal evolutionary dynamics of copper utilization and its link to oxygen. *PLoS One* **3**(1), https://doi.org/10.1371/journal.pone.0001378.

Rijkenberg, M. J. A., Middag, R., Laan, P., Gerringa, L. J., van Aken, H. M., Schoemann, V., de Jong, J. T. M., & de Baar, H. J. W. (2014). The distribution of dissolved iron in the West Atlantic Ocean. *PloS One*, **9**(6).

Ripperger, S., & Rehkämper, M. (2007). Precise determination of cadmium isotope fractionation in seawater by double spike MC-ICPMS. *Geochim. Cosmochim. Acta*, **71**(3), 631-642.

Ripperger, S., Rehkämper, M., Porcelli, D., & Halliday, A. N. (2007). Cadmium isotope fractionation in seawater—A signature of biological activity. *Earth Planet. Sci. Lett.*, **261**(3-4), 670-684.

Rivera-Duarte, I., Flegal, A. R., Sañudo-Wilhelmy, S. A., & Véron, A. J. (1999). Silver in the far North Atlantic Ocean. *Deep-Sea Research II*, **46**, 979-990.

Robinson, L. F., Adkins, J. F., Frank, N., Gagnon, A. C., Prouty, N. G., Roark, E. B., & van de Flierdt, T. (2014). The geochemistry of deep-sea coral skeletons: A review of vital effects and applications for palaeoceanography. *Deep. Res. Part II Top. Stud. Oceanogr.*, **99**, 184–198. http://dx.doi.org/10.1016/j.dsr2.2013.06.005.

Rohatgi, A. (2019) WebPlotDigitizer (version 4.2; April 2019). https://automeris.io/WebPlotDigitizer [accessed 2020-06-22].

Rolison, J. M., Stirling, C. H., Middag, R., Gault-Ringold, M., George, E., & Rijkenberg, M. J. A. (2018). Iron isotope fractionation during pyrite formation in a sulfidic Precambrian ocean analogue. *Earth Planet. Sci. Lett.*, **488**, 1-13. https://doi.org/10.1016/j.epsl.2018.02.006.

Roshan, S., & Wu, J. (2015a). The distribution of dissolved copper in the tropical-subtropical north Atlantic across the GEOTRACES GA03 transect. *Mar. Chem.*, **176**, 189-198, doi:10.1016/j.marchem.2015.09.006.

Roshan, S., & Wu, J. (2015b). Cadmium regeneration within the North Atlantic. *Global Biogeochem. Cycles*, **29**(12), 2082-2094.

Roshan, S., & Wu, J. (2018). Dissolved and colloidal copper in the tropical South Pacific. *Geochim. Cosmochim. Acta*, **233**, 81-94, doi:10.1016/j.gca.2018.05.008.

Roshan, S., DeVries, T., Wu, J., & Chen, G. (2018). The internal cycling of zinc in the ocean. *Global Biogeochem. Cycles*, **32**(12), 1833-1849, doi:10.1029/2018GB006045.

Roshan, S., DeVries, T., Wu, J., John, S., & Weber, T. (2020). Reversible scavenging traps hydrothermal iron in the deep ocean. Earth and Planetary Science Letters, 542, 116297.

Rühlemann, C., Müller, P. J., & Schneider, R. R. (1999). Organic carbon and

Rouxel, O., Shanks III, W. C., Bach, W., & Edwards, K. J. (2008). Integrated Fe-and S-isotope study of seafloor hydrothermal vents at East Pacific Rise 9–10 N. *Chem. Geol.*, **252**(3-4), 214-227.

Rouxel, O., Toner, B. M., Manganini, S. J., & German, C. R. (2016). Geochemistry and iron isotope systematics of hydrothermal plume fall-out at East Pacific Rise 9°50′N. *Chem. Geol.* **441**, 212-234. https://doi.org/10.1016/j.chemgeo.2016.08.027.

Rouxel, O., Toner, B., Germain, Y., & Glazer, B. (2018). Geochemical and iron isotopic insights into hydrothermal iron oxyhydroxide deposit formation at Loihi Seamount. *Geochim. Cosmochim. Acta*, **220**, 449-482. https://doi.org/10.1016/j.gca.2017.09.050.

Rosenthal, Y., Lam, P., Boyle, E. A., & Thomson, J. (1995). Authigenic cadmium enrichments in suboxic sediments: Precipitation and postdepositional mobility. *Earth Planet. Sci. Lett.*, **132**(1-4), 99-111.

carbonate as paleoproductivity proxies: Examples from high and low productivity areas of the tropical Atlantic. In *Use of Proxies in Paleoceanography* (pp. 315-344). Springer, Berlin, Heidelberg.

Rushdi, A. I., McManus, J., & Collier, R. W. (2000). Marine barite and celestite saturation in seawater. *Mar. Chem.*, **69**(1-2), 19-31.

Ryan, B. M., Kirby, J. K., Degryse, F., Scheiderich, K., & McLaughlin, M. J. (2014). Copper isotope fractionation during equilibration with natural and synthetic ligands. *Environ. Sci. Technol.*, **48**(15), 8620-8626.

Saito, M. A., Moffett, J. W., & DiTullio, G. R. (2004). Cobalt and nickel in the Peru upwelling region: A major flux of labile cobalt utilized as a micronutrient. *Global Biogeochem. Cycles* **18**, 1–14.

Saito, M. A., Bertrand, E. M., Dutkiewicz, S., Bulygin, V. V., Moran, D. M., Monteiro, F. M., Follows, M. J., Valois, F. W., & Waterbury, J. B. (2011). Iron conservation by reduction of metalloenzyme inventories in the marine diazotroph *Crocosphaera watsonii*. *Proc. Natl. Acad. Sci.*, **108**(6), 2184-2189.

Saito, M. A., Noble, A. E., Tagliabue, A., Goepfert, T. J., Lamborg, C. H., & Jenkins, W. J. (2013). Slow-spreading submarine ridges in the South Atlantic as a significant oceanic iron source. *Nat. Geosci.*, **6**(9), 775-779.

Samanta, M., Ellwood, M. J., Sinoir, M., & Hassler, C. S. (2017). Dissolved zinc isotope cycling in the Tasman Sea, SW Pacific Ocean. *Mar. Chem.*, **192**, 1–12. http://dx.doi.org/10.1016/j.marchem.2017.03.004.

Samanta, M., Ellwood, M. J., & Strzepek, R. F. (2018). Zinc isotope fractionation by *Emiliania huxleyi* cultured across a range of free zinc ion concentrations. *Limnol. Oceanogr.*, **63**, 660–671.

Sarmiento, J. L., & Gruber, M. (2006). Carbon Cycle. In *Ocean Biogeochemical Dynamics* (pp. 318-358). Princeton, NJ: Princeton University Press.

Sarmiento, J. L., Gruber, N., Brzezinski, M. A., & Dunne, J. P. (2004). High-latitude controls of thermocline nutrients and low latitude biological productivity. *Nature*, **427**(6969), 56-60.

Sclater, F. R., Boyle, E., & Edmond, J. M. (1976). On the marine geochemistry of nickel. *Earth Planet. Sci. Lett.*, **31**(1), 119-128.

Schönbächler, M., Carlson, R. W., Horan, M. F., Mock, T. D., & Hauri, E. H. (2007). High precision Ag isotope measurements in geologic materials by multiple-collector ICPMS: An evaluation of dry versus wet plasma. *Intl J. Mass Spectrom.*, **261**(2-3), 183-191.

Sedwick, P. N., Church, T. M., Bowie, A.R., Marsay, C. M., Ussher, S. J., Achilles, K. M., Lethaby, P. J., Johnson, R. J., Sarin, M. M., McGillicuddy, D. J. (2005). Iron in the Sargasso Sea (Bermuda Atlantic Time-series Study region) during summer: Eolian imprint, spatiotemporal variability, and ecological implications. *Global Biogeochem. Cycles*, 19, GB4006. https://doi.org/10.1029/2004GB002445.

Sharma, M., Polizzotto, M., & Anbar, A. D. (2001). Iron isotopes in hot springs along the Juan de Fuca ridge. *Earth Planet. Sci. Lett.* **194**(1-2), 39-51. https://doi.org/10.1016/S0012-821X(01)00538-6.

Sherman, D. M. (2013). Equilibrium isotopic fractionation of copper during oxidation/reduction, aqueous complexation and ore-forming processes: Predictions from hybrid density functional theory. *Geochim. Cosmochim. Acta*, **118**, 85-97.

Sherman, D. M., Little, S. H., & Vance, D. (2015). Reply to comment on" Molecular controls on Cu and Zn isotopic fractionation in Fe-Mn crusts". *Earth Planet. Sci. Lett.*, **411**, 313-315.

Sherman, D. M., & Peacock, C. L. (2010). Surface complexation of Cu on birnessite (δ-MnO2): Controls on Cu in the deep ocean. *Geochim. Cosmochim. Acta*, **74**(23), 6721-6730.

Schlitzer, R., et al. (2018). The GEOTRACES intermediate data product 2017. *Chem. Geol.*, **493**, 210-223.

Schlitzer, R. (2019) eGEOTRACES - Electronic Atlas of GEOTRACES Sections and Animated 3D Scenes, http://egeotraces.org [accessed 2020-08-31].

Schmitt, A. D., Galer, S. J., & Abouchami, W. (2009a). Mass-dependent cadmium isotopic variations in nature with emphasis on the marine environment. *Earth Planet. Sci. Lett.*, **277**(1-2), 262-272.

Schmitt, A. D., Galer, S. J., & Abouchami, W. (2009b). High-precision cadmium stable isotope measurements by double spike thermal ionisation mass spectrometry. *Journal of Analytical Atomic Spectrometry*, **24**(8), 1079-1088.

Schmitz, B. (1987). Barium, equatorial high productivity, and the northward wandering of the Indian continent. *Paleoceanography*, **2**(1), 63-77.

Scholz, F., McManus, J., & Sommer, S. (2013). The manganese and iron shuttle in a modern euxinic basin and implications for molybdenum cycling at euxinic ocean margins. *Chem. Geol.*, **355**, 56–68, doi:10.1016/j.chemgeo.2013.07.006.

Scholz, F., Siebert, C., Dale, A. W., & Frank, M. (2017). Intense molybdenum accumulation in sediments unearth a nitrogenous water column and implications for the reconstruction of paleo-redox conditions based on molybdenum isotopes. *Geochim. Cosmochim. Acta*, **213**, 400-417.

Schulz, K. G., Zondervan, I., Gerringa, L. J. A, Timmermans, K. R., Veldhuis, M. J. W., & Riebesell, U. (2004). Effect of trace metal availability on coccolithophorid calcification. *Nature,* **430**, 673–676.

Scott, C., & Lyons, T. W. (2012). Contrasting molybdenum cycling and isotopic properties in euxinic versus non-euxinic sediments and sedimentary rocks: Refining the paleoproxies. *Chem. Geol.,* **324–325**, 19–27, doi:10.1016/j.chemgeo.2012.05.012.

Semeniuk, D. M., Cullen, J. T., Johnson, W. K., Gagnon, K., Ruth, T. J., & Maldonado, M. T. (2009). Plankton copper requirements and uptake in the subarctic Northeast Pacific Ocean. *Deep Sea Research Part I: Oceanographic Research Papers*, **56**(7), 1130-1142.

Semeniuk, D. M., Bundy, R. M., Payne, C. D., Barbeau, K. A., & Maldonado, M. T. (2015). Acquisition of organically complexed copper by marine phytoplankton and bacteria in the northeast subarctic Pacific Ocean. *Mar. Chem.* **173**, 222–233.

Serno, S., Winckler, G., Anderson, R. F., Hayes, C. T., Ren, H., Gersonde, R., & Haug, G. H. (2014). Using the natural spatial pattern of marine productivity in the Subarctic North Pacific to evaluate paleoproductivity proxies. *Paleoceanography*, **29**(5), 438-453.

Severmann, S., Johnson, C. M., Beard, B. L., German, C. R., Edmonds, H. N., Chiba, H., & Green, D. R. H. (2004). The effect of plume processes on the Fe isotope composition of hydrothermally derived Fe in the deep ocean as inferred from the Rainbow vent site, Mid-Atlantic Ridge, 36°14′ N. *Earth Planet. Sci. Lett.*, **225**(1-2), 63-76. https://doi.org/10.1016/j.epsl.2004.06.001.

Severmann, S., Johnson, C. M., Beard, B. L., & McManus, J. (2006). The effect of early diagenesis on the Fe isotope compositions of porewaters and authigenic minerals in continental margin sediments. *Geochim. Cosmochim. Acta*, **70**(8). 2006-2022. https://doi.org/10.1016/j.gca.2006.01.007.

Severmann, S., McManus, J., Berelson, W. M., & Hammond, D. E. (2010). The continental shelf benthic iron flux and its isotope composition. *Geochim. Cosmochim. Acta*, **74**(14), 3984-4004. https://doi.org/10.1016/j.gca.2010.04.022.

Shaked, Y., Xu, Y., Leblanc, K., & Morel, F. M. M. (2006) Zinc availability and alkaline phosphatase activity in Emiliania huxleyi: Implications for Zn-P co-limitation in the ocean. *Limnol. Oceanogr.*, **51**, 299–309.

Shemesh, A., Mortlock, R. A., Smith, R. J., & Froelich, P. N. (1988). Determination of Ge/Si in marine siliceous microfossils: Separation, cleaning and dissolution of diatoms and radiolaria. *Mar. Chem.* **25**, 305-323.

Shen, G. T., Boyle, E. A., & Lea, D. W. (1987). Cadmium in corals as a tracer of historical upwelling and industrial fallout. *Nature*, **328**(6133), 794.

Shiel, A. E., Weis, D., & Orians, K. J. (2010). Evaluation of zinc, cadmium and lead isotope fractionation during smelting and refining. *Science of the Total Environment*, **408**(11), 2357-2368.

Sieber, M., Conway, T. M., de Souza, G. F., Hassler, C. S., Ellwood, M. J., & Vance, D. (2019a). High-resolution Cd isotope systematics in multiple zones of the Southern Ocean from the Antarctic Circumnavigation Expedition. *Earth Planet. Sci. Lett.*, **527**, doi:10.1016/j.epsl.2019.115799.

Sieber, M., Conway, T. M., de Souza, G. F., Obata, H., Takano, S., Sohrin, Y., & Vance, D. (2019b). Physical and biogeochemical controls on the distribution of dissolved cadmium and its isotopes in the Southwest Pacific Ocean. *Chem. Geol.*, **511**, 494-509.

Sieber, M., Conway, T. M., de Souza, G. F., Hassler, C. S., Ellwood, M. J., & Vance, D. (2020). Cycling of zinc and its isotopes across multiple zones of the Southern Ocean: Insights from the Antarctic Circumnavigation Expedition. *Geochim. Cosmochim. Acta*, **268**, 310-324, doi:10.1016/j.gca.2019.09.039.

Siebert, C., Nägler, T. F., von Blanckenburg, F., and Kramers, J. D. (2003). Molybdenum isotope records as a potential new proxy for paleoceanography. *Earth Planet. Sci. Lett.*, **211**, 159–171, doi:10.1016/S0012-821X(03)00189-4.

Siebert, C., Pett-Ridge, J. C., Opfergelt, S., Guicharnaud, R. A., Halliday, A. N., & Burton, K. W. (2015). Molybdenum isotope fractionation in soils: Influence of redox conditions, organic matter, and atmospheric inputs. *Geochim. Cosmochim. Acta*, **162**, 1–24, doi:10.1016/j.gca.2015.04.007.

Sigman, D. M., & Boyle, E. A. (2000). Glacial/interglacial variations in atmospheric carbon dioxide. *Nature*, **407**(6806), 859-869.

Sigman, D. M., & Hain, M. P. (2012). The Biological Productivity of the Ocean: Section 1, *Nature Education Knowledge*, **3**(10):21.

Sigman, D. M., Hain, M. P., & Haug, G. H. (2010). The polar ocean and glacial cycles in atmospheric CO_2 concentration, *Nature*, **466**, 47-55, doi:10.1038/nature09149.

Skulan, J. L., Beard, B. L., & Johnson, C. M. (2002). Kinetic and equilibrium Fe isotope fractionation between aqueous Fe (III) and hematite. *Geochim. Cosmochim. Acta*, **66**(17), 2995-3015.

Sinoir, M., Butler, E. C. V., Bowie, A. R., Mongin, M., Nesterenko, P. N., & Hassler, C. S. (2012). Zinc marine biogeochemistry in seawater: A review. *Mar. Freshw. Res.,* **63**, 644–657.

Sorensen, J. V., Gueguen, B., Stewart, B. D., Peña, J., Rouxel, O., & Toner, B. M. (2020). Large nickel isotope fractionation caused by surface complexation reactions with hexagonal birnessite. *Chem. Geol*., **537**, 119481.

Staubwasser, M., Schoenberg, R., von Blanckenburg, F., Krüger, S., & Pohl, C. (2013) Isotope fractionation between dissolved and suspended particulate Fe in the oxic and anoxic water column of the Baltic Sea. *Biogeosciences*, **10**, 233-245. doi:10.5194/bg-10-233-2013.

Sternberg, E., Jeandel, C., Robin, E., & Souhaut, M. (2008). Seasonal cycle of suspended barite in the Mediterranean sea. *Geochim. Cosmochim. Acta*, **72**(16), 4020-4034.

Stevenson, E. I., Fantle, M. S., Das, S. B., Williams, H. M., & Aciego, S. M. (2017). The iron isotopic composition of subglacial streams draining the Greenland ice sheet. *Geochim. Cosmochim. Acta*, **213**, 237-254.

Sun, W.-P., Hu, C.-Y., Han, Z.-B., Shen, C., & Pan, J.-M. (2016). Zn/Si records in diatom opal from Prydz Bay, East Antarctica. *Marine Geology* **381**, 34-41.

Sunda, W. G. (2012). Feedback interactions between trace metal nutrients and phytoplankton in the ocean. *Front. Microbiol.*, **3**(204), doi:10.3389/fmicb.2012.00204.

Sunda, W. G., & Huntsman, S. A. (1995). Iron uptake and growth limitation in oceanic and coastal phytoplankton. *Mar. Chem.,* **50**, 189–206.

Sunda, W. G., & Huntsman, S. A. (2000). Effect of Zn, Mn, and Fe on Cd accumulation in phytoplankton: implications for oceanic Cd cycling. *Limnol. Oceanogr.*, **45**(7), 1501-1516.

Sweere, T. C., Dickson, A. J., Jenkyns, H. C., Porcelli, D., Elrick, M., van den Boorn, S. H., & Henderson, G. M. (2018). Isotopic evidence for changes in the zinc cycle during Oceanic Anoxic Event 2 (Late Cretaceous). *Geology*, **46**(5), 463-466.

Tabouret, H., Pomerleau, S., Jolivet, A., Pécheyran, C., Riso, R., et al. (2012). Specific pathways for the incorporation of dissolved barium and molybdenum into the bivalve shell: An isotopic tracer approach in the juvenile Great Scallop (*Pecten maximus*). *Mar. Environ. Res.*, **78**, 15-25, doi:10.1016/j.marenvres.2012.03.006.

Tagliabue, A., Aumont, O., DeAth, R., Dunne, J. P., Dutkiewicz, S., Galbraith, E., Misumi, K., Moore, J. K., Ridgwell, A., Sherman, E., Stock, C., Vichi, M., Völker, C., & Yool, A. (2016). How well do global ocean biogeochemistry models simulate dissolved iron distributions?. *Global Biogeochem. Cycles*, **30**(2), 149-174.

Tagliabue, A., Bowie, A. R., Boyd, P. W., Buck, K. N., Johnson, K. S., & Saito, M. A. (2017). The integral role of iron in ocean biogeochemistry. *Nature*, **543**(7643), 51-59.

Tagliabue, A., Bowie, A. R., DeVries, T., Ellwood, M. J., Landing, W. M., Milne, A., Ohnemus, D. C., Twining, B. S., & Boyd, P. W. (2019). The interplay between regeneration and scavenging fluxes drives ocean iron cycling. *Nat. Commun.*, 10**(**1), 1-8.

Takano, S., Tanimizu, M., Hirata, T. , & Sohrin, Y. (2014). Isotopic constraints on biogeochemical cycling of copper in the ocean. *Nat. Commun.* **5**, 5663.

Takano, S., Tanimizu, M., Hirata, T., Shin, K. C., Fukami, Y., Suzuki, K., & Sohrin, Y. (2017). A simple and rapid method for isotopic analysis of nickel, copper, and zinc in seawater using chelating extraction and anion exchange. *Anal. Chim. Acta* **967**, 1–11.

Tankéré, S. P. C., Muller, F. L. L., Burton, J. D., Statham, P. J., Guieu, C., & Martin, J. M. (2001). Trace metal distributions in shelf waters of the northwestern Black Sea. *Cont. Shelf Res.* **21**, 1501–1532.

Tegler, L. A., Dunlea, A. G., Romaniello, S. J., Anbar, A. D., & Horner, T. J. (2018). More Clear than Mud: Dating Deep-Sea Clays with Osmium Isotopes to Unravel Seawater Metal Cycling through the Cenozoic. *In 2018 Ocean Sciences Meeting*. AGU.

Tesoriero, A. J., & Pankow, J. F. (1996). Solid solution partitioning of Sr^{2+}, Ba^{2+}, and Cd^{2+} to calcite. *Geochim. Cosmochim. Acta*, **60**(6), 1053-1063.

Tessin, A., Chappaz, A., Hendy, I., & Sheldon, N. (2019). Molybdenum speciation as a paleo-redox proxy: A case study from Late Cretaceous Western Interior Seaway black shales. *Geology*, **47**, 59–62, doi:10.1130/G45785.1.

Thébault, J. Chauvaud, L. L'Helguen, S., Clavier, J., Barats, A., et al. (2009). Barium and molybdenum records in bivalve shells: Geochemical proxies for phytoplankton dynamics in coastal environments? *Limnol. Oceanogr.*, **54**(3), 1002-1014, doi:10.4319/lo.2009.54.3.1002.

Thibon, F., Blichert-Toft, J., Albarede, F., Foden, J., & Tsikos, H. (2019). A critical evaluation of copper isotopes in Precambrian Iron Formations as a paleoceanographic proxy. *Geochim. Cosmochim. Acta*, *264*, 130-140.

Thompson, C. M., & Ellwood, M. J. (2014). Dissolved copper isotope biogeochemistry in the Tasman Sea, SW Pacific Ocean. *Mar. Chem.* **165**, 1–9.

Torres, M. E., Brumsack, H. J., Bohrmann, G., & Emeis, K. C. (1996). Barite fronts in continental margin sediments: a new look at barium remobilization in the zone of sulfate reduction and formation of heavy barites in diagenetic fronts. *Chem. Geol.*, **127**(1-3), 125-139.

Tossell, J. A. (2005). Calculating the partitioning of the isotopes of Mo between oxidic and sulfidic species in aqueous solution. *Geochim. Cosmochim. Acta*, **69**, 2981–2993, doi:10.1016/j.gca.2005.01.016.

Tribovillard, N., Algeo, T. J., Lyons, T., & Riboulleau, A. (2006). Trace metals as paleoredox and paleoproductivity proxies: an update. *Chem. Geol.*, **232**(1-2), 12-32.

Turekian, K. K. (1968). Deep-sea deposition of barium, cobalt and silver. *Geochim. Cosmochim. Acta,* **32**(6), 603-612.

Turner, D. R., Whitfield, M., & Dickson, A. G. (1981). The equilibrium speciation of dissolved components in freshwater and sea water at 25°C and 1 atm pressure. *Geochim. Cosmochim. Acta,* **45**, 855–881.

Twining, B. S., & Baines, S. B. (2013). The trace metal composition of marine phytoplankton. *Annual Review of Marine Science*, **5**, 191-215.

Twining, B. S., Baines, S. B., & Fisher, N. S. (2004) Element stoichiometries of individual plankton cells collected during the Southern Ocean Iron Experiment (SOFeX). *Limnol. Oceanogr.,* **49**, 2115–2128.

Twining, B. S., Baines, S. B., Vogt, S., & Nelson, D. M. (2012) Role of diatoms in nickel biogeochemistry in the ocean. *Glob. Biogeochem. Cycles*, **26** (4), GB4001, doi:10.1029/2011GB004233.

Twining, B. S., Nodder, S. D., King, A. L., Hutchins, D. A., LeCleir, G. R., DeBruyn, J. M., Maas, E. W., Vogt, S., Wilhelm S. W.,. & Boyd, P. W. (2014). Differential remineralization of major and trace elements in sinking diatoms. *Limnol. Oceanogr.*, **59**(3), 689-704.

van Geen, A., Luoma, S. N., Fuller, C. C., Anima, R., Clifton, H. E., & Trumbore, S. (1992). Evidence from Cd/Ca ratios in foraminifera for greater upwelling off California 4,000 years ago. *Nature*, **358**(6381), 54.

van Geen, A., McCorkle, D. C., & Klinkhammer, G. P. (1995). Sensitivity of the phosphate-cadmium-carbon isotope relation in the ocean to cadmium removal by suboxic sediments. *Paleoceanography*, **10**(2), 159-169.

van Helmond, N. A. G. M., Jilbert, T., & Slomp, C. P. (2018). Hypoxia in the Holocene Baltic Sea: Comparing modern versus past intervals using sedimentary trace metals. *Chem. Geol.*, **493**, 478-490, doi:10.1016/j.chemgeo.2018.06.028.

Vance, D., Archer, C., Bermin, J., Perkins, J., Statham, P. J., Lohan, M. C., Ellwood, M. J., & Mills, R. A. (2008). The copper isotope geochemistry of rivers and the oceans. *Earth Planet. Sci. Lett.* **274**, 204–213.

Vance, D., Little, S. H., Archer, C., Cameron, V., Andersen, M. B., Rijkenberg, M. J. A., & Lyons, T. W. (2016). The oceanic budgets of nickel and zinc isotopes: the importance of sulfidic environments as illustrated by the Black Sea. *Philos. Trans. R. Soc. A Math. Phys. Eng. Sci.* **374**, 20150294.

Vance, D., Little, S. H., de Souza, G. F., Khatiwala, S., Lohan, M. C., & Middag, R. (2017). Silicon and zinc biogeochemical cycles coupled through the Southern Ocean. *Nat. Geosci.,* **10**, 202–206.

Vance, D., de Souza, G. F., Zhao, Y., Cullen, J. T., & Lohan, M. C. (2019). The relationship between zinc, its isotopes, and the major nutrients in the North-East Pacific. *Earth Planet. Sci. Lett.*, **525**, doi:10.1016/j.epsl.2019.115748.

Velasquez, I. B., Ibisanmi, E., Maas, E. W., Boyd, P. W., Nodder, S., & Sander, S. G. (2016). Ferrioxamine Siderophores Detected amongst Iron Binding Ligands Produced during the Remineralization of Marine Particles. *Front. Mar. Sci.* **3**, 172. https://doi.org/10.3389/fmars.2016.00172.

Vihtakari, M., Ambrose Jr., W. G., Renaud, P. E., Locke V, W. L., Carroll, M. L., et al. (2017). A key to the past? Element ratios as environmental proxies in two Arctic bivalves. *Palaeogeogr. Palaeoclimatol. Palaeoecol.*, **465**, 316-332, doi:10.1016/j.palaeo.2016.10.020.

Voegelin, A. R., Nägler, T. F., Samankassou, E., & Villa, I. M. (2009). Molybdenum isotopic composition of modern and Carboniferous carbonates. *Chem. Geol.*, **265**, 488-498, doi:10.1016/j.chemgeo.2009.05.015.

Volk, T., & Hoffert, M. I. (1985). Ocean carbon pumps: Analysis of relative strengths and efficiencies in ocean-driven atmospheric CO_2 changes. *The carbon cycle and atmospheric CO_2: natural variations Archean to present*, **32**, 99-110.

Von Allmen, K., Böttcher, M. E., Samankassou, E., & Nägler, T. F. (2010). Barium isotope fractionation in the global barium cycle: First evidence from barium minerals and precipitation experiments. *Chem. Geol.*, **277**(1-2), 70-77.

Vorlicek, T. P., Chappaz, A., Groskreutz, L. M., Young, N., & Lyons, T. W. (2015). A new analytical approach to determining Mo and Re speciation in sulfidic waters. *Chem. Geol.*, **403**, 52–57, doi:10.1016/j.chemgeo.2015.03.003.

Vorlicek, T. P., Helz, G. R., Chappaz, A., Vue, P., Vezina, A., & Hunter, W. (2018). Molybdenum Burial Mechanism in Sulfidic Sediments: Iron-Sulfide Pathway. *ACS Earth and Space Chemistry*, **2**, 565–576, doi:10.1021/acsearthspacechem.8b00016.

Waeles, M., Baker, A. R., Jickells, T., & Hoogewerff, J. (2007). Global dust teleconnections: aerosol iron solubility and stable isotope composition. *Environmental Chemistry*, **4**(4), 233-237.

Wagner, M. E. (2013). *Silver as a novel tracer for Late Quaternary Southern Ocean biological and geophysical processes*. PhD thesis, University of Michigan, 189p.

Wagner, M., Hendy, I. L., McKay, J. L., & Pedersen, T.F. (2013). Influence of biological productivity on silver and redox-sensitive trace metal accumulation in Southern Ocean surface sediments, Pacific sector. *Earth Planet. Sci. Lett.*, **380**, 31-40.

Wagner, M., Chappaz, A., & Lyons, T.W. (2017). Molybdenum speciation and burial pathway in weakly sulfidic environments: Insights from XAFS. *Geochim. Cosmochim. Acta*, **206**, 18–29, doi:10.1016/j.gca.2017.02.018.

Waldron, K. J., & Robinson, N. J. (2009). How do bacterial cells ensure that metalloproteins get the correct metal? *Nature Reviews Microbiology*, **7**(1), 25.

Wang, D., Xia, W., Lu, S., Wang, G., Liu, Q., Moore, W. S., and Arthur Chen, C. T. (2016). The nonconservative property of dissolved molybdenum in the western Taiwan Strait: Relevance of submarine groundwater discharges and biological utilization. *Geochemistry, Geophysics, Geosystems*, **17**, 28–43, doi:10.1002/2014GC005708.

Wang, R. M., Archer, C., Bowie, A. R., & Vance, D. (2019a). Zinc and nickel isotopes in seawater from the Indian Sector of the Southern Ocean: The impact of natural iron fertilization versus Southern Ocean hydrography and biogeochemistry. *Chem. Geol.*, **511**, 452-464.

Wang, Z., Li, J., Wei, G., Deng, W., Chen, X., Zeng, T., Wang, X., Ma, J., Zhang, L., Tu, X., Wang, Q., & McCulloch, M. (2019b). Biologically controlled Mo isotope fractionation in coral reef systems. *Geochim. Cosmochim. Acta*, **262**, 128-142, doi:10.1016/j.gca.2019.07.037.

Wang, S.-J., Rudnick, R. L., Gaschnig, R. M., Wang, H., & Wasylenki, L. E. (2019c). Methanogenesis sustained by sulfide weathering during the Great Oxidation Event. *Nat. Geosci.*, **12**, 296-300, doi:10.1038/s41561-019-0320-z.

Wasylenki, L. E., Anbar, A. D., Liermann, L. J., Mathur, R., Gordon, G. W., & Brantley, S. L. (2007). Isotope fractionation during microbial metal uptake measured by MC-ICP-MS. *J. Anal. At. Spectrom.*, **22**, 905-910, doi:10.1039/b705476a.

Wasylenki, L. E., Rolfe, B. A., Weeks, C. L., Spiro, T. G., and Anbar, A. D. (2008). Experimental investigation of the effects of temperature and ionic strength on Mo isotope fractionation during adsorption to manganese oxides. *Geochim. Cosmochim. Acta*, **72**, 5997–6005, doi:10.1016/j.gca.2008.08.027.

Wasylenki, L. E., Swihart, J. W., & Romaniello, S. J. (2014). Cadmium isotope fractionation during adsorption to Mn oxyhydroxide at low and high ionic strength. *Geochim. Cosmochim. Acta*, **140**, 212-226.

Weber, T., John, S. G., Tagliabue, A., & DeVries, T. (2018). Biological uptake and reversible scavenging of zinc in the global ocean. *Science*, **361**, 72–76.

Wefing, A. M., Arps, J., Blaser, P., Wienberg, C., Hebbeln, D., & Frank, N. (2017). High precision U-series dating of scleractinian cold-water corals using an automated chromatographic U and Th extraction. *Chem. Geol.*, **475**, 140-148.

Wei, W., & Algeo, T. J. (in press). Secular variation in the elemental composition of marine shales since 840 Ma: Tectonic and seawater influences. *Geochim. Cosmochim. Acta*, doi: 10.1016/j.gca.2020.01.033.

Welch, S. A., Beard, B. L., Johnson, C. M., & Braterman, P. S. (2003). Kinetic and equilibrium Fe isotope fractionation between aqueous Fe(II) and Fe(III). *Geochim. Cosmochim. Acta*, **67**, 4231-4250. https://doi.org/10.1016/S0016-7037(03)00266-7.

Wichard, T., Mishra, B., Myneni, S. C. B., Bellenger, J. P., & Kraepiel, A. M. L. (2009). Storage and bioavailability of molybdenum in soils increased by organic matter complexation. *Nat. Geosci.*, **2**, 625–630, doi:10.1038/ngeo589.

Willbold, M., & Elliott, T. (2017). Molybdenum isotope variations in magmatic rocks. *Chem. Geol.*, **449**, 253-268.

Winckler, G., Anderson, R. F., Jaccard, S. L., & Marcantonio, F. (2016). Ocean dynamics, not dust, have controlled equatorial Pacific productivity over the past 500,000 years. *Proceedings of the National Academy of Sciences*, **113**(22), 6119-6124.

Wolgemuth, K., & Broecker, W. S. (1970). Barium in sea water. *Earth Planet. Sci. Lett.*, **8**(5), 372-378.

Woodland, S. J., Rehkämper, M., Halliday, A. N., Lee, D.-C., Hatterndorf, B., & Günther, D. (2005) Accurate measurement of silver isotopic compositions in geological materials including lowPd/Ag meteorites. *Geochim. Cosmochim. Acta*, **69**(8). doi:10.1016/j.gca.2004.10.012.

Wuttig, K., Townsend, A. T., van der Merwe, P., Gault-Ringold, M., Holmes, T., Schallenberg, C., Latour, P., Tonnard, M., Rijkenberg, M. J. A., Lannuzel, D., & Bowie, A. R. (2019). Critical evaluation of a seaFAST system for the analysis of trace metals in marine samples. *Talanta*, **197**, 653-668.

Xie, R. C., Galer, S. J., Abouchami, W., Rijkenberg, M. J., De Baar, H. J., De Jong, J., & Andreae, M. O. (2017). Non-Rayleigh control of upper-ocean Cd isotope fractionation in the western South Atlantic. *Earth Planet. Sci. Lett.*, **471**, 94-103.

Xie, R. C., Galer, S. J. G., Abouchami, W., & Frank, M. (2019a) Limited impact of eolian and riveringe sources on the biogeochemical cycling of Cd in the tropical Atlantic. *Chem. Geol.* **511**, 371-379. https://doi.org/10.1016/j.chemgeo.2018.10.018.

Xie, R., C., Rehkämper, M., Grasse, P., van de Flierdt, T., Frank, M., & Xue, Z. (2019b). Isotopic evidence for complex biogeochemical cycling of Cd in the eastern tropical South Pacific. *Earth Planet. Sci. Lett.* **512**, 134-146. https://doi.org/10.1016/j.epsl.2019.02.001.

Xu, Y., Feng, L., Jeffrey, P. D., Shi, Y., & Morel, F. M. (2008). Structure and metal exchange in the cadmium carbonic anhydrase of marine diatoms. *Nature*, **452**(7183), 56.

Xue, Z., Rehkämper, M., Schönbächler, M., Statham, P. J., & Coles, B. J. (2012). A new methodology for precise cadmium isotope analyses of seawater. *Analytical and Bioanalytical Chemistry*, **402**(2), 883-893.

Xue, Z., Rehkämper, M., Horner, T. J., Abouchami, W., Middag, R., van de Flierd, T., & de Baar, H. J. (2013). Cadmium isotope variations in the Southern Ocean. *Earth Planet. Sci. Lett.*, **382**, 161-172.

Yang, S.-C., Lee, D.-L., & Ho, T.-Y. (2012). The isotopic composition of Cadmium in the water column of the South China Sea. *Geochim. Cosmochim. Acta*, **98**, 66-77. https://doi.org/10.1016/j.gca.2012.09.022.

Yang, S.-C., Lee, D.-L., Ho, T.-Y., Wen, L.-S., & Yang, H.-H. (2014). The isotopic composition of dissolved cadmium in the water column of the West Philippine Sea. *Front. Mar. Sci.* **1**(61). https://doi.org/10.3389/fmars.2014.00061

Yang, S.-C., Lee, D.-C., & Ho, T.-Y. (2015). Cd isotopic composition in the suspended and sinking particles of the surface water of the South China Sea: The effects of biotic activities. *Earth Planet. Sci. Lett.*, **428**, 63-72.

Yang, S.-C., Zhang, J., Sohrin, Y., & Ho, T.-Y. (2018). Cadmium cycling in the water column of the Kuroshio-Oyashio Extension region: Insights from dissolved and particulate isotopic composition. *Geochim. Cosmochim. Acta*, **233**, 66-80.

Yang, T., Chen, Y. Zhou, S., & Li, H. (2019). Impacts of aerosol copper on marine phytoplankton: A review. *Atmosphere*, **10**(7), 414, doi:10.3390/atmos10070414.

Yang, S.-C., Hawco, N. J., Pinedo-González, P., Bian, X., Huang, K.-F., & John. S. G. (2020). A new purification method for Ni and Cu stable isotopes in seawater provides evidence for widespread Ni isotope fractionation by phytoplankton in the North Pacific. *Chem. Geol.* **547**, 119662. https://doi.org/10.1016/j.chemgeo.2020.119662.

Yee, D., & Morel, F. M. M. (1996). In vivo substitution in carbonic of zinc by cobalt of a marine anhydrase diatom. *Limnol. Oceanogr.,* **41**, 573–577.

Zhang, R., John, S. G., Zhang, J., Ren, J., Wu, y., Zhu, Z., Liu, S., Zhu, X., Marsay, C. M., & Wenger, F. (2015). Transport and reaction of iron and iron stable isotopes in glacial meltwaters on Svalbard near Kongsfjorden: From rivers to estuary to ocean. *Earth Planet. Sci. Lett.,* **424**, 201-211. https://doi.org/10.1016/j.epsl.2015.05.031.

Zhang, R., Jensen, L. T., Fitzsimmons, J. N., Sherrell, R. M., & John, S. (2019). Dissolved cadmium and cadmium stable isotopes in the western Arctic Ocean. *Geochim. Cosmochim. Acta*, **258**, 258-273, https://doi.org/10.1016/j.gca.2019.05.028.

Zhang, Y., Amakawa, H., & Nozaki, Y. (2001). Oceanic profiles of dissolved silver: precise measurements in the basins of western North Pacific, Sea of Okhotsk, and the Japan Sea. *Marine Chemistry*, **75**, 151-163.

Zhang, Y., Obata, H., & Nozaki, Y. (2004). Silver in the Pacific Ocean and the Bering Sea. *Geochemical Journal*, **38**, 623-633.

Zhao, Y., Vance, D., Abouchami, W., & de Baar, H. J. W. (2014). Biogeochemical cycling of zinc and its isotopes in the Southern Ocean. *Geochim. Cosmochim. Acta,* **125**, 653–672. http://dx.doi.org/10.1016/j.gca.2013.07.045.

Zhu, X. K., O'Nions, R. K., Guo, Y., & Reynolds, B. C. (2000). Secular variation of iron isotopes in North Atlantic deep water. *Science*, **287**(5460).

Zirino, A., & Yamamoto, S. (1972). A pH-dependent model for the chemical speciation of copper, zinc, cadmium, and lead in seawater. *Limnol. Oceanogr.* **17**, 661–671.